General Disclaimer

One or more of the Following Statements may affect this Document

- This document has been reproduced from the best copy furnished by the organizational source. It is being released in the interest of making available as much information as possible.

- This document may contain data, which exceeds the sheet parameters. It was furnished in this condition by the organizational source and is the best copy available.

- This document may contain tone-on-tone or color graphs, charts and/or pictures, which have been reproduced in black and white.

- This document is paginated as submitted by the original source.

- Portions of this document are not fully legible due to the historical nature of some of the material. However, it is the best reproduction available from the original submission.

Produced by the NASA Center for Aerospace Information (CASI)

PB81-172348

NBS: Nondestructive Evaluation of Nonuniformities in 2219 Aluminum Alloy Plate - Relationship to Processing

(U.S.) National Bureau of Standards
Washington, DC

Prepared for

National Aeronautics and Space Administration
Washington, DC

Dec 80

U.S. Department of Commerce
National Technical Information Service
NTIS

NBS-114A (REV. 9-78)

U.S. DEPT. OF COMM. BIBLIOGRAPHIC DATA SHEET	1. PUBLICATION OR REPORT NO. NBSIR 80-2069	2. Gov't. Accession No.	3. Recipient's Accession No. PB81 172348

4. TITLE AND SUBTITLE

Nondestructive Evaluation of Nonuniformities in 2219 Aluminum Alloy Plate - Relationship to Processing

5. Publication Date

December 1980

6. Performing Organization Code

7. AUTHOR(S) L. Swartzendruber, L. Ives, W. Boettinger, S. Coriell, D. Ballard, D. Laughlin, R. Clough, F. Biancaniello, P. Blau, J. Cahn, R. Mehrabian, G. Ecke and L. Mordfin

8. Performing Organ. Report No.

9. PERFORMING ORGANIZATION NAME AND ADDRESS

NATIONAL BUREAU OF STANDARDS
DEPARTMENT OF COMMERCE
WASHINGTON, DC 20234

10. Project/Task/Work Unit No.

11. Contract/Grant No.

Government Order W-14,637

12. SPONSORING ORGANIZATION NAME AND COMPLETE ADDRESS *(Street, City, State, ZIP)*

National Aeronautics and Space Administration
Washington, DC 20546

13. Type of Report & Period Covered

Technical
August 1979 - Sept. 1980

14. Sponsoring Agency Code

15. SUPPLEMENTARY NOTES

☐ Document describes a computer program; SF-185, FIPS Software Summary, is attached.

16. ABSTRACT *(A 200-word or less factual summary of most significant information. If document includes a significant bibliography or literature survey, mention it here.)*

The compositional homogeneity, microstructure, hardness, electrical conductivity and mechanical properties of 2219 aluminum alloy plates are influenced by the process variables during casting, forming and thermomechanical treatment.

17. KEY WORDS *(six to twelve entries; alphabetical order; capitalize only the first letter of the first key word unless a proper name; separated by semicolons)*

Aging; electrical conductivity; hardness; homogeneity; microstructure; precipitating; segregation; solidification; thermal mechanical treatment.

18. AVAILABILITY ☒ Unlimited

☐ For Official Distribution. Do Not Release to NTIS

☐ Order From Sup. of Doc., U.S. Government Printing Office, Washington, DC 20402, SD Stock No. SN003-003-

☒ Order From National Technical Information Service (NTIS), Springfield, VA. 22161

19. SECURITY CLASS (THIS REPORT)	21. NO. OF PRINTED PAGES
UNCLASSIFIED	
20. SECURITY CLASS (THIS PAGE)	**22. Price**
UNCLASSIFIED	

USCOMM-DC

PB81-172346

NBSIR 80-2069

NBS: Nondestructive Evaluation of Nonuniformities in 2219 Aluminum Alloy Plate - Relationship to Processing

L. Swartzendruber, W. Boettinger, L. Ives, S. Coriell, D. Ballard,
D. Laughlin, R. Clough, F. Biancaniello, P. Blau, J. Cahn and
R. Mehrabian, *Metallurgy Division*
G. Free, *Electrical Measurements and Standards Division*
H. Berger and L. Mordfin, *Office of Nondestructive Evaluation*

National Measurement Laboratory
National Bureau of Standards
U.S. Department of Commerce
Washington, DC 20234
Phone: (301) 921-2811

December 1980
Technical Report
For the Period August 1979 - September 1980
NASA Government Order W-14,637

U.S. DEPARTMENT OF COMMERCE
NATIONAL BUREAU OF STANDARDS

PRODUCT OF:
NATIONAL TECHNICAL
INFORMATION SERVICE
U.S. DEPARTMENT OF COMMERCE
SPRINGFIELD, VA. 22161

NBSIR 80-2069

NBS: NONDESTRUCTIVE EVALUATION OF NONUNIFORMITIES IN 2219 ALUMINUM ALLOY PLATE - RELATIONSHIP TO PROCESSING

L. Swartzendruber, W. Boettinger, L. Ives, S. Coriell, D. Ballard,
D. Laughlin, R. Clough, F. Biancaniello, P. Blau, J. Cahn and
R. Mehrabian, *Metallurgy Division*
G. Free, *Electrical Measurements and Standards Division*
H. Berger and L. Mordfin, *Office of Nondestructive Evaluation*

National Measurement Laboratory
National Bureau of Standards
U.S. Department of Commerce
Washington, DC 20234
Phone: (301) 921-2811

December 1980
Technical Report
For the Period August 1979 - September 1980
NASA Government Order W-14,637

U.S. DEPARTMENT OF COMMERCE, Philip M. Klutznick, *Secretary*
Jordan J. Baruch, *Assistant Secretary for Productivity, Technology, and Innovation*
NATIONAL BUREAU OF STANDARDS, Ernest Ambler, *Director*

Nondestructive Evaluation of Nonuniformities in 2219 Aluminum Alloy Plate - Relationship to Processing

ABSTRACT

The compositional homogeneity, microstructure, hardness, electrical conductivity and mechanical properties of 2219 aluminum alloy plates are influenced by the process variables during casting, rolling and thermo-mechanical treatment. The details of these relationships have been investigated for correctly processed 2219 plate as well as for deviations caused by improper quenching after solution heat treatment. Primary emphasis has been placed on the reliability of eddy current electrical conductivity and hardness as NDE tools to detect variations in mechanical properties.

Experimental studies were carried out on an industrial size semi-continuous cast ingot and on various smaller laboratory cast ingots. The major phases present in as-cast 2219 aluminum alloy are α-aluminum solid solution, θ-$CuAl_2$ and Cu_2FeAl_7. The positive and negative macrosegregation of alloying elements was investigated. This macrosegregation is predictable and is caused by interdendritic fluid flow during casting. It cannot be completely eliminated from the finished alloy plate by thermomechanical treatment or scalping and leads to moderate variations in composition across the plate thickness.

Experiments conducted on correctly heat treated samples from the laboratory ingot indicate that mechanical properties are maintained as long as the copper content is above the maximum solid solubility limit (~5.5% Cu). Such was the case for a commercial alloy plate examined in this report. Hence the observed property variation across this as-received plate was not due to composition variation.

A comprehensive series of thermomechanical heat treatments on 2219-T87* aluminum alloy was performed. The hardness and electrical conductivity were monitored at each stage of the treatment and the mechanical properties of the finished material were determined. The results were utilized to determine curves (C curves) that can be used to assess the effect of various quenching treatments on the final mechanical and NDE properties of the processed material. These C curves were also used to develop correlations between the mechanical and electrical conductivity. Such a correlation was found to exist for alloys (of a single lot) and for improper quenching from solution heat treatment. Wider excursions from the correct heat treatment cycle can destroy this correlation.

The precipitation behavior of the 2219 aluminum alloy was examined. The principal age-hardening phase in properly processed material is θ'. The θ" phase is also present and contributes to strength. A pre-aging heat treatment, or other temperature excursion, following solution heat treatment that results in dwell times which are significant in relation to the C curves, results in the nucleation and rapid growth of θ and/or θ' precipitates. The relationship of precipitation kinetics to the C curves and the influence of the various precipitates on mechanical properties and NDE behavior is discussed.

One dimensional heat flow calculations for the cooling of aluminum plates of various thicknesses were carried out for three models of heat transfer, viz. (a) symmetric cooling of the plate from both top and bottom surfaces, (b) asymmetric cooling of the plate from the top surface only with an insulated bottom surface, and (c) symmetric cooling of the plates for a specified time followed by an abrupt reduction of the heat transfer coefficient at the bottom surface to zero (insulated surface). The temperature-time curves for various cooling conditions were combined with C curve data to calculate plate properties, e.g., yield strength and hardness, as a function of position in the plate. Such calculations for symmetric cooling are in general agreement with property variations observed in as-received and properly heat treated plate. The minimum properties expected under the "worst" quench malfunctions were also predicted as a function of plate thicknesses.

Results of a Round Robin to determine the inter-laboratory precision in eddy current conductivity and hardness measurements on a series of 2219 aluminum alloys heat treated to various conditions are discussed.

TABLE OF CONTENTS

		Page No.
I.	INTRODUCTION	1
II.	STUDIES ON AS-RECEIVED PLATES	3
III.	SOLIDIFICATION-SEGREGATION STUDIES	7
	1. Microsegregation in Cast 2219 Aluminum Alloy	9
	(a) Calculation of Microsegregation for Al-Cu-Mn-Fe-Si Alloy System	9
	(b) Second Phase Particles Formed During Solidification of 2219 Aluminum Alloy	12
	2. Macrosegregation in Cast 2219 Aluminum Alloy	15
	(a) DC Cast Ingot	15
	(b) Macrosegregation in Laboratory Cast Ingot	17
	3. Thermomechanical Treatment and Evaluation of Laboratory Ingot	19
IV.	DETERMINATION OF C CURVES	21
	1. Thermomechanical Treatment	22
	2. Effects of % Stretch and Aging Treatment on Properties	23
	3. Mechanical and Electrical Measurements	24
	4. Measurements on As-Received and Reprocessed 2219-T87* Plate	26
	5. Measurements After Solution Heat Treatment and Pre-Aging	27
	6. Measurements After Stretching	27
	7. Measurements after Final Aging	28
	8. Calculation of C Curves	29
	9. Discussion	32

Page No.

V. ELECTRON MICROSCOPY STUDIES 41

1. Experimental Procedure 43

2. Results 46

(a) Solutionized Structure 46

(b) Stretched and Aged Structure 48

(c) Microstructure After Quench Treatment 51

3. Discussion 56

VI. HEAT FLOW - PROPERTY PREDICTIONS 62

1. Heat Flow Model 62

2. Heat Flow Calculations and Property Predictions 63

(a) Symmetric Cooling 64

(b) Asymmetric Cooling 65

(c) Abrupt Variations in Rate of Heat Extraction From The Bottom Surface 66

3. Summary of "Worst" Property Predictions 67

VII. ROUND ROBIN RESULTS 69

1. Samples 69

2. Equipment 70

3. Results 71

4. Discussion 73

VIII. CONCLUSIONS 75

1. As-received Plate 75

2. Solidification Segregation Studies 75

3. C-Curve Determination and Relationship Between Mechanical Properties and Conductivity 76

4. Electron Microscopy Studies 77

5. Heat Flow Calculations - Property Predictions 78

6. Round Robin Results 79

	Page No.
APPENDIX	80
ACKNOWLEDGEMENT	85
REFERENCES	86
TABLES	88
FIGURES	127

I. INTRODUCTION

This is a comprehensive technical report of our investigations in the past eight months on 2219 aluminum alloy. The aim of this work was to develop specific relationships between process variables used during casting, working and heat treatment of the alloy, and the resulting microstructures and properties including eddy current conductivity and hardness nondestructive evaluation (NDE) responses.

The work was initiated at the National Bureau of Standards at the request of the National Aeronautics and Space Administration. It was motivated by government and aerospace industry concerns on the possibility that substrength aluminum alloys may have been used in aircraft and space vehicle structures(1). These concerns originated from the discovery of "soft" spots† in an anodized 2124-T851 aluminum alloy machined part in June 1979. The part was machined from a ∿ 14 cm (5.5 inch) thick plate of the alloy produced in the Reynolds Metal Company McCook Plant in Chicago, Illinois. The "soft" spots were apparently due to improper processing of the plate (1). Furthermore, it was established that the same plant was producing a variety of other aluminum alloy plates including the 2219 aluminum alloy which was the subject of this investigation. Serious concerns were also expressed about the viability of test techniques used to find suspect metal (2).

Specific aims of our investigation included the following:

1. To establish the processing conditions and mechanisms responsible for the occurrence of "soft" spots;

2. To establish direct correlations between process variables and the composition and microstructures of the plates;

---

† "Soft" spots denote areas of a plate with mechanical properties below Federal Specifications.

3. To determine the relationships between composition, microstructure and the mechanical properties, hardness, and electrical conductivity of the plates;

4. To develop correlations between electrical conductivity and hardness and tensile properties for a wide range of metallurgical microstructures for future use in the development of accurate specifications for 2219 aluminum alloy plates; and

5. To develop predictive heat flow and time-temperature precipitation models in order to determine the ranges of possible degradation of properties due to improper processing conditions.

The investigations carried out were reported in detail in separate monthly reports. This report covers all our investigations on 2219 aluminum alloy. In the following, we describe details of our work in the following areas:

1. Studies carried out on as-received plates of 2219 aluminum alloy;
2. Solidification - segregation studies;
3. Determination of time-temperature precipitation diagrams, i.e. C curves, and the relationships between mechanical properties and NDE responses;
4. Electron microscopy studies done on a wide range of metallurgical microstructures produced, and
5. Predictions of heat flow conditions during malfunctions of the quench from the solution heat treatment temperature and the resulting mechanical property degradations.
6. Results of a Round-Robin for hardness and conductivity measurements conducted on a set of 2219-T87* aluminum alloys.

II. STUDIES ON AS-RECEIVED PLATES

Four sets of 2219 aluminum alloy† plates were used in this investigation. They were:

1. A 12.7 cm (5 inch) thick plate in the T851 temper†† obtained from NASA (Reynolds Lot No. 7950777-DI).
2. A 0.635 cm (1/4 inch) thick plate in the T87* temper††† obtained from Martin Marietta (Reynolds Lot No. 7430252-A).
3. A 0.635 cm (1/4 inch) thick plate in the as-fabricated F temper obtained from Reynolds Metals and identified with the Lot No. 7952505-E.
4. A 3.81 cm (1 1/2 inch) thick plate in the T851 temper obtained from NASA Goddard. This plate was originally purchased from Generation Metals and was designated by the No. 313-812. The mill source of this plate is not known and it was primarily used for casting of some small samples for preliminary examination of the as-cast structure of the alloy.

While all the plates noted above were used in the different portions of this study, the primary work on the thermomechanical treatments was carried out on the 0.635 cm thick plate in the T87* temper. On the other hand, it was expected that across thickness variations in properties due to macrosegregation in the original direct chill (DC) cast ingot or normal

---

† The composition of 2219 aluminum alloy according to ASTM Spec. B211 (or QQ-A-250/30) is 5.8-6.8 wt% Cu. 0.20-0.40 wt% Mn, 0.30 wt% Fe max, 0.20 wt% Si max, 0.02 wt% Mg max, 0.10 wt% Zn max, 0.02-0.10 wt% Ti, 0.05-0.15 wt% V, 0.10-0.25 wt% Zr, others less than 0.15 wt% total.

†† The T851 heat treatment consists of solution heat treatment, a 2-1/4% stretch and aging at 177°C for 18 hr.

††† T87* is a modified T87 thermomechanical treatment used by the Reynolds McCook plant. It consists of a 5%, instead of a 7%, stretch followed by a 16 hour aging treatment at ~172°C. Hereafter, this Reynolds heat treatment which was used in this program will be denoted as T87*.

thermal resistance of the plate during quench from the solution temperature would be most pronounced in the thickest plate. Therefore, the 12.7 cm. thick plate in the T851 temper was carefully examined for chemical, microstructural and property variation across its thickness. The findings from this study are presented below. Average hardness, electrical conductivity and tensile properties of the thinner plates along with their microstructures were also determined. These findings will be discussed in the appropriate subsequent sections of this report.

The data obtained for the composition, hardness, conductivity and tensile properties of the 12.7 cm thick plate are shown in Figures 1 and 2. These data essentially establish the maximum variations in properties due to the macrosegregation remaining in the plate from the original DC cast ingot and the normal variation in cooling rate experienced during quench from the solution heat treatment temperature. The first plot in Figure 1 shows that there is approximately 0.6 wt% variation in copper content across the plate. This was determined by molecular absorption spectrometry (wet chemistry). The abrupt changes in copper content at the edges of the plate are due to the depleted region (negatively segregated region) next to the chill face in the original ingot. The scalping apparently removed the positive chill face segregation leaving some of the depleted region intact which ended up in the plate. The negative segregation at the plate centerline is due to the same type of segregation noted in the DC cast ingot†.

The variation of the composition of copper and other alloying elements was also determined by emission spectroscopy by the Inorganic Analytic Research Division at NBS. Table I summarizes the maximum and minimum values for each element obtained across the 12.7 cm thick plate.

---

†Macrosegregation across a DC ingot of 2219 aluminum alloy cast at the McCook plant is shown in a subsequent section.

The copper variation across the plate determined by emission spectroscopy agrees within experimental error with the wet chemistry results. The Fe, Si, Zn, and, to a lesser degree, Mn profiles across the thickness have the same general shape as the Cu profile with maximum and minimum values given in the Table I. On the contrary, the Ti and V profiles have their maximum at the center. The Zr, Ni and Mg profiles are relatively flat. This behavior correlates well with the equilibrium partition coefficient, k, for these alloying additions in Al as determined from the binary diagrams. Elements in the first group have partition coefficients less than one whereas elements in the second group have coefficients greater than one.

The Rockwell hardness and conductivity, %IACS (percent International Annealed Copper Standard), measurements were made across the plate thickness. The hardness was measured according to ASTM E-18 on a Wilson bench Rockwell hardness tester. The conductivity was measured both on a portable Super Halec Eddy Current Instrument†, and on the NBS conductivity bridge described in a later section. While minor variations were noted in the absolute measured values between the two instruments, the trend shown in Figure 1 is a representative one.

---

† This instrument is manufactured by Hocking Electronic Ltd. in St. Albans, England. All references to commercial equipment in this report are for identification purposes only and in no way constitute any endorsement or evaluation of the relative merits of such equipment.

The following conclusions could be drawn from the data on Figures 1 and 2. First, the variations in hardness and tensile properties can be ascribed to the changes in cooling rate across the plate during the quench and to the fact that the center of the plate did not experience as much mechanical deformation as the outside to break-up the segregated as-cast microstructure of the ingot†. Second, variations in electrical conductivity, especially the abrupt variation near the surfaces of the plate, may also be influenced by changes in copper composition in these locations. This raises an important question regarding the effect of alloy composition on electrical conductivity.

---

† The results of Section III indicate that copper variations of the order seen in this as-received plate do not significantly affect mechanical properties obtained after heat treatment.

III. SOLIDIFICATION-SEGREGATION STUDIES

Engineering alloys, such as 2219 aluminum alloy, solidify over a range of temperatures and liquid concentrations. As a consequence, the elements (such as copper) that are combined to make up the alloy of a given nominal composition segregate during solidification. Segregation in cast ingots, such as semi-continuous Direct Chill (DC) cast ingots of 2219 aluminum alloy, can generally be divided into two categories: long range segregation (macrosegregation), and short range segregation (microsegregation). Macrosegregation occurs over distances approaching the dimensions of an ingot-from chill face to centerline in DC cast ingots. Microsegregation on the other hand, occurs on the dendritic scale-on the order of 1/100 to 1/1000 of a centimeter in the ingots in question.

Figure 3 shows the copper composition variation across the short transverse direction of a DC cast ingot from the Reynolds McCook plant. The ingot was not scalped. This figure indicated that even heavy scalping will not remove the compositional variation. It does end up in the ingot, if only at the center. Furthermore, very long homogenization heat treatments at high temperatures are not effective in eliminating the concentration gradients. Such segregation may effect the heat treatment response of the alloy and its properties including responses to non-destructive evaluation techniques used for quality control.

The second type of segregation, microsegregation, reveals itself, for example, when the cast structure is etched by chemical reagents. It manifests itself as alloy element concentration gradients across dendrite arms. The regions between dendrite arms are usually rich in solute elements, contain equilibrium and/or non-equilibrium second phases and microporosity. The important influence of this type of segregation and the spacings, (dendrite arm spacings), over which it occurs, on the properties of castings and wrought materials produced from cast ingots is now well documented. A detailed quantitative understanding of the variation in composition, of an alloy during freezing (solidification "path") and the resulting microsegregation are also prerequisities to the successful quantitative analysis of the large scale segregation (macrosegregation).

In this program we have undertaken a comprehensive experimental and theoretical study aimed at establishing:

(a) The degree of micro- and macrosegregation that can occur in as-cast ingots of 2219 aluminum alloy, and

(b) The influence that these segregations may have on both the thermo-mechanical treatment response of the alloy and its properties including non-destructive measurements used for quality assurance.

These experimental studies were carried out on both a DC cast ingot received from the Reynolds McCook plant and various smaller ingots cast in our laboratories under controlled conditions.

1. Microsegregation in Cast 2219 Aluminum Alloy

A series of calculations and experiments have been performed to determine the phases present in cast 2219 aluminum alloy with the ultimate aim of calculating the degree of micro- and macrosegregation and identifying the second phases present in the as-cast ingots. Such segregation may have significant effects on the heat treatment response of this alloy, and its properties, including non-destructive evaluation techniques used for quality control.

(a) Calculation of Microsegregation for Al-Cu-Mn-Fe-Si Alloy System

Calculation of expected microsegregation for the n component alloy was performed using the assumption of local equilibrium at the interface, complete diffusion in the liquid phase, no diffusion in the solid phase and no fluid flow in the interdendritic "mushy" region. During solidification of primary α-aluminum, the situation is governed by (n-1) differential equations (3)

$$\frac{df_L}{dC_{Li}} = -\frac{1}{1-k_i^\alpha}\frac{f_L}{C_{Li}} \qquad i = 1, \ldots n-1 \qquad (1)$$

where f_L is the weight fraction liquid, C_{Li} is the liquid concentration of the i th alloying element, and k_i^α is the i th equilibrium partition coefficient for the solidification of the α-aluminum phase. In general, k_i^α is a function of C_{L1}, C_{L2}, ... $C_{L(n-1)}$, but because the tie lines of this multi-component phase diagram are not known we have assumed that k_i^α is constant and is determined from the binary diagrams of aluminum with each alloying addition.

Solution to equation (1) in this case is:

$$\frac{C_{Li}}{C_{oi}} = (1-f_s)^{k_i^\alpha - 1} \qquad (2)$$

where C_{oi} is the original composition of the i th component and f_s is the weight fraction solid $(1-f_L)$. We calculate this solidification path (C_{Li} vs f_s) to determine at what fraction solid the interdendritic liquid becomes saturated with respect to a second solid phase, i.e., when the solidification path encounters a multivariant eutectic (or peritectic). After this point, the solidification is governed by a different set of differential equations(3).

Present interest in 2219 aluminum alloy seems to require the examination of the Al-Cu-Mn-Fe-Si quinary system. Other elements are present in small quantities as grain refiners or impurities and have been neglected. This choice is reasonable since most phases present in low Mg aluminum alloys are contained in this system. Values for k_i^α are shown below.

Equilibrium Partition Coefficients for
Solidification of Primary α-Aluminum Phase

	k_i^α
Al-Cu	0.17
Al-Mn	0.95
Al-Fe	0.02
Al-Si	0.13

As an example, Table II shows the calculated solidification path (concentration of the interdendritic liquid as a function of f_s) for an alloy Al-6.3 wt% Cu-0.3 wt% Mn-0.2 wt% Fe-0.1 wt% Si (Note max levels in the nominal alloy composition on Fe and Si are .3 and .2 wt% respectively).

To examine the solidification "path" in the five component phase diagram is difficult and can only be done approximately. Fortunately, there are no compounds in this system which do not appear in the ternary subsystems (4). Many possibilities exist, depending on the initial alloy composition, for the formation of second phases in the interdendritic region. If we examine the solidification "path" (Table II) in various ternary system combinations of these different components these possibilities become apparent. In Figure 4 are shown the solidification "paths" plotted in the Al-Cu-Mn, Al-Cu-Fe and Al-Cu-Si ternary systems.

In the absence of Fe and Si the solidification "path" intersects the monovariant eutectic trough of $L \rightarrow \alpha\text{-Al}+CuAl_2$ at $f_s = 0.86$. Hence in this ternary system $CuAl_2$ is the second phase to form and the third phase to form would be $Cu_2Mn_3Al_{20}$ by way of the ternary eutectic $L \rightarrow \alpha\text{-Al}+CuAl_2+Cu_2Mn_3Al_{20}$.

In the Al-Cu-Fe ternary system, the solidification "path" would intersect the monovariant eutectic trough $L \rightarrow \alpha\text{-Al}+Cu_2FeAl_7$ at $f_s = 0.78$. Hence, in this case Cu_2FeAl_7 is the second phase to form and the third phase to form would be $CuAl_2$ by way of the ternary eutectic $L \rightarrow \alpha\text{-Al}+Cu_2FeAl_7+CuAl_2$.

In the Al-Cu-Si ternary, the solidification "path" would intersect the monovariant eutectic trough $L \rightarrow \alpha\text{-Al}+CuAl_2$ at $f_s = 0.86$. Hence $CuAl_2$ would be the second phase to form and the third phase to form would be Si by way of the ternary eutectic $L \rightarrow \alpha\text{-Al}+CuAl_2+Si$.

From these three systems, we note that the eutectic $L \rightarrow \alpha\text{-Al}+Cu_2FeAl_7$ is encountered at the lowest volume fraction solidified, and hence it seems reasonable that Cu_2FeAl_7 is the second phase to form in the quinary alloy. Additional evidence for this is found in Figure 5 which shows a projection of the quaternary tetrahedron Al-Cu-Fe-Si into the Al-rich corner (4). The

coordinates of this diagram are relative percentages of Fe, Si, and Cu. In this figure α-aluminum is always present and hence regions represent the solidification of two solid phases and lines represent the solidification of three solid phases (ternary eutectic) etc. Examination of the compositions reached in the interdendritic liquid show that Cu_2FeAl_7 is the second phase to form. During the subsequent freezing of α-aluminum and Cu_2FeAl_7 the liquid composition most likely moves toward the line representing the ternary eutectic $L \rightarrow \alpha\text{-}Al + Cu_2FeAl_7 + CuAl_2$. Examination of this quaternary diagram is important because it excludes the possibility of either $(Mn,Fe)_2Si_2Al_9$ or $(Mn,Fe)_3Si_2Al_{12}$ being the second phase to form. Such a conclusion might have been reached by examining the Al-Fe-Si or the Al-Mn-Si ternary systems alone. In this analysis, we have for the most part neglected Mn due to its relatively high equilibrium partition coefficient.

(b) Second Phase Particles Formed During Solidification of 2219 Aluminum Alloy

The major second phase particles formed during solidification were identified using differential etching, microprobe analysis techniques and electron diffraction. Samples from a semi-continuous DC cast ingot and from two laboratory ingots were examined. The DC cast ingot was obtained from the Reynolds McCook plant through their Research Laboratory in Richmond, VA. The section was marked 2219-13402-9B. The laboratory ingots were cast from two lots of 2219 aluminum alloy plate: 3.81 cm (1-1/2 inches) thick from NASA Goddard and 12.7 cm (5 inches) thick from NASA Marshall†.

---

† Average composition of the NASA Marshall 12.7 cm thick plate of 2219 aluminum alloy (Reynolds Lot No. 7950777-DI) determined by emission spectroscopy is 6.3 wt% Cu, 0.36 wt% Mn, 0.23 wt% Fe, 0.07 wt% Si, 0.12 wt% Zr, 0.07 wt% V, 0.03 wt% Ti, 0.03 wt% Ni, 0.01 wt% Mg, and 0.03 wt% Zn.

A sample of 2219 aluminum alloy from NASA Goddard was melted and solidified in a graphite crucible with a cooling rate of approximately 0.4 K/s. On cooling, the start of primary solidification occured at 644 °C and a eutectic arrest occurred at 543 °C. These temperatures can be considered accurate to within about ± 5 °C.

Typical as-cast microstructures of the alloy in optical and SEM micrographs are shown in Figures 6 and 7. For this particular alloy, only three phases appear to be present in the cast microstructure. The aluminum solid solution (α) plus two phases which occur along with the α-phase in the interdendritic regions. The rounded irregular interdendritic phase is $CuAl_2$ and the bladelike phase is Cu_2FeAl_7 which is sometimes referred to as β-AlCuFe. These findings are in line with the theoretical predictions summarized above. Phase identification was made based on the known morphology of the phases occurring in aluminum alloys (5) known etching response of the phases, electron microprobe analysis, and electron diffraction.

Table III summarizes the etching response determined on cast 2219 aluminum alloy. The etching response is somewhat different than published elsewhere (6) and may reflect the presence of Mn in 2219 aluminum alloy.

Electron microprobe analysis was performed on the phases in cast 2219 aluminum alloy by the Center for Analytical Chemistry at NBS. The analysis was performed in the energy dispersive x-ray spectrometry mode with composition values derived with the NBS theoretical matrix correction FRAMEC (7). Table IV gives examples of microprobe results. The quantitative analysis differs somewhat from exact stochiometry but the composition range of Cu_2FeAl_7 is known to vary between 12-20 wt% Fe and 29-39 wt% Cu (8).

Transmission electron microscopy, TEM, was applied to the study of the as-cast structure. The specimens for TEM were removed from a 10 to 1 reduced cross section laboratory ingot cast in this program. A description of this ingot is given in the next section. The details of specimen preparation for TEM and the methodology used in the analysis is presented in a subsequent section under electron microscopy studies.

Figures 8 to 10 show TEM micrographs and selected area diffraction patterns which provide positive identification of the rounded particles as $CuAl_2$ (Θ phase) and the bladelike particles as the Cu_2FeAl_7 phase. The dark interdendritic phase in Figure 8 is principally Θ-$CuAl_2$. An example of the Θ-$CuAl_2$ phase from another region is shown in Figure 9, together with an electron diffraction pattern which provides positive identification of this phase. The phase adjacent to Θ-$CuAl_2$ is α-Al. An example in which the Cu_2FeAl_7 phase was idenitified is shown in Figure 10; again the diffraction pattern agrees with the known tetragonal structure of this phase.

The nature of the row of small plate-like particles present along the boundary separating the two adjacent dendrites in Figure 8 was not established. However, the diffraction pattern could not be rationalized with either the structure of Cu_2FeAl_7 or Θ-$CuAl_2$.

Regions within the dendrites were also examined for the presence of precipitates. Bands of faintly visible particles can be seen in Figure 8. On close examination, these particles were found to be Θ' precipitates†. An example showing the three different {001} habit variants of Θ' is shown in Figure 11, The Θ' precipitates were found to be associated with subboundaries such as those shown in Figure 12, and probably formed there during cooling in the solid state. Many of the randomly scattered dislocations visible in

---

† See Section V for a detailed discussion of the Θ, Θ', and Θ'' phases.

Figure 12 were almost certainly introduced during specimen preparation. The θ' precipitates did not occur in association with these dislocations. Particles other than θ' were occasionally found within the dendrites. These, however, were probably second phases not associated with the primary solidification process. Large numbers of intragranular particles, comparable to those seen in processed plate materials in the solution heat treated and quenched state discussed later, were not observed within dendrite regions of the ingot specimen.

2. Macrosegregation in Cast 2219 Aluminum Alloy

A series of experiments and measurements has been performed to determine the degree of macrosegregation in semi-continuous DC cast and laboratory cast ingots of 2219 aluminum alloy. The former gave an indication of the maximum composition variations expected in the final plate product while the latter was used in the preparation of control specimens to establish the effect of composition on measured NDE responses.

(a) DC Cast Ingot

A section of as-cast 2219 aluminum alloy was obtained from the Reynolds McCook plant through their Research Laboratories in Richmond, Virginia. The section was marked 2219-13402-9B. It extended from the chill face to the centerline of the casting in the short transverse direction. Measurement of macrosegregation was performed in a direction perpendicular to the chill face as shown in the inset of Figure 3.

Chemical analysis for Cu was performed using two methods, x-ray fluorescence using standards of Al-Cu alloys and wet chemistry. The latter was performed by the Center for Analytical Chemistry at NBS by atomic absorption spectrometry. Both methods yielded similar results. The wet chemistry data is shown in Figure 3 and should be considered accurate to $\pm$ 0.04 wt%.

As seen in Figure 3, extremely high positive segregation is noted at the chill face (∿18 wt% Cu) followed by a negative segregation region that extends almost 2.5 cm (1") into the ingot. The minimum composition (∿4.7 wt% Cu) occurs at ∿0.6 cm from the chill. A relatively uniform composition region (∿6.4 wt%Cu) extends from ∿3 cm to 18 cm from the chill followed by a region of negative segregation at the ingot centerline.

This composition profile can be readily correlated to that found in the as-received heat treated plate of Figure 1. The outermost surface of the DC cast ingot was scalped prior to the plate forming operation leaving some of the negatively segregated region which ended up at the top and bottom surfaces of the plate. The negative segregation at the ingot centerline is of essentially the same magnitude as that found in the plate.

The main phases present in this ingot are the same as that reported in the previous section on cast 2219 aluminum alloy; namely, α-Al solid solution, $CuAl_2$ and Cu_2FeAl_7. Figure 13 shows an SEM view of the interdendritic eutectic phases in this ingot. The solidification "path" described previously applies; namely, primary solidification of α-Al followed by the eutectic $L \rightarrow \alpha\text{-Al}+Cu_2FeAl_7$ and finally the ternary eutectic $L \rightarrow \alpha\text{-Al}+Cu_2FeAl_7+CuAl_2$.

Figure 14 shows micrographs from the ingot taken at the chill face, 0.5 cm from the chill face and 1.7 cm from the chill face. These positions correspond to approximately 18, 4.7 and 6.1 wt% Cu as documented in Figure 3. These micrographs show cored dendritic α-Al plus differing amounts of interdendritic "eutectic". In agreement with their compositions, the material near the chill face has the highest fraction of interdendritic eutectic (or particles of $CuAl_2$ and Cu_2FeAl_7) whereas the material 0.5 cm from the chill has the least. The material 1.7 cm from the chill has an intermediate fraction of "eutectic" and is fairly typical of the rest of the ingot except near the centerline.

(b) Macrosegregation in Laboratory Cast Ingot

Following the work of Mehrabian and Flemings on macrosegregation in multicomponent systems[9] a special geometry unidirectional ingot was cast with 2219 aluminum alloy to demonstrate the mechanisms responsible for the positive and the negative macrosegregation noted in the DC cast ingot and to obtain controlled composition samples differing from the nominal. These samples have been used for thermomechanical treatments and nondestructive evaluation.

The geometry of the casting is shown in the inset of Figure 15 and employs a reduction in area of approximately 10 to 1 to cause macrosegregation. The bottom section of the casting is 11.8 cm square and 9.5 cm high while the top section of the casting is 3.7 cm square and 12 cm high. An investment mold of plaster was preheated to 540 °C and placed directly on a water cooled chill block. The mold has an open bottom so that molten metal came into direct contact with the chill. This, coupled with the preheated mold, guaranteed directional solidification of the ingot. The mold was filled with molten 2219 aluminum alloy (obtained from NASA Marshall as 12.7 cm (5") thick plate) at about 700 °C after being degassed with hexachloroethane. The casting was analyzed for average composition variation (macrosegregation) in the direction perpendicular to the chill. The variation in copper, iron and manganese content determined by atomic absorption spectrometry as a function of distance from the bottom chill in the as-cast ingot is shown in Figure 15. As expected from previous studies of macrosegregation noted above, high positive segregation (∿7.3 wt% Cu) is observed at the chill face while negative segregation (∿3.6 wt% Cu) occurs in the region of the cross section change. Iron, and to a lesser extent manganese, also show a high level at the chill face, drop to a minimum near the cross section change and rise again in the rest of the ingot. This similarity of shape of these profiles with the

copper profile is an indication that the equilibrium partition coefficients for Cu, Fe and Mn (0.17, 0.02, and 0.95 respectively) are all less than one. Because the partition coefficient for Mn is close to one, macrosegregation of Mn is less than Cu or Fe.

Chill face and cross section change segregation both result from the flow of segregated interdendritic liquid to feed solidification shrinkage. It should be noted that the laboratory ingot exhibits a lower positive chill face segregation and no adjacent negative segregation compared to the DC cast ingot. The occurrence of these phenomena near the chill face of the DC cast ingot can be readily ascribed to the formation of an extensive air gap which results in the abrupt reheating of the ingot surface during solidification and the exudation of the solute rich interdendritic liquid from the adjacent region. On the other hand, the negative segregation at the DC ingot center line and the section reduction of the laboratory ingot are due to the extensive flow of interdendritic liquid from the hotter to the cooler regions of the ingots at these locations.

The phases present in this ingot are the same as those described above for the DC cast ingot. Figure 16 shows the three phases present. Similar results are obtained in this ingot regarding the variation of the fraction of interdendritic "eutectic" as the copper content changes with distance from the bottom chill surface.

The relative levels of Cu, Fe and Mn are also important because they are the major components which determine the phases present as second phases along with α-Al in cast or heat treated 2219 aluminum alloy. For example, samples cut from different parts of this ingot and processed in the T87* condition (see next subsection) contained different amounts and types of inclusions.

A second laboratory ingot of 2219 aluminum alloy with a 10 to 1 reduction in cross section was also cast in a manner identical with the first ingot with eight thermocouples inserted through the mold at different distances from the bottom chill face. Figure 17 shows the temperature-time curves for the eight thermocouples and the distance from the chill face of each. The liquidus and solidus temperatures for this alloy are approximately 644 (±5) and 543 (±5) °C respectively and hence, from these curves the local solidification time as a function of position has been determined. This data will be used to theoretically calculate expected macrosegregation in this ingot for comparison with the experimental composition data presented in Figure 15.

3. Thermomechanical Treatment and Evaluation of Laboratory Ingot

The effect of variations in alloy composition due to macrosegregation on the heat treatment response of 2219 aluminum alloy and its properties including non-destructive measurements used for quality assurance has been evaluated using samples taken from the reduced cross section laboratory ingot.

Samples, ∿3.7 cm square and ∿1.3 cm (∿1/2") thick in the solidification direction, were cut from the ingot at different distances from the bottom chill face to obtain specimens with differing compositions. The samples, of course, contained composition gradients through their thickness, but were relatively uniform in perpendicular directions due to the unidirectional solidification. As a reference point, eddy current measurements were conducted on as-cast samples. Measurements were made with the coil on the surfaces which were perpendicular to the solidification direction. The conductivity along with the previously determined copper content is shown in Figure 18.

---

† All electrical conductivity measurements were made on the NBS conductivity bridge as described elsewhere in this report.

These data indicate the same trend as observed in the as-received 12.7 cm (5 inch) thick plate described in the previous section; i.e., increases in copper content correspond approximately to decreases in conductivity.

The samples were then thermomechanically treated as follows:

(a) homogenization heat treated for 48 hours at 535 °C,

(b) hot rolled at 440 °C to 1/4 of their initial thickness (0.32 cm, 1/8"),

(c) solution heat treated at 535 °C for 75 minutes,

(d) stretched 5% and aged at 172 °C for 16 hours†.

Hardness and electrical conductivity measurements were carried out on both surfaces of these 0.3 cm thick samples. In Figures 19 and 20 are plotted hardness and conductivity respectively as a function of the original distance of these surfaces from the bottom chill face along with the copper content. Not until the copper content drops below ∿5.5 wt% does the hardness drop significantly. On the other hand, the variation in electrical conductivity appears to follow the same general trend as that established for the as-cast structure in Figure 18. Note that the variation in copper content shown in Figures 15 to 17 is that obtained in the as-cast ingot. Some averaging of variations in composition has occurred during the rolling operation which manifests itself in the conductivity data scatter noted in Figure 20.

Tensile tests were conducted on the thermomechanically treated samples. Figure 21 shows tensile and yield strength of these samples as a function of the original distance from the bottom chill along with the Cu content. Tensile data beyond the 14 cm point is unreliable due to porosity present near the top of the casting. Again notable reduction of properties correspond to reductions in copper content below ∿5.5 wt%.

---

† This is the modified T87 treatment practiced at the Reynolds McCook plant which is referred to herein as T87* in this report. No interrupted quench experiments were performed on the cast samples.

IV. DETERMINATION OF C CURVES

A comprehensive thermomechanical treatment program was undertaken to provide samples for establishing the effect of process variables on the microstructural, mechanical, and NDE properties of 2219-T87* aluminum alloy, and to establish TTT curves (C curves) that could be used in assessing the effect of various quenching treatments on the final properties of the processed material.

The C curves are a family of C-shaped curves used to characterize the effects of quenching on the final properties of the finished material. Their use for aluminum alloys was pioneered by W. L. Fink and L. A. Willey (10). To determine these curves, specimens are first solution heat treated and then given a series of (nearly) isothermal anneals (referred to here as "pre-aging" treatments)† prior to cold working and the final low temperature aging. The final properties are then measured and the effects of the pre-aging treatment are assessed. In using the C curves, a "rule of additivity" developed by Cahn (11) is used. This rule is also used in determination of the C curves but is much less important there because the pre-aging is nearly isothermal.

The extent to which the "rule of additivity" is applicable to aluminum is not yet completely verified. However, previous experience by Staley (12) indicates that this rule can be applied with good approximation to some aluminum alloys. The differences we note in the present study between the "sequence A" and "sequence B" heat treatments of the 2219 aluminum alloy also gives some indication as to how closely this rule is followed. We use the results on these two sequences in a subsequent section to set limits on what might be obtained under "best" and "worst" quenching conditions for a 2219-T87* aluminum alloy plate.

---

† The term "pre-aging heat treatment" is being used in place of the term interrupted quench or slack-quench. Since the definition of these terms is not firmly established, we use "pre-aging sequence A" (monotonic quench) and "pre-aging sequence B" (quench with re-heat) herein.

1. Thermomechanical Treatment

The treatments were carried out using, as starting material, the 0.635 cm (1/4") thick plate of Reynolds 2219-T87* obtained from Martin Marietta. The plate width was 1.22 m (4 ft.) and the plate length was 1.83 m (6 ft.). Three samples of the plate were removed for chemical analysis 0.6 m (2 ft.) from the plate end, one from each edge and one from the middle. These samples were analyzed using emission spectroscopy by the Center for Analytical Chemistry at NBS. Results of this analysis are shown in Table V.

The plate was then cut into bars approximately 2.5 x 17 cm with the long axis parallel to the rolling direction of the original plate. A jig was constructed to hold four bars for simultaneous heat treatment. The samples were instrumented with calibrated thermocouples as illustrated in Figure 22. Each set of specimens were then given one of two heat treatment sequences which we refer to as sequence A and sequence B. These treatments, which are identical to the T87* treatment except for the interrupt from the solution heat treatment, consisted of:

(i) solution heat treat at 535°C for 75 minutes

(ii) sequence A alloys; direct transfer to salt bath
sequence B alloys; water quench followed by transfer to salt bath (salt bath temperature was varied between 250°C and 475°C; time in salt bath was varied between 2 and 3600 seconds)

(iii) water quench

(iv) mechanically stretch to 5% permanent strain

(v) age in air for 16 hours at 172°C.

The time-temperature profiles of these sequences are schematically illustrated in Figure 23. Typical examples of time-temperature curves obtained for the solutionizing and pre-aging heat treatments are shown in Figures 24 and 25. Only three of each group of four specimens were given the 5% stretch and final aging.

Of these three, two were machined into the tensile test specimens illustrated in Figure 26. The surfaces of these tensile test specimens were milled to a 63 μm finish or better.

2. Effects of % Stretch and Aging Treatment on Properties

In order to assess the effects of % stretch and aging treatments on basic mechanical properties of the 2219 plate materials, a short study was performed. The values of the variables used in the study were the following:

Percent stretch: 0, 2-1/4, 5 and 7.

Aging treatment after stretching: (a) 16 hrs. at 172°C, (b) 18 hrs. at 177°C. Prior to stretching and aging specimens taken from the 0.635 cm (1/4") thick plate were solution heat treated at 535°C for 75 minutes, then quenched in ice water. After stretching and aging, flat tensile specimens were machined in the longitudinal tensile axis direction.

The effects of % stretch and heat treatments (a) and (b) above are presented in Figures 27 and 28. Both yield strength and ultimate tensile strength increased with increasing % stretch; however, little improvement was observed between 5 and 7% for either aging treatment. The lower temperature, shorter time treatment ((a) above) seemed to respond more to the 2-1/4% stretch than did treatment (b) insofar as tensile properties were concerned.

The effects of % stretch on elongation and reduction of area were less clear. While one might expect to see a decrease in ductility as strength level increases, this was not marked in the case of elongation. If the single high value at 7% stretch for treatment (a) is discounted, a slight decrease is indicated. For reduction of area, on the other hand, the 2-1/4% stretch appears to give the highest values.

Except for the fact that unstretched hardness values differed, hardness data tended to follow the same trend as ultimate strength in that no appreciable gains were noted once 5% stretch was reached. Aging treatments were differentiated only at lower values of % stretch.

In summary, from the present study:

(1) there was no significant improvement in strength or hardness between 5 and 7% stretch. In fact, there was an indication that some loss of ultimate strength and hardness occurred at the 7% stretch for aging treatment (a).

(2) With one exception, elongation tended to decrease as % stretch increased.

(3) Reduction in area showed a maximum at 2-1/4% stretch, but considering data scatter this effect was not sharply defined.

(4) The main differences between the two aging treatments studied were seen in strength and hardness for the case of the 2-1/4% stretch.

3. Mechanical and Electrical Measurements

The hardness and conductivity of all specimens were monitored before the solution heat treatment, after the solution and pre-aging treatments, after the 5% stretch, after the final aging treatment, and after machining into tensile test specimens. Rockwell B hardness measurements were made according to ASTM E-18 on a Wilson bench model Rockwell hardness tester. Each time hardness was measured two measurements were taken on the sample surface at a random location except within 5 cm of the sample center and, for the tensile test specimens, outside the gage. The yield strength (0.2% offset) and ultimate tensile strength were determined on a calibrated Satec System Inc. Baldwin Model 60 CG Universal Testing System.

On all samples after the final aging treatment, and on all samples after machining into tensile test samples, measurements of electrical conductivity were made using the NBS conductivity bridge. This bridge has extremely high sensitivity and the signal to noise ratio is on the order of 2×10^6. Conductivity can be measured at any frequency between 5 kHz and 100 kHz. The bridge was completed recently and its accuracy and precision are still being evaluated. Changes of .01% IACS are clearly evident.

Due to the newness of the bridge, its full capabilities were not utilized in the present tests. Instead it was operated as most commercial bridges using a fixed frequency (10 kHz) for all measurements. To determine the conductivity the bridge unbalance voltage when the coil was placed on the samples was measured. The bridge output voltage is proportional to change in impedance of the coil. This voltage was then related to the unbalance voltage when the coil was placed on the standards, using a linear relationship. The bridge was calibrated using two Boeing electrical conductivity standards of 28.81 ± .28% IACS and 35.07 ± .35% IACS. These standards had their last calibration in 1976.

The tests were done with the bridge being calibrated at the start and finish of the measurements. The elapsed time between calibrations was approximately 20 minutes. During this time span, no drift of the instrumentation was evident. The temperature of the standards and test pieces was 23 ± .2°C. To determine the conductivity of the test pieces a linear relationship was assumed between conductivity and bridge unbalance. Due to the lack of recent calibration of the calibration standards the conductivities of the test pieces should be understood in a relative sense. The changes measured are accurately measured with respect to the standards and are repeatable but should be understood only as an indication of change and not in an absolute sense.

Conductivity measurements of each sample before treatment, after the solutionizing and pre-aging treatment, and after the 5% stretch were made at 23 ± 1°C using a Hocking Electronics Super Halec model portable eddy current instrument operated at 10 kHz with a digital voltmeter attached to the readout. Before each measurement, the readout was calibrated using three reference samples of 37.8, 33.2 and 32.2 % IACS which were previously measured on the NBS conductivity bridge. Although some loss of precision is unavoidable with this procedure, the values obtained should be comparable to within ± 0.3% IACS with measurements made on the NBS conductivity bridge.

Data on hardness and conductivity measurement for all the samples subjected to various heat treatments are listed in Table VI. Table VII gives the time-temperature data of the heat treated specimens which will be used later in the determination of C curves. Table VII also summarizes the hardness (average of the two measured values before machining) and conductivity after final aging, the yield strengths, ultimate tensile strengths, percent elongation, and percent reduction in area for each sample.

4. Measurements on As-Received and Reprocessed 2219-T87* Plate

Two hardness measurements were made on each of the 289 samples cut from the as received 0.635 cm (1/4") thick plate of 2219-T87*. The average hardness obtained was 78.4 HRB with a standard deviation of 1.0 HRB. One conductivity measurement was made on each of the samples. The average conductivity obtained was 33.6% IACS with a standard deviation of 0.3% IACS.

The longitudinal and transverse yield strengths (0.2% offset) and ultimate tensile strengths were measured on twelve samples cut from the same plate. The longitudinal specimens gave a yield of 56.4(5) ksi and a tensile of 69.8 ksi. The transverse specimens gave a yield of 56.4(7) ksi and a tensile of 70.9 (7) ksi. (Numbers in parentheses represent error in last digit at the one sigma level.)

About twelve samples from the as-received 2219-T87* were reprocessed to the T87* with no pre-aging treatments. These reprocessed samples gave an average hardness of 78.1 HRB with a standard deviation of 1.1 and an average conductivity of 33.6 % IACS with a standard deviation of 0.4% IACS. These reprocessed samples gave a yield strength of 55.4(8) ksi and a tensile strength of 69.4(8) ksi. These results show that the reprocessed 2219-T87* closely achieves the mechanical and electrical properties of the original plate with perhaps a small degradation (on the order of 1%) in the measured mechanical properties.

5. Measurements After Solution Heat Treatment and Pre-Aging

The hardness obtained after solution heat treatment and pre-aging is plotted as a function of conductivity in Figure 29. In this Figure, sequence A and sequence B alloys are indicated by different symbols. It is seen that, within the scatter of the data, the sequence A alloys fall on a regular sequence, whereas the sequence B alloys do not. The sequence A data were least squares fitted to the quadratic equation.

$$H = a_0 + a_1 C + a_2 C^2 \qquad (3)$$

where H is the Rockwell B hardness and C the conductivity in % IACS. The values obtained for the constants were: $a_0 = -541$, $a_1 = 3918$, and $a_2 = -0.648$. The fit gave a residual standard deviation of 3.1 hardness units. This least squares curve and a scatter band (approximately 95% confidence level) are also shown in Figure 29.

6. Measurements After Stretching

The hardness obtained after solution treatment, pre-aging, and stretching is plotted as a function of conductivity in Figure 30. In this figure, sequence A and sequence B alloys are again indicated by different symbols. As for the case before stretching, sequence A alloys fall on a regular sequence (within the scatter of the data), whereas sequence B alloys do not. When the sequence A alloys were least squares

fitted to the quadratic equation (Equation (3)), the values obtained for the constants were: $a_0 = -208$, $a_1 = 19.5$, and $a_2 = -0.353$. The fit gave a residual standard deviation of 2.3 hardness units. The sequence A least squares fit and a scatter band (approximately 95% confidence level) are also shown in Figure 30.

The dislocations introduced by the stretching result in an increase in hardness and a decrease in electrical conductivity. In Figure 31, we plot the change in hardness vs. change in conductivity. No trend or correlation is evident from this plot. Upon stretching to 5% permanent strain the hardness appears to increase, on average, about 18 HRB, and the conductivity to decrease, on average, about 0.5% IACS.

7. Measurements After Final Aging

The hardness and conductivity data of Table VI after final aging are plotted in Figure 32. In contrast to the measurements after preaging and after stretching, sequence A and sequence B alloys now appear to follow the same trend. (In making this plot, the hardness and conductivity measurements before and after machining were averaged.) The data were least squares fitted to a quadratic equation (Equation (3)). The values obtained for the constants were: $a_0 = -736$, $a_1 = 51.4$ and $a_2 = -0.811$. The fit gave a residual standard deviation of 2.4 hardness units. The least squares fit and a scatter band (approximately 95% confidence level) are also shown in Figure 32.

As described previously, when the samples were machined into tensile test specimens, approximately 0.6 mm was machined from the surface. The hardness and conductivity were measured both before and after the machining procedure. The measurements after machining vs. those before machining are plotted in Figures 33 and 34, along with a linear least squares fit and scatter band. These measurements indicate that there is no detectable difference in either the hardness or conductivity after machining the surface.

8. Calculation of C Curves

The data on hardness, conductivity, yield strength, tensile strength and time-temperature history tabulated in Table VII have been used to determine a set of C curves for both sequence A and sequence B alloys.

Following Evancho and Staley (13) and Cahn (11, 14), we have used the following parameterization to represent the C curves: It is assumed that the value of a resulting property, σ, can be represented as

$$\sigma = (\sigma_m - \sigma_o) \exp(-K_{1x}\tau_x) + \sigma_o \tag{4}$$

where σ_m is the maximum achievable property, σ_o is the minimum or "intrinsic" value of the property achieved under the given conditions, τ_x is given by

$$\tau_x = \int_{t_s}^{t_o} \frac{dt}{C_x(T(t))} \tag{5}$$

with t_s being the start of the quench from solution heat treatment temperature, t_o the time to achieve a temperature less than about 120°C, and $C_x(T)$ given by

$$C_x(T) = K_{1x}\, K_2 \exp\left(\frac{K_3 K_4^2}{RT(K_4-T)^2}\right) \exp\left(\frac{K_5}{RT}\right) \tag{6}$$

where K_2, K_3, K_4, and K_5 are constants to be determined, T is the absolute temperature, and K_{1x} is an arbitrary constant taken to be

$$K_{1x} = -\ln\left(\frac{\sigma_x - \sigma_o}{\sigma_m - \sigma_o}\right) . \tag{7}$$

K_{1x} is chosen so that for $\tau_x > 1$, σ is less than σ_x so that τ_x becomes a critical parameter for achieving some specified value σ_x of the property in question.

To determine the parameters σ_m, σ_o, K_2, K_3, K_4, K_5 the following procedure was used:

(i) the temperature from 535°C (the solutionizing temperature) to 119°C is divided into 35 intervals,

(ii) the time, t_i, spent in each of the temperature intervals is taken from a chart recorder and used to numerically calculate the integral of Equation (5) according to

$$\tau_x \approx \sum_{i=1}^{n} \frac{t_i}{C_x(T_i)} \tag{8}$$

where T_i is the average temperature in the interval, and

(iii) using an iterative, non-linear, fitting routine, values of the parameters which minimize the least squares deviation between measured and calculated values are obtained.

The computer program to do the least squares fit is listed in Appendix A. This program was adapted from a non-linear least squares routine described in detail elsewhere (15). The data input portion of the program as listed is designed to read data in format shown in Table VII. A card with the word END on it is required at the end of the list of temperature intervals and at the end of all input data. Initial guesses are supplied by the user for the parameters σ_m, K_2, K_3, K_4, K_5, and σ_o, along with other interactive input to search for a set of values which minimizes the least squares deviation. Briefly, the operator tells the program what combination of parameters to vary and what step size to use in calculating derivatives. The program calculates the necessary partial derivatives numerically, then sets up and solves a matrix equation and determines new values for the parameters. If these new parameters actually reduce the least square deviation, they are accepted. This procedure is continued until no further reduction in the least square error can be obtained. If a successful fit is not obtained, initial parameters and step sizes are changed and another attempt made.

The set of parameters obtained for the C curves for sequence A and sequence B alloys are given in Table VIII. These C curves are represented in Figures 35 through 42.

An interesting question related to these C curves is: to what precision are the parameters determined? For purposes of comparing the fits we define a quantity, e.s.d., called here the "estimated standard deviation", by

$$\text{e.s.d.} = \sqrt{\frac{\sum(\sigma_i - \sigma_{ci})^2}{N - 6}} \qquad (9)$$

where σ_i is the measured value of the property in question for the ith sample, σ_{ci} is the calculated value, and N is the total number of samples. First, consider the value of K_5. In Table IX, we show the effect of various choices on the other parameters and on the estimated standard deviation for the hardness. There is practically no effect on e.s.d. for values of K_5 between 30,000 and 40,000. The variation of the C curves obtained for three choices of K_5 is shown in Figure 43. These curves vary in minor details. We have chosen the value of 32,000 cal/mol for K_5 because it is close to the known activation energy for diffusion of copper in aluminum, and because it can be used to give a consistent fit to all the sequence A properties using constant values for K_3 and K_4 (as shown in Table VIII). When the value of K_5 is chosen at 32,000 and the other parameters are fitted, the effect of varying one parameter only on the e.s.d. can be determined. This is plotted in Figure 44 for e.s.d. from the sequence A data.

The set of values given in Table VIII for the C curve parameters can be used to obtain relationships between the mechanical and electrical properties. Since the C curves, for a given sequence, vary only on their value of K_2, these relationships can be computed parametrically using a parameter Q such that each property σ is given by

$$\sigma = (\sigma_m - \sigma_o) \exp\left(\frac{-Q}{K_2}\right) + \sigma_o \qquad (10)$$

where K_2, σ_m, and σ_o are the appropriate values for the property being calculated. A series of such plots which display the correlations for both sequence A and sequence B alloys are shown in Figure 45 through 50. These plots also show the appropriate data and scatter bands (approximately 95% confidence level). The scatter bands were obtained from a least squares quadratic fit to all the data and represent ±2 residual standard deviations from this fit. As an example, the residuals (difference between the data and the fit) for the plot of yield strength vs. hardness are displayed in Figure 51. Figure 52 shows a normal probability plot of the hardness residuals plotted in Figure 51. This type of plot provides a graphical test of how well the residuals follow a Gaussian statistical distribution - a straight line indicates a so called normal (or Gaussian) distribution. The nearly straight line obtained and the absence of gaps in the plot indicate that the data are consistent with a normal distribution. The same test was applied to all the fits in Figures 45 to 50 with similar results.

9. Discussion

The C curves calculated above give a self-consistent description of the measured variations in mechanical and electrical properties of 2219-T87* that were produced by the quench procedures used here. Not only do the curves predict, within the scatter of the data, the properties as a function of heat treatment, but they can also be used to calculate the relationship between properties. For example, Figure 48 compares the measured data with the C-curve predicted relationship between ultimate tensile strength and electrical conductivity. Although the correlations for both sequence A and sequence B alloys fall within the scatter band, the two correlations are noticeably different. However,

note that the difference between sequence A and sequence B is less significant at the higher tensile strengths. This trend is also true for the other correlations as well.

If the time-temperature curve during the quench from the solutionizing temperature is known, the C curves can be used to predict the final properties of the alloy if the "rule of additivity" is assumed. The extent to which additivity applies to 2219 has not been fully tested. Previous experience (12) with other aluminum alloys has indicated that it can be applied with good approximation. The most important factor is the rate of temperature decrease while the temperature is in the vicinity of the "nose" of the C curve. In this respect, 2219 aluminum alloy is less quench sensitive than, for example, 7050. For 7050, the nose of the C curve lies at a lower temperature (see Figure 53) where the time to reach this temperature would be longer for a given heat transfer coefficient when compared with the temperature at the nose of the C curve for the 2219 aluminum alloy. Also, for a sequence B type quench, the temperature would be more likely to reach the nose of the C curve for 7050 than for 2219.

The difference between the C curves for sequence A and sequence B is small but significant. For example, using Figures 35 and 36 we can see that a sample which spent 20 seconds at 420 °C during the quench would have a yield strength of 51 ksi for sequence A, which would meet the minimum specification for a 7.6 cm (3 inch) plate, but only 49 ksi for sequence B. In the absence of further data, the best method for applying the C curves would be to use the sequence A curves if the time-temperature curve monotonically decreases from the solutionizing temperature and the sequence B curve otherwise. The C curves presented in Figures 36 through 42 are probably somewhat biased towards shorter

critical times at temperatures above 475 °C and below 250 °C. This is not considered a problem in applying these curves since the quench time spent at these temperatures is usually much shorter than the critical times for most heat flow conditions.

If we use the correlations presented in Figures 45 through 50 between yield strength and ultimate tensile strengths which are specified by Federal Specification QQ-A-250/30) and the hardness and conductivity we can construct a table for 2219-T87* giving the minimum hardnesses and maximum conductivities corresponding to the specified minimum strengths as follows:

	Tensile Strength			Yield Strength		
Thickness - inches	Specified minimum ksi	HRB min.	% IACS max	Specified minimum ksi	HRB min.	% IACS max.
0.020 - 0.249	64	72.6	34.3	52	74.0	34.2
0.250 - 3.000	64	72.6	34.3	51	72.6	34.4
3.001 - 4.000	62	70.2	34.8	50	71.2	34.7
4.001 - 5.000	61	69.0	35.1	49	69.7	35.0

However, care must be utilized in using such a table. The above refers to Rockwell B hardness measurements made on a bench unit for full conformance to ASTM E-18. Even under such controlled conditions there is considerable scatter in the hardness measurements, generally greater than ± 1 Rockwell B hardness unit at the one sigma level. This scatter is due in part to the measurement itself and in part to inhomogeneity in the material over a size range greater than the hardness indentation diameter.

When making measurements with portable units, which generally make smaller indentations and, because of size limitations, cannot control test conditions with the precision of a bench unit, hence, greater scatter in the hardness can be expected. Ideally, enough hardness measurements would be made in a localized area to determine both the mean and the variance in that area. Practically speaking, it it generally required to make several, at least three, measurements in a localized area and to use the mean of these measurements.

Converting the readings of a portable hardness tester to Rockwell B units poses a separate problem. It cannot be considered satisfactory to calibrate the portable tester with brass standards when using the tester on aluminum. Since aluminum standards are not generally available, calibration of a portable unit must proceed by measuring a range of aluminum alloy samples on a bench tester according to ASTM E-18, then using these samples to calibrate the scale of the portable unit, with a large number of measurements (at least five) being made on each sample.

Although the conductivity measurement averages over a larger sample area than the Rockwell B hardness measurements, considerable scatter in the measurement remains. Again, this scatter is due in part to the measurement itself and in part to inhomogeneity in the material over a size range greater than the probe diameter. Thus, for critical applications, it is also desirable to make several eddy current measurements in a localized area and to use the mean of these measurements. Calibration of conductivity measuring instruments is a critical factor. Generally, the differences in conductivity can be measured with much greater precision than absolute values. Figure 54 presents an example of this problem, where the yield strength vs. conductivity curves determined by four laboratories on different lots of material are compared.

Since the hardness and conductivity of plates are generally measured on the surface, the degradation in properties from surface to center under normal conditions of heat extraction due to only resistance in heat flow in the plate itself must be taken into account. For example, for a 12.7 cm (5 in.) thick plate using sequence A cooling, the yield strength in the center of the material is as much as about 3 ksi less than the yield strength at the surface. (This assumes a plate of uniform composition.) Accordingly, to meet the specification of a minimum yield strength of 49 ksi for a 12.7 cm plate, the hardness and conductivity measured on the surface must correspond to those for a yield strength of 52 ksi. For sequence B cooling, the surface to center degradation can be more severe, up to about 6 ksi difference between the surface and the center of a 5 inch plate. These effects are considered in more detail in the next section.

Because of the poor inter-laboratory correlation between yield strength and conductivity measurements seen in Figure 54 some further remarks on the sources of error in conductivity measurements and on its usefulness as an NDE tool for sorting out bad material are required.

Electrical conductivity measurements were made on the various types of metal samples that are discribed elsewhere in the report. The greatest number of measurements were made on samples which were approximately 5 to 6 mm thick, 25 mm wide, and 150 mm long. In order to insure the highest accuracy of measurement all possible physical effects which might cause error had to be evaluated. These effects could in general be classified as coil-metal field interactions and temperature effects.

The coil-metal interactions can be further subdivided into lift-off effects, edge effects and field penetration through the metal. The errors due to field penetration through the metal are considered to be negligible due to the thickness of the samples and the frequency

used (10 to 20 kHz). To insure that no penetration error was present, a test was run using a second coil as the detector. This coil was placed on the metal so that it was concentric with the driving coil but with the metal sample between the two coils. The bridge was then run at its normal power level and the detecting coil was connected to the detector of the system. No appreciable field could be detected even at the highest levels of detector sensitivity.

Errors due to lift-off effects (changes in distance between the coil surface and the metal surface) were made negligible by adjustment of the phase of the bridge detector. The lift off compensation is accurate as long as the separation distance between the two surfaces is less than 0.14 mm. A test sample holder was constructed which held the metal surface against the coil surface with a constant pressure for all samples. This also insured that any distortion of coil geometry due to the pressure would be the same for all samples.

Some test samples were measured immediately after the 5% stretch and before the surface was machined. The surface of these samples was slightly mottled by the mechanical stretch. This could introduce some error due to lift off or lift off related effects. Several coils of different diameter, i.e., 12.7 mm and 6.35 mm were used to measure these samples. No change in value could be seen at the 0.01% IACS level using the two coils. Thus it has been assumed that in this case the surface had no effect on the measurement.

Errors due to edge effects are still in the process of being evaluated. The sample width was 25.4 mm and measurements were made along the center-line of the sample. Initially tests were run moving the coil away from

the centerline until a change of 0.01% IACS was noted. These tests were done using both coils. The data from these tests showed that the coil need not be perfectly centered to achieve good measurements. It was only at the end of the tests and after several discussions with others in the field that it was realized that edge effect errors could still exist and not be detected due to the symmetry of the test samples. Further tests are now being done to characterize the error that might be present in the measurement. It is thought that this error should be less than 0.1% IACS.

Errors in the measurement due to temperature variation were minimized by keeping the test samples and the standards in a partially enclosed area. Thus variations in ambient temperature were decreased at the test site. The samples and the standards were kept in contact except during the time an individual sample was being measured. Ambient temperature was monitored at a distance of 25 mm from the side of the coil. The sample holder eliminated any temperature variation that might be due to human contact with the coil and being near the test samples. At random intervals a test sample was monitored for several minutes to determine if any temperature drift was occuring during the measurement.

Errors due to drift of the instrumentation over the period of time that it took to do a series of measurements are considered negligible. To test this assumption standard inductors were placed in the bridge circuit replacing the coil. These standards were well insulated thermally so that their electrical properties would not be effected by changes in ambient temperature. The bridge was then balanced and the detector was left at its highest sensitivity for time intervals up to two hours. During this time there was no apparent drift in the balance point.

Thus instrumentation drift was also considered negligible during the time of sample testing.

A final error that was present in the experiment was the assumption that the coil imbalance due to changes in metal conductivity were linear. Some error was introduced into measurement values by this assumption, but is thought to be less than 0.1% IACS at the midpoint of the two standards, i.e., 31.9% IACS and less at conductivities which approach the value of the standards being used. Further measurements with newly constructed coils and with the variable frequency capabilities of the bridge are being completed to determine the exact error that is present due to this assumption.

Due to the lack of recent calibration of the calibration standards the conductivities of the test pieces should be understood in a relative sense. The changes measured are accurately measured with respect to the standards and are repeatable but should be understood only as an indication of change and not in an absolute sense. However, on an absolute scale, the measurements are expected to be good within a few tenths of one IACS percent.

The use of conductivity as an indirect hardness measurement in aluminum alloys has been a well-established and useful technique for a considerable time (16,17). It is well known, however, that hardness is a multiple valued function of conductivity. The results established here confirm this for 2219. Indeed there is a different branch of the curve for each stage in the processing of the material. Therefore, supplemental hardness measurements are generally required. This, along with the problems of precision and accuracy discussed above, complicates the use of conductivity. Careful consideration must be given to part geometry, heat treatment history, and condition of the sample microstructure.

At present, eddy current conductivity measurements should always be considered in a relative, rather than an absolute sense. A conservative interpretation of Figure 54 would require that the conductivity of 2219-T87* should vary no more than 1% IACS from that of a piece of known good material from the same lot, with a definite degradation of material properties evident for a variation of greater than 2% IACS.

V.. ELECTRON MICROSCOPY STUDIES

Electron microscopy studies were carried out to determine the direct relationships between thermomechanical processing and microstructure. An additional advantage of this approach lies in the fact that physical properties including hardness, yield strength and possibly NDE responses can then be correlated to microstructure.

Direct determination of microstructural changes is especially important in a complex material such as 2219 aluminum alloy where a variety of process dependent, interrelated and often competing phase transformations may occur. Indirect measurement methods such as hardness or electrical conductivity are in general not capable of distinguishing between the various often simultaneous changes in several phase components. Thus, when solely based on such measurement, the capability of predicting the influence of changing processing conditions on physical behavior is at best limited.

Aluminum alloy 2219 as indicated earlier has a nominal concentration of ~6.3 wt%Cu with other minor constituents (see Table I). The precipitation characteristics of this alloy are dominated by the presence of Cu and are similar to those exhibited by the binary Al-6.3wt%Cu alloy. The aluminum rich end of the Al-Cu phase diagram is shown in Figure 55. At equilibrium the solid consists of a two phase mixture of α-aluminum and the intermetallic compound, Θ-Al_2Cu. This equilibrium, however, is not achieved at low temperatures or with rapid cooling rates. Instead, copper rich G.P. zones, and the metastable Θ'' and Θ' phases that are indicated in Figure 55 may form. The outstanding mechanical properties of Al-Cu alloys are based on the precipitation of a fine dispersion of G.P. zones and the metastable phases. The final microstructural state will depend on the thermomechanical processing history. Although

the behavior of the 2219 aluminum alloy is in its essentials similar to the comparable Al-Cu binary alloy, the presence of the minor elemental constituents has important consequences.

The influence on aging response of the various minor constituents is complex. When in solution, the presence of Fe in Al-Cu binary alloys is deleterious, both with respect to reducing the peak hardness achieved on artificial aging and in reducing the aging rate (18). The elements Mn and Si, on the other hand, have the opposite effect although in an alloy containing 4.5wt%Cu, Mn was found to be deleterious (18). Age-hardening at room temperature was not observed in an alloy containing 4wt%Cu and 0.5wt%Mn (19) while the comparable binary alloy without Mn exhibits significant age-hardening. The element Zr has been shown to have an effect on aging behavior which in many respects is similar to Mn (18). The response to a given element addition can also be strongly influenced by the aging treatment. Although an Al-4wt%Cu alloy with a 0.5wt%Mn does not exhibit two stage aging at 160°C, pre-aging at 120°C does lead to this response (20). When the concentration of additional elements exceeds the solubility limit, a negative effect on age hardening is often observed (18). This is associated with the formation of copper containing compounds that themselves do not contribute to hardening but reduce the relative concentration of available Cu in the matrix. In general, a decrease in available Cu is accompanied by a significant reduction in age-hardening. Several insoluble Cu bearing compounds are found in 2219 aluminum alloy. However, these have little effect during normal processing since excess copper is available at the solution treatment temperature. Finally, it should be pointed out that the elements Zn, V, Mn and Ti play an important role in achieving grain

refinement during casting and in controlling recrystallization and grain growth during thermomechanical treatment (21).

This portion of the investigation was concerned mainly with evaluating the effect of an abnormal quench from the solution treatment temperature on the properties of a material given an otherwise normal T87* treatment. The majority of the specimens subjected to electron microscopy examination were taken after the quench step or after final aging. Some additional specimens given a T851 treatment were examined. The T851 treatment differs from T87* in that a stretch of 2-1/4% rather than 5% is employed and final aging is carried out at 177°C for 18 hours instead of 172°C for 16 hours. Specimens obtained from the 10 to 1 reduced cross-section ingot in the as-cast state were also studied as described in a previous section. The purpose here was to confirm, by means of electron diffraction, the identification of interdendritic phases that had been examined optically and in the SEM. It was also of interest to determine what, if any, precipitates might exist within the primary dendrites to answer the question concerning the origin of the numerous insoluble precipitates found distributed throughout the material after processing. In studying aged specimens, special consideration was given to correlating microstructural observations with the C-curve behavior described in the previous section.

1. Experimental Procedure

With the exception of the as-cast ingot all specimens were prepared from rolled plate stock. Specifications describing the condition of the starting materials and details of the methods employed in the various laboratory processing steps are given elsewhere in this report. Identification of the specimens is by number. In discussing a particular specimen, the number will be stated together with a brief description which will serve to identify that aspect of the processing sequence which was unique to

the specimen. For convenience, a complete list of specimens that were examined in the TEM and those examined in the SEM that are discussed in this section is given in Table X. The processing treatment for each specimen is indicated. Additional information on these specimens is given in Table VI.

To prepare a specimen for TEM examination, a thin section was cut along a plane normal to the original rolling direction of the plate. In the case of the as-cast ingot, the section was parallel to the solidification direction. Except for a few samples prepared early in the investigation in which spark machining was used, all sections were cut using a low speed diamond saw. The thickness of these sections was approximately 0.2 mm. Disks 3 mm in diameter were punched from the sections and jet electropolished in a solution consisting of 30% HNO_3 and 70% methyl alcohol by volume. The electropolishing solution was cooled to about -60°C. In a few instances, to minimize the introduction of mechanical damage in the very soft specimens that had been solution heat treated but not stretched or aged, 1 mm thick sections were cut and electrochemically thinned using the so called window method (22).

TEM studies were conducted with three instruments, a JEOL 200 A operated at 200 kV, a JEOL 100B and a JEOL 100CX. In the latter two instruments observations were carried out at 100 kV. The JEOL 100CX, is designed to function in either the conventional transmission mode or the scanning transmission (STEM) mode which employs a highly focused electron probe a few nm in diameter. The JEOL 100CX was also equipped with an energy dispersive x-ray analysis system supplied by the Kevex Corporation. When applied to a suitably thin foil, it is possible with this system utilizing the STEM mode of operation to obtain an elemental analysis of a column of material through the thickness of the foil as small as 10 nm

in diameter. Analysis is applicable to elements having atomic numbers higher than Ne. The results reported in this investigation were corrected for background level and the relative elemental concentrations were calculated by means of a program termed "Foil" that was supplied by the manufacturer (Kevex). Despite these correction procedures, the results are subject to considerable uncertainty. Accurate determination of elemental composition can be complicated by a number of factors, especially when the region of interest may be a small particle within a matrix having a different composition. If a layer of matrix material overlays the particle, then the contribution of the matrix must be taken into account. Preparation of the foil specimen may alter the near surface composition or leave a deposit differing in composition from the particle of interest. If the specimen is not sufficiently thin, effects due to beam spreading, absorption and fluorescence may be introduced. It is only with the accumulation of a number of measurements together with other information such as electron diffraction data that confidence can be gained in a quantitative analysis. Despite the complications that exist in analyzing small particles, even a qualitative analysis can provide information not available by other means.

Some specimens subject to TEM study were also examined by means of scanning electron microscopy. The SEM samples were mechanically polished then electropolished and lightly etched in Keller's solution. Large θ and θ' precipitates produced during altered quench treatments were readily observed by this method. Large particles remaining at the end of the solution heat treatment were, of course, also visible. This method has a considerable advantage in that large areas can be examined at relatively low magnifications, and a representative picture of precipitate concentration and distribution can be obtained. To achieve the same

result by means of TEM study would require the preparation and examination of a large number of specimens. TEM and STEM are, in general, necessary for the identification of precipitates, especially when they are less than a micrometer in diameter. Precipitates responsible for age hardening are not readily amenable to SEM study.

2. Results

The observations reported below were made on specimens derived from rolled plate stock. The results are divided into subsections under the following headings: Solution Heat Treated and Quenched Structure, Stretched and Aged Structure, and Microstructure After Quench Treatment.

(a) Solution Heat Treated and Quenched Structure - In order to study the as-solutionized structure, specimens taken from 3.81 cm thick plate in T851 condition (specimen #879-55) and from 0.635 cm thick plate in the T87* condition were solution treated at 535°C for 75 minutes and quenched in ice water. The microstructure of these two materials did not appear to differ with the exception of the extensive recrystallization and grain growth that occurred in the T87* material and not in T851. The latter effect is shown in Figures 56 and 57. Figure 56 shows the as-received grain structure of 2219 aluminum alloy plates in the T87* and T851 conditions. There is no discernable difference between the two structures. Figure 57(a) and 57(b) show the grain structures after solution heat treatment and quench of the two plates. The anomalous grain growth in the T87* plate is ascribed to the higher prior cold work (5%) in this plate versus 2 1/4% in the T851 plate. This observation was verified by solution heat treatment of a 2219-F (as-fabricated) plate obtained from the Reynolds McCook plant, Figure 57(c).

A TEM micrograph of the resolutionized T851 (specimen #879-26) is shown in Figure 58. Numerous particles are present ranging in size from

a few tens of nm to nearly a μm in diameter. There was considerable variability both in the size and distribution of these particles. In some regions, observed at the same magnification as Figure 58, no particles were visible while at other locations numerous larger particles were found. Some of the large particles are visible in SEM and optical micrographs contained elsewhere in this report.

The TEM sample shown in Figure 58 was prepared specifically to avoid mechanical damage and the attendant introduction of dislocations. The dislocations visible in Figure 58, and in Figure 59 from the same sample, are arranged in subboundaries and arrays. This is typical of materials that have been deformed and subsequently annealed.

A number of particles were analyzed both by electron diffraction and by energy dispersive x-ray analysis utilizing the STEM instrument. A STEM micrograph of resolutionized T87* material (specimen #197) is shown in Figure 60. X-ray spectra and electron diffraction patterns were obtained from the labeled particles in Figure 60. The precipitate labeled Q is shown at a higher magnification in Figure 61, together with its associated x-ray spectrum and electron diffraction pattern. According to the diffraction pattern, the crystal structure is appropriate to the Cu_2FeAl_7 phase, which has been identified previously in the interdendritic regions of as-cast ingot specimens. The concentrations of Al, Cu and Fe determined from the x-ray spectrum are in approximate agreement with the composition of the Cu_2FeAl_7 phase. Note, however, that there is a small Mn peak indicating that this element has partitioned to the particle. X-ray analysis of particles L and E in Figure 60 also indicated that they were probably the Cu_2FeAl_7 phase.

The precipitate at R in Figure 60 was not conclusively identified. This precipitate is shown at a higher magnification in Figure 62 with its

x-ray spectrum. The relative concentrations of Al, Cu and Mn suggest that R may be the phase $Cu_2Mn_3Al_{20}$. The small V peak in the spectrum also indicates that significant partitioning of that element to the particle has occurred. The x-ray spectrum from the α-aluminum matrix is shown in Figure 62 for reference. Only Al and Cu are indicated to be present. Because of their low concentrations, the elements Fe, Mn and V found in the above particles were not detected in the matrix. Other elements, Ti, Zr and Si which according to chemical analysis are present in the material were not detected in the matrix.

The above brief study of a few precipitates occuring in resolutionized and quenched specimens was by no means exhaustive. It is quite likely that further study would reveal the existence of other phases consistent with the composition and solution heat treatment temperature of the 2219 aluminum alloy. In particular, none of the small particles examined in Figure 60 were found to be Θ-$CuAl_2$.

Even though the above samples had been held at room temperature (~20°C), for as long as several days in some cases, there was no evidence of the formation of G.P. zones.

(b) Stretched and Aged Structure - Deformation by stretching the as-quenched material in tension leads to a high density of relatively uniformly distributed dislocations. Figure 63 shows the dislocation structure in a resolutionized and quenched T851 specimen after stretching in tension by 2-1/4% (specimen #1). The accompanying diffraction pattern in Figure 63 (after tilting to a [100] zone orientation) is characteristic of the α-aluminum matrix structure. Reflections that might be associated with the formation of G.P. zones, Θ" or Θ' precipitates are not observed. Aging the above structure for 18 hours at 177°C to complete

the T851 processing sequence produced the structure shown in Figure 64(a) (specimen #1A). The diffraction pattern included in Figure 63(a) was taken along a [100] α-aluminum zone axis. The square array of large spots are from the α-aluminum matrix. The pattern of small spots identifies the closely spaced fine precipitates as θ'. The microstructure in the as-received T851 plate specimen is shown in Figure 64(b) and is essentially identical to that of the reprocessed material. For comparison, the T87* "structure" is shown in Figure 65 (specimen #142). Qualitatively, the microstructures of the T851 and T87* processed specimens are similar, despite the somewhat enhanced strength properties of T87*.

Although the diffraction patterns in Figures 64 and 65 indicate that the principal precipitate phase present is θ', a close examination of both the T87* and T851 materials reveals a concentration of much finer precipitates having a similar morphology and orientation to θ'. These fine precipitates are visible among the larger θ' precipitates in Figure 66(a) taken at a higher magnification than Figures 64 and 65. Their small size, shape and orientation tentatively identifies them as θ". The diffraction pattern corresponding to Figure 66(a) is shown in 66(b). Each of the spots can be identified as originating from the α-aluminum matrix or one of the three θ' variants. Any contribution the θ" precipitates might make is overwhelmed by matrix and θ' reflections. However, by carrying out the appropriate dark field experiment, it is possible to demonstrate that the small precipitates in Figure 66(a) are in fact θ". A schematic drawing of the diffraction pattern of Figure 66(b) is shown in Figure 67 eliminating all spots except for those eminating from the matrix and one variant each of θ' and θ". Reflections produced by double diffraction are also excluded. Because of the close proximity of θ' to θ" reflections in this and other orientations, θ" cannot be displayed

separately under dark field imaging. However, by comparing a dark field image obtained from the overlapping $(003)_{\theta''}$ and $(002)_{\theta'}$ reflections with a dark field image obtained from the $(101)_{\theta'}$ reflection which contains only θ', the presence of θ" can be deduced. This is illustrated in Figure 68. Figure 68(a) was imaged with a $(101)_{\theta''}$ reflection and only θ' precipitates lying on horizontally oriented (020) matrix planes are visible. Figure 68(b) was imaged with overlapping $(003)_{\theta''}$ and $(002)_{\theta'}$ reflections, and here both the small θ" and larger θ' precipitates are seen. Weak images from the θ' habit variant lying on (200) matrix planes are also visible since the imaging conditions did not entirely exclude the contribution of nearby reflections from that variant. The dark field imaging conditions for Figures 68(a) and (b) are indicated in Figure 67. The specimen from which the micrographs in Figures 66 and 68 were obtained was subjected to a quench interrupt at 400°C for 15s on cooling from the solution heat treatment temperature at 535°C. Otherwise, the specimen (#94) was processed according to T87* practice. Similar observations of θ" precipitates were made in specimens processed according to T851, and T87* and after a number of altered (sequence A and B) quench treatments, as will be described later.

Omitting the 2-1/4% stretch normally included in the T851 process leads to the microstructure shown in Figure 69 (specimen #879-35). Bands of θ' precipitates are present within a fine dispersion of much smaller homogeneously distributed θ" precipitates, rather than a predominance of uniformly distributed θ' precipitates seen in Figure 64 after normal T851 processing. Although a similar specimen given the T87* process without stretching was not examined in the TEM, a similar result would be expected. The shorter aging time and slightly lower aging temperature of the T87* process is not expected to lead to a substantial difference in the precipitation behavior.

A higher magnification view of the microstructure in Figure 69 is shown in Figure 70. It can be seen that a region free of θ" precipitates surrounds the larger θ' precipitates. Positive identification of the θ" precipitates is afforded by the diffraction pattern included in Figure 70. Only α-aluminum matrix reflections and θ" reflections are present, θ' precipitates were not present in sufficient numbers to contribute to the diffraction pattern. The short streaks located at $\{1\ 0\ \frac{1}{2}\}$, {001} and $\{1\ 0\ \frac{3}{2}\}$ with respect to the α-aluminum lattice serve to identify the precipitates as θ"(3).

The bands of θ' precipitates in Figure 69 can be associated with the presence of dislocation arrays and subboundaries similar to those shown in Figures 58 and 59 which exist after quenching from the solution heat treatment step. The initial precipitation of θ' is known to occur heterogeneously at dislocations. After quenching from solution heat treatment, the majority of the dislocations are located in rather widely separated arrays and subboundaries as shown in Figure 58. Deformation by stretching increases the density and leads to a relatively uniform distribution of dislocations throughout the structure (Figure 63). These dislocations now act as sites for the nucleation of θ' precipitates during aging. This process, of course, accounts for the high concentration of θ' precipitates in stretched materials.

(c) Microstructure After Quench Treatment - The microstructure of selected specimens subjected to altered quench treatments (pre-aging treatments) was studied after the pre-aging quench treatment step and, in many cases, after completion of the T87* process. When the cooling rate from the solution treatment temperature is sufficiently fast a supersaturated solid solution of copper in aluminum is obtained. The only additional phases present at the end of the quench are those that exist at the solution treatment

temperature. A slow rate of cooling, a pre-aging treatment, or other thermal cycle prior to stretching and aging may result in the growth of an existing phase or the precipitation of additional and new phases. The microstructural studies described here were concerned with the detection and identification of these changes. Specimens given a "sequence A" pre-aging treatment will be considered first followed by those given a reheat cycle after initially quenching "sequence B".

SEM micrographs of specimens given quench interrupts at 400°C for 15, 30 and 60s (specimens #93, 81 and 85) are shown in Figures 71(b), (c) and (d), respectively. For reference, Figure 71(a) shows the as-quenched structure (specimen #197) in the absence of any pre-aging. A progressive increase in the concentration and size of visible precipitates is evident in advancing from (a) to (d). Precipitates are present both within grains and along grain boundaries, but the largest precipitates appear to form along grain boundaries. Grain boundaries are known to act as preferential sites for the nucleation of the Θ-$CuAl_2$ phase. When the shapes of the precipitates could be sufficiently well resolved, as in Figure 71(d) for example, it was clear that many precipitates had the form of needles. The needle-like appearance may in fact be the result of thin plates or disks viewed edge-on. Since the Θ' phase has the required lamellar shape and the pre-aging temperature is appropriate to the formation of this phase, many of the precipitates seen in Figure 71 may be Θ'. However, to be consistent with {001} habit exhibited by Θ', a pattern of alignment along three directions with an appropriate angular relationship would be expected in each grain. That this was not the case can be seen by closely examining Figure 71(d).

Observations after pre-aging treatments at 450°C were similar to those at 400°C. A specimen given a pre-aging at 450°C for 30s (specimen #69)

is shown in Figure 72. The distribution of precipitates is displayed at a relatively low magnification in Figure 72(a) and at a higher magnification in Figure 72(b). Consistent with the slightly poorer strength properties that were measured after a pre-aging at 400°C for 30s, the concentration of precipitates in Figure 71(c) appears to be greater than in Figure 72(b). In assessing precipitate concentrations with this method, it must be cautioned that grain orientations and etching rate can have a considerable effect on the observations.

A TEM micrograph of precipitates formed as a result of a pre-aging treatment at 400°C for 60s (Figure 71(d)) is shown in Figure 73. A second micrograph of the same specimen with dislocations in contrast is shown in Figure 74. Misfit dislocations at many particle interfaces and strain induced dislocations in the surrounding lattice are present. The misfit dislocations are a result of the loss of coherency between precipitate and matrix. Electron diffraction patterns obtained from various precipitates indicated that most were either the θ or θ' phase. A duplicate specimen (#86) which was taken through the remainder of the T87* process is shown in Figure 75. The large precipitates were produced during the pre-aging treatment while the small θ' precipitates dispersed throughout the structure were formed during aging. Note the precipitate free zone surrounding the large precipitates. There was little evidence of θ" precipitates in this specimen. The θ" phase was readily observed after a pre-aging treatment at 400°C for 15s as has been demonstrated in Figures 66 through 68.

Figure 76 is a dark field micrograph of a specimen given an interrupt at 450°C for 60s (specimen #105). The two precipitates visible in bright contrast were determined to be θ. A third, larger inclusion to which the two θ precipitates appear to be joined was not identified. The larger of the two θ precipitates, in addition to its junction with the unidentified

particle, is also associated with a matrix grain boundary.

Precipitates that are Θ' are indicated in Figure 77. This specimen (#6) had been given a pre-aging quench treatment at 350°C for 15s The precipitates are thin plates parallel to {001} matrix planes as is characteristic of Θ'. The presence of pre-existing particles from the solution treatment step together with the small size and low concentration complicates the identification of particles that may have formed during the pre-aging period. Note that a second much smaller particle appears in conjunction with each of the larger Θ' particles.

SEM micrographs of specimens given a sequence B quench treatment are shown in Figure 78. It may be recalled that in this treatment the specimen is quenched into ice water from the solution treatment temperature, isothermally annealed, and then quenched again into ice water. Analogous to sequence A behavior the precipitate size and visible concentration increased with longer pre-aging times. Grain boundaries were also decorated with precipitates as was observed for sequence A treatments. The Widmanstatten pattern of precipitates formed after an anneal at 400°C for 30s (specimen #232, Figure 78(c)) provides a strong clue to their likely identity as Θ'. This was confirmed by electron diffraction. A TEM micrograph of this specimen is shown in Figure 79, displaying the morphology and orientation appropriate to the Θ' phase. The identity of precipitates formed at 450°C has not been confirmed by TEM studies.

A feature that seemed to be characteristic of sequence B specimens and not of sequence A specimens was the appearance of a vein-like pattern of precipitates. This is evident in Figures 78(a) and (c), and, although not shown, was also seen in the specimen of Figure 78(b). The presence of these veins of precipitates is reminiscent of the bands of Θ precipitates observed in specimens aged without stretching, Figure 69. In that case,

it was concluded that the bands were a result of heterogeneous nucleation of θ' at subboundaries. A similar explanation may be advanced here. It was also noted that veining was much less evident in large recrystallized grains.

The hardnesses of specimens shown in Figures 71, 72 and 78 are listed in Table XI. The hardness measurements were taken after completing the T87* process and reflect the influence of the altered quench treatment. Comparing sequence A and B specimens it appears that for the same hardness a higher precipitate concentration occurs in sequence B specimens. For example, compare Figure 71(c) to Figure 78(c) both with a hardness of ∿67HRB and Figure 72(b) to Figure 78(a) having a hardness of ∿72HRB. It is also interesting to note that the hardness of specimens pre-aged at 400°C decreases with time at about the same rate in sequence A and B while at 450°C the change is more rapid in sequence B. On the basis of these observations it is apparent that the precipitation process and its effect on properties differs for the two quench treatments.

Utilizing the STEM instrument x-ray analyses were carried out on a number of the precipitates observed in sequence B specimens. Figure 80 is a TEM micrograph from specimen #249 reheated to 450°C and held 15s. Precipitates labeled A, B, and C were found to consist of Al and Cu and are probably θ or θ'. The indicated Al concentration was higher than the stoichiometric value of 45.9wt% probably because the particles were embedded in the α-Al matrix. For example, the indicated Al concentration in precipitate B was 84wt%. The x-ray spectrum of B is shown in Figure 81(a). The same spectrum is shown in Figure 81(b) on an expanded vertical scale to demonstrate the presence of a small Mn peaks at about 5.9 kev. A very small Mn peak could also be detected in spectra from precipitates B and C. In general, Mn appears to partition to the θ and/or θ' precipitates.

The spectrum of precipitate Z is shown in Figure 81(c). In this case, in addition to Cu and Al there is a small Zr peak. Close examination of Z in Figure 79 suggests that there are two rather than one precipitate present. Thus, the spectrum in Figure 81(c) may be a composite obtained from two precipitates. Other precipitates examined in this specimen were found to contain Cu and Fe in addition to Al and were probably the Cu_2FeAl_7 phase which remained after solution heat treatment.

3. Discussion

Although this investigation did not embrace a complete study of the precipitation behavior of 2219 aluminum alloy, the observations, as expected, indicate that its behavior is similar to the binary Al-6.3wt%Cu alloy. The age hardening response of Al-Cu alloys has been studied in detail by Hardy (23) and the precipitate species determining this response have been identified by Silcock, Heal and Hardy (24). Details, as they are presently understood, of the nucleation and growth mechanisms of the four species, G.P. zones, Θ'', Θ' and Θ-$CuAl_2$, that occur in Al rich Al-Cu alloys have been summarized by Lorimer (25). In an extensive investigation employing electron microscopy, Hornbogen (26) has analyzed the precipitation processes and determined the nucleation diagrams for a series of Al-Cu alloys ranging up to 6 wt%Cu. The nucleation diagrams constructed by Hornbogen provide a useful means of describing the aging behavior of Al-Cu alloys. Two of these diagrams, one for 5wt%Cu and the other for 1.95wt%Cu are reproduced in Figures 82(a) and (b) respectively. The Al-5wt%Cu alloy is essentially a close binary counterpart of the 2219 aluminum alloy which, at the solution heat treatment temperature of 535°C, contains approximately 5wt%Cu in solid solution. By employing the nucleation diagram in Figure 82(a), the aging behavior of 2219 aluminum alloy, insofar as it is similar to the binary alloy, can be described as follows.

On cooling to a temperature between 520 and 400°C and holding, the equilibrium phase Θ-$CuAl_2$ nucleates heterogeneously at grain boundaries and grows. Below 480°C not only is Θ formed at grain boundaries but the metastable phase Θ' appears. This precipitate also nucleates heterogeneously, however, the preferred sites in this case are dislocations. If the specimen is held for a sufficiently long period of time, the Θ' precipitates transform to Θ. At temperatures approaching 200°C, however, the transformation $\Theta' \rightarrow \Theta$ becomes very slow. It is clear from this diagram and the fact that Θ nucleates only at grain boundaries and existing Θ' precipitates, that Θ' will be the first precipitate to form within grains. Because Θ' itself nucleates heterogeneously at dislocations, the presence of dislocations will have a profound effect on the initial concentration and distribution of both Θ' and Θ precipitates. The temperature range of the nucleation diagram just described, 210°C to 480°C, corresponds to the region that was explored in the sequence A and B quench treatments.

At temperatues below 210°C formation of metastable Θ'' is indicated. Although not shown in Figure 82(a), it is generally believed that G.P. zones precede and are a prerequisite for the formation of Θ'' precipitates (25), that is, the sequence G.P. Zones $\rightarrow \Theta''$ is required. G.P. zones form homogeneously throughout the matrix so Θ'' will also appear to be distributed homogeneously. Although some controversy may exist (25,27) it is generally believed that the reaction $\Theta'' \rightarrow \Theta'$ does not occur. Therefore, the curve $\underline{V}$ in Figure 82(a) is not valid. The continued formation of Θ' which initially nucleates at dislocations is thought to be autocatalytic. Since Θ' is the more stable phase, it grows at the expense of nearby Θ'' precipitates which dissolve to support this growth.

The effect on microstructure of the preaging stretch in the T851 and T87* processes can now be explained. Without the stretch, it was demonstrated that the majority of the dislocations present in as-quenched specimens were at subboundaries. Thus, on aging the predominant precipitate phase was θ", with θ' in bands at subboundaries. Although the experiment was not carried out, it is expected that continued aging would have caused the width of the θ' bands to increase expanding into regions occupied by θ". Stretched specimens contain a high dislocation density and a correspondingly high concentration of sites for the nucleation of θ', consequently the major precipitate phase is θ'. Local regions that happen to be free of dislocations are occupied by θ". This accounts for the clusters of θ" precipitates that were observed in some stretched and aged specimens.

An attempt will now be made to rationalize the microstructure of 2219 aluminum alloy specimens exposed to sequence A and B quench treatments with the binary nucleation diagrams. A summary of the precipitate species observed in sequence A and B specimens before stretching and aging is as follows: (1) Both quench treatments resulted in a significant increase in the amount of θ at grain boundaries, (2) At 450°C, with increasing time, sequence A specimens exhibited initially θ and then θ' precipitates within grains, (3) A similar observation was made at 400°C except θ' was observed earlier in the process and may have preceded the appearance of θ within grains, (4) All specimens given a sequence B treatment at 400°C and 450°C exhibited a predominance of θ' often arranged in a vein-like pattern.

The formation of θ at grain boundaries is in good agreement with binary behavior. On the other hand, the early appearance in sequence A specimens at 450°C of significant amounts of θ in the interior of grains in the absence of θ' is not predicted by the binary nucleation diagram.

However, on examination of specimens quenched into ice water from solution heat treatment, it was established that 2219 aluminum alloy contains a significant concentration of insoluble precipitates. Boundaries at these precipitates as well as α-Al matrix grain boundaries can act as sites for the nucleation of θ. Indeed, θ phase was sometimes noted at such precipitate boundaries. The observation of θ' at 400°C earlier than at 450°C indicates an increase in nucleation rate at lower temperatures and is consistent with the binary alloy behavior. This tendency for θ' to nucleate readily at low temperatures may also explain the significantly higher concentration of that phase in sequence B specimens than in sequence A specimens. The cycle to ice water and reheating that was not experienced by sequence A specimens resulted in the relatively profuse nucleation of θ' which subsequently grew at the reheat temperature. The observation of veins can be accounted for by the presence of subboundaries at which θ' has precipitated. It is not clear why similar veins were not observed in sequence A specimens when θ' precipitates were detected.

The primary effect of the large θ and θ' precipitates formed during sequence A and B quench treatments is the removal of available Cu atoms from the matrix. As a result, after aging, regions exist surrounding each of these relatively large precipitates that are free of the fine precipitates which are responsible for age-hardening. When extensive growth of θ and θ' phases occurred during long interrupt or reheat periods, the concentration of Cu in the matrix was found to be so reduced that θ" precipitates were no longer observed after a T87* treatment. As seen in the phase diagram of Figure 55, the available Cu concentration throughout the matrix can be reduced to a point where the aging temperature (172°C) lies above the θ" solidus. Under these circumstances the nucleation diagram shown in Figure 82(a) for 5wt%Cu is no longer applicable at any

point in the matrix and diagrams at lower Cu concentrations must be used. For example, Figure 82(b) shows the diagram at 1.95wt%Cu. The aging temperature of 172°C is now above the nucleation curve for θ" and that phase no longer forms. Furthermore, the nucleation curve for θ' is displaced to the right and the formation of θ' is retarded in comparison with the 5wt%Cu.

Having considered the effect of altered quench treatments on microstructure, the relationship between microstructure and physical properties will now be examined. In comparison with properly quenched material, the hardness of specimens exposed to sequence A and B quench treatments was lower both before and after stretching and aging. The reduced hardness before stretching and aging can be attributed to a diminished solid solution hardening contribution associated with the loss of Cu atoms from the matrix. The large θ and θ' precipitates which are responsible for this loss, contribute little to hardness. Similarly, the reduced matrix Cu concentration also leads to a higher electrical conductivity. After stretching and aging, hardness is determined mainly by the concentration of θ' and θ" precipitates. The concentration of θ' and θ" precipitates is, in turn, determined by the amount of Cu in solution.

The C curves, whether determined before stretching and aging or after the completion of the T87* process, can be related to the concentration of Cu in solid solution. The C-curves may, therefore, be regarded as nucleation curves (or more properly as the time-temperature-transformation curves) for the formation of θ and θ'. In the temperature range considered, the C curves do not distinguish between θ and θ'. Formation of the two phases overlaps and, moreover, with sufficient time θ' transforms to θ. The C curves are not a simple function of time and temperature but depend both on path and on the initial microstructural state of the material. Thus, the same C curves are not obtained for sequence A and B

quench treatments. These differences were also reflected in the different microstructures that resulted from the two treatments.

VI. HEAT FLOW-PROPERTY PREDICTIONS

A heat flow model is developed and used here to calculate almost all conceivable heat flow conditions anticipated during the quench of 2219 aluminum alloy plates from the solutionizing temperature of 535°C. The calculated time-temperature data is then coupled to the C curves established in the previous section. The variations in properties across different thickness plates for the worst and the best heat flow conditions are thus predicted.

1. Heat Flow Model

The heat flow calculations were carried out for the cooling of a flat plate from an initial temperature of T_0. The differential equation and the boundary conditions for the temperature distribution in the plate, $T(x,t)$, are

$$(\partial T/\partial t) = \alpha(\partial^2 T/\partial x^2), \tag{11}$$

$$\left.\begin{aligned} &T(x,0) = T_0 \qquad 0 \leq x \leq L, \\ &k(\partial T/\partial x) - h_1(T-T_f) = 0 \qquad x = 0, \\ &k(\partial T/\partial x) + h_2(T-T_f) = 0 \qquad x = L, \end{aligned}\right\} \tag{12}$$

where x is the spatial variable, L is plate thickness, t is the time, α is the thermal diffusivity, T_0 and T_f are the initial and final temperatures of the plate, respectively, k is the thermal conductivity, and h_1 and h_2 are the heat transfer coefficients at the top and bottom surfaces of the plate, respectively. In terms of the dimensionless variables, $\eta = x/L$, $\Theta = (T-T_f)/(T_0-T_f)$, $Fo = \alpha t/L^2$, $Bi_1 = h_1 L/k$, and $Bi_2 = h_2 L/k$, the above equations are:

$$(\partial\theta/\partial Fo) = \partial^2\theta/\partial\eta^2 \tag{13}$$

$$\left.\begin{aligned} &\theta(\eta,0) = 1 && 0 \le \eta \le 1 \\ &\partial\theta/\partial\eta - Bi_1\theta = 0 && \eta = 0 \\ &\partial\theta/\partial\eta + Bi_2\theta = 0 && \eta = 1 \end{aligned}\right\} \tag{14}$$

Using results of Carslaw and Jaeger for constant heat transfer coefficients (28), we find:

$$\theta(\eta,Fo) = 2\sum_{n=1}^{\infty} C_n\{(\lambda_n/Bi_1)\cos\lambda_n\eta + \sin\lambda_n\eta\}\exp(-Fo\lambda_n^2), \tag{15}$$

with

$$\left.\begin{aligned} C_n &= \{[(\lambda_n/Bi_1)\sin\lambda_n - \cos\lambda_n + 1]d_2\}/\{\lambda_n[d_1d_2 + (d_1/Bi_2) + (d_2/Bi_1)]\} \\ d_1 &= 1 + (\lambda_n/Bi_1)^2 \\ d_2 &= 1 + (\lambda_n/Bi_2)^2 \end{aligned}\right\} \tag{16}$$

λ_n's are the positive roots of $[\lambda^2 - Bi_1Bi_2]\sin\lambda - (Bi_1 + Bi_2)\lambda\cos\lambda = 0$ with $\lambda_{n+1} > \lambda_n$.

The thermophysical properties used in the calculations that follow were:

Initial temperature T_0 = 535°C
Water temperature T_f = 40°C
Thermal Conductivity k = 1.2W/cm.K
Thermal Diffusivity α = 0.5 cm^2/s
Heat Transfer Coefficient* h = 0.8 W/cm^2K

2. Heat Flow Calculations and Property Predictions

The heat flow calculations were carried out using the computer code MOLID (29). These included the following:

(a) Symmetric cooling of the plate from both top and bottom surfaces under normal experimental conditions, $h_1 = h_2 = 0.8$ $W/cm^2.K$.

---

*This heat transfer coefficient was deduced from simultation of temperature-time data on the computer and comparison of same with actual data obtained in laboratory and commercial practice. This value approximates the normal condition during water quench from the solutionizing temperature.

(b) Asymmetric cooling of plates, where heat is withdrawn from only the top surface, $h_2 = 0$ for all times.

(c) Symmetric cooling of plates from both top and bottom followed by an abrupt variation in the heat transfer coefficient on the bottom surface of the plate, $h_2 = 0$, at different dimensionless times.

Time-temperature data from the computer program was then combined with equations (4) to (6) for the determination of C curves using the values of the constants reported in Table VIII. The numerical procedure for the determination of a given property, e.g., yield strength, was as follows. Equation (5) is integrated, using the calculated time-temperature data and equation (6) for a given position in the plate, and the quality $K_{1X}\tau_X$ is determined. Using the values of σ_m and σ_o from Table VIII, the value of σ, in this case yield strength, is established. These computations are carried out numerically and simultaneously with the heat flow calculations.

Finally, for a given sequence (A or B) of heat treatment, the values of the constants K_3, K_4 and K_5 are identical for all properties in question, while σ_m, σ_o and K_2 differ according to Table VIII. Under these conditions, it follows from equations (4) to (6) that the quantity $K_2 \ln[(\sigma-\sigma_o)/(\sigma_m-\sigma_o)]$ remains the same for all properties, e.g., hardness, tensile strength, and conductivity, for a given sequence. Thus, from the yield strength results one can readily obtain all the other properties without further heat flow calculations.

(a) Symmetric Cooling

Results for the symmetric heat flow from both sides of a plate using dimensionless variables $Bi_1 = Bi_2 = Bi = hL/k = 5.0$, and 0.5 are shown in Figures 83 and 84. Using the thermophysical properties listed above the following relationships between the Biot number and plate thickness, and Fourier number and time are deduced:

$$Bi = 0.67L \text{ and } t = 2(Fo)\ L^2 \qquad (17)$$

For example, equation (17) and Figures 83 and 84 show that the centers of 7.5 cm and 0.75 cm thick plates would reach a temperature of 200°C from an initial temperature of 535°C in ∿27 seconds and ∿1.2 seconds, respectively.

Figure 85 shows the actual calculated time-temperature data at four locations in a 15.24 cm (6") thick plate.

(b) Asymmetric Cooling

In these calculations it was assumed that heat was withdrawn from only the top surface of the plate. The time-temperature profiles developed are of course equally valid for plates with twice the thickness subjected to symmetric cooling from both surfaces. The data generated was 86 coupled to equations (4) to (6) as described above to permit determination of yield strength in the plates. Figure shows calculated minimum yield strengths in the plates versus plate thickness for constants from Table VIII for both sequences of heat treatments. The data are more representative of sequence A heat treatment in that a continuous decrease in temperature was calculated for all the cases. The minimum yield strength for each plate thickness represents the bottom surface which was assumed to be insulated. On the other hand, it could also represent the centerline of a plate with twice the thickness which is cooled from both sides. For example, the curve for sequence A in Figure 86 shows that the insulated bottom of a 12.7 cm (5 inch) thick plate would have a yield strength of 45.9 ksi which is only ∿6% lower than the minimum Federal Specification QQA-250/30 requires. On the other hand, the same curve also predicts a yield strength of 51.8 ksi for the same plate cooled symmetrically from both sides. The latter value

exceeds the minimum specification of 49 ksi for 12.7 cm (5 inch) thick 2219 aluminum alloy plates.

(c) Abrupt Variations in Rate of Heat Extraction From the Bottom Surface

The time-temperature data generated were for cases in which a plate was subjected to symmetric cooling for a certain length of dimensionless time, $Fo=\tau$*, followed by abrupt insulation of the bottom surface. It was assumed that this would represent an extreme case of formation of an air gap or steam pocket in commercial practice.

Figure 87 shows the calculated time-temperature profiles for a 12.7 cm thick plate cooled symmetrically for 6.45 seconds ($Fo=\tau=0.02$), followed by an abrupt change in the heat transfer coefficient h_2 from 0.8 W/cm^2K to 0. The data shows significant recalescence in temperature at locations near the bottom surface. This reheating phenomenon can then lead to deterioration of properties if it results in additive times that intersect the C curves for the alloy.

Calculated hardness and yield strengths for this 12.7 cm thick plate for a variety of τ values are shown in Figures 88 to 90. The value of $\tau=\infty$ is equivalent to complete symmetrical cooling, while $\tau=0$ depicts conditions under which the bottom surface is insulated for all times. Figures 88 and 89 show the predicted hardness and yield strength values using the C curves and constants developed earlier for sequence A. It is interesting to note that the lowest predicted properties are for $\tau=0.02$ (6.45 seconds). Trial and error showed that these should represent about the worst conditions. For example, these correspond to minimum values of hardness and yield strength of 59.1 HRB and 42.6 ksi, respectively at $X/L = 0.9$ ($\sim$11.4 cm from the top surface). This represents a maximum deterioration in yield strength of 13% below specification. If sequence B values are employed the minimum predicted yield strength at the same location

* This τ is not to be confused with

is 39 ksi. The latter probably represents the worst possible case under the assumptions of these calculations.

Time-temperature profiles for a 7.62 cm thick plate at a location 6.67 cm from the top surface for a variety of heat flow conditions are shown in Figure 91. The calculated minimum yield strengths for sequences A and B are shown in Figures 92 and 93, respectively. It is interesting to note that the lowest predicted yield strength from Figure 93 is ∿45.3 ksi which is only 11% lower than that specified in Federal Specification QQ-A-250/30.

Predicted data for a 15.24 cm (6 inch) thick plate are shown in Figures 44 to 96. As anticipated the deterioration in yield strength is most severe for sequence B.

3. Summary of "Worst" Property Predictions

Similar calculations as shown above were carried out for all plate thicknesses of up to 15.24 cm (6 inches). The data for the worst properties (lowest yield strength, tensile strength and hardness; and highest conductivity %IACS) were established using the computer model and trial and error methodology described above. The data generated are shown in Figures 97 through 100.

Figure 92 shows the predicted minimum hardness in different thickness plates when the "worst possible" heat flow conditions prevailed. For example, under the "worst" conditions a 15.24 cm (6 inch) thick plate should show a minimum hardness of ∿55 HRB somewhere close to (X/L = 0.9) its bottom surface. Figure 97 shows similar data for maximum predicted conductivities.

The predictive "worst possible case" yield and ultimate tensile strength data are shown in Figures 99 and 100. Figure 99 also shows the minimum yield strengths noted in Federal Specification QQ-A-250/30. These predictions show

that under the "worst" heat flow conditions, sequence B in Figure 99, plates thinner than ∿4 cm should meet the specifications. On the other hand, a 15.24 cm (6 inch) thick plate could have locations with yield strength of ∿37 ksi.

VII. ROUND ROBIN RESULTS

Round robin measurements of eddy current conductivity and Rockwell B hardness were conducted by five laboratories on thirty samples of 2219-T87* aluminum alloy. Each laboratory made six Rockwell B hardness measurements and three eddy current conductivity measurements on each sample. Yield and tensile strengths of each sample were measured by NBS. Thus, the results obtained are pertinent only to the interlaboratory precision of conductivity and hardness measurements and not to yield and tensile strength measurements. Details and results are described herein.

1. Samples

The samples were fabricated from the same 0.635 cm (1/4 inch) thick plate of 2219-T87* aluminum alloy used for the work described in Section IV. Three samples from this plate were chemically analyzed with the results shown in Table V. The plate was cut into bars 2.54 cm (1 inch) wide by 18 cm (7 inches) long with the long axis parallel to the rolling direction. The samples were given thermomechanical processing in groups of four as described in section IV.1.

Following the final aging treatment, one bar from each set of four bars was machined into the space shown in Figure 101. Two of the bars from each set were machined into tensile test specimens and the yield strength (0.2% offset) and ultimate tensile strength were determined on a calibrated Satec System Inc. Baldwin Model 60 CG Universal Testing System*. The two determinations were averaged and these averages are reported here as the yield strengths and tensile strengths of the round robin samples. In no case did the two values for yield and tensile strength determined for each sample set differ by more than one percent.

In all, thirty samples were circulated in the round robin. These included two exceptions to the sequence A or sequence B thermomechanical treatments described in Section IV. Sample number 276 received no stretch, and sample number 5 received only a 2-1/2% stretch. All five laboratories readily determined that the zero stretch sample did not fit property in a plot of hardness versus conductivity. The results from this sample will generally be excluded in the analysis below. However, the 2-1/2% stretch sample could not be distinguished in this manner. For four samples, numbers 34, 38, 323, and 324, no yield or tensile strength data were available.

2. Equipment

A total of five laboratories participated in the round robin. The following equipments were used in the measurements by these laboratories:

1. A conductivity bridge constructed at NBS with an 1.3 cm diameter probe operated at 15 kHz. The bridge was calibrated using two Boeing conductivity standards of 28.81 ± 0.28% IACS and 35.07 ± 0.35% IACS. The temperature of the standards and the round robin samples was 23 ± 0.2°C. Hardness measurements were made on a Wilson bench model Rockwell hardness tester. The tester was checked and gave correct readings on three Wilson test blocks with Rockwell B hardnesses 81.0, 59.7 and 39.0.
2. A Nortec NDT 5A Conductivity meter operated at 60 kHz. Two Boeing standards, 29.3 and 41.6% IACS, were used for calibration. The calibration was checked against a third Boeing standard of 35.6% IACS. Both the test specimens and the conductivity standards were maintained at the same temperature (approximately 23°C) during measurement. Hardness was measured on a Wilson bench modern hardness tester.

3. A model NDT-5A Nortec conductivity meter with an 0.95 cm (0.375 inch) model 3049C probe operated at 150 kHz. Calibration was with Boeing standards. Measurements were made at 22 ± 2°C. Hardness was measured using a Wilson Rockwell Hardness Tester Model 3-OR-7. The hardness tester was checked using a Wilson Rockwell B test block with a hardness of 69.4.
4. A Nortec NDT-5A conductivity meter with an 1.3 cm (0.5 inch) diameter type 3049D probe operated at 60 kHz. Calibration of the meter was made using aluminum standard blocks with conductivities 29.8 to 42.8% IACS at 23.9°C. A CCO Industries Rockwell B tester with digital readout. The hardness tester was checked using a calibration block with a Rockwell B hardness of 79.1.
5. A magnetest FM-120 conductivity meter with an 1.3 cm (0.5 in) diameter model 709 probe operated at 60 kHz. Two blocks with conductivities of 42.0% IACS and 29.0% IACS were used as references. The reference blocks and test samples were placed together on a large aluminum block for 30 minutes prior to measurement to insure temperature equality. Hardness was measured on a Model MC-4, Kentral Hardness Tester calibrated using a Wilson Test block with a Rockwell B hardness of 84.0.

3. Results

Each of the five laboratories made six hardness measurements and three conductivity measurements on each of the thirty samples. These measurements, along with the yield strength, tensile strengths, and heat treatments, are listed in Table XII.

Table XIII gives the average of all hardness and conductivity measurements, along with the respective standard deviations. The maximum observed single sample standard deviations are 2.4 HRB for the hardness measurements, and 0.57 %IACS for the conductivity measurements. The average of the observed standard deviations for all samples is 1.15 HRB for hardness and 0.30% IACS for conductivity.

Figure 102 is a plot of hardness vs. conductivity for the thirty samples as obtained by the five laboratories. Each point on this plot represents the average of the six hardness measurements vs. the average of the three conductivity measurements made on one sample by one laboratory. The group of five measurements which appear below the main sequence are from sample No. 276. This sample is the one that received no stretching during the thermomechanical processing of the alloy. Figure 103 shows the same relationship using the average hardness and conductivity computed using all the measurements by all five laboratories on each sample. The results in Figure 103 have been least squares fitted to the quadratic equation

$$H = a_0 + a_1 c + a_2 c^2 \tag{17}$$

where H is the Rockwell B hardness and c is the conductivity in % IACS. The values for a_0, a_1, and a_2 found are -652.95, 47.04, and -0.7521, respectively. The residual standard deviation was 0.93 HRB.

Figure 104 shows the yield strength (at 0.2% offset) plotted as a function of the conductivity determined by averaging the results obtained for each sample by the five laboratories. The results have been least squares fitted to the quadratic equation

$$Y = b_0 + b_1 c + b_2 c^2 \tag{18}$$

where Y is the yield strength. The values obtained for b_0, b_1, and b_2 are -158.97, 15.76 and -0.2806, respectively, with a residual standard deviation of 1.3 ksi.

By least squares fitting, the yield strength vs. the conductivity measured by each individual lab, the five curves displayed in Figure 105 are obtained. Each data set was fitted to Equation (18). The parameters obtained are listed in Table XIV.

Figure 106 shows the yield strength (at 0.2% offset) as a function of the average hardness determined by averaging the results obtained for each sample by the five laboratories. The results have been least squares fitted to the quadratic equation

$$Y = c_0 + c_1 H + c_2 H^2. \tag{19}$$

The values obtained for c_0, c_1, and c_2 were 27.98, -0.1350, and 0.005906, respectively. The residual standard deviation for this fit was 1.2 ksi.

By least squares fitting, the yield strength vs. the hardness measured by each individual lab, the five curves displayed in Figure 107 are obtained. Each data set was fitted to Equation (19). The parameters obtained are listed in Table XV.

4. Discussion

The results of this round robin show that, for the range of conductivities from 33 to 37% IACS, an inter-laboratory agreement of about ± 0.6% IACS (at the two sigma level) can currently be expected. For the single lot of 2219-T87* aluminum alloy measured here, a conductivity measurement by any of the five laboratories would predict the yield strength to about ±2.6 ksi and a hardness measurement (using a bench type hardness tester) could predict the yield

strength to about ± 2.4 ksi (two sigma levels). Thus, *for a single lot of material*, conductivity provides almost as good a screening test as do bench hardness measurements. It is believed that the interlaboratory agreement in the conductivity measurement could be further improved if all laboratories used conductivity standards certified by a single laboratory.

The large lot to lot variations in yield strength vs. conductivity (see Figure 54) cannot be explained as errors in the measurement of conductivity. The relative role of different processing variables in these lot to lot variations is not presently clear. It should be re-emphasized that, when NDT measurements are being made on a sample of 2219-T87* from an unknown lot, eddy current conductivity measurements alone are not sufficient to screen for mechanical properties. Hardness measurements, or better yet, yield strength measurements, must be made somewhere on the sample. Once this is done, the remainder of the material can be screened using appropriate eddy current measurements.

VIII. CONCLUSIONS

1. <u>As-received Plate</u>

1.1 Moderate variations in composition, hardness, electrical conductivity and mechanical properties were noted across the thickness of a 12.7 cm (5 inch) thick 2219-T851 aluminum alloy plate. Composition variations, which influence measured conductivities, can be traced to the original ingot. The variations in hardness and tensile properties are mainly due to changes in cooling rate across the plate during the quench and are probably influenced to some extent by inhomogeneous mechanical deformation during processing.

2. <u>Solidification Segregation Studies</u>

2.1 Macrosegregation of copper in Direct Chill (DC) cast ingots of 2219 aluminum alloy cannot be completely eliminated by chill face scalping and subsequent thermomechanical treatment. Macrosegregation does remain in the finished plate product. However, good scalping practice should limit copper content to above the solid solubility limit with no deterioration in mechanical properties.

2.2 Elements with equilibrium partition coefficients less than unity exhibit macrosegregation similar to copper while those with coefficients greater than unity are opposite to copper. The magnitude of deviations from the nominal are related to the deviation of the coefficient from unity.

2.3 The major phases present in cast 2219 aluminum alloy in this study have been determined by electron microprobe analysis and electron diffraction. They are α-aluminum solid solution, θ-$CuAl_2$ and Cu_2FeAl_7. These phases are also present in the heat treated finished plate product.

2.4 Predictable macrosegregation has been obtained in laboratory ingots of 2219 aluminum alloy. Both positive and negative segregation similar to DC cast ingots are observed and are caused by the flow of segregated interdendritic liquid.

2.5 Electrical conductivity determined by eddy current measurements of cast 2219 aluminum alloy is inversely related to copper content. This fact complicates the relationship of conductivity to mechanical properties used for nondestructive evaluation of the finished plate product.

2.6 Because of large copper content variation near the chill face, surface hardness and eddy current measurements may be very sensitive to scalping depth in their ability to evaluate the condition of finished alloy plate.

2.7 Hardness, yield strength and ultimate tensile strength of heat treated 2219 aluminum alloy decrease significantly when the average copper content drops below approximately 5.5 wt%.

3. <u>C-curve Determination and Relationship Between Mechanical Properties and Conductivity</u>

3.1 No significant difference in either strength or hardness was detected between alloys stretched between 5 and 7% permanent strain during the thermomechanical processing of 2219 aluminum alloy.

3.2 The functional form developed by Cahn and used previously by Staley for 7075-T6 and 6061-T6 aluminum alloy was found to give an adequate representation of the C curves for 2219-T87* if the form was modified to include a minimum value for each property in question. Some deficiency in this form at the highest and lowest temperatures was noted.

3.3 An efficient computer program was developed for using time-temperature and property measurement data to establish C curve parameters.

3.4 Time temperature precipitation curves (C curves) were determined for hardness, yield strength, tensile strength and electrical conductivity. The C curves can be used to determine the correlations between these properties. C curves could not be developed for elongation, probably because this property is more sensitive to grain size and other factors.

3.5 A small but significant difference was found between the C curves for sequence A (direct transfer to salt bath) and sequence B (water quench and reheat in salt bath) type quenches. For a given salt bath time and temperature, sequence B quenches resulted in a greater degradation of mechanical properties.

3.6 The scatter in hardness and conductivity was found to be large. This scatter can be expected to complicate NDE measurements and should be properly taken into account when establishing NDE procedures and specifications.

3.7 Because the "nose" of the C curves for 2219 is at a relatively high temperature, 2219 aluminum alloy is not as sensitive to the types of abnormal quenches studies here as some of the other high strength aluminum alloys such as 7050.

4. <u>Electron Microscopy Studies</u>

4.1 The age-hardening response of 2219-T87* and T851 is determined principally by the formation of Θ' precipitates with some contribution by Θ'' precipitates.

4.2 An abnormal quench treatment which results in dwell times significant with respect to the C curves leads to heterogeneous nucleation and rapid growth of θ and θ' precipitates.

4.3 The nucleation and growth behavior of the θ and θ' precipitates formed during an abnormal quench depends on the pre-existing microstructural state of the material and on the thermal "path".

4.4 The large incoherent θ and θ' precipitates formed during an abnormal quench consume copper available from the matrix and thereby reduce the concentration of θ' and θ" precipitates that contribute to precipitation hardening during subsequent aging.

4.5 The C curves are a measure of the concentration of large θ and θ' precipitates formed during the quench treatment.

5. Heat Flow Calculations - Property Predictions

5.1 Calculated plate properties, e.g., yield strength and hardness, decrease monotonically with increasing distance from surface to centerline of a plate for fixed heat transfer conditions.

5.2 For symmetric cooling and (sequence A) C curves, the calculated minimum yield strength (at the center of the plate) is 54.9, 53.7, and 51.8 ksi for 2.54, 7.62, and 12.7 cm (1, 3, and 5 inch) thick plates, respectively.

5.3 For asymmetric cooling and (sequence A) C curves, the calculated minimum yield strength (at the bottom surface of the plate) is 54.4, 50.7, 45.9 ksi for 2.54, 7.62, 12.7 cm (1, 3, and 5 inch) thick plates, respectively.

5.4 For plate thicknesses greater than 2.54 cm, (sequence B) C curves yield lower properties values than (sequence A) C curves. For example, for asymmetric cooling and (sequence B) C curves the calculated minimum yield strength is 54.6, 48.0, 41.5 ksi for 2.54, 7.62, and 12.7 cm (1, 3, and 5 inch) thick plates, respectively.

5.5 Interrupted (abnormal) cooling, in which the heat transfer coefficient at the bottom surface changes from the same value as at the top surface to a zero value, can result in lower property values than found for asymmetric cooling. For example, for a 12.7 cm (5 inch) thick plate and (sequence B) C curves interrupted cooling yields a minimum yield strength of 39.0 ksi compared with 41.5 ksi for asymmetric cooling.

5.6 For "worst case "interrupted asymmetric cooling and for the 2219 aluminum alloy lot studied here, plates with thicknesses less than about 5 cm (2 inches) will not suffer yield strength degradation below levels in Federal Specification QQ-A-250/30.

6. Round Robin Results

6.1 Round robin results show that, for the range of conductivities from 33 to 37% IACS, an interlaboratory agreement of about ±0.6% IACS (at the two sigma level) can currently be expected. Agreement could be improved if all laboratories used conductivity standards certified by a single laboratory.

6.2 When NDE measurements are being made on a sample of 2219-T87* from an unknown lot, eddy current conductivity measurements alone are not sufficient to screen mechanical properties. Hardness measurements (or better yet, yield strength measurements) must be made somewhere on the sample.

APPENDIX A

Listing of the interactive program used for least squares fitting the data in Table VII to C curves as described in the text of this report. The language is Fortran V and the program was compiled and operated on the NBS Univac 1108. The data format called for in subroutine READD for the data as displayed in Table VII with the exception that the headings "sequence A" and "sequence B" are removed and END statements placed after the list of temperature intervals and at the end of all data to be used.

```
SWARTZ*SOFTAL(1).MAIN(19)
                INTEGER VP
                COMMON /RW/ IR,IW,R,IPROP
                COMMON /PAR/ P(10),VP(10),PAD(10),E(10)
                COMMON/RD/T(100),ISN(200),HRB(200),PIACS(200),YS(200),UTS(200),
               *RA(200),EL(200)
                COMMON /RT/ TI(200,100),NE,NS
                IR=5
                IW=6
                R=1.9872
                CALL READD
        100     WRITE(IW,101)
        101     FORMAT('  C CURVE FIT WHAT PROPERTY?',/,
               *' ANSWER: 0=EXIT, 1=HRB, 2=%IACS, 3=YS , 4=UTS')
                READ(IR,102,ERR=100) IPROP
        102     FORMAT(I1)
                IF(IPROP.EQ.0) GO TO 112
                I=IPROP
                IF(I.NE.1.AND.I.NE.2.AND.I.NE.3.AND.I.NE.4)GOTO 100
        98      WRITE(IW,103)
        103     FORMAT('  GIVE INITIAL VALUES FOR PARAMETERS',/,
               *' SIGN, K2, K3, K4, K5, SIG0,  FREE FORMAT')
                READ (IR,104,ERR=98) (P(J),J=1,6)
        104     FORMAT()
        99      IF(P(1).EQ.0) GO TO 110
        97      WRITE(IW,105)
        105     FORMAT('  GIVE STEP SIZE FOR EACH PARAMETER, FREE FORMAT')
                READ(IR,104,ERR=97) (E(J),J=1,6)
        200     WRITE(IW,201)
        201     FORMAT('  DO A LEAST SQUARES FIT?, 1=YES, 2=CALC.TABLE',
               *' 3=OUT TO FILE')
                READ(IR,102,ERR=200) NDEC
                IF(NDEC.NE.1) GO TO 111
                CALL MINLSQ
                GO TO 200
        110     CONTINUE
                GO TO 100
        111     CONTINUE
                IF(NDEC.EQ.3) CALL GRDFIN(3)
                IF(NDEC.NE.2) GO TO 100
                CALL GRDFIN(0)
                GO TO 200
        112     CONTINUE
                END
```

```
SWARTZ*SOFTAL(1).READD(7)
      SUBROUTINE READD
      INTEGER VP
      COMMON /RW/ IR,IW,R,IPROP
      COMMON /PAR/ P(10),VP(10),PAD(10),E(10)
      COMMON /RD/ T(100),ISN(200),HRB(200),PIACS(200),YS(200),UTS(200),
     *RA(200),EL(200)
      COMMON /RT/ TI(200,100),NE,NS
      WRITE(IW,90)
90    FORMAT('  ADD IN TEMP. INTERVAL DATA, FOLLOWED BY',
     *' PROPERTY AND TIME DATA')
      READ(IR,100)NHD
100   FORMAT(A2)
      IF(NHD.NE.'TE')GO TO 900
      NB=0
      NE=0
91    READ(IR,100)NDEC
      IF(NDEC.EQ.'EN')GO TO 105
101   READ(0,102) N1
102   FORMAT()
      NB=NE+1
      NE=NE+N1
      READ(0,102) ND,(T(J),J=NB,NE)
      GO TO 91
C NE IS TOTAL NUMBER OF TEMPERATURES READ IN
105   CONTINUE
      NS=0
C NS KEEPS  TRACK OF NUMBER OF SAMPLES
110   READ(IR,100)NHD
      IF(NHD.EQ.'EN') GO TO 901
      NS=NS+1
      READ(0,102)ISN(NS),HRB(NS),PIACS(NS),YS(NS),UTS(NS),
     *EL(NS),RA(NS)
      NER=NE-1
      READ(IR,102,ERR=902) (TI(NS,J),J=1,NER)
      GO TO 110
900   WRITE(IW,120)
120   FORMAT( '  FIRST CARD DOES NOT READ TEMP RANGES')
      RETURN
901   WRITE(IW,121)NE,NS
121   FORMAT('  NO. OF TEMPS. READ=',I4,/,'   NO. OF SAMPLES=',I4)
      RETURN
902   WRITE(IW,122)
122   FORMAT('  ERROR IN READING TIME DATA')
      RETURN
      END
```

```
SWARTZ*SOFTAL(1).MINLSQ(9)
      SUBROUTINE MINLSQ
      DOUBLE PRECISION A,AA,B
      INTEGER VP
      COMMON /RW/ IR,IW,R,IPROP
      COMMON /PAR/ P(10),VP(10),PAD(10),E(10)
      COMMON /RD/ T(100),ISN(200),HRB(200),PIACS(200),YS(200),UTS(200),
     *RA(200),EL(200)
      COMMON /RT/ TI(200,100),NE,NS
      COMMON /LSM/ A(10,10),AA(10,10),B(10)
      DIMENSION SIGC(200),PSI(200),SMEM(200),SP(200),Z(10,200),C(10)
C PICK PARAMETERS TO BE VARIED
      JNIT=0
101   WRITE(IW,102)
102   FORMAT('  LIST PARAMETERS TO BE VARIED',/,' 1=SIGM , 2=K2, ',
     *'3=K3, 4=K4, 5=K5, 6=SIG0,  BLANK=RETURN, FORMAT 5I1')
      READ(IR,103,ERR=101) (VP(J),J=1,6)
103   FORMAT(6I1)
      NPV=0
      DO 104 J=1,6
      IF(VP(J).EQ.0) GO TO 105
104   NPV=J
105   IF(NPV.EQ.0) RETURN
2011  JNIT=JNIT+1
      NOIT=0
202   CONTINUE
C ZERO LEAST SQUARES MATRIX
      DO 206 J=1,NPV
      DO 205 K=J,NPV
      A(J,K)=0.
205   A(K,J)=0.
206   C(J)=0.
C
C EVALUATE PARTIAL DERIVATIVES
C
```

```
      CALL CALC(SIGC)
      DO 207 J=1,NS
      IF(IPROP.EQ.1) PSI(J)=HRB(J)-SIGC(J)
      IF(IPROP.EQ.2) PSI(J)=PIACS(J)-SIGC(J)
      IF(IPROP.EQ.3) PSI(J)=YS(J)-SIGC(J)
      IF(IPROP.EQ.4) PSI(J)=UTS(J)-SIGC(J)
 207  SMEA(J)=SIGC(J)
      DO 209 J=1,NPV
      JDO=VP(J)
      P(JDO)=P(JDO)+E(JDO)
      CALL CALC(SP)
      DO 208 I=1,NS
 208  Z(J,I)=(SP(I)-SIGC(I))/E(JDO)
      P(JDO)=P(JDO)-E(JDO)
 209  CONTINUE
C
C FILL LEAST SQUARES MATRIX
C
      DO 213 J=1,NPV
      DO 211 K=J,NPV
      DO 210 I=1,NS
 210  A(J,K)=A(J,K)+Z(J,I)*Z(K,I)
 211  A(K,J)=A(J,K)
      DO 212 I=1,NS
 212  C(J)=C(J)+PSI(I)*Z(J,I)
 213  CONTINUE
      DO 214 J=1,NPV
 214  B(J)=C(J)
C
C INVERT MATRIX
C
      CALL DPINVS(NPV,+1,ISIG)
      WRITE (IW,1004) ISIG
1004  FORMAT('  DPINVS CALLED, ISIG=',I3)
C
C INCREMENT NO. OF ITERATIONS
C
      NOIT=NOIT + 1
      IF(ISIG.NE.0) GO TO 101
      DC=0
      DO 216 J=1,NPV
 216  DC=DC+ C(J)*B(J)
      IF(DC.GT.0) GO TO 218
      DO 217 J=1,NPV
 217  B(J)=-B(J)
 218  J=0
 219  J=J+1
      IF(J.GT.6) GO TO 220
      PAD(J)=P(J)
      GO TO 219
 220  CONTINUE
      DO 223 J=1,NPV
      JDO=VP(J)
      IF(DABS(B(J)).GT.ABS(10.*PAD(JDO))) GO TO 223
2230  IF(DABS(B(J)).LT.ABS(0.5*PAD(JDO))) GO TO 2231
      B(J)=0.5*B(J)
      GO TO 2230
2231  PAD(JDO)=PAD(JDO)+B(J)
 223  CONTINUE
 224  CONTINUE
      Y0=SQEK(P)
      YT=SQEK(PAD)
      IF(YT.LT.Y0) GO TO 229
      WRITE(IW,1006) NOIT
1006  FORMAT('  IT. NO.',I4,' CHI SQUARE FAILED TO IMPROVE')
      GO TO 101
 229  WRITE(IW,1090) JNIT,NOIT,(PAD(J),P(J),J=1,6)
      DO 230 J=1,6
 230  P(J)=PAD(J)
1090  FORMAT('  SEQ.NO.',I4,'  IT.NO.',I4,/,
     *'  NEW PAR. VALUES  PREV. PAR. VALUES',/,(2E12.4))
      WRITE(IW,1091) YT
1091  FORMAT(/' LEAST SQUARE ERROR=',E12.4,/,
     *' DO ANOTHER ITERATION?,  1 = YES')
      READ (IR,1092) NTEST
1092  FORMAT (I1)
      IF(NTEST.EQ.1) GO TO 202
      GO TO 101
      END
```

```
SWARTZ*SOFTAL(1).DPINVS(3)
      SUBROUTINE DPINVS(N,K,ISIG)
      DOUBLE PRECISION A,AA,B,C,HOLD,X
      COMMON /LSM/ A(10,10),AA(10,10),B(10)
      COMMON /RW/ IR,IW,R,IPROP
      ISIG=0
      IF(K.LT.0) GO TO 20
      DO 15 I=1,N
      DO 15 J=1,N
      IF(I.EQ.J)   GO TO 10
      AA(I,J)=0.
      GO TO 15
   10 AA(I,J)=1.
   15 CONTINUE
   20 DO 65 L=1,N
      C=0.
      DO 25 J=L,N
      X=DABS(A(J,L))
      IF (X.LE.C) GO TO 25
      C=X
      J1=J
   25 CONTINUE
   26 IF((C-1.0E-8).LE.0.) GO TO 120
      IF(J1.EQ.L) GO TO 40
      DO 28 J=L,N
      HOLD=A(L,J)
      A(L,J)=A(J1,J)
   28 A(J1,J)=HOLD
      IF (K.LT.0) GO TO 35
      DO 32 J=1,N
      HOLD=AA(L,J)
      AA(L,J)=AA(J1,J)
   32 AA(J1,J)=HOLD
      IF(K.EQ.0) GO TO 40
   35 HOLD=B(L)
      B(L)=B(J1)
      B(J1)=HOLD
   40 CONTINUE
      DO 60 I=1,N
      IF(I.EQ.L) GO TO 60
      Z1=A(I,L)/A(L,L)
      DO 45 J=L,N
   45 A(I,J)=A(I,J) - Z1*A(L,J)
      IF(K.LT.0) GO TO 55
      DO 50 J=1,N
   50 AA(I,J)=AA(I,J)-Z1*AA(L,J)
      IF(K.EQ.0) GO TO 60
   55 B(I)=B(I)-Z1*B(L)
   60 CONTINUE
   65 CONTINUE
   68 DO 95 L=1,N
      Z1=A(L,L)
      DO 70 J=L,N
   70 A(L,J) = A(L,J)/Z1
      IF(K.LT.0) GO TO 80
      DO 75 J=1,N
   75 AA(L,J)=AA(L,J)/Z1
      IF(K.EQ.0) GO TO 95
   80 B(L)=B(L)/Z1
   95 CONTINUE
      GO TO 150
  120 ISIG=-1.
      WRITE(IW,130)
  150 RETURN
  130 FORMAT(///20X,42H MARTIX IS SINGULAR, NO INVERSE OBTAINABLE ///)
      END
SWARTZ*SOFTAL(1).SQEK(4)
      FUNCTION SQEK(PIN)
      INTEGER VP
      COMMON /RW/ IR,IW,R,IPROP
      COMMON /PAR/ P(10),VP(10),PAD(10),E(10)
      COMMON /RD/ T(100),ISN(200),HRB(200),PIACS(200),YS(200),UTS(200),
     *RA(200),EL(200)
      COMMON /RT/ TI(200,100),NE,NS
      DIMENSION PIN(10),HOLD(10),SC(200)
      SQEK=0.
      DO 1 J=1,6
      HOLD(J)=P(J)
    1 P(J)=PIN(J)
      CALL CALC(SC)
      DO 2 J=1,NS
      IF(IPROP.EQ.1) Y=HRB(J)
      IF(IPROP.EQ.2) Y=PIACS(J)
      IF(IPROP.EQ.3) Y=YS(J)
      IF(IPROP.EQ.4) Y=UTS(J)
      X=Y-SC(J)
    2 SQEK=SQEK+X*X
      XN=NS
      SQEK=SQRT(SQEK/(XN-6.))
      DO 3 J=1,6
    3 P(J)=HOLD(J)
      RETURN
      END
```

```
SWARTZ*SOFTAL(1).CALC(9)
      1              SUBROUTINE CALC(SC)
      2              INTEGER VP
      3              COMMON /RW/ IR,IW,R,IPROP
      4              COMMON /PAR/ P(10),VP(10),PAD(10),E(10)
      5              COMMON /RD/ T(100),ISN(200),HRB(200),PIACS(200),YS(200),UTS(200),
      6             *RA(200),EL(200)
      7              COMMON /RT/ TI(200,100),NE,NS
      8              COMMON /TP/ TAU(200)
      9              DIMENSION SC(200),ECALC(200)
     10              XX=ALOG(P(2))
     11              T0=273.15
     12              CP=P(3)*P(4)*P(4)/R
     13              CP2=P(5)/R
     14        C
     15        C CALCUALTE TAU'S
     16        C
     17              NER=NE-1
     18              DO 2 K=1,NER
     19              TEMP=(T(K)+T(K+1))/2.
     20              D1=(TEMP+T0)*(P(4)-TEMP-T0)**2
     21              IF(D1.LT.1.E-35) D1=1.E-35
     22              D2=TEMP+T0
     23              ECALC(K)=XX + CP/D1 + CP2/D2
     24              IF(ECALC(K).GT.50.) ECALC(K)=50.
     25        2     IF(ECALC(K).LT.-50.) ECALC(K)=-50.
     26              DO 3 J=1,NS
     27              TAU(J)=0.
     28              DO 4 K=1,NER
     29        4     TAU(J)=TAU(J)+TI(J,K)*EXP(-ECALC(K))
     30        3     CONTINUE
     31        1     CONTINUE
     32        C
     33        C DETERMINE THE CALCUATED VALUE OF THE PARAMETER BEING FITTED
     34        C
     35              DO 5 J=1,NS
     36              IF(TAU(J).GT.50.) TAU(J)=50.
     37        5     SC(J)=(P(1)-P(6))*EXP(-TAU(J)) + P(6)
     38              RETURN
     39              END
```

```
SWARTZ*SOFTAL(1).GRDFIN(12)
      1              SUBROUTINE GRDFIN(IDEC)
      2              INTEGER VP
      3              COMMON /RW/ IR,IW,R,IPROP
      4              COMMON /PAR/ P(10),VP(10),PAD(10),E(10)
      5              COMMON /RD/ T(100),ISN(200),HRB(200),PIACS(200),YS(200),UTS(200),
      6             *RA(200),EL(200)
      7              COMMON /RT/ TI(200,100),NE,NS
      8              COMMON /TP/TAU(200)
      9              DIMENSION SC(200)
     10              DEFINE FILE 3(204,120,M,NAS)
     11              WRITE(IW,101) (P(J),J=1,6)
     12       101    FORMAT('  PARAMETER VALUES ARE:  ',/,' SIGM=',E10.4,5X,
     13             *' K2=',E10.4,5X,' K3=',E10.4,5X,'K4=',E10.4,5X,
     14             */,'  K5=',E10.4,5X,'SIG0=',E10.4)
     15              CALL CALC(SC)
     16              IF(IPROP.EQ.1) IO='   HRB'
     17              IF(IPROP.EQ.2) IO=' %IACS'
     18              IF(IPROP.EQ.3) IO='  Y.S.'
     19              IF(IPROP.EQ.4) IO='U.T.S.'
     20              WRITE(IW,102) IO
     21       102    FORMAT('  SAMPLE NO.',2X,'  TAU',8X,A6,7X,'CALC. VALUE')
     22              DO 103 J=1,NS
     23              IF(IPROP.EQ.1)WRITE(IW,104)ISN(J),TAU(J), HRB(J),SC(J)
     24              IF(IPROP.EQ.2)WRITE(IW,104)ISN(J),TAU(J),PIACS(J),SC(J)
     25              IF(IPROP.EQ.3)WRITE(IW,104)ISN(J),TAU(J),   YS(J),SC(J)
     26              IF(IPROP.EQ.4)WRITE(IW,104)ISN(J),TAU(J),  UTS(J),SC(J)
     27       103    CONTINUE
     28       104    FORMAT(I4,3E13.4)
     29              YT=SQEK(P)
     30              WRITE(IW,105) YT
     31       105    FORMAT('  NORMALIZED LEAST SQUARE ERROR=',F10.4)
     32              IF(IDEC.NE.3) RETURN
     33              FIND(3'1)
     34              WRITE(3'NAS,102) IO
     35              DO 106 J=1,NS
     36              IF(IPROP.EQ.1)WRITE(3'NAS,104)ISN(J),TAU(J),HRB(J),SC(J)
     37              IF(IPROP.EQ.2)WRITE(3'NAS,104)ISN(J),TAU(J),PIACS(J),SC(J)
     38              IF(IPROP.EQ.3)WRITE(3'NAS,104)ISN(J),TAU(J),YS(J),SC(J)
     39              IF(IPROP.EQ.4)WRITE(3'NAS,104)ISN(J),TAU(J),UTS(J),SC(J)
     40       106    CONTINUE
     41              WRITE(3'NAS,110)
     42       110    FORMAT(1H ,'END')
     43              RETURN
     44              END
```

ACKNOWLEDGEMENT

We are indebted to W. F. Brown of NASA-Lewis, G. A. Rodney of Martin Marietta, S. A. Levy of Reynolds Aluminum, and R. J. Schwinghamer of Marshall Space Flight Center for their aid in carrying out the round robin measurements. We thank C. H. Brady for the metallography presented in this report. The efforts of P. A. Boyer, R. L. Parke, and R. D. Robbins are also greatly appreciated. We also thank J. J. Fillibin for his aid in plotting and analysis of the data. We would also like to thank D. E. Newbury and B. I. Diamondstone for chemical analysis, C. J. Bechtoldt for some x-ray measurements, and R. F. Boisvert for advice and assistance on the heat flow calculations. Appreciation is also extended to R. V. Drew, D. E. Harrison, D. M. G. Summers, and L. J. Toms for the preparation of the manuscript. Finally, we are indebted to Dr. S. A. Levy and associates of the Metallurgical Research Division of Reynolds Metals Company for frequent consultation and for the ingot and plates made available for this study.

REFERENCES

1. Aluminum Inspections Pressed, Staff Report, Aviation Week and Space Technology, Aug. 6, 1980, p. 14.

2. Aluminum Concern Extended to Testing, Staff Report, Aviation Week and Space Technology, Aug. 13, 1980, p. 17.

3. M. C. Flemings, Solidification Processing, McGraw Hill, New York, 1974.

4. G. Phragmen, J. Inst. of Metals, 77 (1950), p. 489.

5. Metals Handbook, Vol. 8, ASM (1973), p. 126.

6. F. Keller and G. W. Wilcox, Alcoa Research Lab., Tech. Report #7 (1958).

7. R. L. Myklebust, C. E. Fiori, and K. J. F. Heinrich, NBS Technical Note 1106, U. S. Govt. Printing Office, Washington, D.C., Sept. 1979.

8. L. F. Mondolfo, Aluminum Alloys: Structure and Properties, Butterworths, Boston (1976), p. 491.

9. R. Mehrabian and M. C. Flemings, Met. Trans., Vol. 1 (1970), p. 455.

10. W. L. Fink and L. A. Willey, Trans. AIME, Vol. 175, (1948), p. 414.

11. J. W. Cahn, Acta Met. Vol. 4, (1956), p. 572.

12. J. T. Staley, Industrial Heating, Vol. 44, (1977), p. 6.

13. J. W. Evancho and J. T. Staley, Met. Trans., Vol. 5, (1974), p. 43.

14. J. W. Cahn, Acta Met., Vol. 4, (1956), p. 449.

15. W. Wilson and L. J. Swartzendruber, Computer Phys. Comm., Vol. 7, (1974), p. 151.

16. R. C. McMaster, Nondestructive Testing Handbook, 1959, Ch. 42, p. 18.

17. H. V. Pellegrini, Metal Progress, March 1980, p. 60

18. A. Chitty, J. Inst. of Metals, Vol. 86, (1957-58), p. 65.

19. S. Matsuo, Trans. Nat. Res. Inst. Metals, Vol. 13, No. 2, (1971), p. 57

20. Y. Baba, Trans. Japan Inst. Metals, Vol. 10, (1969), p. 188.

21. W. A. Denn, Aluminum, Vol. 1, Chap. 6, American Society for Metals, (1967).

22. G. Thomas, Transmission Electron Microscopy of Metals, John Wiley & Sons, New York, (1962), pp. 153-158.

23. H. K. Hardy, J. Inst. Metals. Vol. 79, (1951), p. 321.

24. J. M. Silcock, T. J. Heal and H. K. Hardy, J. Inst. Metals, Vol. 82, (1953-54), p. 239.

25. G. W. Lorimer, Precipitation Processes in Solids, Met. Soc. of AIME, (1976), p. 87.

26. E. Hornbogen, Aluminum, Vol. 43, Part I, p. 41; Part II, p. 115; Part III, p. 163; Part IV, p. 166, (1967).

27. V. A. Philips, Acta Met., Vol. 23, (1975), p. 751.

28. H. S. Carslaw and J. C. Jaeger, Conduction of Heat in Solids, 2nd edition, (1959).

29. J. M. Hyman, LA-7595M Manual, Los Alamos Scientific Laboratory.

Table I

Center and Near Edge Composition of 12.7 cm (5 inch) thick 2219-T851 Aluminum Alloy Plate (Reynolds Lot No. 7950777-DI).

Element	Composition (wt%)	
	Approximately 2 cm from edge	Center
Cu*	6.6	5.8
Cu	6.5	5.9
Mn	0.36	0.35
Fe	0.24	0.21
Si	0.071	0.064
Zn	0.033	0.030
Ti	0.030	0.041
V	0.070	0.079
Zr	0.11	0.12
Ni	0.029	0.029
Mg	0.010	0.009

*Values determined by solution molecular absorbtion spectrometry, others by emission spectroscopy.

Table II

Solidification "Path" During Formation of α-Aluminum Phase

f_s	C_L^{Cu} wt%	C_L^{Mn} wt%	C_L^{Fe} wt%	C_L^{Si} wt%
0	6.30	0.3	0.20	0.10
.1	6.87	0.30	0.22	0.11
.2	7.56	0.303	0.25	0.121
.3	8.44	0.306	0.27	0.136
.4	9.64	0.309	0.33	0.156
.5	11.22	0.312	0.394	0.183
.6	13.48	0.315	0.49	0.222
.7	17.13	0.318	0.65	0.29
.8	23.94	0.324	0.97	0.41
.85	30.43	0.330	1.28	0.52
.9	42.58	0.336	1.91	0.74
.95	75.66	0.348	3.766	1.35

Table III

Summary of Etching Response of Phases in Cast 2219 Aluminum Alloy

Etchant	$CuAl_2$ (rounded irregular)	Cu_2FeAl_7 (blades)
unetched	light gray	slightly darker than $CuAl_2$
1/2%HF 15s @ 20°C	no attack	outlined - dark brown
1%NaOH 15s @ 50°C	light brown	no attack
10%NaOH 5s @ 70°C	violet brown	light brown
25%HNO_3 45s @ 20°C	dark reddish black	dark blue gray to black
20%N_2SO_4 30s @ 70°C	no attack	no attack
H_3PO_4 60s @ 50°C	no attack - outlined	no attack - outlined
Keller's	outlined - not colored	outlined darkened

Table IV

Examples of Electron Microprobe Analysis of Phases in Cast 2219 Aluminum Alloy

	wt% Al	wt% Cu	wt% Mn	wt% Si	wt% Fe
rounded irregular ($CuAl_2$)	51.3	49.5	0	0.4	0
blades (Cu_2FeAl_7)	53.9	36.3	2.2	0.4	8.6
$CuAl_2$ exact	45.9	54.1	-	-	-
Cu_2FeAl_7 exact	50.8	34.2	-	-	15.0

TABLE V

Report of Analysis of three samples from the 0.635 cm thick plate of 2219-T87* aluminum alloy. Samples were analyzed by emission spectroscopy. The values labeled 2219 are typical values for a standard of this alloy. Duplicate determinations are given in weight percent.

Sample	Si	Fe	Cu	Mn	Mg	Cr	Ni	Zn	Ti	V	Zr
2219	.15	.20	6.3	.28	.02	.01	.01	.03	.06	.12	.16
LEFT	.08	.04	6.65	.34	.004	.003	.027	.029	.044	.084	.107
	.08	.03	6.79	.35	.007	.001	.025	.0295	.043	.081	.107
MIDDLE	.08	.05	6.51	.34	.005	.003	.027	.029	.045	.084	.107
	.08	.04	6.79	.35	.006	.002	.026	.029	.044	.080	.106
RIGHT	.08	.04	6.70	.34	.005	.002	.026	.029	.045	.083	.108
	.08	.04	6.88	.35	.007	.002	.027	.029	.045	.084	.108

TABLE VI

Summary of hardness and conductivity data obtained during thermo-mechanical heat treatment of a 0.635 cm (1/4") thick plate of 2219 aluminum alloy.

COLUMN 1: SEQUENCE (1=A , 2=B)
COLUMN 2: SAMPLE NUMBER
COLUMNS 3, 4, AND 5: HRB, HRB, %IACS FOR AS RECEIVED PLATE
COLUMNS 6, 7, AND 8: HRB, HRB, %IACS AFTER SOLUTION TREAT AND QUENCH
COLUMNS 9, 10, AND 11: HRB, HRB, %IACS AFTER STRETCH
COLUMNS 12, 13, AND 14: HRB, HRB, %IACS AFTER AGEING
COLUMNS 15, 16, AND 17: HRB, HRB, %IACS AFTER MACHINING TO TENSILE SPECIMEN
A .0 INDICATES THAT NO MEASUREMENT WAS TAKEN

1	1	80.3	78.5	33.6	33.8	31.6	.0	.0	.0	.0	.0	.0	.0	.0	.0	.0
1	2	79.9	78.0	33.7	34.2	40.0	.0	.0	.0	.0	.0	.0	.0	.0	.0	.0
1	3	80.4	78.3	33.4	36.8	36.7	.0	.0	.0	.0	.0	.0	.0	.0	.0	.0
1	4	80.0	78.3	33.4	39.0	39.0	.0	.0	.0	.0	.0	.0	.0	.0	.0	.0
1	5	80.0	77.7	33.3	36.0	37.6	.0	.0	.0	.0	.0	.0	.0	.0	.0	.0
1	6	79.4	78.7	33.3	35.0	35.0	.0	.0	.0	.0	.0	.0	.0	.0	.0	.0
1	7	80.1	78.7	33.4	38.8	38.0	.0	.0	.0	.0	.0	.0	.0	.0	.0	.0
1	8	80.0	79.1	33.3	37.8	36.7	.0	.0	.0	.0	.0	.0	.0	.0	.0	.0
1	10	79.1	77.7	33.4	42.7	39.2	31.2	57.8	53.9	30.6	76.2	76.7	34.5	.0	.0	.0
1	11	80.0	79.0	33.4	40.2	38.0	31.3	61.2	59.1	30.5	76.2	76.6	34.3	75.8	76.0	33.4
1	12	80.0	77.9	33.3	49.2	48.2	31.5	59.0	55.7	30.6	75.0	76.9	34.2	76.1	74.0	33.5
1	13	79.8	78.7	33.3	39.7	39.3	32.3	.0	.0	.0	.0	.0	.0	.0	.0	.0
1	14	79.7	78.8	33.3	39.9	38.2	32.5	54.7	59.0	31.8	70.8	71.8	34.4	.0	.0	.0
1	15	80.0	78.7	33.4	39.1	36.3	32.4	55.0	57.1	31.8	71.3	73.3	35.0	71.2	70.0	33.7
1	16	80.4	79.3	33.4	34.3	37.1	32.7	52.9	52.1	32.1	69.5	69.5	35.4	72.5	72.2	34.4
1	17	79.1	79.5	33.3	31.7	31.0	33.9	.0	.0	.0	.0	.0	.0	.0	.0	.0
1	18	79.1	78.3	33.3	33.9	33.3	33.7	47.3	47.7	33.5	61.5	64.3	36.6	.0	.0	.0
1	19	80.0	79.7	33.4	33.7	30.0	34.0	46.4	46.6	33.9	60.7	58.8	36.6	64.7	66.5	35.9
1	20	79.3	79.0	33.6	30.0	32.0	33.5	47.9	48.5	33.2	64.3	64.3	35.9	65.0	66.3	35.6
1	21	80.0	78.7	33.4	21.6	23.4	35.7	.0	.0	.0	.0	.0	.0	.0	.0	.0
1	22	79.1	79.0	33.2	23.1	22.4	35.6	37.2	37.0	35.7	52.0	47.0	37.3	.0	.0	.0
1	23	80.2	79.3	33.2	21.8	22.5	35.6	39.3	39.0	35.7	48.4	45.8	37.9	49.3	49.2	37.9
1	24	79.9	77.8	33.3	22.2	23.2	35.7	36.0	35.8	35.7	44.6	43.4	37.7	47.2	48.1	37.9

1	25	80.0	78.2	33.2	34.8	38.3	30.6	.0	.0	.0	.0	.0	.0	.0	.0	.0
1	26	79.3	78.6	33.3	41.0	40.2	30.7	58.5	59.5	29.6	75.8	76.7	33.5	.0	.0	.0
1	27	79.7	77.8	33.3	42.7	40.6	30.5	58.2	61.7	29.4	77.4	77.3	33.4	76.0	76.3	33.6
1	28	80.1	77.8	33.1	41.5	38.5	30.1	59.9	63.3	29.0	78.1	78.7	33.1	76.8	76.7	33.5
1	29	79.9	78.1	33.3	40.7	41.8	30.6	.0	.0	.0	.0	.0	.0	.0	.0	.0
1	30	80.0	78.4	33.2	40.1	39.0	30.5	58.7	61.8	29.4	76.1	75.3	33.8	.0	.0	.0
1	31	79.3	78.9	33.5	43.7	40.5	30.6	56.5	58.2	29.8	77.0	76.1	34.1	76.7	76.8	34.4
1	32	80.0	77.9	33.2	38.7	37.3	30.5	58.4	58.7	29.6	75.6	77.1	33.8	76.3	76.8	33.7
1	33	80.1	77.5	33.1	43.1	37.1	30.5	.0	.0	.0	.0	.0	.0	.0	.0	.0
1	34	79.7	78.2	33.1	42.3	38.9	30.5	58.0	57.2	29.7	77.0	74.3	33.5	.0	.0	.0
1	35	79.7	78.6	33.3	42.0	39.7	30.5	61.0	56.8	29.6	76.2	75.7	33.6	77.2	75.8	33.8
1	36	79.2	78.3	33.3	36.4	38.7	30.6	57.8	60.8	29.9	76.6	75.0	33.9	76.3	76.4	33.7
1	37	79.5	77.1	33.2	34.8	37.2	30.7	.0	.0	.0	.0	.0	.0	.0	.0	.0
1	38	78.3	78.3	33.3	33.2	33.8	30.9	.0	.0	.0	.0	.0	.0	.0	.0	.0
1	39	80.3	78.3	33.6	36.8	34.9	30.8	.0	.0	.0	.0	.0	.0	.0	.0	.0
1	40	80.0	78.8	33.3	36.5	31.9	30.7	.0	.0	.0	.0	.0	.0	.0	.0	.0
1	69	76.9	77.1	33.6	32.6	34.7	31.6	.0	.0	.0	.0	.0	.0	.0	.0	.0
1	70	78.6	77.4	33.7	34.9	37.2	31.8	52.0	55.2	30.9	72.6	72.2	34.4	.0	.0	.0
1	71	75.8	77.0	33.8	37.3	35.3	31.8	54.1	57.8	30.9	72.1	71.7	34.7	73.0	73.5	35.0
1	72	78.9	78.6	33.5	37.0	35.0	31.5	58.1	56.8	30.6	72.6	73.3	34.0	72.7	72.7	34.5
1	77	79.3	78.3	33.5	37.2	39.2	31.4	.0	.0	.0	.0	.0	.0	.0	.0	.0
1	78	78.8	79.5	33.2	40.5	38.1	31.4	55.5	59.5	30.5	72.8	75.3	34.6	.0	.0	.0
1	79	79.2	79.2	33.7	39.7	41.8	31.6	55.0	56.4	30.8	72.0	72.3	34.5	74.0	71.3	34.7
1	80	79.5	78.5	33.7	39.0	41.3	31.8	60.6	59.2	31.0	69.3	69.0	35.3	72.7	72.8	35.0
1	93	79.9	79.3	33.6	40.3	38.9	31.6	.0	.0	.0	.0	.0	.0	.0	.0	.0
1	94	80.0	79.9	33.7	37.8	39.6	31.7	50.8	54.4	30.5	74.2	74.8	34.4	.0	.0	.0
1	95	81.6	80.0	33.7	7.2	35.5	31.8	53.5	56.1	30.9	72.3	72.2	34.3	74.8	73.8	34.7
1	96	80.0	79.0	33.5	39.7	37.0	31.6	54.7	58.6	30.6	72.7	72.9	33.9	74.2	74.8	34.6
1	81	77.9	77.6	33.3	32.1	35.3	32.9	.0	.0	.0	.0	.0	.0	.0	.0	.0
1	82	79.0	79.0	33.1	36.1	36.1	32.9	54.8	54.4	32.1	67.0	65.4	35.6	.0	.0	.0
1	83	79.2	79.0	33.3	36.1	33.1	32.9	52.5	52.0	32.3	66.2	68.0	35.1	71.0	68.6	33.8
1	84	79.0	80.0	33.2	37.1	36.0	32.8	57.8	54.3	32.1	70.0	68.0	35.6	71.7	71.8	35.1
1	85	79.0	77.6	33.2	32.3	26.2	34.1	.0	.0	.0	.0	.0	.0	.0	.0	.0
1	86	79.9	79.4	33.2	17.0	25.0	34.2	46.0	59.2	33.8	58.4	60.6	36.3	.0	.0	.0
1	87	79.1	79.8	33.2	31.8	30.3	34.1	48.1	50.5	33.7	60.4	62.0	36.2	63.2	62.4	37.8
1	88	79.8	80.1	33.1	18.2	24.6	34.1	47.0	45.6	33.9	61.0	60.8	36.0	61.3	61.5	36.5
1	109	80.0	79.3	33.1	.0	.0	.0	.0	.0	.0	.0	.0	.0	.0	.0	.0
1	110	80.8	80.9	33.1	23.7	24.8	34.9	41.3	46.7	34.4	58.8	56.2	36.8	.0	.0	.0

1	111	80.8	80.9	33.1	23.9	23.9	34.9	39.0	45.0	34.5	56.5	56.6	37.0	57.9	57.1	37.2
1	112	80.9	80.1	33.2	28.4	23.3	34.8	40.0	43.8	34.6	52.0	60.2	36.9	58.5	58.8	37.3
1	125	79.0	80.1	33.3	.0	.0	.0	.0	.0	.0	.0	.0	.0	.0	.0	.0
1	106	80.9	79.9	33.3	17.5	26.9	33.7	50.0	51.0	32.8	66.8	65.2	35.9	.0	.0	.0
1	107	80.1	79.9	33.2	27.3	25.8	33.7	49.2	46.6	33.0	68.0	69.2	35.7	66.3	66.8	38.3
1	108	79.2	80.4	33.2	26.5	25.0	33.7	50.0	50.1	33.0	68.0	[illegible].0	35.9	67.1	67.4	36.3
1	101	80.0	79.6	33.3	40.5	42.5	30.4	.0	.0	.0	.0	.0	.0	.0	.0	.0
1	102	81.9	80.1	33.2	41.1	43.4	30.5	54.3	58.8	29.8	78.0	79.0	33.7	.0	.0	.0
1	103	79.6	80.1	33.2	43.2	43.8	30.7	59.6	60.7	30.1	78.5	77.1	33.9	75.5	76.6	34.2
1	104	79.8	80.1	33.2	42.3	43.5	30.6	60.3	59.0	29.9	79.0	77.0	33.9	77.2	77.2	35.3
1	89	80.0	79.3	33.1	41.2	39.5	30.4	.0	.0	.0	.0	.0	.0	.0	.0	.0
1	90	80.0	79.9	33.0	40.8	44.2	30.2	60.3	58.3	29.6	78.0	79.1	32.9	.0	.0	.0
1	91	80.1	80.0	33.1	45.5	47.7	30.3	61.3	60.0	29.6	77.0	79.1	33.7	77.3	76.4	34.0
1	92	80.7	79.4	33.1	42.0	42.2	30.3	60.5	59.1	30.3	77.1	77.9	33.9	76.9	76.3	33.8
1	113	79.1	77.1	33.7	.0	.0	.0	.0	.0	.0	.0	.0	.0	.0	.0	.0
1	114	77.1	78.0	33.7	42.8	43.3	30.7	60.5	59.5	29.9	76.0	78.1	33.5	.0	.0	.0
1	115	79.6	79.0	33.5	41.0	40.7	30.6	60.0	60.0	29.9	77.1	79.2	33.7	78.9	79.1	33.8
1	116	79.2	79.0	33.5	39.2	39.3	30.7	55.0	60.5	29.9	79.1	78.4	33.2	78.2	79.0	33.8
1	117	79.5	78.6	33.3	.0	.0	.0	.0	.0	.0	.0	.0	.0	.0	.0	.0
1	118	78.0	78.1	33.3	40.8	40.2	30.4	57.6	55.0	29.6	80.1	73.4	33.0	.0	.0	.0
1	119	79.4	79.4	33.3	39.7	38.3	30.5	57.1	58.5	29.6	75.0	78.1	32.9	78.2	77.5	33.9
1	120	79.6	78.9	33.3	40.8	40.8	30.4	58.2	59.6	29.7	78.6	78.4	33.1	77.9	78.3	33.6
1	121	79.0	78.0	33.2	.0	.0	.0	.0	.0	.0	.0	.0	.0	.0	.0	.0
1	122	78.9	78.2	33.1	43.8	44.8	30.2	59.0	61.0	29.5	77.1	77.1	33.2	.0	.0	.0
1	123	79.5	79.5	33.0	41.2	42.7	30.2	58.5	48.3	29.5	79.2	79.4	33.0	77.7	77.3	33.7
1	124	79.0	79.0	33.1	43.5	44.2	30.4	62.0	64.1	29.6	79.2	80.4	33.5	77.8	78.3	33.4
1	125	79.0	78.1	33.0	35.3	37.2	30.6	58.6	58.4	29.7	80.0	76.1	33.7	.0	.0	.0
1	126	78.9	78.0	33.1	36.6	39.4	30.5	54.0	58.0	29.5	76.1	77.2	33.6	.0	.0	.0
1	127	78.8	79.0	33.1	37.5	36.8	30.6	58.3	62.0	29.8	75.6	80.3	32.6	77.7	78.0	33.8
1	128	78.6	79.1	33.3	33.8	36.2	30.5	59.0	61.4	29.6	78.5	79.7	33.3	77.6	78.0	33.8
1	129	79.2	78.4	33.8	34.3	34.1	32.1	.0	.0	.0	.0	.0	.0	.0	.0	.0
1	130	79.6	78.8	33.9	32.5	31.4	32.1	51.2	53.1	31.5	70.9	70.0	34.5	.0	.0	.0
1	131	79.4	78.8	33.9	32.2	31.9	32.2	52.8	49.7	31.6	67.7	68.2	34.5	71.7	70.2	.0
1	132	78.2	79.4	33.8	32.9	33.2	32.3	52.3	52.0	31.7	71.9	71.9	34.1	72.9	72.7	.0
1	133	79.0	78.1	33.6	.0	.0	.0	.0	.0	.0	.0	.0	.0	.0	.0	.0
1	134	78.0	77.2	33.6	28.8	29.4	33.8	49.3	48.4	33.4	67.0	67.2	36.0	.0	.0	.0
1	135	78.6	77.9	33.5	28.3	30.2	33.7	46.0	48.8	33.1	65.0	63.0	35.6	65.5	66.6	36.3
1	136	79.0	79.5	33.4	27.6	27.9	33.7	49.9	49.6	33.2	63.5	64.0	35.8	64.4	65.0	36.6

1	137	78.9	77.0	33.4	.0	.0	.0	.0	.0	.0	.0	.0	.0	.0	.0	.0
1	138	78.6	78.6	33.3	21.8	23.2	34.7	43.2	45.9	34.0	61.0	61.1	36.0	.0	.0	.0
1	139	78.0	79.0	33.3	20.3	25.4	34.6	46.0	45.0	34.0	59.0	60.5	35.9	60.0	60.5	36.3
1	140	78.9	78.8	33.3	21.2	23.4	34.7	44.2	42.0	34.1	58.0	61.1	36.3	61.6	61.0	36.5
1	141	78.9	78.8	33.3	36.0	37.3	30.2	.0	.0	.0	.0	.0	.0	.0	.0	.0
1	142	78.6	78.9	33.2	36.8	39.5	30.1	58.1	.0	29.4	78.5	79.9	32.6	.0	.0	.0
1	143	78.1	79.1	33.3	38.6	37.3	30.2	56.3	56.2	29.3	79.3	77.8	33.2	78.9	79.0	.0
1	144	78.6	78.9	33.4	39.5	38.3	30.3	58.4	57.1	29.5	77.0	77.3	33.1	76.8	77.3	.0
1	145	78.6	78.1	33.6	35.7	36.7	30.7	.0	.0	.0	.0	.0	.0	.0	.0	.0
1	146	78.7	77.8	33.5	37.5	37.1	30.8	60.5	59.2	30.4	80.0	77.6	33.7	.0	.0	.0
1	147	78.9	79.0	33.7	38.9	38.5	30.7	53.6	55.5	30.3	76.4	77.1	33.8	77.5	76.2	34.1
1	148	78.5	78.5	33.7	37.3	37.3	30.8	53.6	55.5	30.3	76.0	77.3	33.6	76.2	75.8	34.5
1	149	78.9	78.6	33.6	14.4	16.3	35.6	.0	.0	.0	.0	.0	.0	.0	.0	.0
1	150	78.0	78.9	33.6	14.4	17.4	35.6	35.0	34.2	35.6	51.8	52.2	37.3	.0	.0	.0
1	151	78.1	77.0	33.7	16.3	17.2	35.7	31.9	33.2	35.7	51.7	52.0	37.9	51.4	51.4	36.6
1	152	78.0	77.2	33.7	17.9	18.0	35.8	33.8	38.0	35.6	47.6	54.0	37.2	51.4	51.0	37.9
1	153	79.4	78.8	33.8	13.5	13.0	36.2	.0	.0	.0	.0	.0	.0	.0	.0	.0
1	154	78.9	78.1	33.7	6.5	8.0	36.1	33.9	32.5	36.3	43.0	45.5	37.8	.0	.0	.0
1	155	78.6	78.8	33.6	12.0	13.0	36.1	36.1	39.1	36.2	47.5	47.9	37.3	45.3	46.5	36.3
1	156	78.0	77.9	33.6	12.0	12.9	36.1	30.9	35.0	36.0	46.8	45.4	38.1	47.7	47.9	35.8
1	157	78.2	77.8	33.5	39.0	40.0	30.3	.0	.0	.0	.0	.0	.0	.0	.0	.0
1	158	78.7	78.1	33.4	35.8	36.0	30.1	57.3	57.2	29.7	76.2	78.4	33.2	.0	.0	.0
1	159	79.6	78.8	33.5	37.3	39.8	30.2	58.9	58.5	29.8	78.0	78.1	32.6	78.4	78.4	33.8
1	160	78.6	77.9	33.5	41.1	39.7	30.4	54.8	58.2	29.9	75.6	78.6	33.3	77.1	77.3	33.7
1	161	78.9	77.8	33.7	33.2	31.3	31.3	.0	.0	.0	.0	.0	.0	.0	.0	.0
1	162	78.0	78.0	33.9	33.3	32.7	31.2	56.2	54.5	30.6	77.0	76.0	33.7	.0	.0	.0
1	163	78.4	78.4	33.9	32.3	33.5	31.4	54.0	55.2	30.7	75.0	76.0	33.8	76.3	75.3	34.3
1	164	79.0	78.8	33.8	35.3	36.2	31.2	57.8	56.5	30.7	72.4	75.0	33.3	76.7	75.7	34.1
1	165	79.0	78.8	33.7	40.7	43.1	30.2	.0	.0	.0	.0	.0	.0	.0	.0	.0
1	166	78.0	78.0	33.8	34.1	34.0	30.3	53.8	61.2	29.7	78.1	75.6	33.5	.0	.0	.0
1	167	79.0	78.8	33.8	42.0	41.9	30.5	57.5	56.9	29.7	78.0	78.2	33.5	78.1	78.9	33.4
1	168	79.0	77.7	33.7	41.3	38.3	30.3	61.8	64.0	29.6	78.1	78.5	33.4	77.9	78.3	33.6
1	169	79.0	77.0	33.6	38.0	36.1	30.7	.0	.0	.0	.0	.0	.0	.0	.0	.0
1	170	78.4	76.0	33.5	39.0	36.1	30.6	60.5	57.4	29.9	78.4	76.9	33.4	.0	.0	.0
1	171	78.8	78.0	33.5	38.0	36.9	30.8	60.5	61.2	30.1	76.6	76.5	33.3	78.1	78.6	33.7
1	172	78.1	78.8	33.8	36.6	38.0	30.6	58.0	56.4	30.1	77.8	77.7	33.5	77.2	77.1	33.7
1	173	78.1	76.0	33.9	34.4	34.4	30.6	.0	.0	.0	.0	.0	.0	.0	.0	.0
1	174	78.1	78.0	33.9	34.5	34.0	31.0	55.0	59.6	30.5	78.5	77.2	.0	.0	.0	.0

1	175	78.0	78.4	33.9	33.0	33.5	30.9	53.9	59.4	30.4	78.0	79.0	.0	77.1	76.0	33.6
1	176	78.8	77.7	33.9	33.8	33.5	30.8	55.0	57.1	30.4	77.0	78.9	.0	78.5	76.6	33.6
1	177	75.0	78.1	33.8	34.0	35.0	30.9	.0	.0	.0	.0	.0	.0	.0	.0	.0
1	178	78.2	79.0	33.7	34.1	35.6	30.8	54.4	56.9	30.6	73.6	78.4	.0	.0	.0	.0
1	179	77.1	78.2	33.7	38.0	34.6	30.9	59.4	59.1	30.3	73.9	78.8	.0	77.0	75.7	33.7
1	180	77.6	78.0	33.7	36.5	35.7	31.2	55.2	55.1	30.6	74.1	77.0	.0	76.9	75.5	33.7
1	181	78.1	77.1	33.5	42.3	38.0	31.3	.0	.0	.0	.0	.0	.0	.0	.0	.0
1	182	77.7	77.0	33.5	45.0	40.0	31.5	61.0	58.9	31.1	72.4	75.0	.0	.0	.0	.0
1	183	77.6	78.4	33.6	45.1	38.0	31.5	57.8	57.1	31.4	71.2	77.0	.0	76.0	75.8	34.1
1	184	77.7	78.5	33.6	36.1	37.0	31.4	56.9	54.4	30.8	77.6	78.2	.0	75.6	72.0	33.9
1	185	78.0	78.0	33.5	37.0	35.2	30.8	.0	.0	.0	.0	.0	.0	.0	.0	.0
1	186	77.0	76.2	33.5	37.8	32.1	30.8	60.0	57.9	30.2	79.0	78.6	.0	.0	.0	.0
1	187	77.0	78.1	33.6	31.0	32.2	30.9	57.6	57.5	30.4	79.0	76.2	.0	78.2	77.1	33.8
1	188	77.8	78.9	33.8	33.0	33.1	30.9	54.0	55.5	30.2	76.5	78.0	.0	77.3	75.9	33.7
1	225	78.9	78.6	33.6	.0	.0	.0	.0	.0	.0	.0	.0	.0	78.3	78.2	32.7
1	226	78.0	79.0	33.5	.0	.0	.0	.0	.0	.0	.0	.0	.0	78.0	77.8	33.0
1	227	78.6	77.0	33.3	.0	.0	.0	.0	.0	.0	.0	.0	.0	77.5	77.8	32.5
1	228	79.0	79.5	33.4	.0	.0	.0	.0	.0	.0	.0	.0	.0	78.3	78.3	32.9
1	189	78.3	78.4	33.7	35.0	37.4	30.7	.0	.0	.0	.0	.0	.0	.0	.0	.0
1	190	78.0	77.8	33.8	38.6	36.0	30.7	.0	.0	.0	.0	.0	.0	.0	.0	.0
1	191	78.0	77.0	33.7	38.2	37.1	30.6	.0	.0	.0	.0	.0	.0	.0	.0	.0
1	192	78.0	78.2	33.7	35.5	39.6	30.7	.0	.0	.0	.0	.0	.0	.0	.0	.0
1	193	77.4	79.0	33.9	19.2	17.2	35.6	.0	.0	.0	.0	.0	.0	.0	.0	.0
1	194	78.4	78.4	33.8	19.9	19.6	35.6	40.1	42.0	35.6	56.0	54.0	.0	.0	.0	.0
1	195	78.5	78.4	33.8	15.2	14.0	35.6	42.2	41.0	35.5	52.2	55.0	.0	53.2	54.0	37.3
1	196	79.0	78.8	33.9	19.6	17.9	35.6	41.0	37.0	35.6	54.0	54.9	.0	52.4	52.7	37.4
1	197	78.2	78.0	33.9	41.2	36.9	30.6	.0	.0	.0	.0	.0	.0	.0	.0	.0
1	198	78.0	78.3	33.7	40.6	38.3	30.5	.0	.0	.0	.0	.0	.0	.0	.0	.0
1	199	79.0	78.6	33.6	37.2	38.1	30.5	.0	.0	.0	.0	.0	.0	.0	.0	.0
1	200	78.6	78.6	33.5	40.1	38.0	30.7	.0	.0	.0	.0	.0	.0	.0	.0	.0
1	201	78.0	78.4	33.6	22.0	19.1	35.6	.0	.0	.0	.0	.0	.0	.0	.0	.0
1	202	78.0	77.9	33.7	16.8	18.0	35.6	39.4	35.1	35.6	50.5	52.2	.0	.0	.0	.0
1	203	77.2	78.0	33.6	20.0	19.4	35.7	40.2	41.6	35.5	58.4	54.4	.0	51.2	49.0	37.4
1	204	78.0	78.0	33.7	19.0	17.1	35.6	38.5	38.1	35.5	52.8	52.9	.0	52.0	52.0	37.3
1	223	78.5	77.3	33.7	.0	.0	.0	.0	.0	.0	.0	.0	.0	.0	.0	.0
1	224	77.1	77.4	33.5	.0	.0	.0	.0	.0	.0	.0	.0	.0	.0	.0	.0
1	205	78.6	77.2	33.8	38.9	36.2	30.8	.0	.0	.0	.0	.0	.0	.0	.0	.0
1	206	78.8	77.4	33.8	37.6	32.2	30.6	56.0	58.9	30.0	79.5	76.8	.0	.0	.0	.0

1	207	78.9	77.4	33.8	37.0	35.3	30.8	62.5	59.4	30.2	77.3	77.3	.0	78.1	78.0	33.8
1	208	78.0	76.1	33.9	37.0	39.1	30.8	54.5	56.9	30.2	79.2	77.3	.0	77.6	78.8	33.7
1	209	76.4	78.5	33.9	38.5	37.3	30.6	.0	.0	.0	.0	.0	.0	.0	.0	.0
1	210	78.0	79.0	33.9	37.0	37.3	30.5	.0	.0	.0	.0	.0	.0	.0	.0	.0
1	211	77.2	78.0	33.7	38.7	37.5	30.6	.0	.0	.0	.0	.0	.0	.0	.0	.0
1	212	77.3	78.0	33.7	39.6	40.2	30.5	.0	.0	.0	.0	.0	.0	.0	.0	.0
1	213	78.5	78.0	33.8	39.0	39.0	30.5	.0	.0	.0	.0	.0	.0	.0	.0	.0
1	214	77.0	78.0	33.8	40.8	39.0	30.7	.0	.0	.0	.0	.0	.0	.0	.0	.0
1	215	78.4	78.6	33.7	40.0	39.0	30.6	59.3	63.9	30.0	79.2	80.0	33.3	.0	.0	.0
1	216	78.4	78.2	33.7	39.1	43.9	30.6	60.0	58.2	29.7	78.0	79.5	33.6	.0	.0	.0
1	217	75.3	78.6	33.8	39.1	41.0	30.4	58.4	60.7	29.8	.0	.0	.0	.0	.0	.0
1	218	78.0	77.9	33.8	42.0	39.9	30.7	60.2	61.7	29.8	.0	.0	.0	.0	.0	.0
1	219	79.0	78.0	33.8	38.4	37.4	30.7	60.3	58.7	29.8	.0	.0	.0	.0	.0	.0
1	220	78.0	77.9	33.9	39.1	38.1	30.5	59.9	63.1	29.7	.0	.0	.0	.0	.0	.0
2	221	78.0	77.9	33.9	34.5	38.8	31.6	.0	.0	.0	.0	.0	.0	.0	.0	.0
2	222	78.0	78.2	33.9	35.6	29.4	31.[illegible]	59.3	60.0	30.9	74.4	76.9	34.6	.0	.0	.0
2	229	78.1	78.0	33.8	33.2	37.6	31.6	58.0	57.1	30.9	75.0	75.1	34.4	77.0	74.8	34.2
2	230	78.0	77.9	33.7	34.5	34.5	31.6	55.8	56.2	31.0	75.1	74.2	34.2	76.1	76.2	34.9
2	231	78.0	79.5	33.7	32.6	28.4	33.5	52.9	52.2	33.0	67.0	67.2	35.9	.0	.0	.0
2	232	78.0	78.9	33.8	33.1	34.3	33.5	.0	.0	.0	.0	.0	.0	.0	.0	.0
2	233	78.4	78.9	33.7	25.1	35.8	33.5	53.8	48.3	33.1	68.6	67.0	36.0	68.5	68.9	36.1
2	239	78.0	78.3	33.7	36.2	36.1	33.6	54.3	52.1	33.0	66.4	67.1	36.4	68.0	66.0	36.3
2	240	78.3	78.4	33.8	30.0	31.1	35.4	.0	.0	.0	.0	.0	.0	.0	.0	.0
2	241	78.6	78.8	33.8	28.7	29.6	35.4	45.9	48.0	35.2	52.9	51.3	37.4	.0	.0	.0
2	242	78.0	78.9	33.9	24.6	27.0	35.4	47.1	47.0	35.3	54.4	53.0	37.1	55.0	53.6	37.8
2	248	77.6	78.5	34.0	29.2	27.0	35.4	48.5	48.0	35.5	55.0	55.8	37.6	56.0	56.3	38.0
2	249	78.7	77.9	33.9	33.2	31.4	32.3	.0	.0	.0	.0	.0	.0	.0	.0	.0
2	250	78.4	77.6	33.8	32.7	31.0	32.4	51.5	49.9	31.9	73.8	71.6	34.7	.0	.0	.0
2	251	77.4	77.4	33.8	31.1	31.2	32.4	52.0	52.3	32.1	70.8	72.0	34.9	71.6	72.1	35.0
2	252	78.5	78.7	33.7	33.0	30.4	32.4	48.1	50.6	32.1	71.0	72.9	35.0	72.9	72.7	35.9
2	253	76.8	77.7	33.7	26.0	24.3	33.9	.0	.0	.0	.0	.0	.0	.0	.0	.0
2	259	78.5	78.3	33.7	26.3	25.3	34.1	47.8	47.1	33.8	63.6	65.9	36.2	.0	.0	.0
2	260	78.4	77.5	33.8	25.8	28.0	33.9	51.0	49.5	33.7	65.4	67.4	36.3	65.6	64.9	36.4
2	261	78.1	78.0	33.8	25.9	27.0	34.0	48.0	44.8	33.8	66.1	64.7	36.4	64.2	64.3	36.4
2	234	78.9	77.8	33.7	45.0	47.2	32.6	.0	.0	.0	.0	.0	.0	.0	.0	.0
2	235	78.0	78.2	33.8	45.5	48.3	32.9	60.5	60.3	32.2	.0	.0	35.8	.0	.0	.0
2	236	78.0	78.6	33.6	48.0	45.[illegible]	32.3	58.1	61.1	32.3	.0	.0	35.2	71.4	68.0	35.0
2	237	78.6	78.0	33.5	54.0	49.0	32.6	61.2	58.4	32.3	.0	.0	35.3	64.9	70.2	35.4

2	243	78.1	78.0	33.6	49.1	49.0	34.8	.0	.0	.0	.0	.0	.0	.0	.0	.0
2	244	78.1	78.6	33.7	48.6	50.0	34.7	54.2	55.0	34.8	.0	.0	.0	.0	.0	.0
2	245	78.3	78.7	33.8	46.4	50.5	34.6	56.0	56.0	33.4	.0	.0	36.3	62.9	62.4	36.9
2	246	78.2	77.4	33.8	44.0	48.0	34.8	54.6	54.4	34.5	.0	.0	36.8	59.1	63.0	36.6
1	254	77.9	77.6	33.8	34.0	25.0	31.2	.0	.0	.0	.0	.0	.0	.0	.0	.0
1	255	78.3	78.6	33.8	38.0	35.2	31.2	51.0	54.2	30.7	72.0	75.0	34.6	.0	.0	.0
1	256	78.4	77.4	33.8	33.3	37.8	31.2	55.0	49.1	30.9	76.9	77.0	34.4	76.9	76.2	33.8
1	257	78.8	78.0	33.7	34.0	35.7	31.1	56.3	58.3	30.7	75.9	73.9	34.1	76.8	76.3	33.8
1	262	78.0	78.3	33.8	24.2	29.8	33.2	.0	.0	.0	.0	.0	.0	.0	.0	.0
1	263	77.2	77.3	33.8	31.0	29.0	33.3	47.8	49.6	33.2	63.8	66.9	35.9	.0	.0	.0
1	264	77.4	77.6	33.9	30.4	28.9	33.3	51.9	49.0	33.5	66.0	67.0	36.0	67.1	67.0	35.6
1	265	78.0	77.6	33.8	30.9	32.0	33.3	49.4	49.0	33.0	66.8	66.0	35.6	66.5	66.8	35.6
1	266	77.2	78.0	33.9	.0	.0	.0	.0	.0	.0	.0	.0	.0	.0	.0	.0
1	267	77.0	77.6	34.1	.0	.0	.0	.0	.0	.0	.0	.0	.0	.0	.0	.0
1	268	78.0	77.9	33.9	.0	.0	.0	.0	.0	.0	.0	.0	.0	.0	.0	.0
1	269	77.6	77.4	33.9	.0	.0	.0	.0	.0	.0	.0	.0	.0	.0	.0	.0
1	276	78.5	78.0	33.8	.0	.0	.0	.0	.0	.0	.0	.0	.0	.0	.0	.0
1	277	77.6	77.5	33.8	.0	.0	.0	.0	.0	.0	.0	.0	.0	.0	.0	.0
1	278	78.0	78.1	33.8	.0	.0	.0	.0	.0	.0	.0	.0	.0	.0	.0	.0
1	279	77.8	77.6	33.8	.0	.0	.0	.0	.0	.0	.0	.0	.0	.0	.0	.0
1	272	77.2	78.0	33.7	31.9	28.9	33.8	.0	.0	.0	.0	.0	.0	.0	.0	.0
1	278	73.4	78.0	33.7	29.0	29.0	33.7	46.1	54.0	33.7	.0	.0	35.7	.0	.0	.0
1	274	78.0	76.9	33.7	29.3	31.0	33.7	47.0	51.0	33.4	.0	.0	35.7	66.0	65.0	35.9
1	275	77.1	77.2	33.7	30.4	31.6	33.8	50.4	47.4	33.6	.0	.0	35.7	65.9	65.3	35.8
1	281	77.6	77.4	33.8	43.1	42.9	31.5	.0	.0	.0	.0	.0	.0	.0	.0	.0
1	282	77.6	78.1	33.7	42.6	43.8	31.3	60.5	58.0	30.7	.0	.0	33.6	.0	.0	.0
1	283	78.0	74.0	33.9	43.6	39.0	31.2	58.8	58.4	30.6	.0	.0	34.0	75.8	76.9	33.8
1	284	78.3	76.6	33.9	40.3	37.0	31.4	59.5	59.4	30.7	.0	.0	33.9	75.4	75.0	33.9
1	285	78.0	77.2	33.9	33.6	46.4	32.6	.0	.0	.0	.0	.0	.0	.0	.0	.0
1	286	78.1	77.9	33.9	39.7	42.6	32.3	56.0	56.9	32.2	71.6	73.6	35.1	.0	.0	.0
1	287	77.0	78.1	33.9	41.9	40.4	32.2	56.3	55.9	32.4	73.4	71.2	34.4	72.1	72.0	34.9
1	288	78.0	77.7	33.9	31.0	40.0	32.5	56.2	56.8	32.2	70.0	73.6	34.9	72.8	70.2	35.0
2	289	78.4	77.0	33.8	41.0	40.9	32.9	.0	.0	.0	.0	.0	.0	.0	.0	.0
2	290	77.1	78.0	33.9	42.0	34.5	32.9	56.8	55.0	32.5	68.1	70.8	35.0	.0	.0	.0
2	291	77.6	77.3	33.8	41.3	43.0	33.0	54.0	53.0	32.9	71.0	70.0	35.0	70.8	69.0	35.3
2	292	77.5	78.0	33.8	47.0	42.5	32.7	55.6	56.1	32.4	69.1	69.6	34.9	70.0	69.1	35.3
2	293	77.3	77.6	33.8	45.5	34.9	31.5	.0	.0	.0	.0	.0	.0	.0	.0	.0
2	294	78.0	77.0	33.9	41.0	41.9	31.3	63.3	63.7	30.8	73.0	71.0	34.1	.0	.0	.0

2	295	78.2	78.0	33.8	40.5	45.0	31.3	60.8	59.0	30.7	74.5	74.8	33.9	72.2	75.1	34.2
2	296	78.0	78.0	33.8	48.6	42.9	31.4	65.8	60.4	31.0	74.9	75.0	34.8	73.3	76.5	34.1
2	297	77.1	77.4	33.6	52.7	39.7	33.9	.0	.0	.0	.0	.0	.0	.0	.0	.0
2	298	77.6	78.0	33.8	47.8	55.8	33.5	65.8	63.8	33.1	67.8	68.0	35.7	.0	.0	.0
2	299	77.9	78.1	33.8	53.0	58.1	33.4	63.8	64.3	33.2	68.9	68.4	36.6	63.4	64.2	35.3
2	300	76.6	77.6	33.9	52.9	59.0	33.7	65.2	64.5	33.4	66.8	69.1	36.0	66.5	64.0	35.5
2	301	77.0	78.0	33.8	17.1	18.0	35.6	.0	.0	.0	.0	.0	.0	.0	.0	.0
2	302	77.5	78.0	33.9	14.2	21.1	35.7	42.2	43.4	35.7	55.7	53.8	37.7	.0	.0	.0
2	303	78.0	78.0	33.9	14.1	15.9	35.7	41.9	39.6	35.8	55.0	54.3	37.7	51.3	45.2	37.7
2	304	77.6	76.8	34.1	16.0	23.1	35.8	40.5	41.4	35.9	55.1	55.0	37.9	44.0	44.8	37.7
2	305	77.2	77.5	33.9	20.9	18.3	35.8	.0	.0	.0	.0	.0	.0	.0	.0	.0
2	306	77.5	77.2	33.9	18.0	18.6	35.6	36.5	37.4	35.6	55.6	58.2	37.5	.0	.0	.0
2	307	78.0	77.6	33.9	14.6	17.0	35.7	40.6	37.4	35.7	56.1	57.2	37.7	51.9	55.5	37.6
2	308	76.8	78.2	33.9	19.0	20.6	35.5	42.1	41.5	35.6	53.8	54.9	37.7	55.2	55.5	37.6
2	309	77.0	77.1	34.0	37.7	35.0	31.2	.0	.0	.0	.0	.0	.0	.0	.0	.0
2	310	77.9	78.3	34.0	33.8	32.4	31.3	55.1	57.8	30.6	76.8	76.8	33.5	.0	.0	.0
2	311	78.3	77.8	34.0	31.5	33.9	31.2	55.0	58.6	30.8	75.0	75.1	34.1	75.1	75.3	34.0
2	312	77.9	77.8	34.0	31.9	28.9	31.4	53.5	57.5	30.9	77.9	79.1	34.2	73.0	75.0	33.7
2	313	78.0	78.1	33.9	35.7	38.0	31.8	.0	.0	.0	.0	.0	.0	.0	.0	.0
2	314	78.0	73.0	33.9	29.9	32.9	31.9	60.7	59.8	31.4	75.0	70.5	34.8	.0	.0	.0
2	315	77.9	78.4	34.1	34.0	35.8	31.7	60.8	61.0	31.2	76.0	74.8	34.2	73.1	74.9	34.1
2	316	77.3	78.3	34.1	34.4	34.1	31.8	60.0	64.1	31.3	74.4	75.0	34.3	60.8	71.1	34.1
2	317	78.0	78.2	34.0	42.6	47.3	32.5	.0	.0	.0	.0	.0	.0	.0	.0	.0
2	318	77.9	78.2	34.0	41.6	44.8	32.6	58.5	60.8	32.4	72.0	70.3	34.9	.0	.0	.0
2	319	77.8	77.7	34.1	46.1	45.8	32.3	61.2	58.9	31.9	68.8	67.0	34.7	68.0	65.9	34.6
2	320	77.8	77.8	34.2	39.5	40.1	32.6	62.0	60.0	32.0	65.0	67.7	35.2	68.4	64.0	35.1
2	321	77.5	77.6	34.4	20.6	22.7	35.3	.0	.0	.0	.0	.0	.0	.0	.0	.0
2	322	77.4	78.2	34.4	21.8	26.0	35.3	42.3	45.0	35.0	56.0	56.4	37.3	.0	.0	.0
2	323	78.0	77.0	34.5	25.5	25.0	35.3	41.4	40.0	35.0	52.8	58.0	37.0	.0	.0	.0
2	324	77.9	78.0	34.3	22.3	22.2	35.3	44.0	46.0	35.1	57.9	56.5	37.1	.0	.0	.0
1	325	77.0	78.0	34.4	.0	.0	.0	.0	.0	.0	.0	.0	.0	.0	.0	.0
1	326	76.8	77.4	34.4	.0	.0	.0	.0	.0	.0	.0	.0	.0	.0	.0	.0
1	327	76.7	77.9	34.4	.0	.0	.0	.0	.0	.0	.0	.0	.0	.0	.0	.0
1	328	75.1	76.8	34.4	.0	.0	.0	.0	.0	.0	.0	.0	.0	.0	.0	.0
1	329	77.4	77.4	34.3	.0	.0	.0	.0	.0	.0	.0	.0	.0	.0	.0	.0
1	330	78.0	77.8	34.1	.0	.0	.0	.0	.0	.0	.0	.0	.0	.0	.0	.0
1	331	77.7	78.0	34.3	.0	.0	.0	.0	.0	.0	.0	.0	.0	.0	.0	.0
1	332	77.9	78.0	34.3	.0	.0	.0	.0	.0	.0	.0	.0	.0	.0	.0	.0

TABLE VII

Data for sequence A and sequence B heat treatments used to determine C curves for 2219-T87* in this report. The range between the solutionizing temperature (535°C) and 118°C was divided into 35 equal intervals. First given is a list of the bracketing temperatures. Next, sample numbers are given followed, on the same line, by the Rockwell B hardness, the conductivity in % IACS, the yield strength (0.2% offset) in ksi, the ultimate tensile strength in ksi, the % elongation and the % reduction in area, respectively. For each sample the following four lines give a list of times, in seconds, spent betwwen each of the temperatures listed, respectively. For sequence A alloys the cooling cycle from the solutionizing temperature was performed by a direct transfer from the solutionizing furnace to a salt bath and then to an ice water quench. For sequence B alloys a quench into ice water from the solutionizing temperature was followed by an immediate transfer to a salt bath at elevated temperature and then by another ice water quench.

```
TEMP RANGES
10 535.0 523.1 511.2 499.3 487.4 475.6 463.7 451.8 439.9 428.0
10 416.1 404.2 392.3 380.4 368.6 356.7 344.8 332.9 321.0 309.1
10 297.2 285.3 273.4 261.6 249.7 237.8 225.9 214.0 202.1 190.2
06 178.3 166.4 154.6 142.7 130.8 118.9
```

SEQUENCE A

```
11 76.4 34.3 52.6 64.8 10.8 17.6
     .2 .1 .1 .2 .2 .2 .3 .4 .3 .3
     .4 .4 .6 1. 1.8 27.6 .058 .058 .058 .058
     .058 .058 .058 .058 .058 .058 .058 .058 .058 .058
     .058 .058 .058 .058 .058
12  76.0 34.2 53.2 65.5 11.2 17.6
     .2 .1 .1 .2 .2 .2 .3 .4 .3 .3
     .4 .4 .6 1.0 1.8 27.6 .058 .058 .058 .058
     .058 .058 .058 .058 .058 .058 .058 .058 .058 .058
     .058 .058 .058 .058 .058
15  72.3 34.9 49.6 61.9 13.7 18.3
     .1 .1 .1 .1 .2 .2 .2 .2 .2 .4
     .4 .6 1.0 1.4 4.8 53.8 .03 .03 .03 .03
     .03 .03 .03 .03 .03 .03 .03 .03 .03 .03
     .03 .03 .03 .03 .03
16  69.5 35.4 47.8 61.6 15.4 19.2
     .1 .1 .1 .1 .2 .2 .2 .2 .2 .4
     .4 .6 1.0 1.4 4.8 53.8 .03 .03 .03 .03
     .03 .03 .03 .03 .03 .03 .03 .03 .03 .03
     .03 .03 .03 .03 .03
19  59.8 36.6 42.8 54.1 14.9 25.2
     .2 .2 .2 .2 .2 .3 .3 .3 .4 .5
     .5 .6 .9 3.0 7.0 110.4 .0263 .0263 .0263 .0263
     .026 .026 .026 .026 .026 .026 .026 .026 .026 .026
     .026 .026 .026 .026 .026
20 64.3 35.9 45.9 58.4 13.9 20.0
     .2 .2 .2 .2 .2 .3 .3 .3 .4 .5
     .5 .6 .9 3.0 7.0 110.4 .026 .026 .026 .026
     .026 .026 .026 .026 .026 .026 .026 .026 .026 .026
     .026 .026 .026 .026 .026
23  47.1 37.9 35.1 47.5 15.7 21.3
     .2 .2 .2 .3 .2 .3 .3 .4 .4 .5
     .5 .6 1. 2. 17. 279.2 .3 .3 .3 .3
     .03 .03 .03 .03 .03 .03 .03 .03 .03 .03
     .03 .03 .1 .04 .06
24  44.0 37.7 35.7 47.5 13.9 23.4
     .2 .2 .2 .3 .2 .3 .3 .4 .4 .5
     .5 .6 1.0 2.0 17.0 279.2 .03 .03 0.3 .03
     .03 .03 .03 .03 .03 .03 .03 .03 .03 .03
     .03 .03 .1 .04 .06
31 76.5 34.1 54.1 67.3 10.8 19.3
     1.2 .2 .1 .14 .16 .2 .2 .2 .2 .2
     .32 .28 .34 .28 .4 .4 .6 1.0 1.4 10.6
     40.8 .033 .033 .033 .033 .033 .033 .033 .033 .033
     .033 .033 .033 .1 .1
```

```
32  76.4 33.8 54.5 67.4  9.1 16.1
     1.2 .2 .1 .14 .16 .2 .2 .2 .2 .2
     .32 .28 .34 .28 .4 .4 .6 1.0 1.4 10.6
     40.8 .033 .033 .033 .033 .033 .033 .033 .033 .033
     .033 .033 .033 .1 .1
35  75.9 33.6 54.3 68.0  9.7 19.3
     .1 .1 .1 .1 .2 .2 .1 .2 .2 .2
     .2 .2 .2 .3 .4 .4 .5 .8 1.2 3.0
     51.4 .03 .03 .03 .03 .03 .03 .03 .03 .03
     .03 .03 .03 .08 .12
36  75.8 33.8 53.9 67.6  8.9 14.3
     .1 .1 .1 .1 .2 .2 .1 .2 .2 .2
     .2 .2 .2 .3 .4 .4 .5 .8 1.2 3.0
     51.4 .03 .03 .03 .03 .03 .03 .03 .03 .03
     .03 .03 .03  .08 .12
27 77.3 33.3 54.8 68.7 10.8 12.2
     .8 .3 .12 .18 .1 .2 .12 .16 .2 .2
     .3 .26 .34 .4 .4 .6 1. 1.2 3.4 9.2
     .034 .034 .034 .034 .034 .034 .034 .034 .034 .034
     .034 .034 .034 .1 .1
28     78.4 33.0 56.1 70.1 8.7 12.4
     .8 .3 .12 .18 .1 .2 .12 .16 .2 .2
     .3 .26 .34 .4 .4 .6 1.0 1.2 3.4 9.2
     .034 .034 .034 .034 .034 .034 .034 .034 .034 .034


     .034 .034 .034 .1 .1
71     72.3 34.7 51.2 63.7 12.5 19.6
     .6 .8 1. 1. 1.2 3.2 24.4 .02 .02 .02
     .02 .02 .02 .02 .02 .02 .02 .02 .02 .02
     .02  .02 .02 .02 .02 .02 .02 .02 .02 .02
     .02 .02 .02 .02 .02
72     73.0 33.9 51.7 64.8  8.2 19.3
     .6 .8 1. 1. 1.2 3.2 24.4 .02 .02 .02
     .02 .02 .02 .02 .02 .02 .02 .02 .02 .02
     .02 .02 .02 .02 .02 .02 .02 .02 .02 .02
     .02 .02 .02 .02 .02
79     74.1 34.5 49.4 62.8 10.9 16.4
     .4 .2 .2 .1 .1 .1 .1 .2 .2 .2
     .4 .2 .4 .6 .7 1.3 1.3 1.4 2.4 109.4
     .1 .036 .036 .036 .036 .036 .036 .036 .036 .036
     .036 .036 .036 .036 .03
80     72.3 34.4 51.0 64.4 11.7 12.7
     .4 .2 .2 .1 .1 .1 .1 .2 .2 .2
     .4 .2 .4 .6 .7 1.3 1.3 1.4 2.4 109.4
     .1 .036 .036 .036 .036 .036 .036 .036 .036 .036
     .036 .036 .036 .036 .036
95  72.2 34.3 51.1 64.0 13.3 28.0
     .5 .6 .6 .6 .6 .4 .8 1.0 1.2 1.6
     4.0 6.4 .02 .02 .02 .02 .02 .02 .02 .02
     .02 .02 .02 .02 .02 .02 .02 .02 .02 .02
     .02 .02 .02 .02 .02
96  72.8 33.9 53.0 66.6 13.1 16.8
     .5 .6 .6 .6 .6 .4 .8 1.0 1.2 1.6
     4.0 6.4 .02 .02 .02 .02 .02 .02 .02 .02
     .02 .02 .02 .02 .02 .02 .02 .02 .02 .02
     .02 .02 .02 .02 .02
```

```
83  67.1 35.1 47.0 59.2 13.2 25.2
     .3 .3 .4 .6 .6 .8 1.0 1.4 1.6 3.0
     6.0 20.0 .02 .02 .02 .02 .02 .02 .02 .02
     .02 .02 .02 .02 .02  .02 .02 .02 .02 .02
     .02 .02 .02 .02 .02
84  69.0 35.7 48.6 60.8 10.3 21.5
     .3 .3 .4 .6 .6 .8 1.0 1.4 1.6 3.0
     6.0 20.0 .02 .02 .02 .02 .02 .02 .02 .02
     0.02 .02 .02 .02 .02 .02 .02 .02 .02 .02
     .02  .02 .02 .02 .02
87  61.2 36.2 44.1 55.7 12.0 20.6
     .4 .4 .6 .6 .8 .8 1.0 1.2 2.0 2.4
     14.4 54.4 .02 .02 .02 .02 .02 .02 .02 .02
     0.02 0.02 .02 .02 .02 .02 .02 .02 .02 .02
     0.02 0.02 .02 .02 .02
88  60.9 36.0 42.8 54.1 12.4 25.3
     .4 .4 .6 .6 .8 .8 1.0 1.2 2.0 2.4
     14.4 54.4 .02 .02 .02 .02 .02 .02 .02 .02
     0.02 0.02 .02 .02 .02 .02 .02 .02 .02 .02
     0.02 0.02 .02 .02 .02
111 56.6 36.9 41.3 51.6 13.1 29.0
     .22 .5 .7 .8 1.4 2.2 15.6 108.4 .03 .03
     .03 .03 .03 .03 .03 .03 .03 .03 .03 .03
     .03 .03 .03 .03 .03 .03 .03 .03 .03 .03
     .03 .03 .03 .03 .03
112 56.1 36.8 41.8 52.6 12.4 16.9
     .22 .5 .7 .8 1.4 2.2 15.6 108.4 .03 .03
     .03 .03 .03 .03 .03 .03 .03 .03 .03 .03
     .03 .03 .03 .03 .03 .03 .03 .03 .03 .03
     .03 .03 .03 .03 .03
107 68.6 35.7 46.3 57.3 12.8 21.7
     .22 .5 .7 .8 1.4 2.2 15.6 45.0 .03 .03
     .03 .03 .03 .03 .03 .03 .03 .03 .03 .03
     .03 .03 .03 .03 .03 .03 .03 .03 .03 .03
     .03 .03 .03 .03 .03
108 67.5 35.9 46.8 57.7 14.0 18.8
     .22 .5 .7 .8 1.4 2.2 15.6 45.0 .03 .03
     .03 .03 .03 .03 .03 .03 .03 .03 .03 .03
     .03 .03 .03 .03 .03 .03 .03 .03 .03 .03
     .03 .03 .03 .03 .03
103 78.5 33.7 54.4 67.7  9.9 13.5
     .2 .2 .1 .1 .1 .1 .1 .2 .6 .4
     .6 .3 .3 .6 .6 2.0 0.03 .03 .03 .03
     .03 .03 .03 .03 .03 .03 .03 .03 .03 .03
     .03 .03 .03 .03 .03
104 77.8 33.9 53.9 67.1  9.2 15.9
     .2 .2 .1 .1 .1 .1 .1 .2 .6 .4
     .6 .3 .3 .6 .6 2.0 .03 .03 .03 .03
     .03 .03 .03 .03 .03 .03 .03 .03 .03 .03
     .03 .03 .03 .03 .03
91  78.1 33.7 54.5 67.4  9.4 19.4
     .1 .3 .1 .1 .1 .2 .5 .7 .5 .1
     2.1 .025 .025 .025 .025 .025 .025 .025 .025 .025
     .025 .025 .025 .025 .025 .025 .025 .025 .025 .025
     .025 .025 .025 .025 .025
```

```
92  77.5 33.8 53.7 66.7 11.3 16.8
     .1 .3 .1 .1 .1 .2 .5 .7 .5 .1
     2.1 .025 .025 .025 .025 .025 .025 .025 .025 .025
     .025 .025 .025 .025 .025 .025 .025 .025 .025 .025
     .025 .025 .025 .025 .025
115 78.2 33.7 54.1 67.6 7.7  19.6
     .1 .1 .1 .1 .1 .1 .1 .1 .2 .2
     .2 .2 .2 .3 .6 1.5 .03 .03 .03 .03
     .03 .03 .03 .03 .03 .03 .03 .03 .03 .03
     .03 .03 .03 .03 .03
116 78.8 33.2 54.7 68.4  9.5 14.7
     .1 .1 .1 .1 .1 .1 .1 .1 .2 .2
     .2 .2 .2 .3 .6 1.5 .03 .03 .03 .03
     .03 .03 .03 .03 .03 .03 .03 .03 .03 .03
     .03 .03 .03 .03 .03
119 76.6 32.9 54.4 68.4  8.7 11.9
     .1 .04 .1 .1 .2 .2 .1 .2 .3 .3
     .2 .6 2.5 .018 .018 .018 .018 .018 .018 .018
     .018 .018 .018 .018 .018  .018 .018 .018 .018 .018
     .018 .018 .018 .018 .018
120 78.5 33.1 55.0 67.9 10.1 19.2
     .1 .04 .1 .1 .2 .2 .1 .2 .3 .3
     .2 .6 2.5 .018 .018 .018 .018 .018 .018 .018
     .018 .018 .018 .018 .018 .018 .018 .018 .018 .018
     .018 .018 .018 .018 .018
123 79.3 33.0 54.5 68.4 10.2 12.1
     .2 .1 .1 .1 .1 .1 .1 .1 .1 .2
     .2 .2 .2 .2 .2 .3 .3 .3 .4 .4
     1.2 1.6 .03 .03 .03 .03 .03 .03 .03 .03
     .03 .03 .03 .03 .03
124 79.8 33.4 54.4 68.4  9.1 12.5
     .2 .1 .1 .1 .1 .1 .1 .1 .1 .2
     .2 .2 .2 .2 .2 .3 .3 .3 .4 .4
     1.2 1.6 .03  .03 .03 .03 .03 .03 .03 .03
     .03 .03 .03 .03 .03
127 78.0 33.1 55.2 68.7  7.5 12.4
     .2 .1 .1 .1 .1 .1 .1 .1 .1 .2
     .2 .2 .2 .2 .2 .3 .3 .3 .4 .4
     .4 .4 .4 .8 1. 1. 2.2 4.4 .057 .057
     .057 .057 .057 .057 .057
128 79.1 33.3 54.7 68.3  9.5 11.5
     .2 .1 .1 .1 .1 .1 .1 .1 .1 .2
     .2 .2 .2 .2 .2 .3 .3 .3 .4 .4
     .4 .4 .4 .8 1. 1. 2.2 4.4 .057 .057
     .057 .057 .057 .057 .057
131 67.9 34.5 51.2 64.6 11.3 14.0
     .3 .5 .8 1.1 2.4 2.2 2.2 5.6 21.6 .023
     .023 .023 .023 .023 .023 .023 .023 .023 .023 .023
     .023 .023 .023 .023 .023 .023 .023 .023 .023 .023
     .023 .023 .023 .023 .023
132 71.9 34.0 50.9 63.5  7.8 15.1
     .3 .5 .8 1.1 2.4 2.2 2.2 5.6 21.6 .023
     .023 .023 .023 .023 .023 .023 .023 .023 .023 .023
     .023 .023 .023 .023 .023 .023 .023 .023 .023 .023
     .023 .023 .023 .023 .023
135 64.0 35.6 45.5 56.8 12.3 24.7
     .2 .2 .4 .6 2. 1.8 2.8 13.8 44.4 .015
     .015 .015 .015 .015 .015 .015 .015 .015 .015 .015
     .015 .015 .015 .015 .015 .015 .015 .015 .015 .015
     .015 .015 .015 .015 .015
```

```
136 63.7 35.8 44.5 55.5 13.6 25.0
     .2 .2 .4 .6 2. 1.8 2.8 13.8 44.4 .015
     .015 .015 .015 .015 .015 .015 .015 .015 .015 .015
     .015 .015 .015 .015 .015 .015 .015 .015 .015 .015
     .015 .015 .015 .015 .015
139 59.7 35.8 44.1 54.4 13.5 15.0
     .1  .1 .6 .6 1. 1.2 1.8 6.4 112. .038
     .038 .038 .038 .038 .038 .038 .038 .038 .038 .038
     .038 .038 .038 .038 .038 .038 .038 .038 .038 .038
     .038 .038 .038 .038 .038
140 59.5 36.3 42.0 52.8 16.2 21.4
     .1 .1 .6 .6 1. 1.2 1.8 6.4 112.0 .038
     .038 .038 .038 .038 .038 .038 .038 .038 .038 .038
     .038 .038 .038 .038 .038 .038 .038 .038 .038 .038
     .038 .038 .038 .038 .038
143 78.6 33.2 55.8 69.8  9.9 17.8
     .1 .03 .03 .03 .03 .03 .03 .03 .03 .03
     .03 .03 .03 .03 .03 .03 .03 .03 .03 .03
     .03 .03 .03 .03 .03 .03 .03 .03 .03 .03
     .03 .03 .03 .03 .03
144 77.2 33.0 55.1 69.0  8.7 17.6
     0.1 .03 .03 .03 .03 .03 .03 .03 .03 .03
     .03 .03 .03 .03 .03 .03 .03 .03 .03 .03
     .03 .03 .03 .03 .03 .03 .03 .03 .03 .03
     .03 .03 .03 .03 .03
147 76.8 33.8 53.9 67.4  9.8 16.1
     .1 .4 .5 .6 1. 1. 1.9 4.4 9.4  .03
     .03 .03 .03 .03 .03 .03 .03 .03 .03 .03
     .03 .03 .03 .03 .03 .03 .03 .03  .03 .03
     .03 .03 .03 .03 .03
148 76.2 33.5 53.7 67.6  9.8 16.9
     .1 .4 .5 .6 1. 1. 1.9 4.4 9.4  .03
     .03 .03 .03 .03 .03 .03 .03 .03 .03 .03
     .03 .03 .03 .03 .03 .03 .03 .03 .03 .03
     .03 .03 .03 .03 .03
151 51.9 37.9 37.6 47.1 14.2 27.0
     .22 .5 .7 .8 1.4 2.2 59.6 242. .8 .017
     .017 .017 .107 .107 .017 .017 .017 .017 .017 .017
     .017 .017 .017 .017 .017 .017 .017 .017 .017 .017
     .017 .017 .017 .017 .017
152 50.8 37.2 37.9 48.0 12.6 26.9
     .22 .5 .7 .8 1.4 2.2 59.6 242.0 .8 .017
     .017 .017 .017 .017 .017 .017 .017 .017 .017 .017
     .017 .017 .017 .017 .017 .017 .017 .017 .017 .017
     .017 .017 .017 .017 .017
155 47.7 37.3 35.8 45.4 15.7 35.7
     .3 .7 .7 .9 1. 3.9 601.7 .03 .03 .03
     .03 .03 .03 .03 .03 .03 .03 .03 .03 .03
     .03 .03 .03 .03 .03 .03 .03 .03 .03 .03
     .03 .03 .03 .03 .03
156 46.1 38.1 35.8 45.5 15.3 29.6
     .3 .7 .7 .9 1. 3.9 601.7 .03 .03 .03
     .03 .03 .03 .03 .03 .03 .03 .03 .03 .03
     .03 .03 .03 .03 .03 .03 .03 .03 .03 .03
     .03 .03 .03 .03 .03
```

```
159 78.0 32.4 56.3 70.3 11.0 20.7
     .4 .9 1.8 3.0 55.7 .02 .02 .02 .02 .02
     .02 .02 .02 .02 .02 .02 .02 .02 .02 .02
     .02 .02 .02 .02 .02 .02 .02 .02 .02 .02
     .02 .02 .02 .02 .02
160 77.1 33.3 53.8 66.3 14.1 26.3
     .4 .9 1.8 3.0 55.7 .02 .02 .02 .02 .02
     .02 .02 .02 .02 .02 .02 .02 .02 .02 .02
     .02 .02 .02 .02 .02 .02 .02 .02 .02 .02
     .02 .02 .02 .02 .02
163 75.5 33.8 52.2 64.4  9.3 19.6
     .9 4.1 598.4 .04 .04 .04 .04 .04 .04 .04
     .04 .04 .04 .04 .04 .04 .04 .04 .04 .04
     .04 .04 .04 .04 .04 .04 .04 .04 .04 .04
     .04 .04 .04 .04 .04
164 73.7 33.3 54.1 66.8  9.7 15.0
     .9 4.1 598.4 .04 .04 .04 .04 .04 .04 .04
     .04 .04 .04 .04 .04 .04 .04 .04 .04 .04
     .04 .04 .04 .04 .04 .04 .04 .04 .04 .04
     .04 .04 .04 .04 .04
167 78.1 33.5 55.1 68.7 0.0 14.7
     .4 .1 .1 .1 .1 .1 .1 .1 .1 .2
     .1 .3 .2 .3 .3 .4 .4 .4 .5 .8
     .1 1.4 2.8 6.4 .227 .227 .227 .227 .227 .227
     .227 .227 .227 .227 .227
168 78.3 33.4 54.8 68.3 10.4 16.5
     .4 .1 .1 .1 .1 .1 .1 .1 .1 .2
     .1 .3 .2 .3 .3 .4 .4 .4 .5 .8
     .1 1.4 2.8 6.4 .227 .227 .227 .227 .227 .227
     .227 .227 .227 .227 .227
171 76.5 33.3 54.8 67.4 11.7 21.0
     .2 .1 .1 .1 .2 .3 .1 .3 .2 .3
     .4 .3 .4 .4 .5 .7 .7 .8 1.0 1.7
     2.6 5.0 16.5 .25 .25 .25 .25 .25 .25 .25
     .25 .25 .25 .25 .25
172 77.7 33.5 56.4 70.0 7.2 8.0
     .2 .1 .1 .1 .2 .3 .1 .3 .2 .3
     .4 .3 .4 .4 .5 .7 .7 .8 1.0 1.7
     2.6 5.0 16.5 .25 .25 .25 .25 .25 .25 .25
     .25 .25 .25 .25 .25
175 78.5 33.6 53.5 67.1 11.3 17.6
     .1 .1 .1 .1 .2 .2 .1 .2 .2 .2
     .2 .2 .3 .3 .4 .4 .4 .4 .6 .8
     1.0 1.8 2.8 6.4 42.4 .045 .045 .045 .045 .045
     .045 .045 .045 .045 .045
176 77.9 33.5 54.7 68.6 10.4 14.8
     .1 .1 .1 .1 .2 .2 .1 .2 .2 .2
     .2 .2 .3 .3 .4 .4 .4 .4 .6 .8
     1. 1.8 2.8 6.4 42.4 .045 .045 .045 .045 .045
     .045 .045 .045 .045 .045
179 76.5 33.7 53.2 66.4 9.0 21.5
     .1 .1 .1 .1 .2 .2 .1 .1 .2 .2
     .1 .2 .3 .2 .4 .4 .4 .4 .6 .8
     1. 1.8 2.8 6.4 281.8 .15 .15 .15 .15 .15
     .15 .15 .15 .15 .15
```

```
180 76.0 33.7 52.6 66.0 9.8 14.1
     .1 .1 .1 .1 .2 .2 .1 .1 .2 .2
    .1 .2 .3 .2 .4 .4 .4 .4 .6 .8
    1. 1.8 2.8 6.4 281.8 .15 .15 .15 .15 .15
    .15 .15 .15 .15 .15
183 75.9 34.1 49.6 63.5 11.9 13.5
    .1 .1 .1 .1 .1 .2 .1 .2 .2 .2
    .1 .2 .3 .3 .5 .4 .5 .6 .7 .9
    1.1 1.6 2.8 3.0 588.4 .03 .03 .03 .03 .03
    .03 .03 .03 .03 .03
184 73.5 33.9 51.8 64.8 9.0 16.5
    .1 .1 .1 .1 .1 .2 .1 .2 .2 .2
    .1 .2 .3 .3 .5 .4 .5 .6 .7 .9
    1.1 1.6 2.8 3.0 588.4 .03 .03 .03 .03 .03
    .03 .03 .03 .03 .03
264  66.5  35.9  48.0  60.5   9.0  16.3
    .2 .2 .3 .3 .2 .3 .3 .3 .4 .5
    .8 1. 3.0 56.6 .04 .04 .04 .04 .04 .04
    .04 .04 .04 .04 .04 .04 .04 .04 .04 .04
    .04 .04 .04 .04 .04
265  66.4  35.9  48.0  60.5   9.0  16.3
    .2 .2 .3 .3 .2 .3 .3 .3 .4 .5
    .8  1. 3. 56.6 .04 .04 .04 .04 .04 .04
    .04 .04 .04 .04 .04 .04 .04 .04 .04 .04
    .04 .04 .04 .04 .04
256  76.9  34.3  54.4  68.6   7.9   7.7
    .1 .1 .2 .1 .2 .2 .3 .4 .4 .6
    1. 2.4 11.8 .02 .02 .02 .02 .02 .02 .02
    .02 .02 .02 .02 .02 .02 .02 .02 .02 .02
    .02 .02 .02 .02 .02
257  74.9  34.1  54.8  68.7  8.0  14.0
    .1 .1 .2 .1 .2 .2 .3 .4 .4 .6
    1. 2.4 11.8 .02 .02 .02 .02 .02 .02 .02
    .02 .02 .02 .02 .02 .02 .02 .02 .02 .02
    .02 .02 .02 .02 .02
291  70.5  35.2  48.8  62.4   9.0  16.3
    .2 .2 .2 .1 .2 .2 .1 .1 .2 .2
    .2 .2 .1 .2 .2 .3 .3 .4 .4 .8
    1.6 1.2 2.0 3670. .06 .06 .06 .06 .06 .06
    .06 .06 .06 .06 .06
292  69.4  34.9  49.3  62.4   8.8  13.4
    .2 .2 .2 .1 .2 .2 .1 .1 .2 .2
    .2 .2 .1 .2 .2 .3 .3 .4 .4 .8
    1.6 1.2 2.0 3670. .06 .06 .06 .06 .06 .06
    .06 .06 .06 .06 .06
207  77.3  33.7  54.1  67.4  12.1  19.0
    .6 1. 1. 1.6 5.4 7.6 .09 .09 .09 .09
    .09 .09 .09 .09 .09 .09 .09 .09 .09 .09
    .09 .09 .09 .09 .09 .09 .09 .09 .09 .09
    .09 .09 .09 .09 .09
208  77.8  33.6  55.0  68.9  12.7  16.8
    .6 1. 1. 1.6 5.4 7.6 .09 .09 .09 .09
     .09 .09 .09 .09 .09 .09 .09 .09 .09 .09
     .09 .09 .09 .09 .09 .09 .09 .09 .09 .09
     .09 .09 .09 .09 .09
```

```
287  72.3  34.4  50.2  62.3   8.0  12.8
     .1 .1 .2 .1 .1 .1 .2 .1 .1 .1
     .1 .2 .2 .2 .1 .3 .3 .3 .4 .6
     .6 1.2 4.0 1790.5 .04 .04 .04 .04 .04 .04
     .04 .04 .04 .04 .04
288  72.3  34.4  49.2  61.1   7.6  21.7
     .1 .1 .2 .1 .1 .1 .2 .1 .1 .1
     .1 .2 .2 .2 .1 .3 .3 .3 .4 .6
     .6 1.2 4.0 1790.5 .04 .04 .04 .04 .04 .04
     .04 .04 .04 .04 .04
```

SEQUENCE B

```
229  75.1  34.4  51.8  65.5  10.9  17.0
     .046 .046 .046 .046 .046 .046 .046 .046 .046 .046
     .046 .046 9.25 1.65 0.94 0.75 0.45 0.45 .045 0.35
     0.45 0.25 0.45 0.25 0.25 0.15 0.25 0.25 0.15 0.15
     0.15 0.15 0.25 0.15 0.25
230  7[illegible].7  34.2  52.8  64.8   9.5  16.5
     0.045 .045 .045 .045 .045 .045 .045 .045 .045 .045
     .046 .046 9.25 1.65 .94 .75 .45 .45 .45 .35
     .45 .25 .45 .25 .25 .15 .25 .25 .15 .15
     .15 .15 .25 .15 .15
233  68.8  36.0  46.7  58.6   9.7  22.5
     .026 .026 .026 .026 .026 .026 .026 .026 .026 .026
     .026 .026 27.8 1.65 1.15 .55 .55 .55 .45 .45
     .35 .45 .35 .35 .25 .25 .25 .25 .15 .25
     .15 .25 .25 .15 .35
239  66.8  36.4  47.1  59.5   9.8  15.5
     .026 .026 .026 .026 .026 .026 .026 .026 .026 .026
     .026 .026 27.75 1.65 1.15 .55 .55 .55 .45 .45
     .35 .45 .35 .35 .25 .25 .25 .25 .15 .25
     .15 .25 .25 .15 .35
203  56.4  37.4  38.4  48.4  13.3  28.1
     .02 .02 .02 .02 .02 .02 .02 .02 109.75 1.653
     1.05 .86 .65 .65 .45 .69 1.09 .99 .99 .79
     .69 .79 .59 .59 .59 .59 .59 .49 .59 .49
     .29 .29 .19 .19 .19
204  52.9  37.3  37.8  47.7  15.9  27.5
     .02 .02 .02 .02 .02 .02 .02 .02 109.75 1.65
     1.05 .85 .65 .65 .45 .69 1.05 .99 .99 .79
     .69 .79 .59 .59 .59 .59 .49 .59 .49 .49
     .29 .29 .19 .19 .19
195  53.6  37.2  38.1  48.7  14.0  26.0
     .03 .03 .03 .03 .1 .1 .1 50.1 70.0 1.44
     1.53 .73 .53 .63 .33 .43 .43 .63 .63 .63
     .53 .53 .73 .73 .93 1.23 2.23 9.43 .03 .03
     .03 .03 .03 .03 .03
196  53.6  37.2  38.1  48.7  14.0  26.0
     .03 .03 .03 .03 .1 .1 .1 50.1 70. 1.44
     1.53 .73 .53 .63 .33 .43 .43 .63 .63 .63
     .53 .53 .73 .73 .93 1.23 2.23 9.43 .03 .03
     .03 .03 .03 .03 .03
```

```
295  74.7 33.9  53.5  67.1  10.2  16.4
     .03 .03 .03 .03 .03 .03 .03 .03 .03 .03
     .03 .03 .03 .03 .03 .03 .03 .03 .03 .03
     .03 .03 .03 .03 670.07 3.67 1.47 .97 .77 .77
     .57 .57 .57 .67 .57
296  75.0 33.9  55.4  67.3   8.8  16.5
     .03 .03 .03 .03 .03 .03 .03 .03 .03 .03
     .03 .03 .03 .03 .03 .03 .03 .03 .03 .03
     .03 .03 .03 .03 670.07 3.67 1.47 .97 .77 .77
     .57 .57 .57 .67 .57
299  68.6  36.2  48.2  62.3   7.0  10.1
     .02 .02 .02 .02 .02 .02 .02 .02 .02 .02
     .02 .02 .02 .02 .02 .02 .02 .02 .02 .02
     .02 .02 .02 .02 1930.06 2.96 1.16 .86 .66 .46
     .45 .45 .45 .55 .55
300  66.9  35.9  47.1  62.1   9.6  11.5
     .02 .02 .02 .02 .02 .02 .02 .02 .02 .02
     .02 .02 .02 .02 .02 .02 .02 .02 .02  .02
     .02 .02 .02 .02 1930.06 2.96 1.16 .86 .66 .46
     .45 .45 .45 .55 .55
303  54.6  37.4  38.9  49.6  14.2  20.8
     .03 .03 .03 .03 .03 .03 .03 88.26 2.26 1.86
     2.26 1.66 1.06 .86 .66 .46 .46 .46 .46 .36
     .36 .26 .26 .26 .26 .16 .26 .16 .16 .16
     .16 .26 .16 .26 .26
304  55.0  37.6 38.6  49.3  14.9  25.3
     .03 .03 .03 .03 .03 .03 .03 .03 88.26 2.26 1.86
     2.26 1.66 1.06 .86 .66 .46 .46 .46 .46 .36
     .36 .26 .26 .26 .26 .16 .26 .16 .16 .16
     .16 .26 .16 .26 .26
307  59.7  37.4  39.8  49.6  12.1  27.6
     .03 .03 .03 .03 .03 .03 .03 117.66 1.96 .86
     .66 .46 .46 .46 .56 .66 .56 .46 .36 .36
     .36 .26 .26 .25 .26 .16 .16 .16 .16 .16
     .16 .16 .16 .16 .16
308  54.4  37.3  39.6  50.5  12.1  23.7
     .03 .03 .03 .03 .03 .03 .03 117.66 1.96 .86
     .66 .46 .46 .46 .56 .66 .56 .46 .36 .36
     .36 .26 .26 .26 .26 .16 .16 .16 .16 .16
     .16 .16 .16 .16 .16
242  53.7  37.1  38.3  52.6  10.0  20.1
     .06 .06 .06 .06 .06 .06 .06 .06 .06 .06
     .06 .06 79.30 6.50 1.70 .90 .79 .59 .49 .49
     .4 .3 .3 .3 .3 .3 .3 .3 .3 .3
     .3 .3 .3 .3 .3
248  55.4  37.6  40.3  52.8  11.8  15.5
     .06 .06 .06 .06 .06 .06 .06 .06 .06 .06
     .06 .06 72.3 6.5 1.7 .9 .8 .6 .5 .5
     .4 .3 .3 .3 .3 .3 .3 .3 .3 .3
     .3 .3 .3 .3 .3
260  66.4  36.3  46.4  58.1  10.9  13.7
     .03 .03 .03 .03 .03 .03 .03 .03 25.97 1.87
     1.27 .97 .57 .57 .47 .37 .37 .37 .27 .27
     .27 .17 .27 .17 .17 .17 .17 .17 .17 .16
     .27 .17 .17 .27 .17
```

```
261  66.4  36.3  46.4  58.1  10.9  13.7
     .03 .03 .03 .03 .03 .03 .03 .03 25.97 1.87
      1.27 .97 .57 .47 .47 .37 .37 .37 .27 .27
     .27 .17 .27 .17 .17 .17 .17 .17 .17 .17
      .27 .17 .17 .27 .17
251  71.4  34.9  50.8  63.1  13.0  21.3
     .03 .03 .03 .03 .03 .03 .03 .03 11.68 1.68
     1.08 .68 .48 .48 .38 .38 .48 .28 .28 .18
     .28 .18 .28 .18 .18 .18 .18 .18 .18 .18
     .18 .18 .18 .18 .18
252  71.9  35.0  49.4  61.6  14.5  27.3
     .03 .03 .03 .03 .03 .03 .03 .03 11.68 1.68
     1.08 .68 .48 .48 .38 .38 .48 .28 .28 .18
     .28 .18 .28 .18 .18 .18 .18 .18 .18 .18
     .18 .18 .18 .18 .18
274   66.0  35.9  48.0  59.9  12.2  19.1
      .03 .03 .03 .03 .03 .03 20.78 3.68 1.38 .98
     .58 .48 .48 .38 .38 .38 .28 .28 .28 .28
     .18 .28 .18 .28 .28 .18 .18 .18 .18 .28
     .18 .18 .18 .18 .18
275  65.9  35.8  47.6  59.2  11.7  23.1
     .03 .03 .03 .03 .03 .03 20.78 3.68 1.38 .98
     .58 .48 .48 .38 .38 .38 .28 .28 .28 .28
     .18 .28 .18 .28 .28 .18 .18 .18 .18 .18
     .18 .18 .18 .18 .18
283  76.9  34.0  55.1  69.0   7.9  10.5
     0.3 .03 .03 .03 .03 .03 .03 .03 .03 .03
     .03 .03 .03 .03 .03 .03 22.58 7.28  1.68 1.08
     .78 .48 .58 .48 .58 .58 .38 .28 .28 .28
     .28 .18 .28 .28 .28
284  75.4  33.9  55.2  68.9   6.8  12.0
     .03 .03 .03 .03 .03 .03 .03 .03 .03 .03
     .03 .03 .03 .03 .03 .03 22.58 7.28 1.68 1.08
      .78 .48 .58 .48 .58 .58 .38 .28 .28 .28
     .28 .18 .28 .28 .28
236  71.4  35.1  48.0  60.9   8.6  13.9
     .04 .04 .04 .04 .04 .04 .04 .04 .04 .04
     .04 .04 .04 .04 .04 .04 53.38 3.08 1.59 .88
     .88 .78 .58 .48 .98 1.18 1.08 1.08 .78 .78
     .58 .48 .38 .38 .28
237  70.2  35.3  49.3  62.6   7.5  13.7
     .04 .04 .04 .04 .04 .04 .04 .04 .04 .04
     .04 .04 .04 .04 .04 .04 53.38 3.08 1.59 .88
     .88 .78 .58 .48 .98 1.18 1.08 1.08 .78 .78
     .58 .48 .38 .38 .28
245  62.9  36.5  43.8  56.7   8.9  13.1
     .04 .04 .04 .04 .04 .04 .04 .04 .04 .04
     .04 .04 .04 .04 .04 .04 117.79 3.09 1.29 1.09
     .59 .59 .49 .49 .49 .79 .79 .69 .49 .39
     .39 .29 .29 .19 .29
246  63.0  36.8  43.3  57.1   9.6  20.4
      .04 .04 .04 .04 .04 .04 .04 .04 .04 .04
     .04 .04 .04 .04 .04 .04 117.79 3.09 1.29 1.09
     .59 .59 .49 .49 .49 .79 .79 .69 .49 .39
     .39 .29 .29 .19 .29
```

```
215  79.6  33.3  57.0  70.3  14.5  17.5
      .03 .03 .03 .03 .03 .03 .03 .03 .03 .03
     .03 .03 .03 .03 .03 .03 .03 .03 .03 .03
     .03 .03 .03 .03 .03 .03 .03 .03 .03 .03
     .03 .03 .03 .03 .03
216  78.7  33.4  56.6  69.9  11.4  17.4
     .03 .03 .03 .03 .03 .03 .03 .03 .03 .03
     .03 .03 .03 .03 .03 .03 .03 .03 .03 .03
     .03 .03 .03 .03 .03 .03 .03 .03 .03 .03
     .03 .03 .03 .03 .03
311  75.0  31.9  54.3  67.9   8.6  12.6
     .03 .03 .03 .03 .03 .03 .03 .03 .03 .03
     .03 .03 .03 .03 .03 .03 .03 .03 .03 .03
     54.6 2.16 .96 .76 .56 .46 .36 .36 .26 .36
     .26 .26 .26 .26 .26
312  78.5  32.5  54.2  67.7   9.3  14.5
     .03 .03 .03 .03 .03 .03 .03 .03 .03 .03
     .03 .03 .03 .03 .03 .03 .03 .03 .03 .03
     54.6 2.16 .96 .76 .56 .46 .36 .36 .26 .26
     .26 .26 .26 .26 .26
315  75.4  33.5  52.8  65.7   8.7  13.4
     .03 .03 .03 .03 .03 .03 .03 .03 .03 .03
     .03 .03 .03 .03 .03 .03 .03 .03 .03 .03
     115.28 4.48 1.58 .98 .78 .68 .48 .78 .48 .48
     .28 .28 .28 .28 .28
316  74.7  34.5  52.2  66.0   8.2  13.5
     .03 .03 .03 .03 .03 .03 .03 .03 .03 .03
     .03 .03 .03 .03 .03 .03 .03 .03 .03 .03
     115.28 4.48 1.58 .98 .78 .68 .48 .78 .48 .48
     .28 .28 .28 .28 .28
319  67.9  34.9  49.5  62.8   7.9  16.0
     .03 .03 .03 .03 .03 .03 .03 .03 .03 .03
     .03 .03 .03  03 .03 .03 .03 .03 .03 .03
     232.57 6.27 1.57 .87 .77 .57 .47 .47 .37 .37
     .57 .87 .57 .47 .27
320  66.4  35.5  50.2  63.3   8.4  13.6
     .03 .03 .03 .03 .03 .03 .03 .03 .03 .03
     .03 .03 .03 .03 .03 .03 .03 .03 .03 .03
     232.57 6.27 1.57 .87 .77 .57 .47 .47 .37 .37
     .57 .87 .57 .47 .27
```

TABLE VIII

C curve parameters for aluminum alloy 2219-T87*

Property	Sequence	σ_m	σ_o	K_2 sec	K_3 cal/mol	K_4 °K	K_5 cal/mol	est. std. dev.
Hardness, HRB	A	79.0	46.0	$.86 \times 10^{-10}$	320	900	32,000	2.2
Yield Strength (0.2% offset) ksi	A	55.3	35.4	$.78 \times 10^{-10}$	320	900	32,000	1.5
Tensile Strength ksi	A	69.0	45.1	$.79 \times 10^{-10}$	320	900	32,000	1.7
Conductivity % IACS	A	33.2	37.7	$.59 \times 10^{-10}$	320	900	32,000	0.4
Hardness, HRB	B	80.6	53.6	$.28 \times 10^{-7}$	200	900	25,000	1.9
Yield Strength (0.2% offset) ksi	B	56.5	35.7	$.37 \times 10^{-7}$	200	900	25,000	1.4
Tensile Strength ksi	B	69.5	45.4	$.43 \times 10^{-7}$	200	900	25,000	1.3
Conductivity % IACS	B	32.3	37.4	$.17 \times 10^{-7}$	200	900	25,000	0.4

TABLE IX

Parameters obtained for C curve fits to hardness data for varying values of K_5. (K_5 was chosen and kept fixed while the other parameters were adjusted to obtain a minimum least squares deviation).

σ_m HRB	σ_o HRB	K_2 Sec	K_3 cal/mole	K_4 K	K_5 cal/mole	est. std. dev.
79.2	46.0	$.41 \times 10^{-8}$	240	892	28,000	2.5
79.0	44.9	$.43 \times 10^{-9}$	330	905	30,000	2.2
79.0	46.0	$.78 \times 10^{-10}$	320	900	32,000	2.2
78.5	41.1	$.56 \times 10^{-11}$	335	886	35,000	2.2
78.3	39.3	$.12 \times 10^{-11}$	335	881	37,000	2.2
78.4	40.4	$.23 \times 10^{-13}$	595	921	40,000	2.2
78.1	40.0	$.48 \times 10^{-14}$	570	919	42,000	2.3

Table X. Specimens Examined by Means of Electron Microscopy

Specimen #	Condition
-	As cast 10:1 reduction ingot
879-55†	As-received T851
879-26†	532°C-75min → Quenched 0°C
879-35†	532°C-75min → Quenched 0°C → Age 177°C-18h
1†	532°C-75min → Quenched 0°C → stretched 2 1/4%
1A†	Reprocessed T851
6†	532°C-75min → 350°C-15s → Quenched 0°C
-	As-received T87*
37	535°C-75min → 450°C-15s → Quenched 0°C
69	535°C-75min → 450°C-30s → Quenched 0°C
81	536°C-75min → 400°C-30s → Quenched 0°C
85	535°C-75min → 400°C-60s → Quenched 0°C
86	535°C-75min → 400°C-60s → Quenched 0°C → Stretched 5% → Age 172°C-16h
93	537°C-75min → 400°C-15s → Quenched 0°C
94	537°C-75min → 400°C-15s → Quenched 0°C → Stretched 5% → Age 172°C-16h
105	538°C-75min → 450°C-60s → Quenched 0°C
106	538°C-75min → 450°C-60s → Quenched 0°C → Stretched 5% → Age 172°C-16h
142	Reprocessed T87*
146	535°C-75min → 450°C-15s → Quenched 0°C
150	535°C-75min → 450°C-300s → Quenched 0°C → Stretched 5% → Age 172°C-16h
197	536°C-75min → Quenched 0°C
231	535°C-75min → Quenched 0°C → 400°C-30s → Quenched 0°C → Stretched 5% → Age 172°C-16h
232	535°C-75min → Quenched 0°C → 400°C-30s → Quenched 0°C

249	535°C-75min → Quenched 0°C → 450°C-15s → Quenched 0°C
250	535°C-75min → Quenched 0°C → 400°C-30s → Quenched 0°C → Stretched 5% → Age 172°C-16h
253	535°C-75min → Quenched 0°C → 450°C-30s → Quenched 0°C
322	537°C-75min → Quenched 0°C → 450°C-60s → Quenched 0°C → Stretched 5% → Age 172°C-16h
-	2219 F temper

† Initial material T851 1 1/2" plate

TABLE XI

Hardness of Several Sequence A and B specimens After Completing the T87* Temper.

Specimen	Quench Treatment	† Hardness after T87* Treatment
#197 (Fig. 73a)	quenched directly to 0°C	79.0±0.96 HRB
#93 (Fig. 73b)	sequence A, 400°C-15s	73.2±1.1
#81 (Fig. 73c)	sequence A, 400°C-30s	67.3±1.8
#85 (Fig. 73d)	sequence A, 400°C-60s	60.5±1.2
#69 (Fig. 74 a&b)	sequence A, 450°C-30s	72.4±0.55
#249 (Fig. 79a)	sequence B, 450°C-15s	72.0±1.2
#253 (Fig. 79b)	sequence B, 450°C-30s	65.6±1.4
#232 (Fig. 79c)	sequence B, 400°C-30s	67.2±0.73

†These hardness values were obtained from companion specimens given the same quench treatments as those indicated in the left hand column.

TABLE XII

List of data obtained on round robin samples.

Column 1: Lab number

Column 2: Sample heat treatment code

1 = sequence A (5% stretch)
2 = sequence B (5% stretch)
3 = sequence A (no stretch)
4 = sequence A (2-1/2% stretch)

Column 3: Sample number

Column 4: Yield strength in MPa (0.2% offset) as measured at NBS

Column 5: Ultimate tensile strength in MPa as measured at NBS

Columns 6-11: Hardness measurements, Rockwell B

Columns 12-14: Conductivity measurements, % IACS

1	2	3	4	5	6	7	8	9	10	11	12	13	14
1	4	005	338	440	75.1	77.4	77.6	77.8	78.2	77.5	34.35	34.49	34.46
1	1	014	336	426	72.2	73.3	71.5	71.2	72.1	71.9	34.57	34.71	34.76
1	1	018	304	385	65.9	65.8	66.5	66.0	65.5	65.9	35.49	35.53	35.48
1	1	026	387	483	78.0	78.4	78.4	78.0	79.1	78.0	33.50	33.33	33.32
1	1	034	000	000	78.2	77.1	78.0	78.8	78.0	78.0	33.49	33.53	33.48
1	1	038	000	000	71.9	73.3	73.0	73.0	72.5	73.5	34.18	34.14	34.41
1	1	070	355	443	72.4	74.0	73.6	74.5	74.3	74.5	34.14	34.41	34.41
1	1	102	374	465	78.8	78.9	79.5	78.6	78.6	79.2	33.16	33.39	33.36
1	1	110	287	359	58.1	59.6	59.0	60.0	59.7	60.8	36.56	36.65	36.60
1	1	118	377	470	80.1	80.0	79.6	78.9	79.0	79.4	33.21	33.32	33.33
1	1	122	376	472	78.9	79.6	79.5	78.7	78.3	79.0	33.34	33.37	33.42
1	1	158	379	471	79.1	78.1	79.1	78.2	79.6	78.4	33.29	33.46	33.33
1	1	170	383	474	78.9	79.5	79.1	79.1	78.8	79.1	33.22	33.52	33.40
1	1	174	373	469	78.1	77.8	77.8	78.2	78.5	77.9	33.46	33.59	33.59
1	1	178	365	456	77.5	78.1	77.1	78.2	78.2	78.1	33.46	33.70	33.54
1	2	202	263	331	51.5	51.9	51.0	50.7	49.6	52.2	37.39	37.18	37.22
1	1	206	376	470	78.0	77.0	78.5	79.0	79.0	78.9	33.35	33.31	33.17
1	2	222	376	449	76.4	76.1	76.5	76.1	75.9	75.5	34.41	34.24	34.39
1	2	235	335	426	70.9	71.1	71.8	71.1	74.3	74.2	35.02	34.99	34.92
1	2	241	271	363	55.2	56.5	56.1	54.0	55.4	56.2	37.30	37.32	37.29
1	1	255	376	473	77.2	77.1	77.0	77.0	76.8	77.0	33.78	33.81	33.89
1	2	259	320	402	64.9	66.5	65.9	64.7	64.0	65.0	36.09	36.18	36.18
1	1	263	332	419	68.0	68.0	69.0	69.0	69.0	67.8	35.48	35.48	35.40
1	2	273	330	411	67.8	67.1	67.7	67.8	67.0	67.6	35.62	35.66	35.64
1	3	276	235	388	64.6	65.0	65.0	64.8	65.0	65.0	33.82	33.97	34.12
1	1	290	339	431	72.0	70.8	71.5	70.8	71.2	72.0	34.78	34.92	34.82
1	2	302	267	341	55.8	56.2	55.7	54.1	54.2	54.0	37.27	37.28	37.28
1	2	310	374	467	76.8	77.4	77.0	77.7	78.0	78.0	33.22	33.45	33.46
1	2	323	000	000	56.0	55.2	56.7	56.9	54.5	56.0	36.93	37.04	36.96
1	2	324	000	000	56.0	55.5	56.1	55.5	54.2	56.9	37.00	36.96	36.98
2	4	005	338	440	75.1	75.7	75.8	76.8	76.4	77.1	34.50	34.50	34.60
2	1	014	336	426	72.7	75.2	73.4	72.2	72.6	72.2	34.70	35.00	35.00
2	1	018	304	385	66.2	66.2	65.8	67.7	67.2	66.7	35.80	35.60	35.60
2	1	026	387	483	79.4	79.4	80.5	78.3	78.7	79.8	33.00	33.25	33.40
2	1	034	000	000	79.5	79.8	80.9	78.2	79.0	80.5	33.25	33.30	33.40
2	1	038	000	000	74.8	74.5	74.2	75.1	74.8	74.2	34.40	34.00	34.25

2	1	070	355	443	75.0	75.3	75.8	76.5	75.2	75.3	34.40	34.50	34.00
2	1	102	374	465	79.8	80.2	79.8	79.5	79.5	79.9	33.40	33.25	33.10
2	1	110	287	359	61.1	60.3	61.5	60.3	61.9	62.8	36.75	36.75	36.80
2	1	118	377	470	80.7	80.5	80.1	80.8	80.9	81.5	33.30	33.20	33.20
2	1	122	376	472	79.5	79.1	79.9	79.1	79.1	78.8	33.20	33.10	33.30
2	1	158	379	471	80.0	80.3	80.7	80.8	79.8	81.1	33.25	33.40	33.50
2	1	170	383	474	79.2	80.2	79.9	79.3	80.0	80.3	33.50	33.70	33.60
2	1	174	373	469	78.2	79.3	79.3	78.3	79.2	80.1	33.75	33.60	33.50
2	1	178	365	456	77.9	78.3	78.1	78.2	78.8	78.4	33.50	33.50	33.00
2	2	202	263	331	51.9	51.8	54.4	54.2	54.5	53.4	37.40	37.40	37.40
2	1	206	376	470	79.9	80.0	80.2	80.8	79.8	81.2	33.40	33.20	33.20
2	2	222	361	449	77.5	77.4	77.4	77.0	77.6	77.6	34.50	34.40	34.60
2	2	235	335	426	71.7	72.7	73.8	71.8	68.9	69.1	35.10	35.00	35.20
2	2	241	271	363	56.2	56.3	56.7	55.8	56.3	55.4	37.50	37.50	37.50
2	1	255	376	473	77.8	79.1	78.9	78.8	78.6	78.9	34.10	33.60	33.75
2	2	259	320	402	63.5	64.9	63.9	65.1	65.5	65.8	36.40	36.40	36.30
2	1	263	332	419	69.8	68.7	69.8	69.8	69.9	69.5	35.40	35.40	35.50
2	2	273	330	411	68.2	68.8	68.9	67.1	67.9	68.9	35.80	35.60	35.25
2	3	276	235	388	66.6	65.6	66.2	66.3	66.6	66.2	34.40	34.00	33.90
2	1	290	339	431	73.2	73.7	72.0	73.1	72.8	74.5	34.70	34.80	34.80
2	2	302	267	341	56.0	58.0	55.9	56.0	55.7	56.1	37.50	37.50	37.50
2	2	310	374	467	78.5	78.9	78.0	78.9	78.4	79.8	33.70	33.40	33.40
2	2	323	000	000	57.7	58.2	58.3	57.8	58.0	56.0	37.10	37.10	37.00
2	2	324	000	000	57.1	58.1	59.2	56.9	57.2	57.9	37.20	37.10	37.20
3	4	005	338	440	79.7	77.2	78.0	77.4	77.7	76.1	34.40	34.50	34.60
3	1	014	336	426	75.0	74.9	76.1	73.0	73.2	72.5	35.20	35.10	35.00
3	1	018	304	385	69.6	69.5	69.4	69.1	67.5	68.6	36.00	35.70	35.90
3	1	026	387	483	80.1	80.6	79.7	80.9	80.1	79.7	33.50	33.60	33.70
3	1	034	000	000	80.5	80.2	80.7	80.5	80.2	78.9	33.60	33.50	33.70
3	1	038	000	000	76.3	76.2	75.0	76.2	76.2	75.7	34.60	34.60	34.60
3	1	070	355	443	75.0	76.1	76.5	77.7	76.1	76.5	34.60	34.80	34.30
3	1	102	374	465	79.9	80.5	80.2	79.9	80.0	81.0	33.80	33.60	34.00
3	1	110	287	359	64.1	64.3	63.5	62.0	62.6	62.1	36.50	36.50	36.40
3	1	118	377	470	82.1	81.1	80.5	81.1	81.6	81.1	33.30	33.30	33.30
3	1	122	376	472	80.0	81.0	80.5	80.2	81.6	80.5	33.60	33.40	33.60
3	1	158	379	471	81.5	81.7	81.3	81.9	80.6	80.8	33.40	33.60	33.50
3	1	170	383	474	79.9	81.0	80.1	80.9	81.1	79.5	33.60	33.70	33.60
3	1	174	373	469	79.5	81.5	79.9	81.6	81.0	80.1	33.50	33.70	33.50

3	1	178	365	456	79.8	79.1	79.5	80.2	80.0	80.0	33.40	33.70	33.60
3	2	202	263	331	56.0	55.5	55.0	55.8	56.2	56.0	37.30	37.40	37.50
3	1	206	376	470	80.5	81.3	81.0	80.6	81.2	81.5	33.40	33.50	33.40
3	2	222	361	449	78.3	78.3	79.3	77.5	77.8	77.3	34.60	34.60	34.70
3	2	235	335	426	75.9	74.0	77.5	77.0	74.0	77.2	35.20	35.10	34.80
3	2	241	271	363	59.5	58.7	59.0	59.2	57.0	59.5	37.20	37.10	37.10
3	1	255	376	473	78.9	78.9	79.5	78.7	79.1	79.5	33.80	33.90	33.60
3	2	259	320	402	68.5	67.5	68.2	67.0	68.0	68.5	36.20	36.40	36.30
3	1	263	332	419	70.0	70.5	70.7	70.5	70.5	70.7	35.60	35.50	35.40
3	2	273	330	411	68.2	69.5	69.5	69.0	71.5	70.0	35.50	35.60	35.50
3	3	276	235	388	67.5	67.1	66.5	67.3	66.5	67.5	34.20	34.00	34.00
3	1	290	339	431	74.0	73.8	74.0	74.5	75.0	74.0	34.90	34.90	34.90
3	2	302	267	341	59.0	57.7	57.2	58.0	57.5	57.5	36.10	36.00	36.10
3	2	310	374	467	81.0	79.5	79.2	81.0	79.7	79.5	33.50	33.50	33.50
3	2	323	000	000	57.9	61.3	59.8	61.1	59.5	61.2	37.00	36.90	36.90
3	2	324	000	000	60.0	60.0	60.0	59.1	59.0	59.1	37.00	37.00	37.00
4	4	005	338	440	75.3	75.8	73.4	76.4	75.1	75.2	34.60	34.60	34.90
4	1	014	336	426	72.1	72.8	73.5	71.4	71.4	73.0	35.20	35.20	35.10
4	1	018	304	385	65.9	67.3	65.3	66.6	67.1	66.2	36.20	35.80	36.20
4	1	026	387	483	78.3	79.4	78.6	77.9	77.8	77.7	33.40	33.70	33.70
4	1	034	000	000	78.5	78.6	78.6	78.7	78.5	78.7	33.60	33.40	33.50
4	1	038	000	000	74.2	74.3	74.8	75.4	75.5	75.3	34.60	34.50	34.50
4	1	070	355	443	75.9	75.3	75.9	76.2	75.7	75.7	34.50	34.70	34.20
4	1	102	374	465	79.4	79.1	79.8	78.7	78.7	79.0	33.40	33.60	33.60
4	1	110	287	359	60.7	61.6	61.2	61.2	61.7	62.5	36.70	37.00	36.80
4	1	118	377	470	79.2	79.7	80.1	79.6	79.7	79.7	33.70	33.40	33.50
4	1	122	376	472	79.6	79.6	80.1	79.5	79.9	79.2	33.60	33.30	33.50
4	1	158	379	471	79.2	79.1	79.2	79.5	79.2	80.2	33.40	33.50	33.50
4	1	170	383	474	79.8	79.3	79.0	78.9	79.2	79.0	33.60	33.70	33.50
4	1	174	373	469	79.1	79.3	78.7	79.2	79.4	79.4	33.60	33.90	33.70
4	1	178	365	456	78.2	78.4	78.0	78.7	78.7	79.3	33.80	33.90	33.60
4	2	202	263	331	53.5	52.9	53.8	54.9	54.3	54.7	37.60	37.60	37.70
4	1	206	376	470	78.8	79.0	79.4	78.9	79.8	79.3	33.40	33.50	33.50
4	2	222	361	449	76.6	76.3	77.4	76.8	76.5	77.3	34.80	34.50	3[illegible].50
4	2	235	335	426	73.1	72.8	74.8	72.9	71.6	67.5	35.40	35.60	35.10
4	2	241	271	363	55.9	56.8	57.7	55.3	55.7	55.7	37.70	37.60	37.70
4	1	255	376	473	78.8	77.1	77.3	77.9	77.6	78.1	34.00	34.10	34.10
4	2	259	320	402	65.8	66.1	65.7	65.9	66.1	66.6	36.60	36.60	36.60

4	1	263	332	419	68.7	69.0	69.7	69.0	69.6	68.6	35.60	35.70	35.60
4	2	273	330	411	68.6	68.1	69.3	68.4	67.8	67.3	35.80	35.90	35.90
4	3	276	235	388	65.6	65.8	65.7	65.7	65.4	65.9	34.40	34.20	34.10
4	1	290	339	431	71.9	72.5	72.0	66.8	72.9	72.9	34.90	35.10	35.00
4	2	302	267	341	55.7	57.2	56.9	56.3	57.4	54.5	37.60	37.60	37.60
4	2	310	374	467	77.5	78.4	79.2	79.4	78.7	77.0	33.60	33.70	33.60
4	2	323	000	000	58.6	57.8	57.6	58.3	57.7	57.2	37.40	37.30	37.30
4	2	324	000	000	58.6	58.9	58.0	56.0	57.6	56.9	37.40	37.30	37.40
5	4	005	338	440	74.5	74.5	75.0	76.0	76.0	77.0	34.01	34.10	34.20
5	1	014	336	426	73.5	73.0	73.0	71.5	73.0	72.0	34.50	34.50	34.80
5	1	018	304	385	65.5	65.5	67.0	67.5	67.5	67.5	35.00	35.00	35.10
5	1	026	387	483	79.5	79.0	79.5	78.0	80.0	78.0	32.80	32.80	32.80
5	1	034	000	000	78.5	79.0	79.0	78.5	78.5	79.0	32.95	32.95	32.95
5	1	038	000	000	75.0	74.5	74.5	75.0	74.5	75.0	34.00	34.00	33.90
5	1	070	355	443	75.5	76.0	74.0	75.0	76.0	75.5	34.05	33.95	33.95
5	1	102	374	465	79.5	79.5	80.0	79.5	79.5	79.5	32.90	32.70	32.80
5	1	110	287	359	61.5	60.5	62.0	62.0	62.0	62.0	36.40	36.10	36.10
5	1	118	377	470	79.5	80.0	80.0	80.5	80.5	79.5	32.90	32.80	32.80
5	1	122	376	472	80.0	79.5	79.5	79.0	79.0	79.0	32.90	32.50	32.80
5	1	158	379	471	80.0	79.5	79.5	79.5	79.5	80.0	32.80	32.60	33.10
5	1	170	383	474	80.0	80.0	80.0	78.5	79.5	79.5	33.00	32.95	32.90
5	1	174	373	469	79.0	80.0	79.0	79.0	79.5	79.5	33.10	33.05	33.10
5	1	178	365	456	79.5	79.5	79.0	79.0	79.0	79.0	32.95	33.00	33.00
5	2	202	263	331	53.0	52.0	56.0	54.5	54.5	55.5	37.00	37.00	37.00
5	1	206	376	470	79.5	79.5	80.5	78.5	79.5	80.0	32.60	32.80	32.70
5	2	222	376	449	77.5	78.0	78.5	77.5	77.5	77.0	33.80	33.80	33.80
5	2	235	335	426	74.0	74.0	75.0	75.5	75.5	73.5	34.50	34.60	34.80
5	2	241	271	363	59.0	58.0	59.0	58.5	58.5	58.0	37.05	37.00	37.00
5	1	255	376	473	77.5	79.0	78.0	78.5	78.5	78.0	33.00	33.00	33.00
5	2	259	320	402	67.5	66.5	66.0	66.0	66.0	65.5	35.70	35.80	35.90
5	1	263	332	419	69.0	70.0	70.0	69.0	69.0	69.5	34.90	34.80	34.80
5	2	273	330	411	68.0	68.0	69.0	68.5	69.0	68.5	35.00	35.00	34.90
5	3	276	235	388	68.0	67.0	68.0	67.5	67.5	67.5	33.40	33.30	33.30
5	1	290	339	431	73.0	73.0	73.0	74.0	73.0	73.0	34.30	34.20	34.30
5	2	302	267	341	56.5	57.0	57.5	55.5	56.5	57.0	37.00	37.10	37.00
5	2	310	374	467	80.0	78.5	80.5	79.0	80.0	79.0	32.90	33.00	33.05
5	2	323	000	000	58.0	58.5	60.0	58.0	58.0	58.5	36.50	36.80	36.90
5	2	324	000	000	59.5	57.5	56.5	56.5	57.5	57.5	36.50	36.80	36.60

Table XIII

Summary of measurements by five laboratories on thirty samples of 2219.

Column 1: sample number

Column 2: Yield strength (0.2% offset) in ksi (NBS measurement)

Column 3: Ultimate tensile strength in ksi (NBS measurement)

Column 4: Average of 30 Rockwell B hardness measurements (6 by each of 5 laboratories)

Column 5: Standard deviation of the 30 hardness measurements

Column 6: Average of 15 conductivity measurements in % IACS (3 by each of 5 laboratories)

Column 7: Standard deviation of the 15 conductivity measurements

1	2	3	4	5	6	7
5	49.0	63.8	76.36	1.37	34.45	.22
14	48.7	61.8	72.85	1.19	34.89	.26
18	44.1	55.8	66.93	1.27	35.63	.38
26	56.1	70.0	79.03	.94	33.32	.33
34	.0	.0	79.04	.96	33.37	.25
38	.0	.0	74.61	1.10	34.31	.26
70	51.5	64.2	75.37	1.04	34.33	.27
102	54.2	67.4	79.53	.58	33.34	.36
110	41.6	52.1	61.42	1.39	36.57	.25
118	54.7	68.1	80.23	.80	33.24	.25
122	54.5	68.4	79.57	.71	33.26	.32
158	55.0	68.3	79.91	1.00	33.31	.28
170	55.5	68.7	79.62	.66	33.43	.28
174	54.1	68.0	79.25	.98	33.51	.25
178	52.9	66.1	78.73	.77	33.44	.31
202	38.1	48.0	53.71	1.81	37.33	.22
206	54.5	68.1	79.70	1.06	33.23	.30
222	54.5	65.1	77.21	.84	34.38	.33
235	48.6	61.8	73.24	2.41	35.02	.28
241	39.3	52.6	57.04	1.54	37.32	.25
255	54.5	68.6	78.17	.84	33.70	.39
259	46.4	58.3	66.04	1.30	36.24	.28
263	48.1	60.8	69.41	.80	35.37	.29
273	47.8	59.6	68.43	.96	35.51	.33
276	34.1	56.3	66.30	1.02	33.94	.35
290	49.2	62.5	72.70	1.55	34.75	.27
302	38.7	49.4	56.42	1.22	37.10	.57
310	54.2	67.7	78.82	1.13	33.40	.25
323	.0	.0	58.01	1.63	37.01	.22
324	.0	.0	57.63	1.50	37.03	.26

Table XIV

Parameters obtained in least square fitting Equation (18) to the yield strength vs. the conductivity of the 2219-T87* round robin samples as measured by each of the five participating laboratories.

Lab. No.	b_0	b_1	b_2	Residual Std. Dev. ksi
1	-105.2	12.72	-0.2375	1.4
2	- 63.23	10.08	-0.1962	1.2
3	- 59.80	10.42	-0.2091	1.7
4	-119.0	13.24	-0.2405	1.1
5	-21.50	7.783	-0.1663	1.2

Table XV

Parameters obtained in least squares fitting Equation (19) to the yield strength vs. the Rockwell B hardness of the 2219-T87* round robin samples as measured by each of the five participating laboratories.

Lab. No.	c_0	c_1	c_2	Residual Std. Dev. ksi
1	27.43	-0.0785	0.005372	1.2
2	24.47	-0.0038	0.004773	1.1
3	31.92	-0.2750	0.006877	1.2
4	24.45	-0.0298	0.005176	1.0
5	27.21	-0.1290	0.005948	1.1

Figure 1. Measured average composition (wt.% copper) hardness (HRB) and conductivity (%IACS) versus distance through (bottom to top) an as-received 12.7 cm (5 inches) thick plate of 2219-T851 aluminum alloy (Reynolds Lot No. 7950777-DI). The dotted lines indicate location of top and bottom.

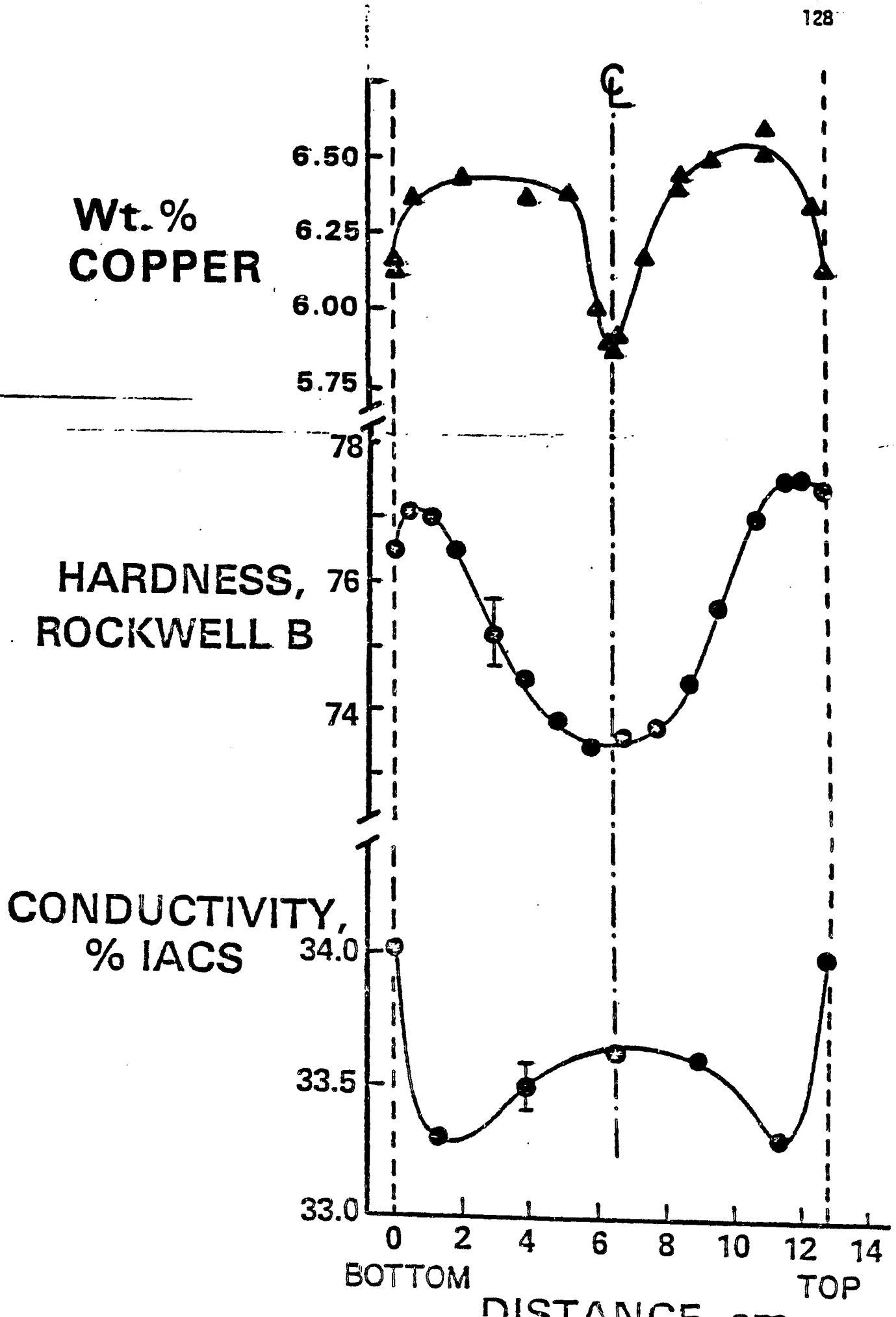
℄
Wt. %
COPPER
6.50
6.25
6.00
5.75
78
HARDNESS,
ROCKWELL B
76
74
CONDUCTIVITY,
% IACS
34.0
33.5
33.0
0
2
4
6
8
10
12
14
BOTTOM
TOP

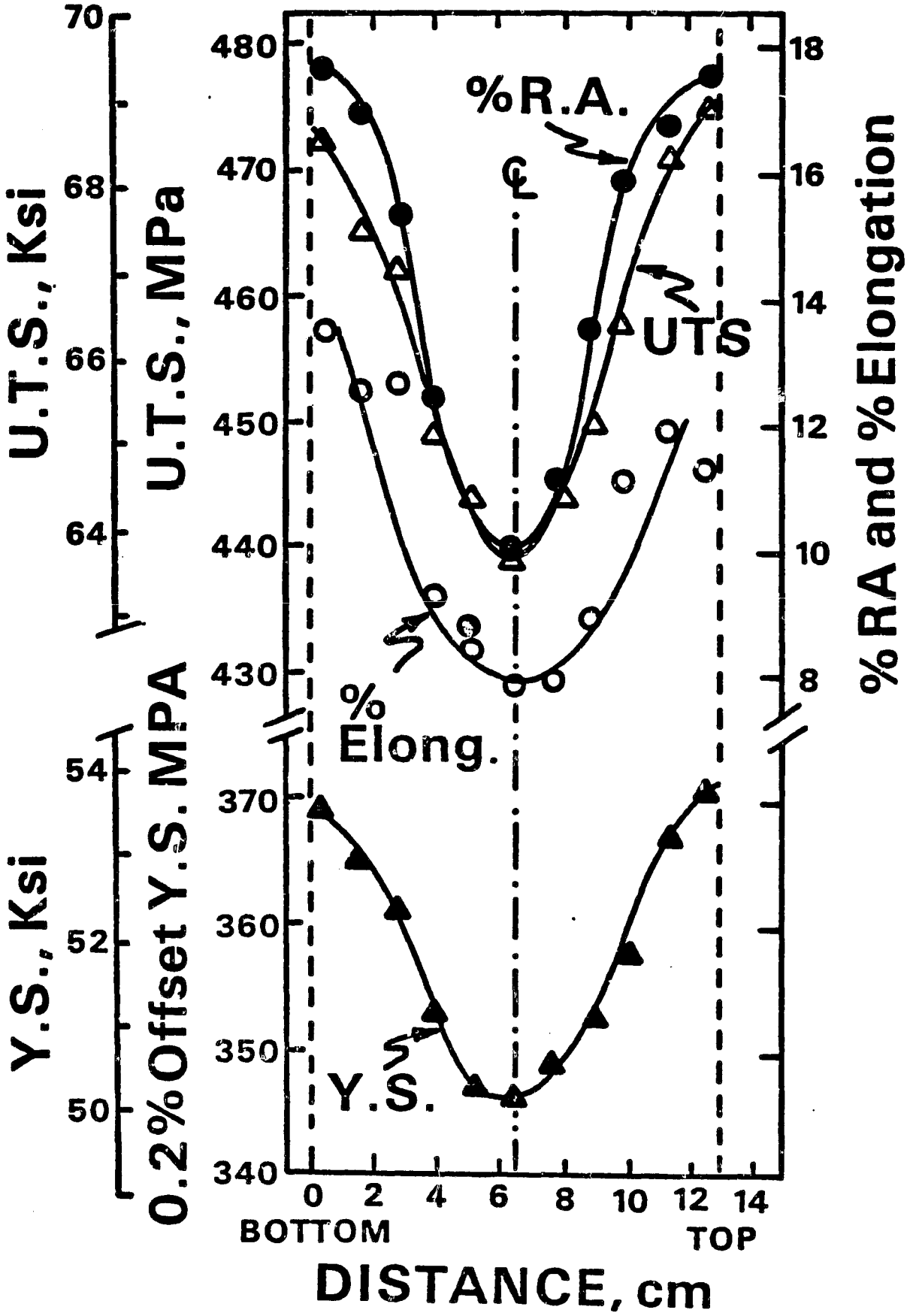

Figure 2. Measured yield stress, ultimate tensile stress, percent elongation and reduction in area versus distance through (bottom to top) an as-received 12.7 cm (5 inches) thick plate of 2219-T851 aluminum alloy (Reynolds Lot No. 7950777-DI).

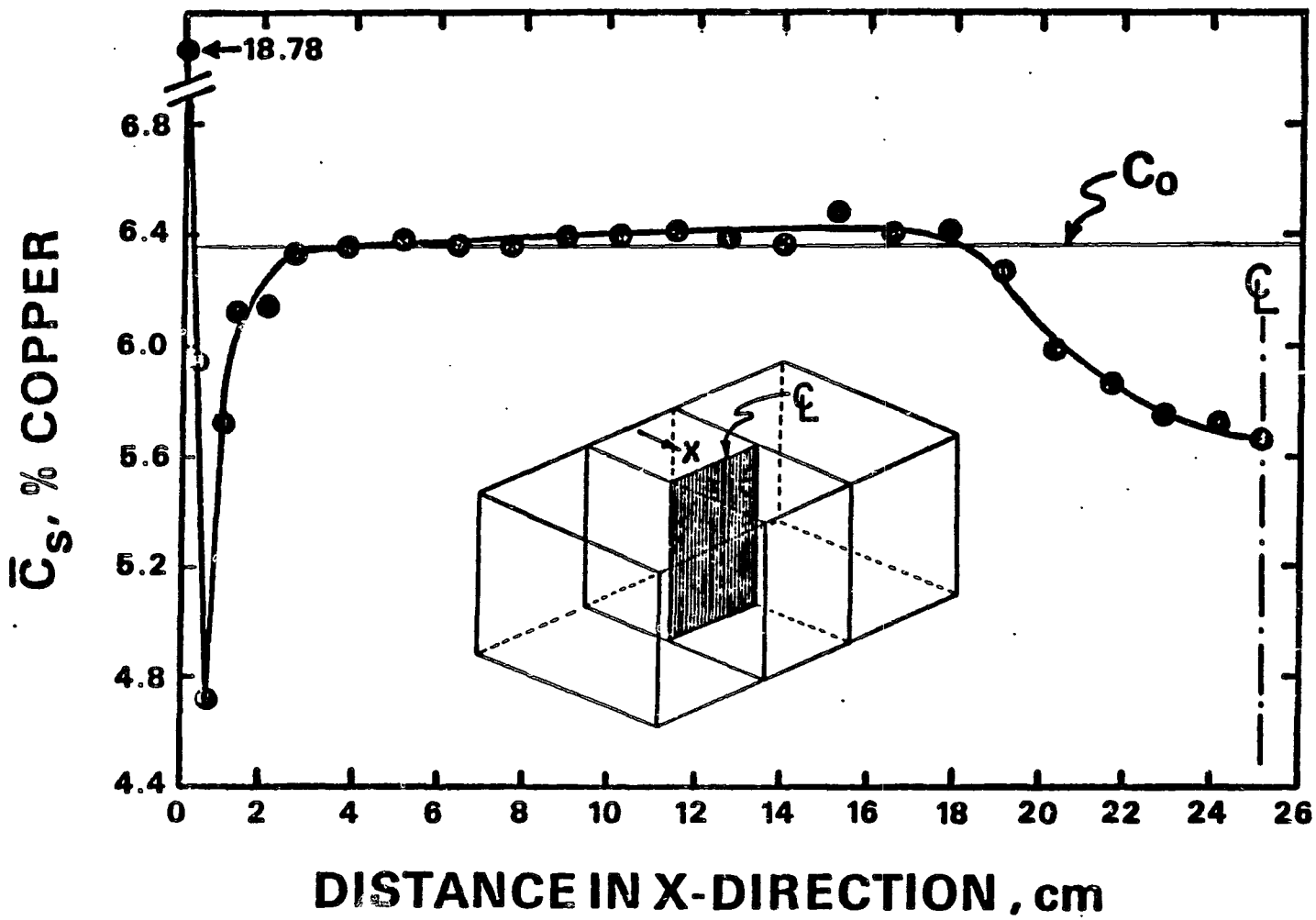

Figure 3. Macrosegregation profile, average copper content versus distance from the chill face, across the short transverse direction of a semi-continuous DC cast ingot of 2219 aluminum alloy. Ingot is from the Reynolds McCook plant. It is idenitified as 2219-13402-9B.

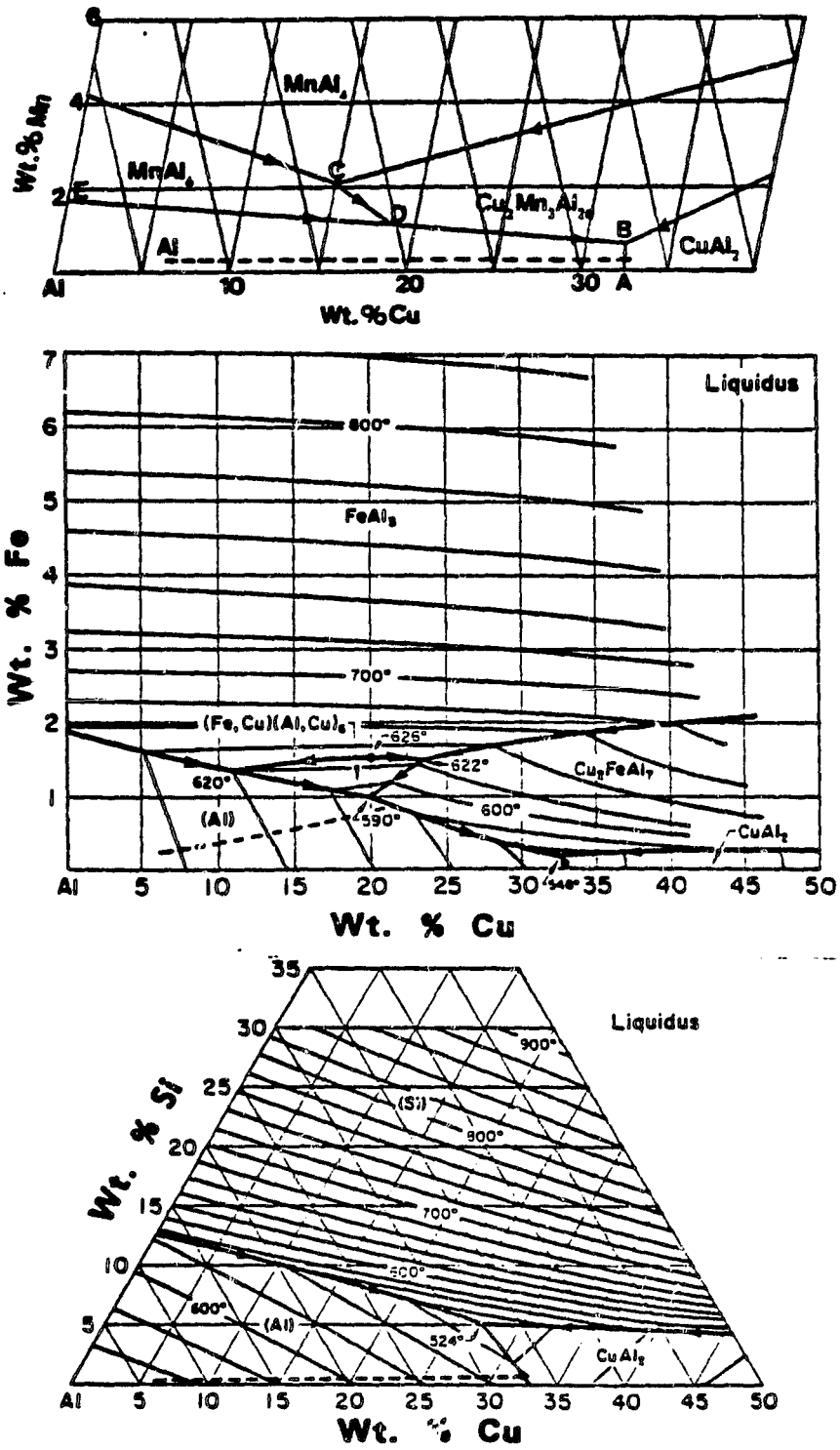

Figure 4. Calculated solidification "path", dashed lines, shown on the liquidus phase diagrams of the aluminum rich corner of Al-Cu-Mn, Al-Cu-Fe and Al-Cu-Si systems. In (a), Mn remains in solution until solidification is completed at the ternary eutectic point. In (b), the solidification "path" intersects the eutectic trough $L \rightarrow \alpha\text{-Al} + Cu_2FeAl_7$ before solidification is completed at the ternary eutectic point. In (c), the "path" intersects the eutectic trough $L \rightarrow \alpha\text{-Al} + Cu_2Al$ before solidification is completed at the ternary eutectic $L \rightarrow \alpha\text{-Al} + Cu_2Al + Si$.

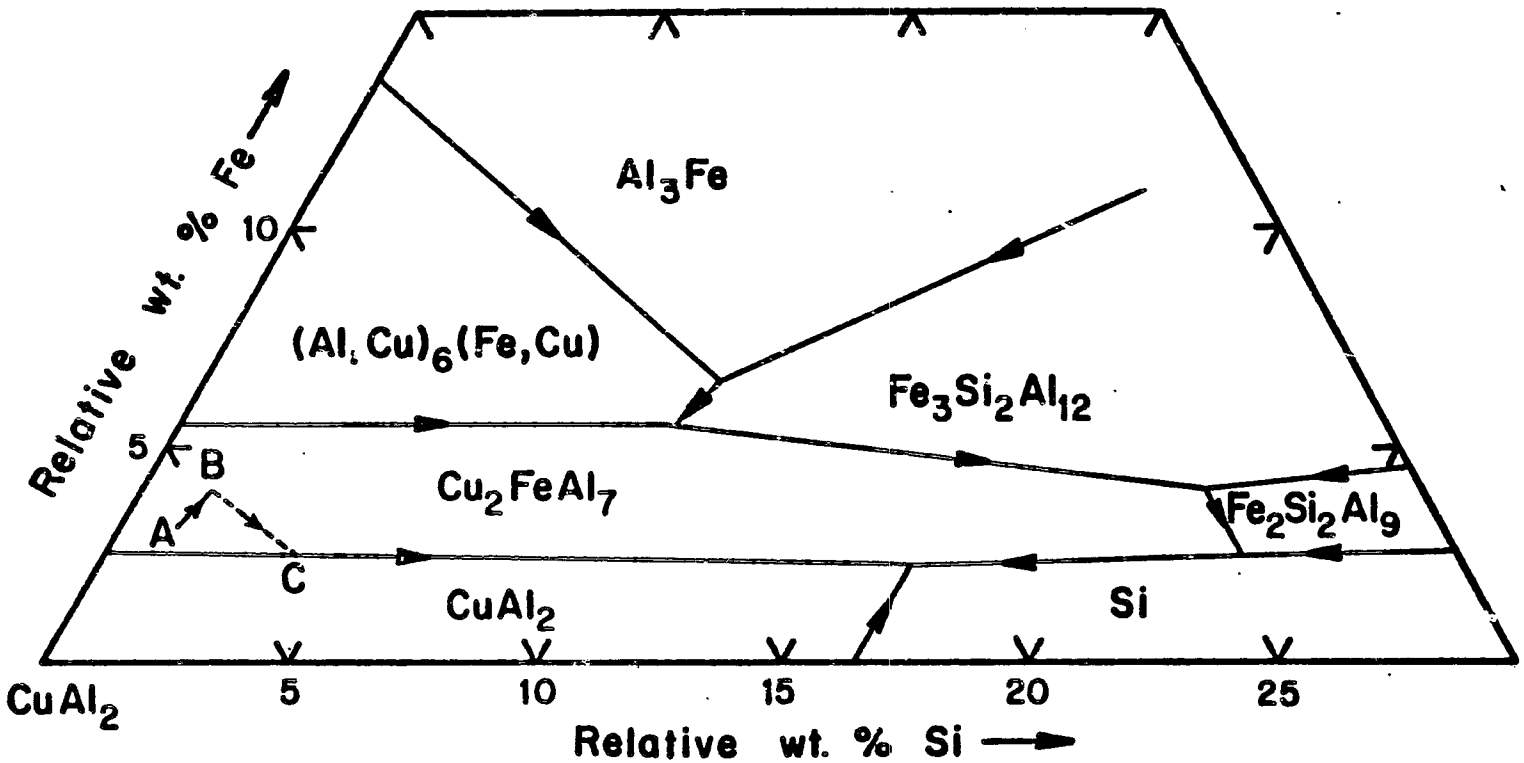

Figure 5. Aluminum rich alloys of the Al-Cu-Fe-Si system showing relative percentage of Fe vs. Si with the remainder copper. Regions represent solidification of α-aluminum in addition to the phase noted. The solidification path (AB) lies in the region for Cu_2FeAl_7. A possible path (BC) of secondary solidification of $L \rightarrow \alpha\text{-Al} + Cu_2FeAl_7$ is shown and intersects the ternary eutectic line $L \rightarrow \alpha\text{-Al} + Cu_2FeAl_7 + CuAl_2$.

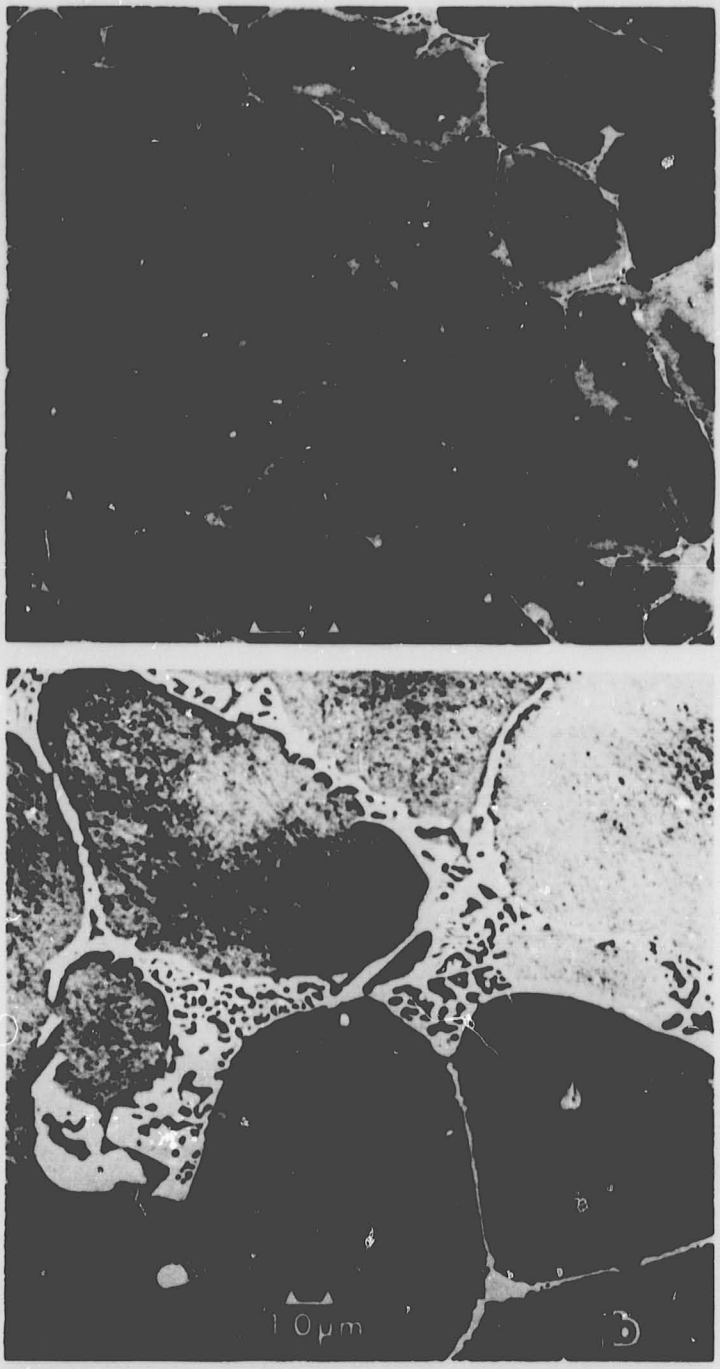

Figure 6. Typical SEM views of the as-cast microstructure of 2219 aluminum alloy. (a) Shows cored dendritics and interdendritic eutectic at 100X. (b) Shows the interdendritic eutectic at 400X.

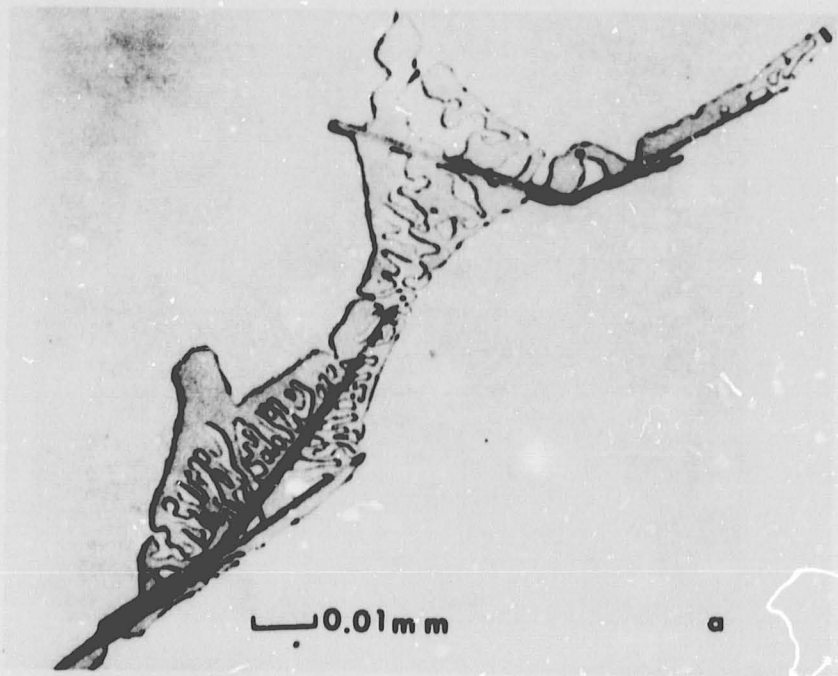

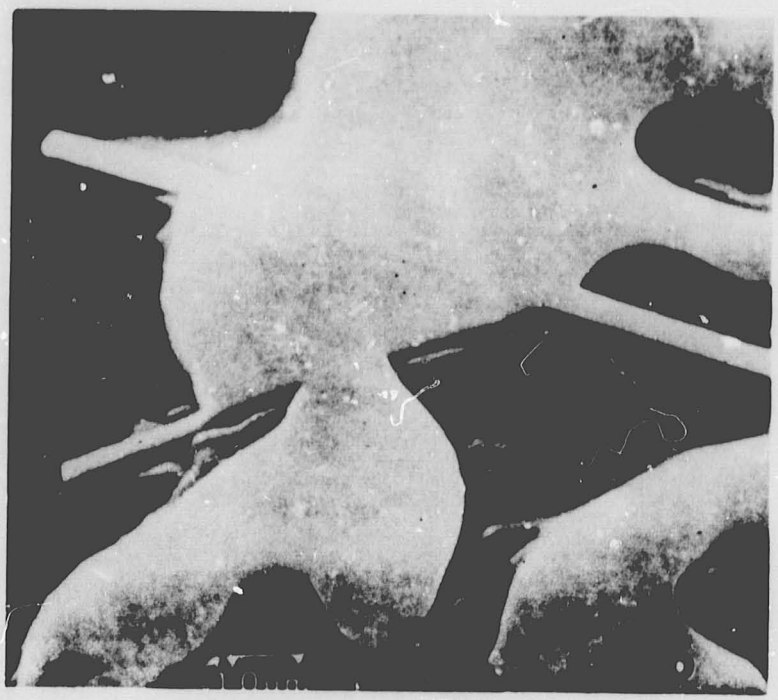

Figure 7. Typical optical and SEM views of the interdendritic region of as-cast microstructure of 2219 aluminum alloy. (a) Optical view, Keller's etch, light phase is α-Al, gray phase $CuAl_2$, dark phase Cu_2FeAl_7. (b) Shows an SEM view at 7500X.

Figure 8. TEM micrograph of as-cast 2219 aluminum alloy. Dark interdendritic phase is θ. Light interdendritic material is α-Al. θ' precipitates are faintly visible within the dendrites. Precipitates along dendrite grain boundary have not been identified.

Figure 10. Cu_2FeAl_7 interdendritic phase identified by electron diffraction in as-cast 2219 aluminum alloy. Diffraction pattern was obtained from light polygonal shaped region.

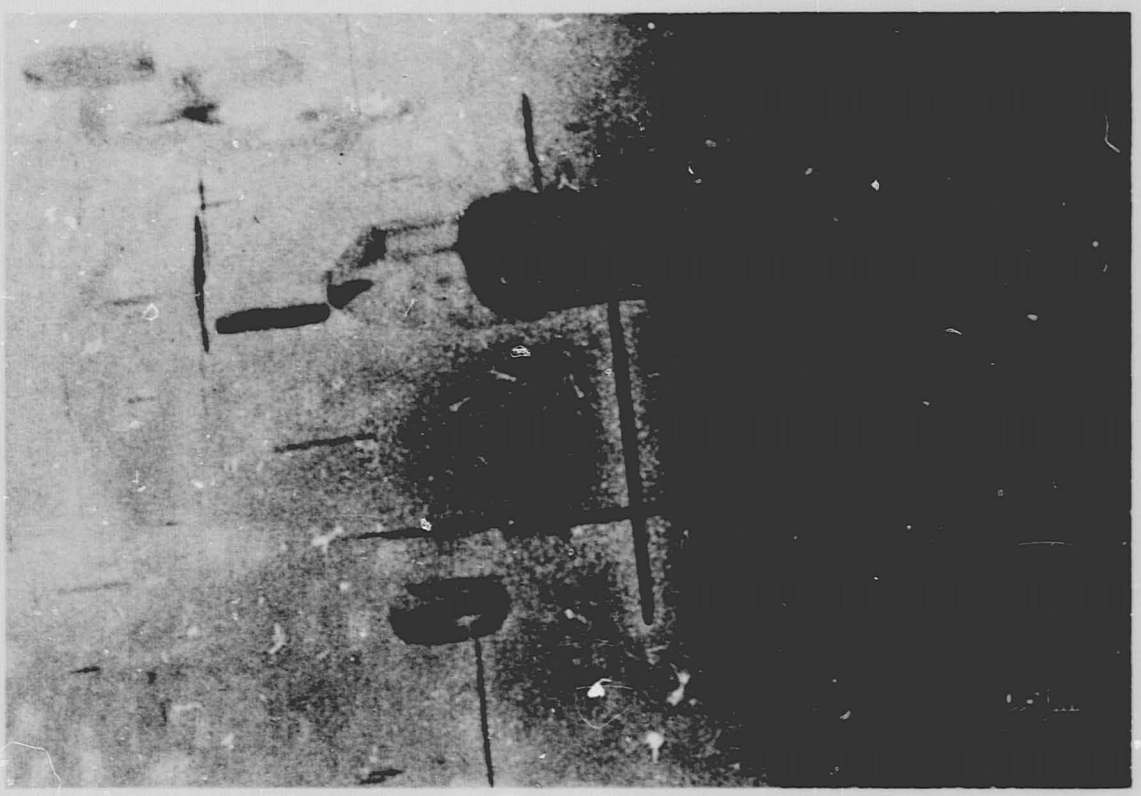

Figure 11. Precipitates within the interior of an α-Al dendrite in as-cast 2219 aluminum alloy. The precipitates are θ'. Three different habit variants are present.

Figure 12. Subboundaries within the interior of an α-Al dendrite in as-cast 2219 aluminum alloy. These subboundaries act as preferred sites for nucleation of θ'.

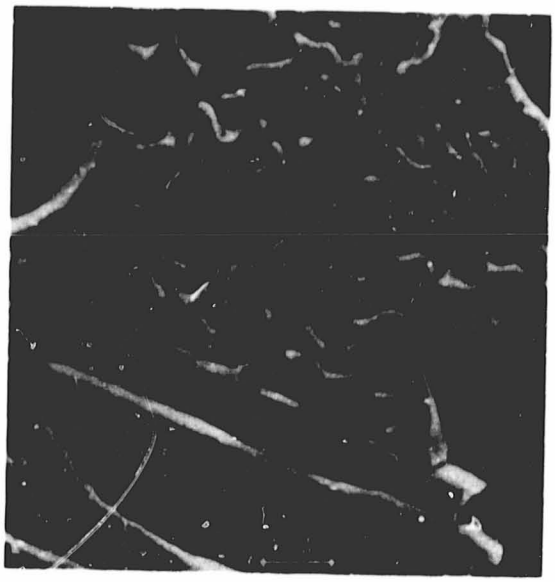

Figure 13. Typical SEM view of interdendritic eutectic near the chill face of DC cast 2219 aluminum alloy; α-Al, irregular rounded particles of $CuAl_2$ and blades of Cu_2FeAl_7.

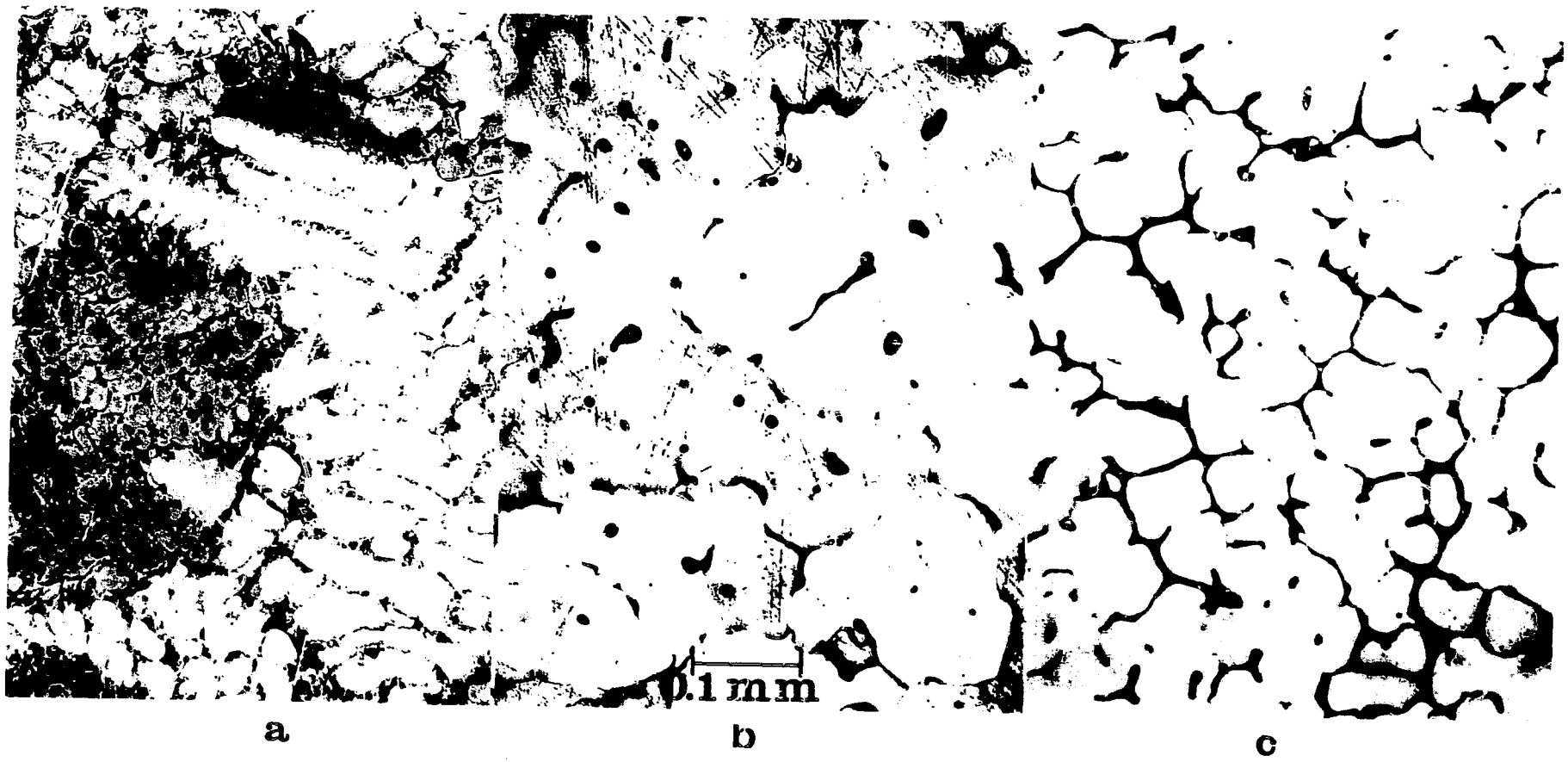

Figure 14. Optical micrographs of DC cast ingot at different distances from the chill surface: (a) chill face (on left), (b) 0.5 cm from chill face (c) 1.7 cm from the chill face.

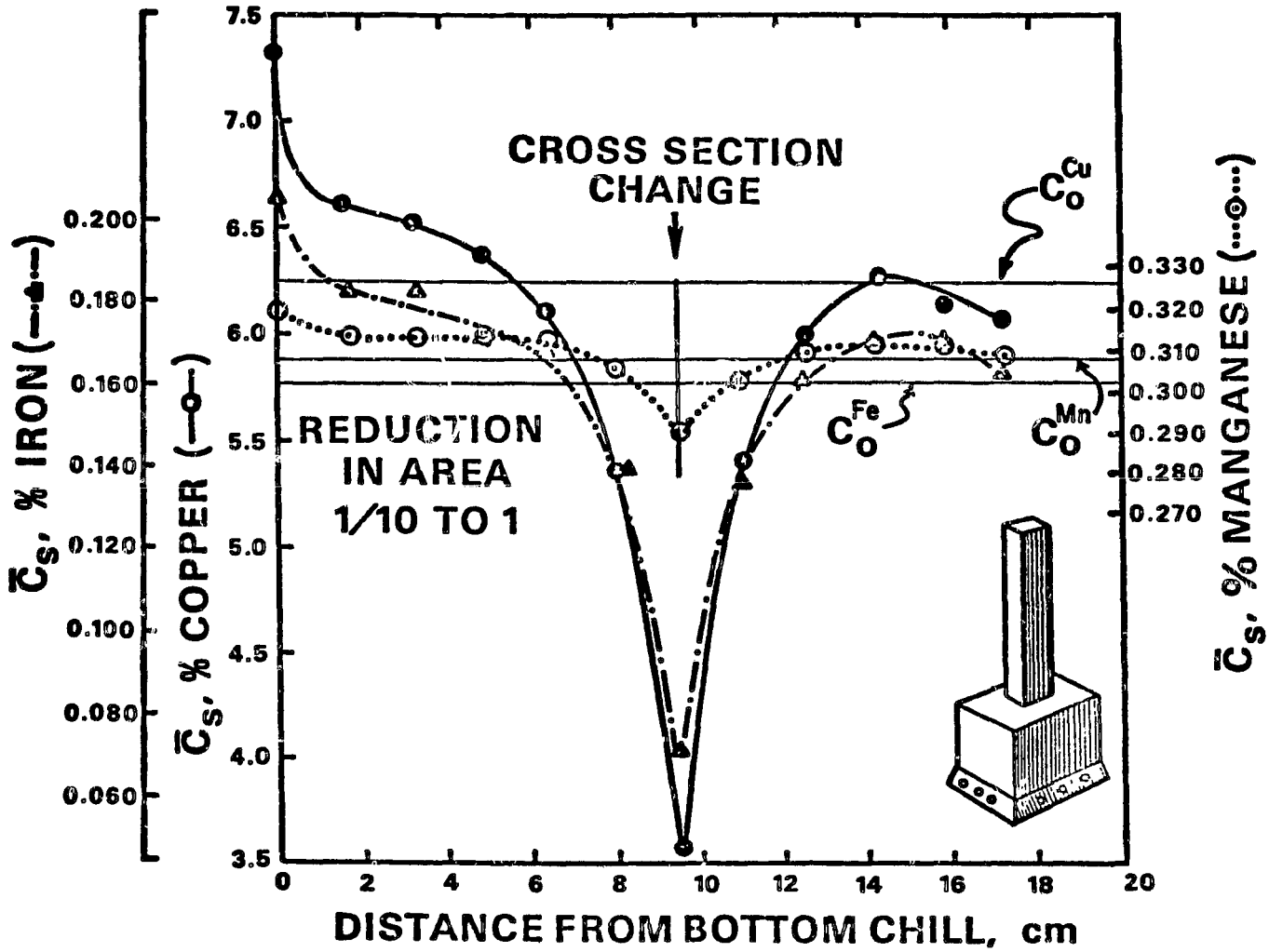

Figure 15. Macrosegregation profile, average copper, iron and manganese content versus distance from the bottom chill, in a unidirectionally solidified reduced cross section laboratory ingot of 2219 aluminum alloy. C_o's denote the average content of each element.

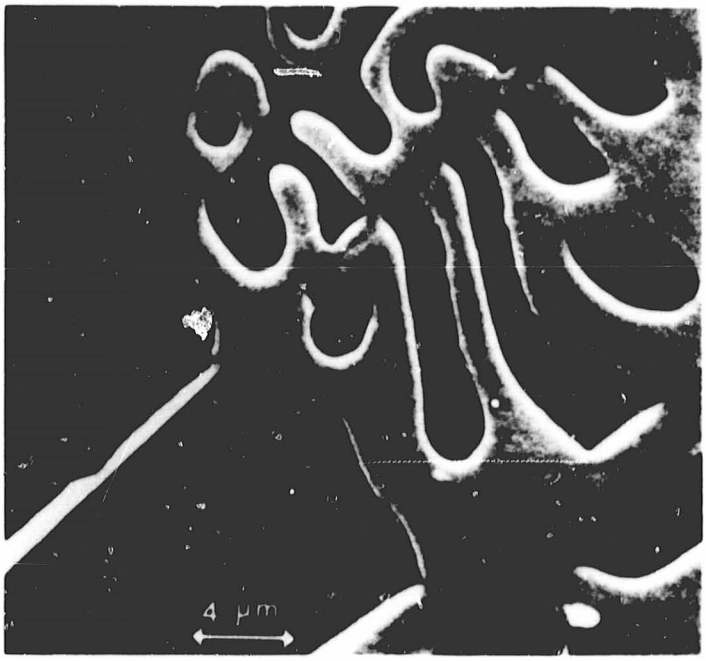

Figure 16. Typical SEM view of interdendritic eutectic near the chill face of laboratory cast 2219 aluminum alloy ingot; α-Al, irregular rounded particles of $CuAl_2$ and blades of Cu_2FeAl_7.

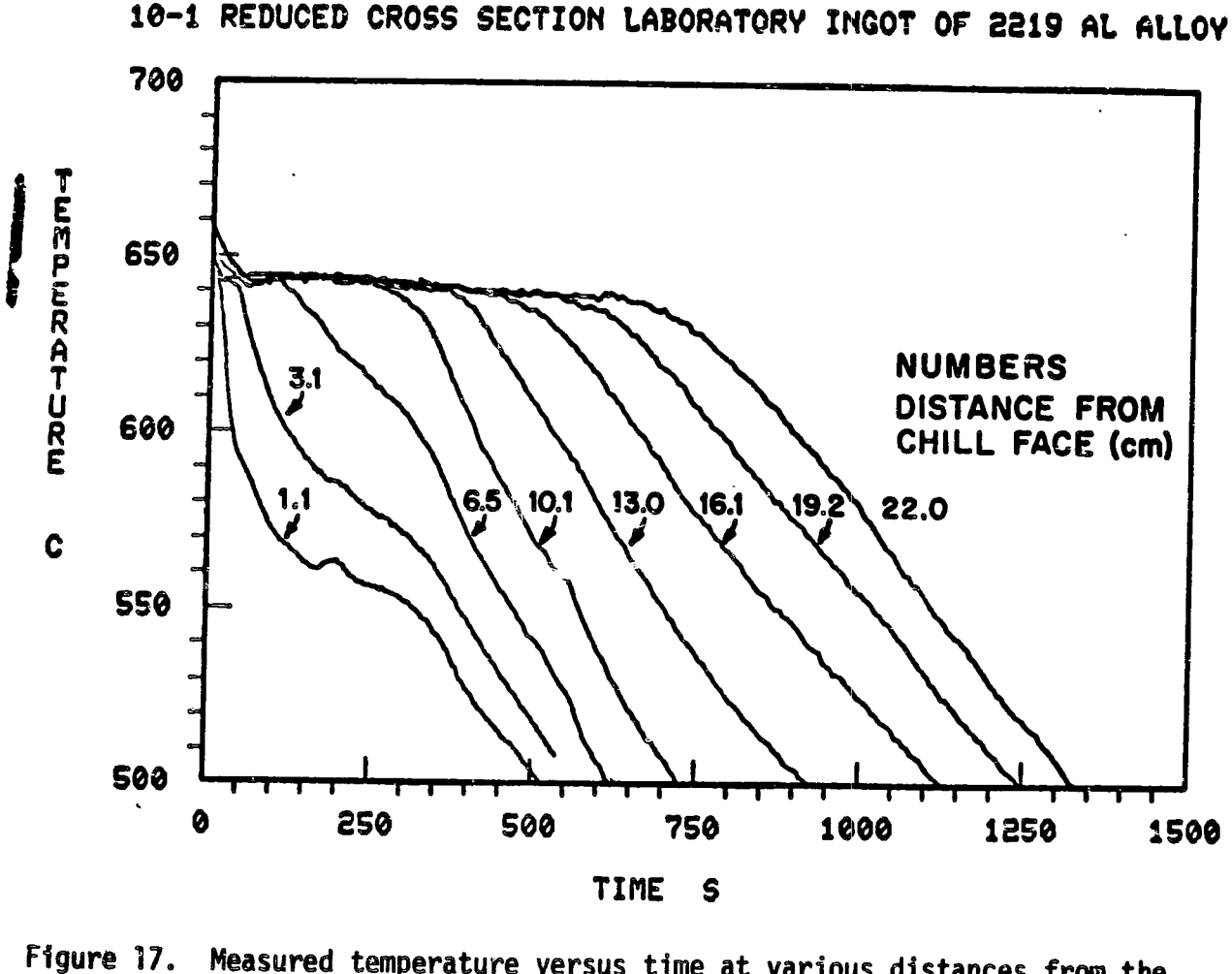

Figure 17. Measured temperature versus time at various distances from the bottom chill during the unidirectional solidification of a 10 to 1 reduced cross section laboratory ingot of 2219 aluminum alloy.

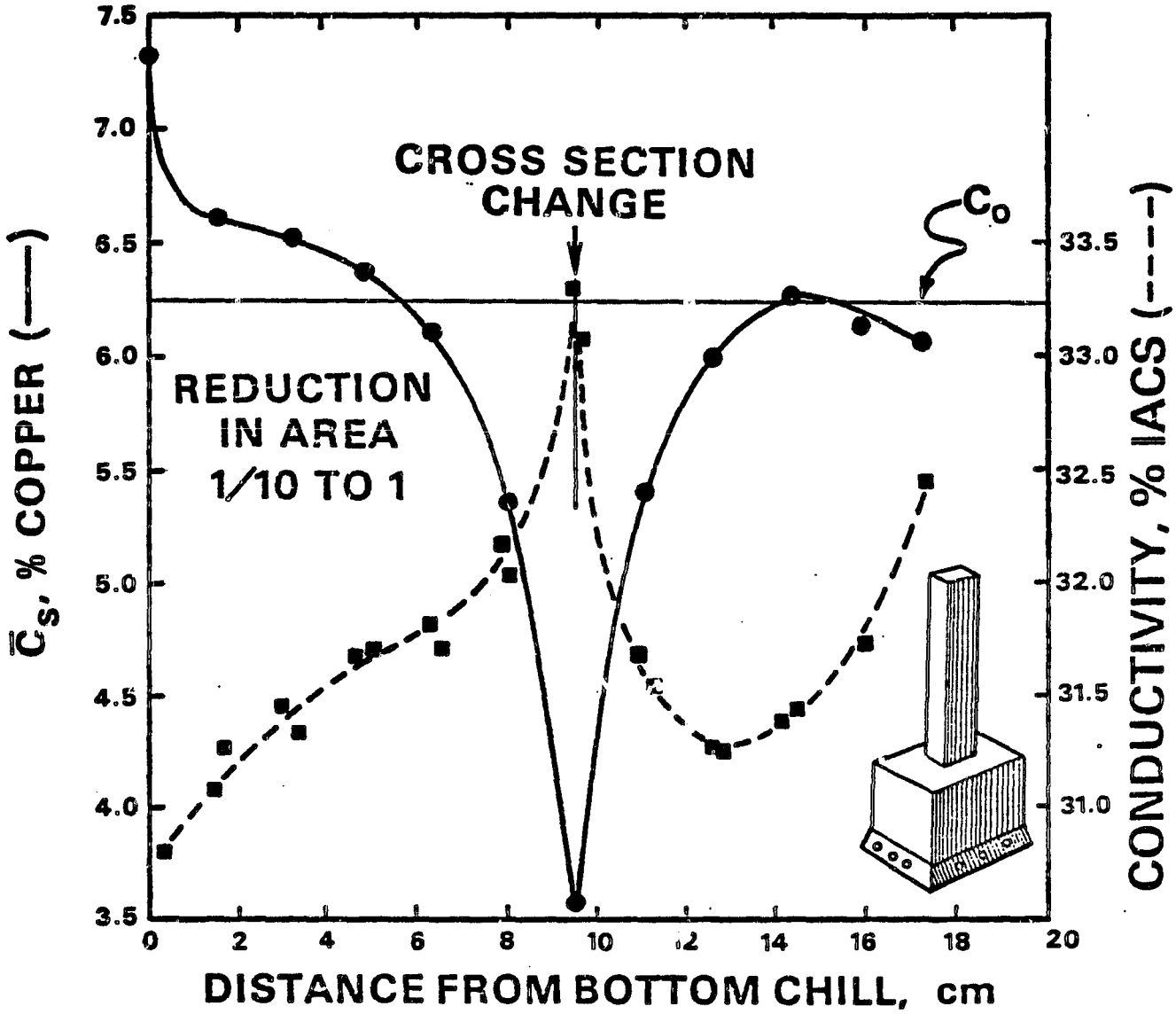

Figure 18. Average copper content and electrical conductivity versus distance from the bottom chill, in a unidirectionally solidified reduced cross section laboratory ingot of 2219 aluminum alloy.

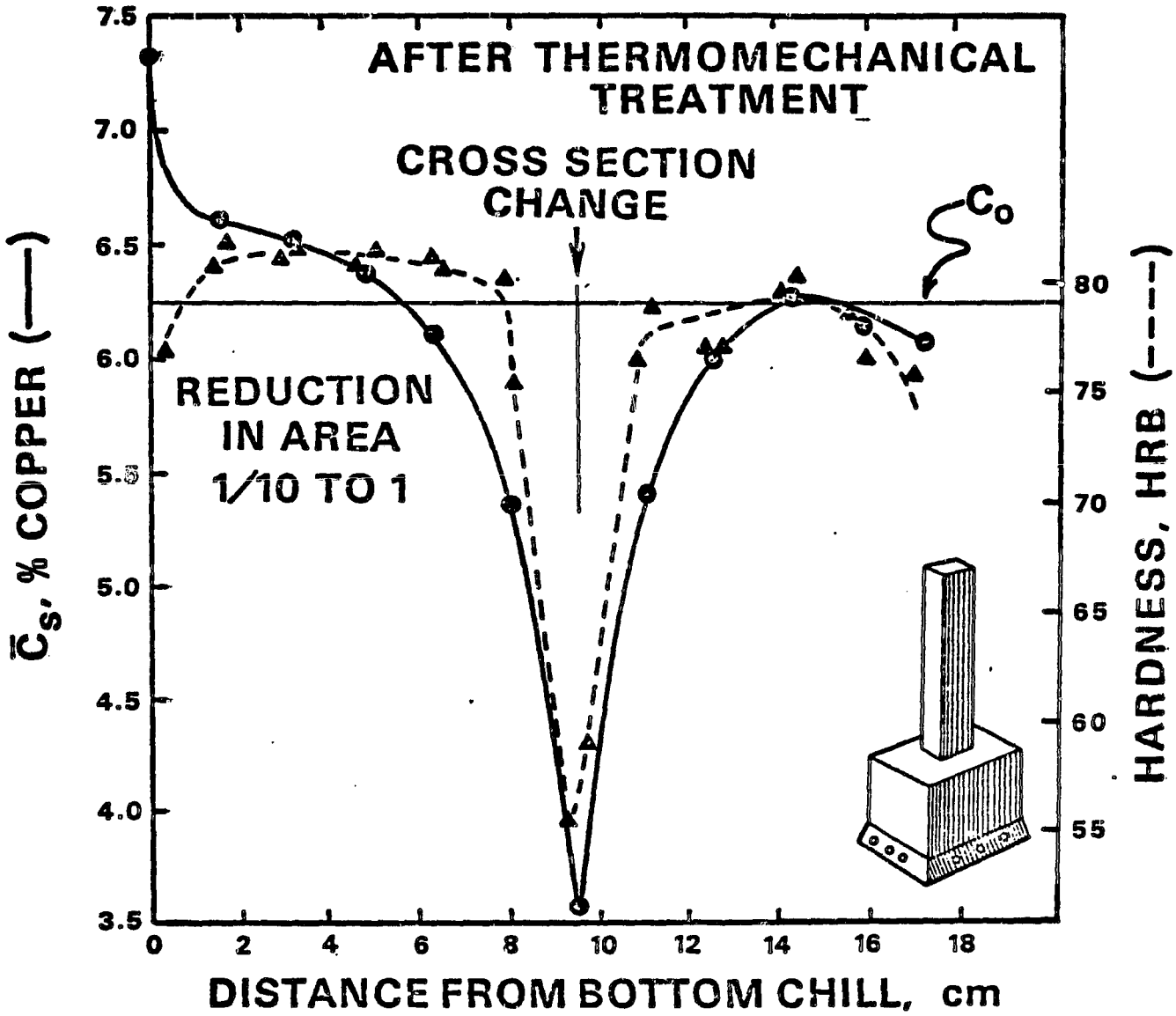

Figure 19. Hardness after thermomechanical treatment to the T87* condition and copper content versus distance from the bottom chill in a unidirectionally solidified reduced cross section laboratory ingot.

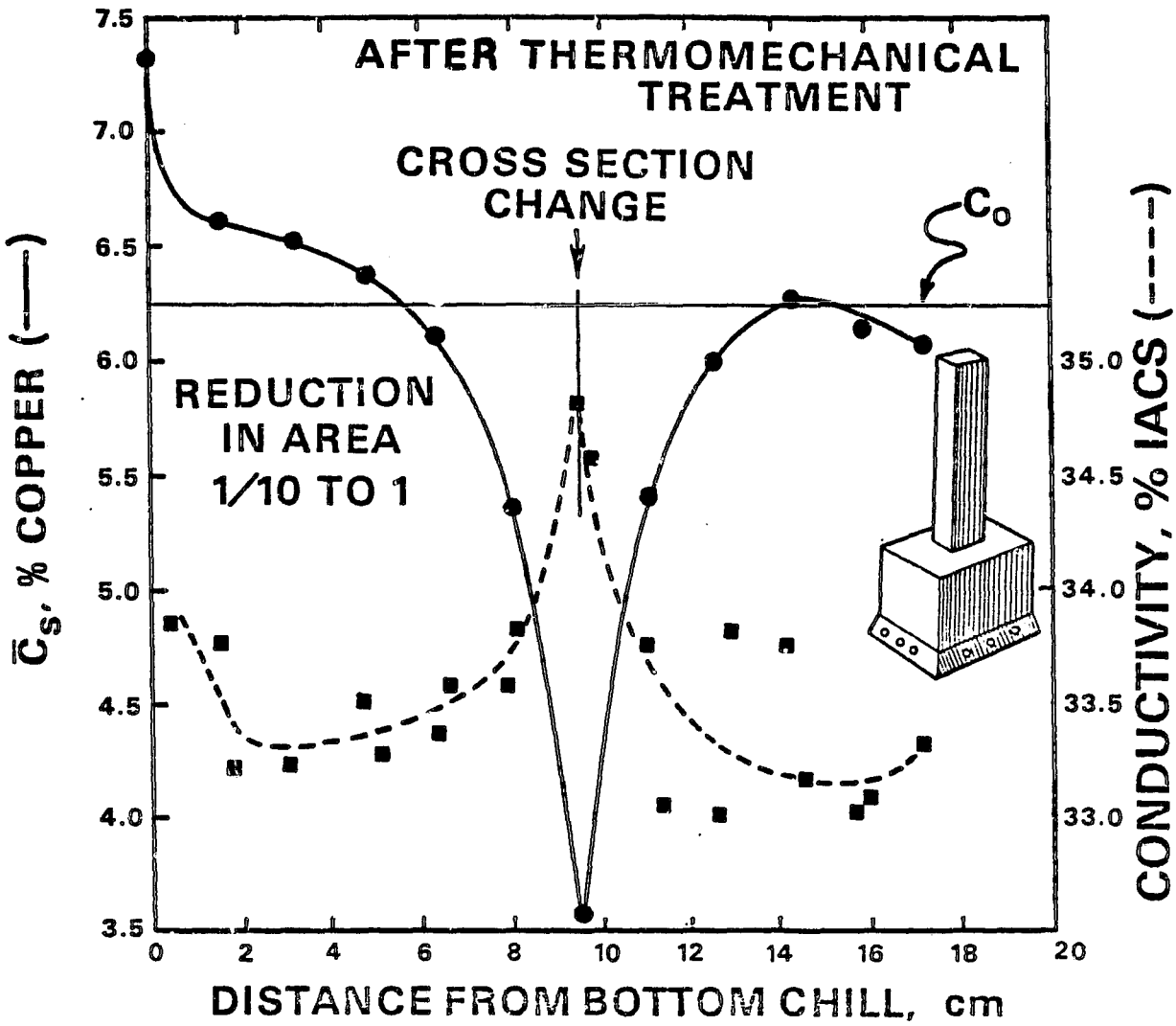

Figure 20. Conductivity after thermomechanical treatment to the T87* condition and copper content versus distance from the bottom chill in a unidirectionally solidified reduced cross section laboratory ingot.

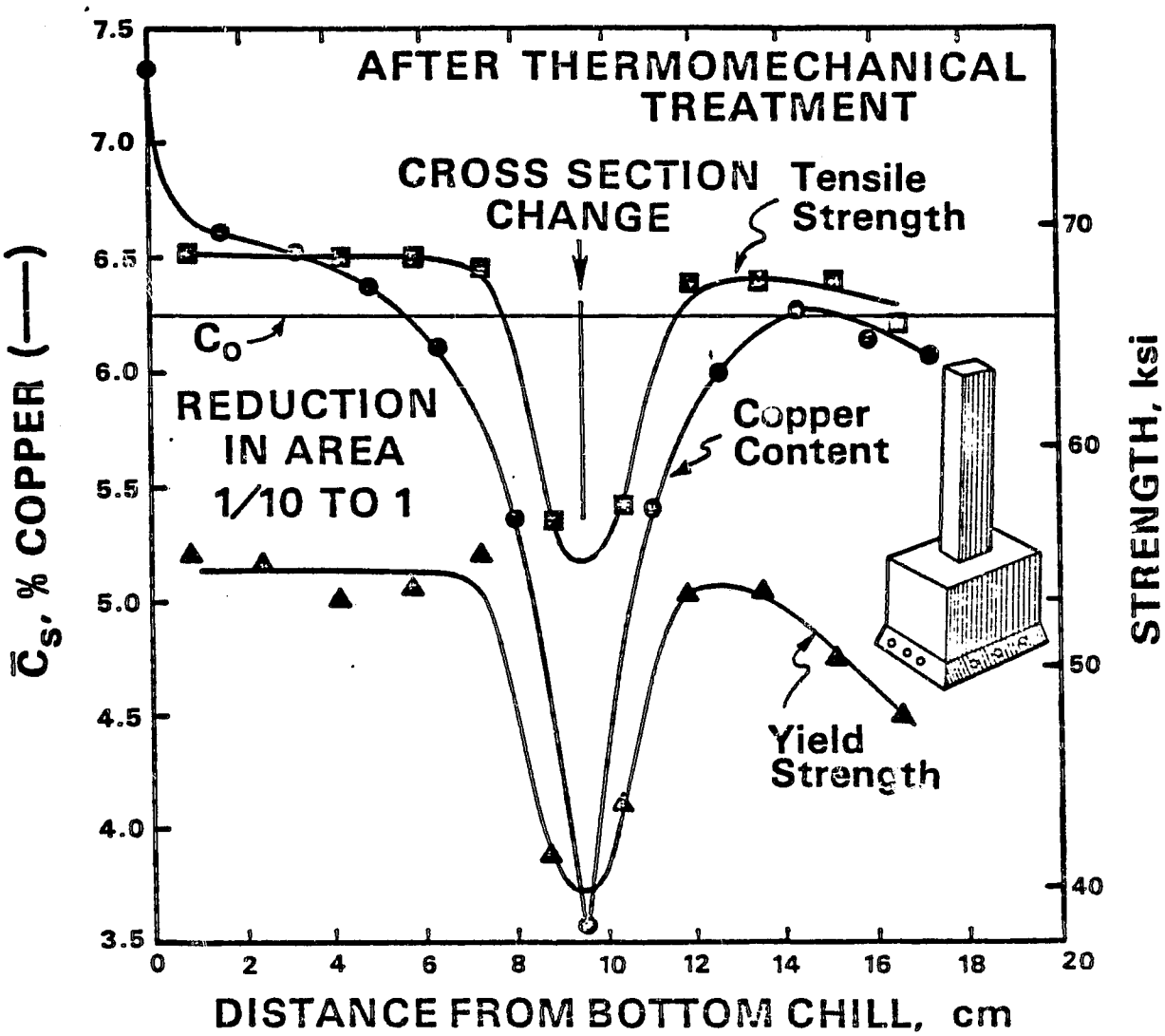

Figure 21. Tensile and yield strength after thermomechanical treatment to T87* condition and copper content versus distance from the bottom chill in a unidirectionally solidified reduced cross section laboratory ingot of 2219 aluminum alloy.

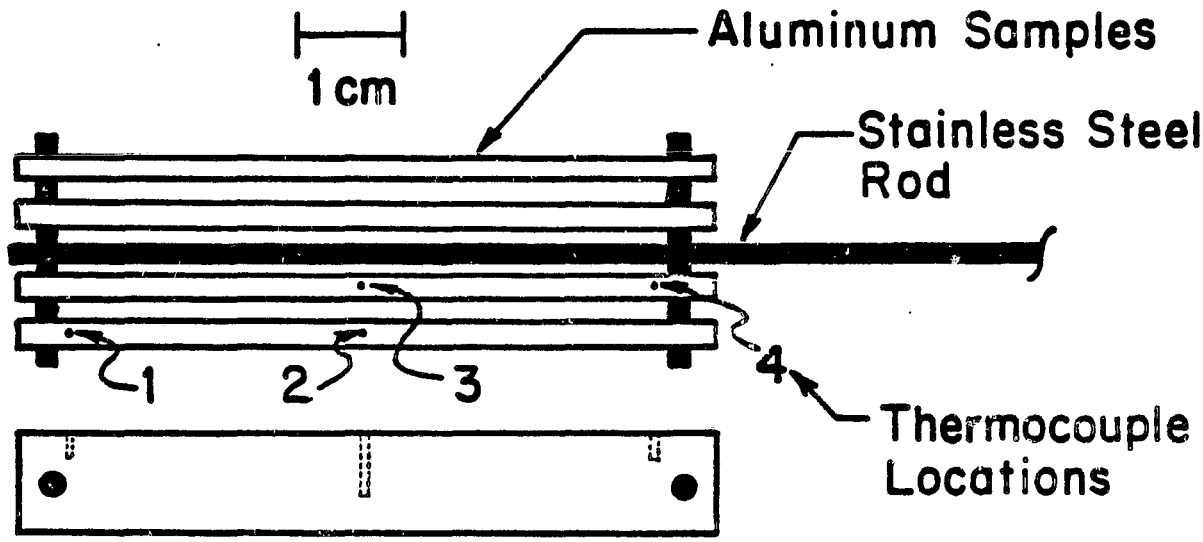

Figure 22. Schematic of jig for holding four aluminum alloy plates ~ 0.64 cm x 2.5 cm x 17 cm (1/4" x 1" x 6-1/2") for simultaneous heat treatment. Four thermocouples are buried in the samples as shown. Samples are held in place with stainless steel rods.

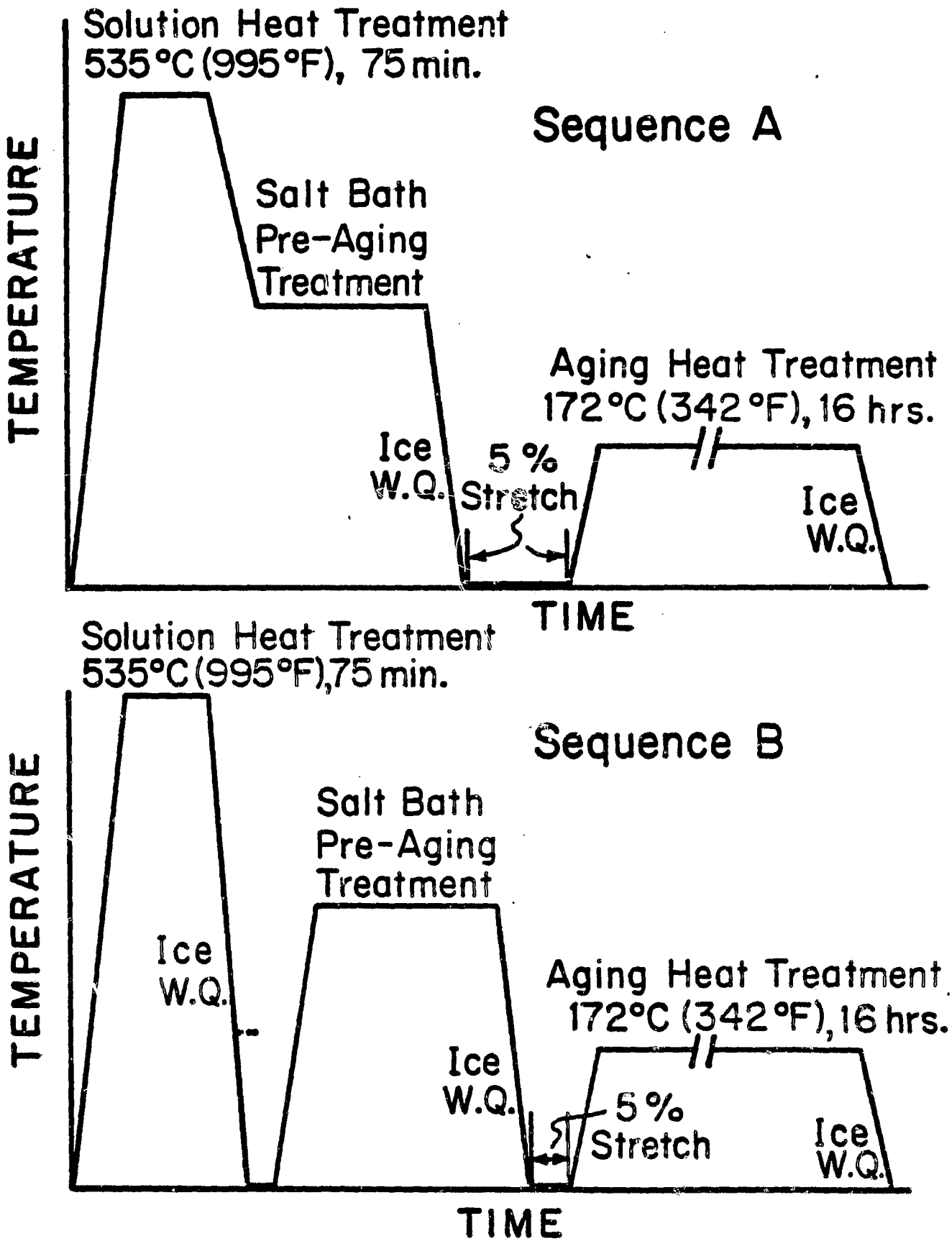

Figure 23. Schematic representation of the thermomechanical treatment sequences given the 2219-T87* aluminum alloys used in this study.

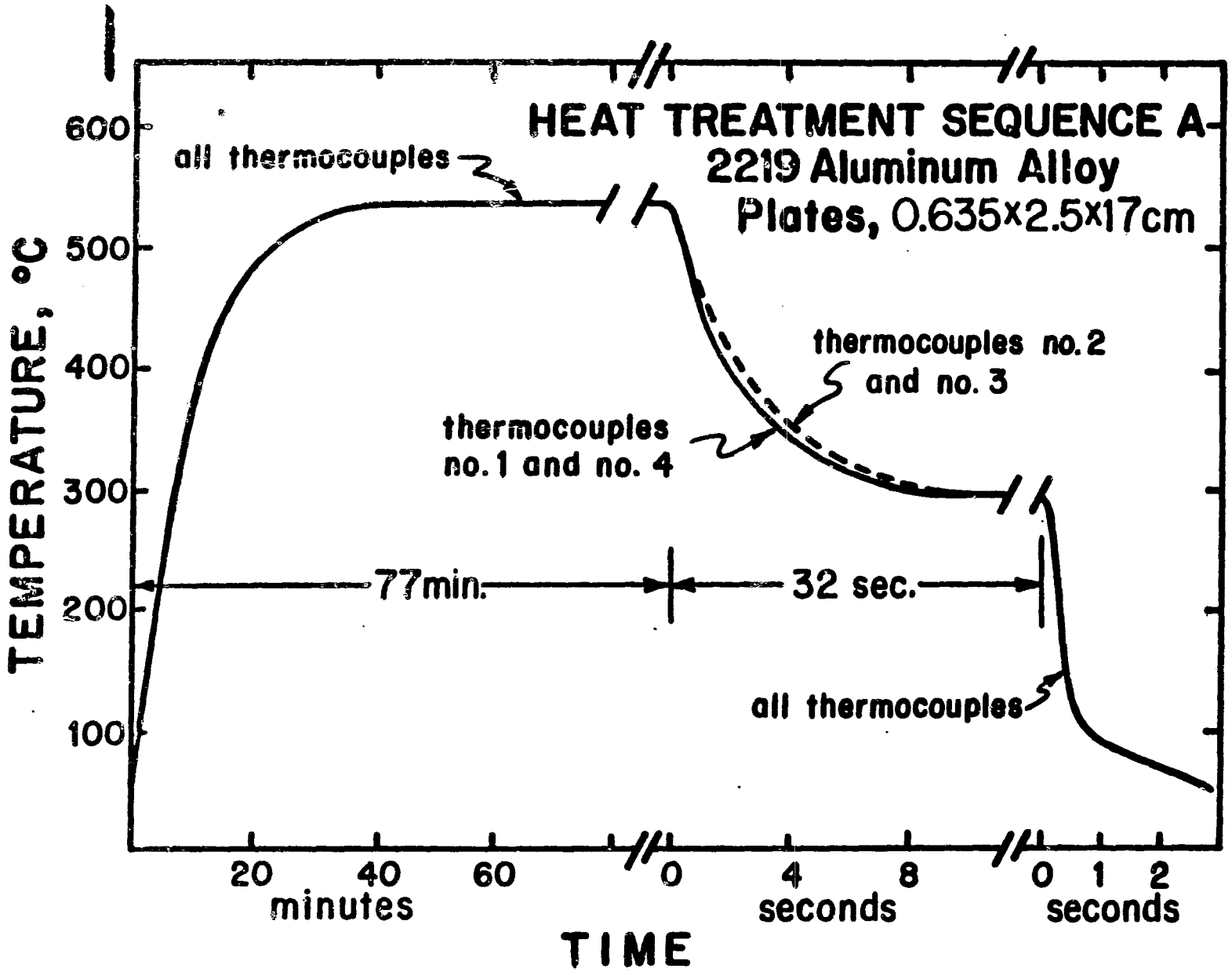

Figure 24. Temperature vs. time profiles from the four thermocouples in an aluminum alloy plate ∿ 0.64 cm x 2.54 cm x 17 cm (1/4" x 1" x 6-1/2") given a simultaneous heat treatment of the sequence A type. (Thermocouple placement in illustrated in Figure 1).

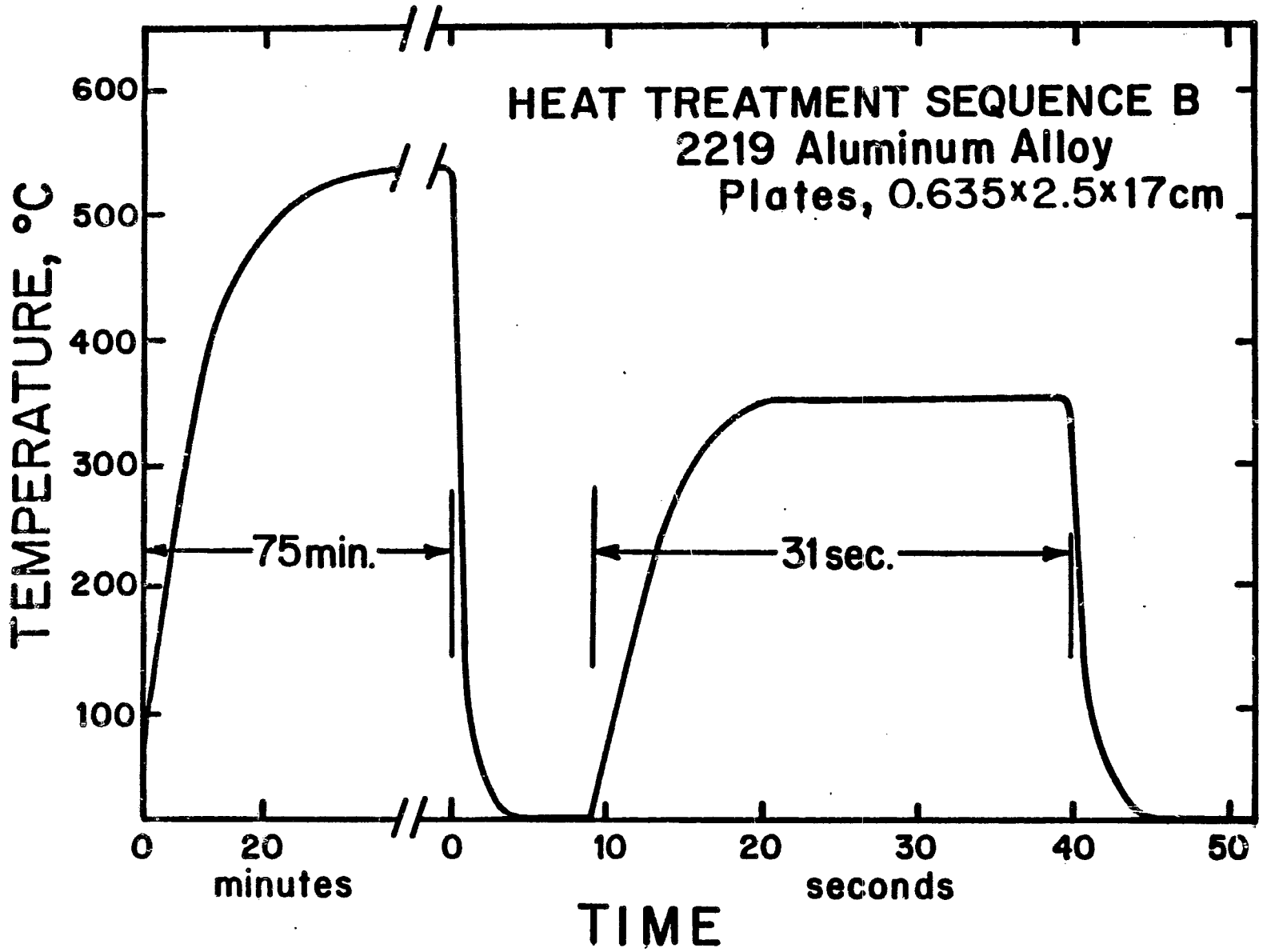

Figure 25. Temperature vs. time profiles for alloy plates ∿ 0.64 cm x 2.54 cm x 17 cm (1/4" x 1" x 6-1/2") given a heat treatment of the sequence B type. Temperature represents the average of thermocouples placed as illustrated in Figure 1.

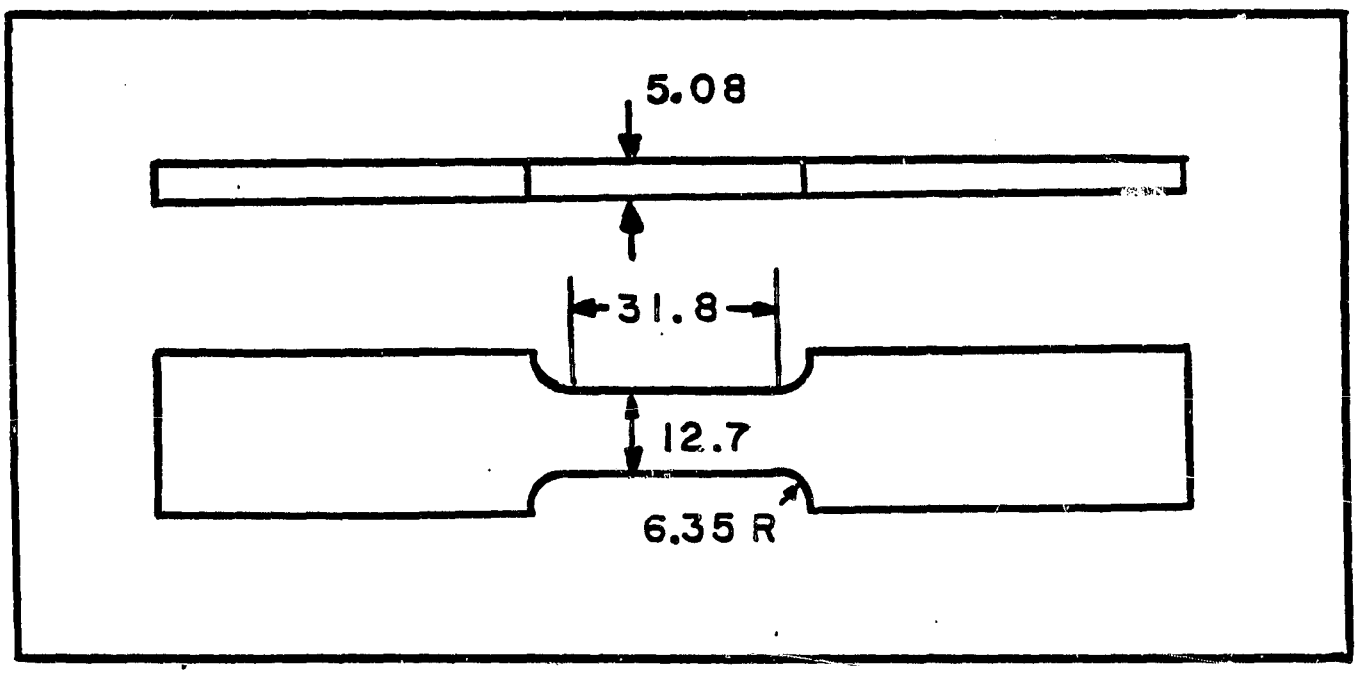

Figure 26. Schematic of tensile test specimen. Dimensions are in mm.

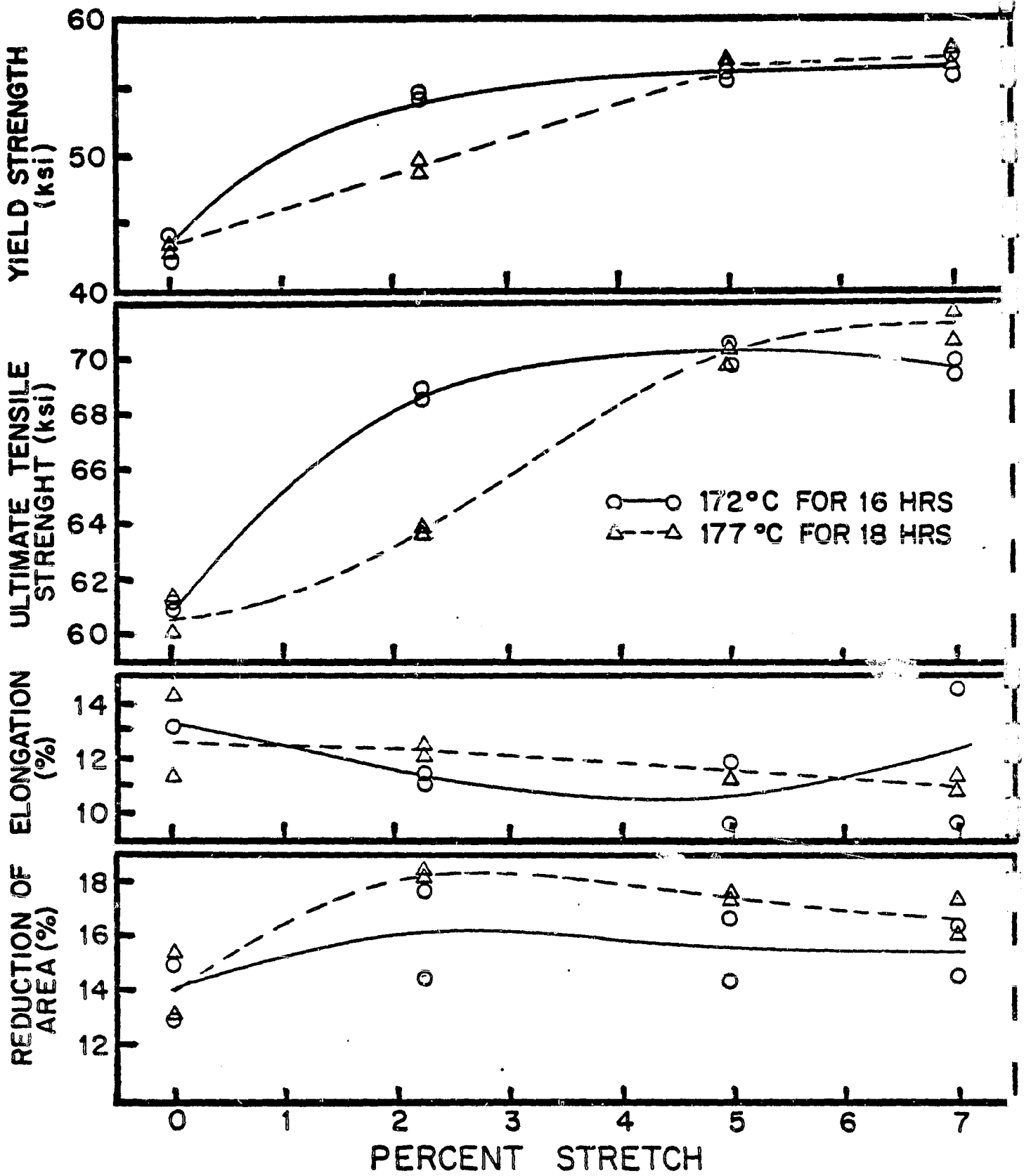

Figure 27. Mechanical properties as a function of stretching for 2219 aluminum alloy. Samples were solutionized and quenched prior to stretching, then aged for 16 hours at 172°C (solid lines and circles) or for 18 hours at 177°C (dotted lines and triangles.

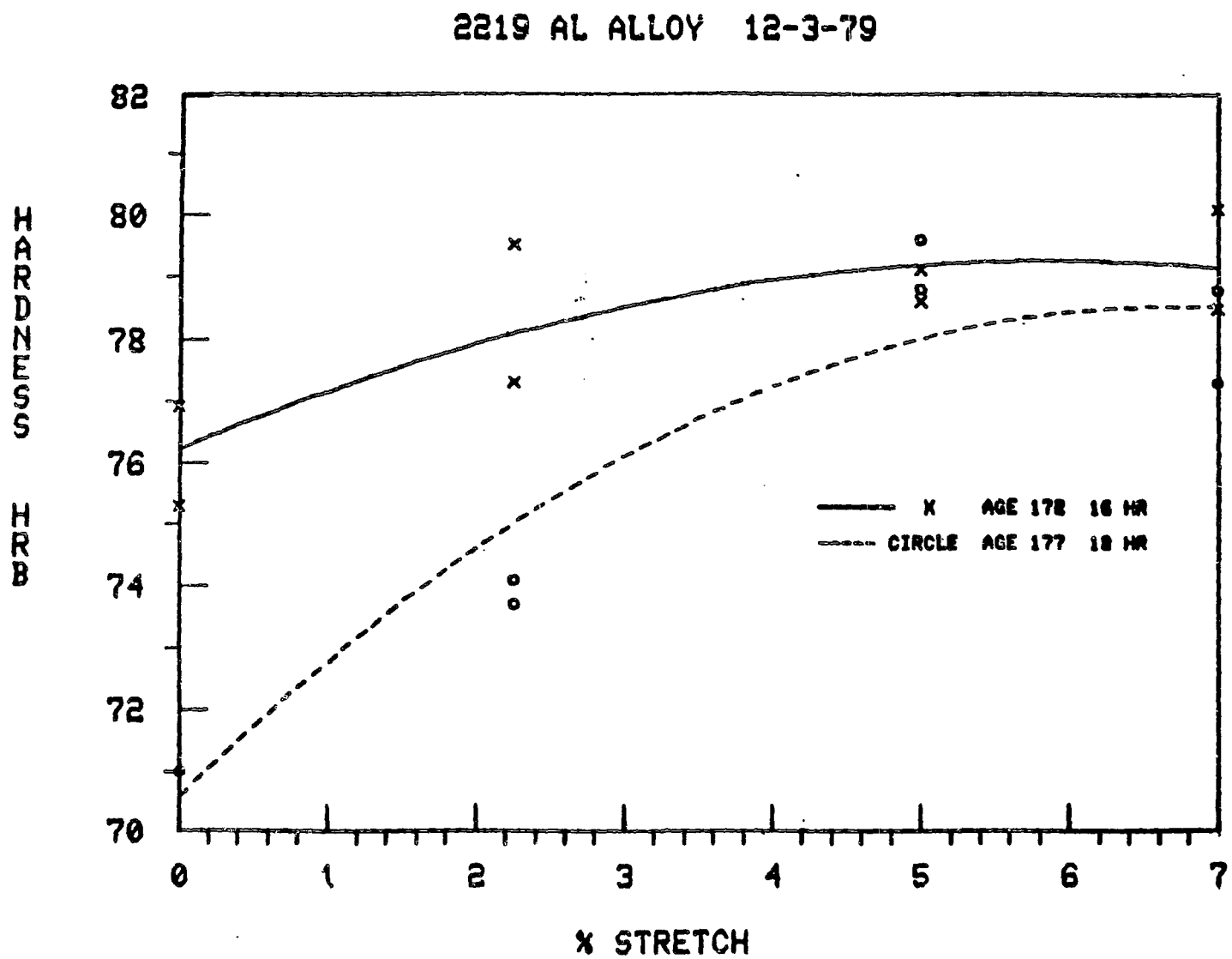

Figure 28. Rockwell B hardness as a function of stretching for 2219 aluminum alloy. Samples were solutionized and quenched prior to stretching, then aged for 16 hours at 172°C (solid lines and crosses) or for 18 hours at 177°C (dotted lines and circles).

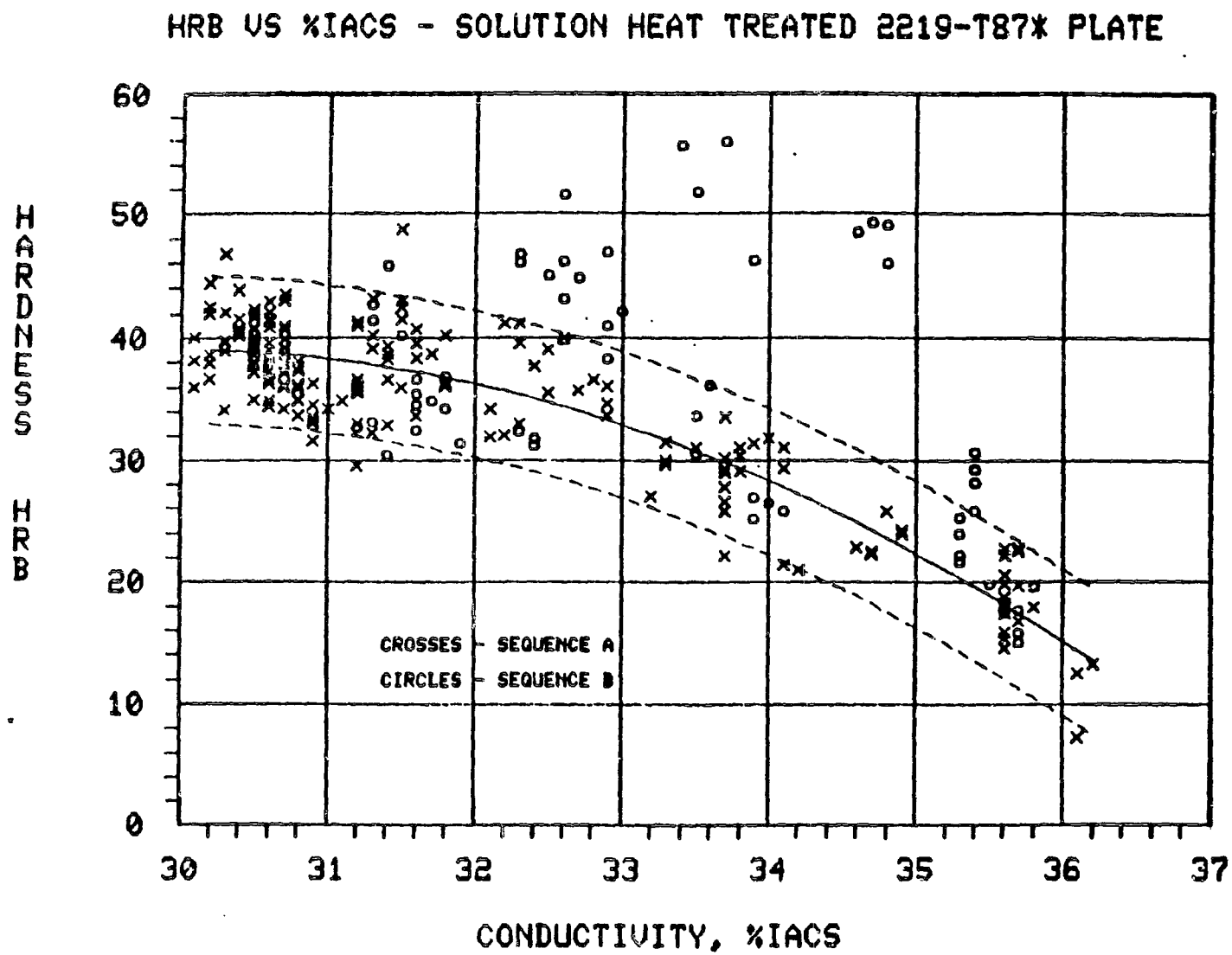

Figure 29. Hardness vs. conductivity for 2219 aluminum alloy given a solution heat treatment and a salt-bath pre-aging treatment. Pre-aging treatments varied between 250°C and 475°C in temperature and between 2 and 3600 seconds in time.

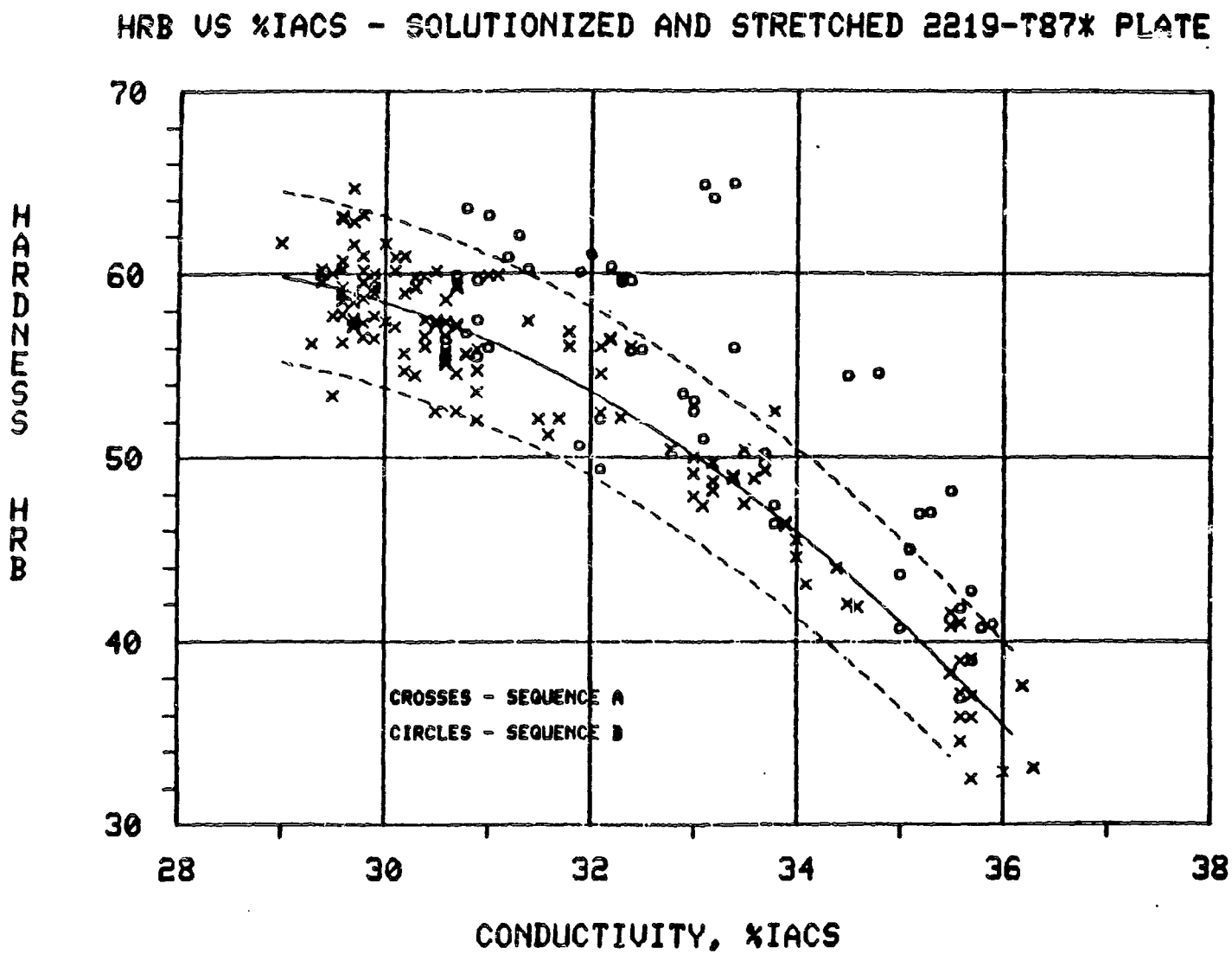

Figure 30. Hardness vs. conductivity for 2219 aluminum alloy given a 5% stretch after a solution heat treatment and a salt-bath pre-aging treatment.

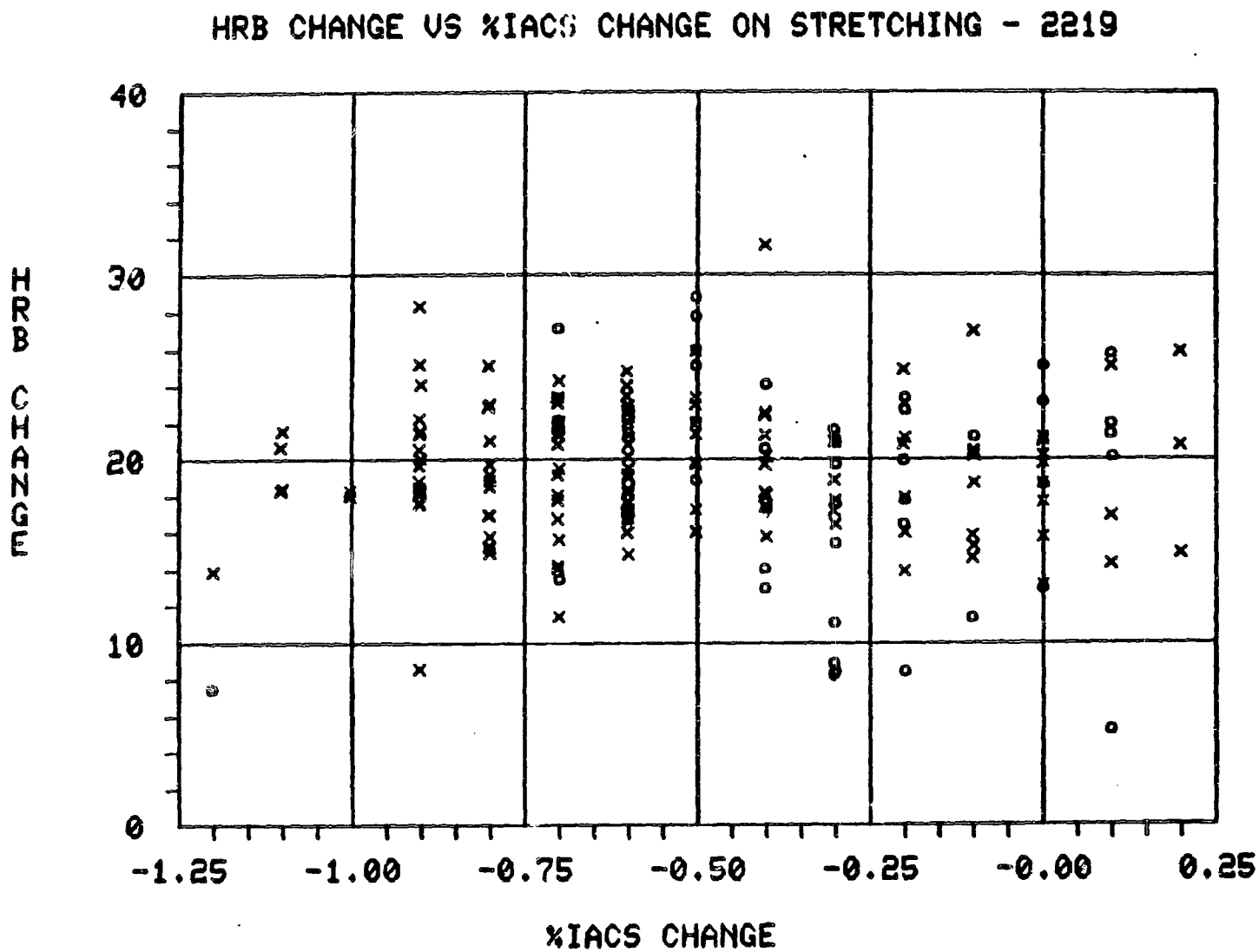

Figure 31. The change in sample hardness vs. the change in sample conductivity which occurs in solutionized and pre-aged 2219 aluminum alloy upon stretching to 5% permanent strain.

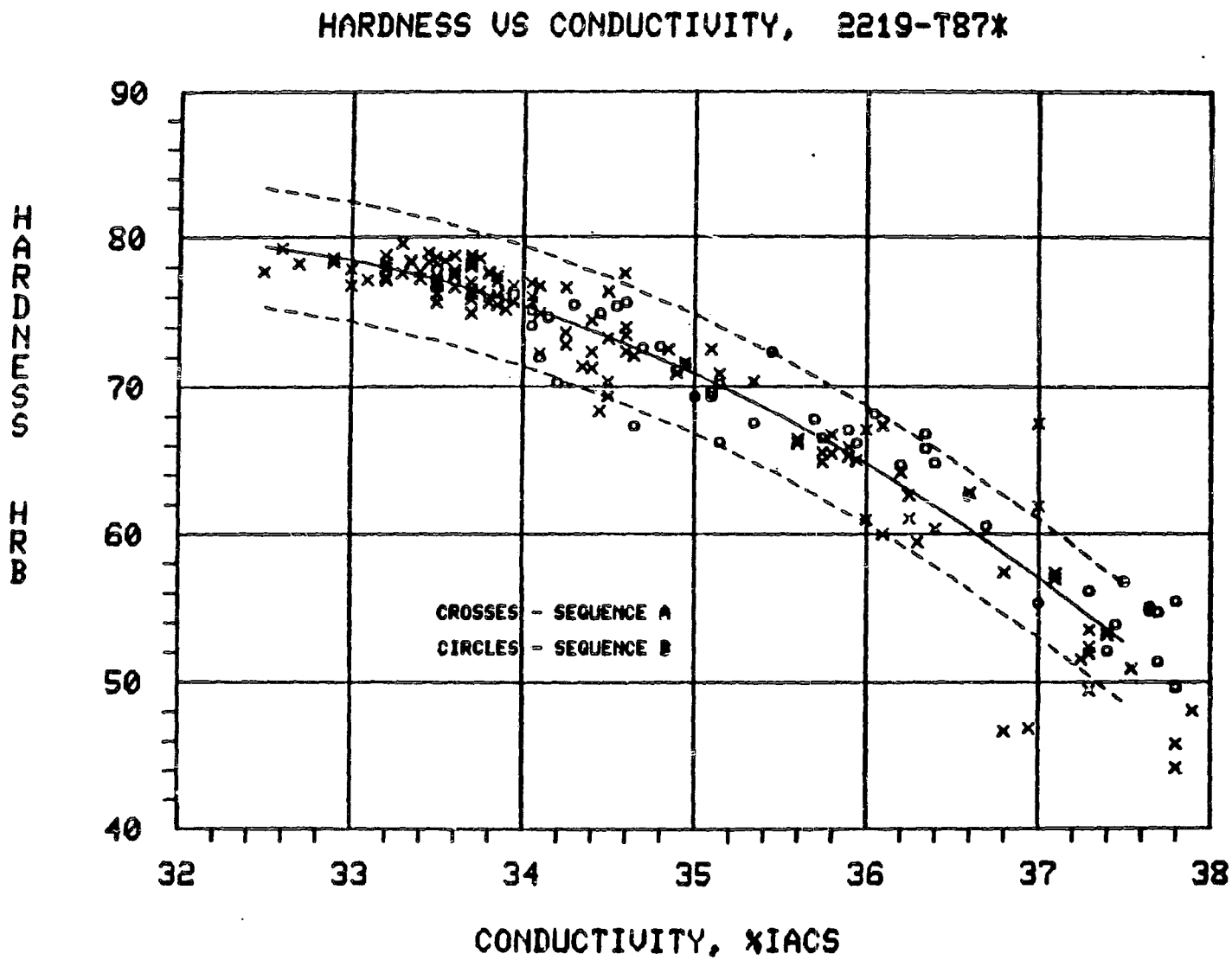

Figure 32. Hardness vs. conductivity for 2219-T87*. The solid line represents a least squares quadratic fit to all the data and the dotted lines a scatter band (approx. 95% confidence level).

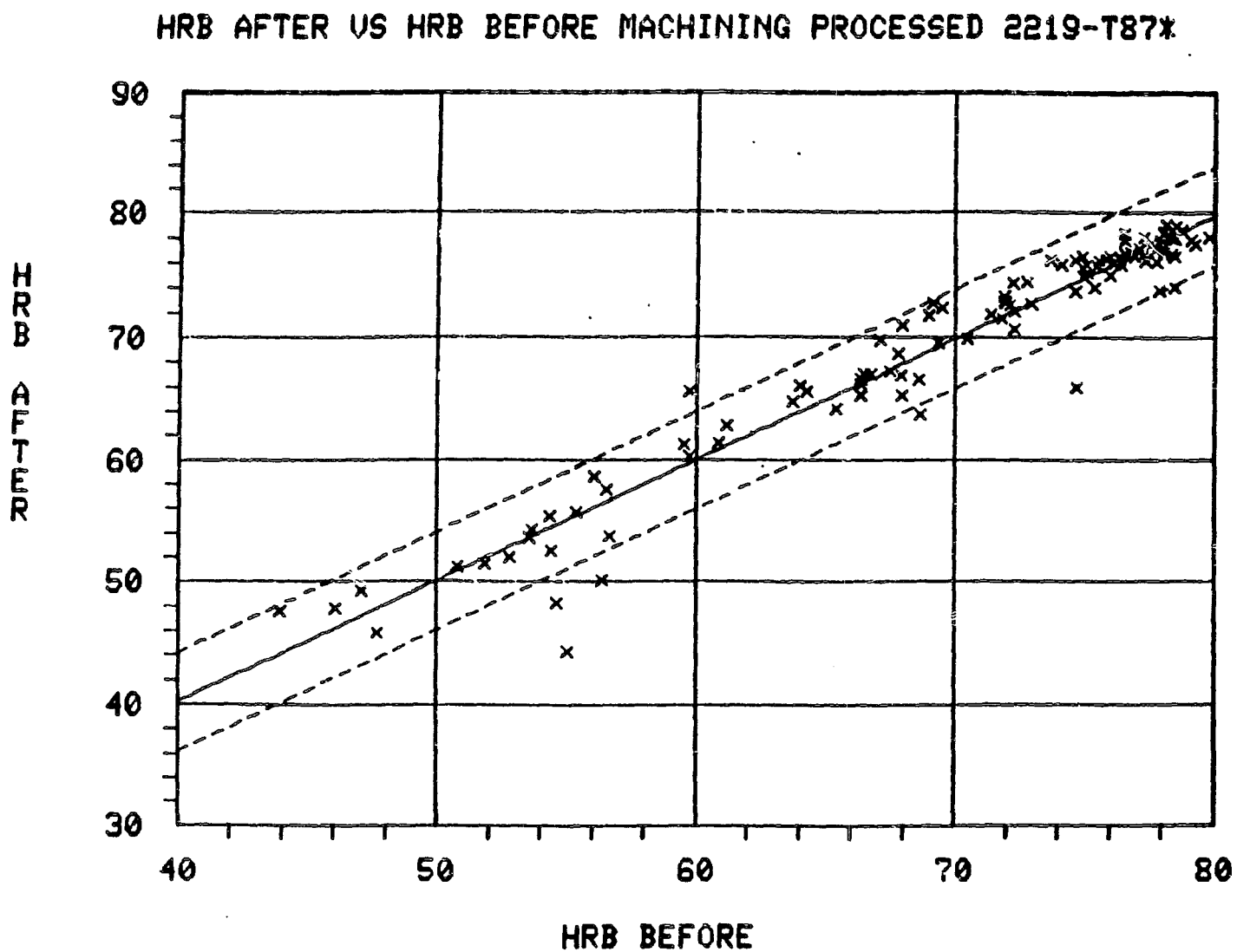

Figure 33. The hardness obtained after machining approximately 0.6 mm from the surface of aged 2219-T87* alloys plotted as a function of the hardness obtained before machining. The solid line is a linear least squares fit to the data points and the dotted lines are the scatter band (∿ 95% confidence level).

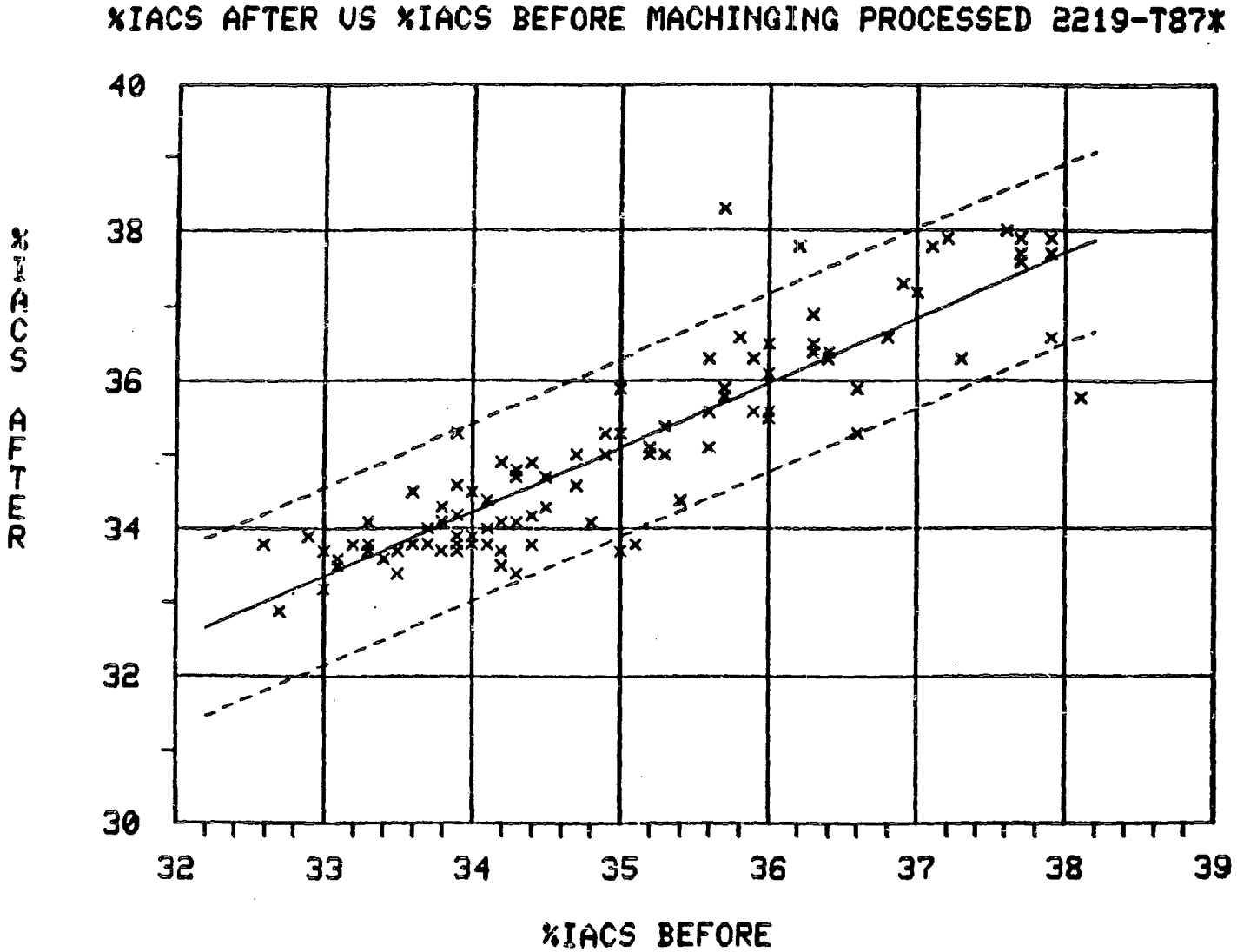

Figure 34. Conductivity obtained after machining approximately 0.6 mm from the surface of aged 2219-T87* alloys plotted as a function of the conductivity before machining. The solid line is a linear least squares fit to the data points and the dotted lines are the scatter band (∿ 95% confidence level).

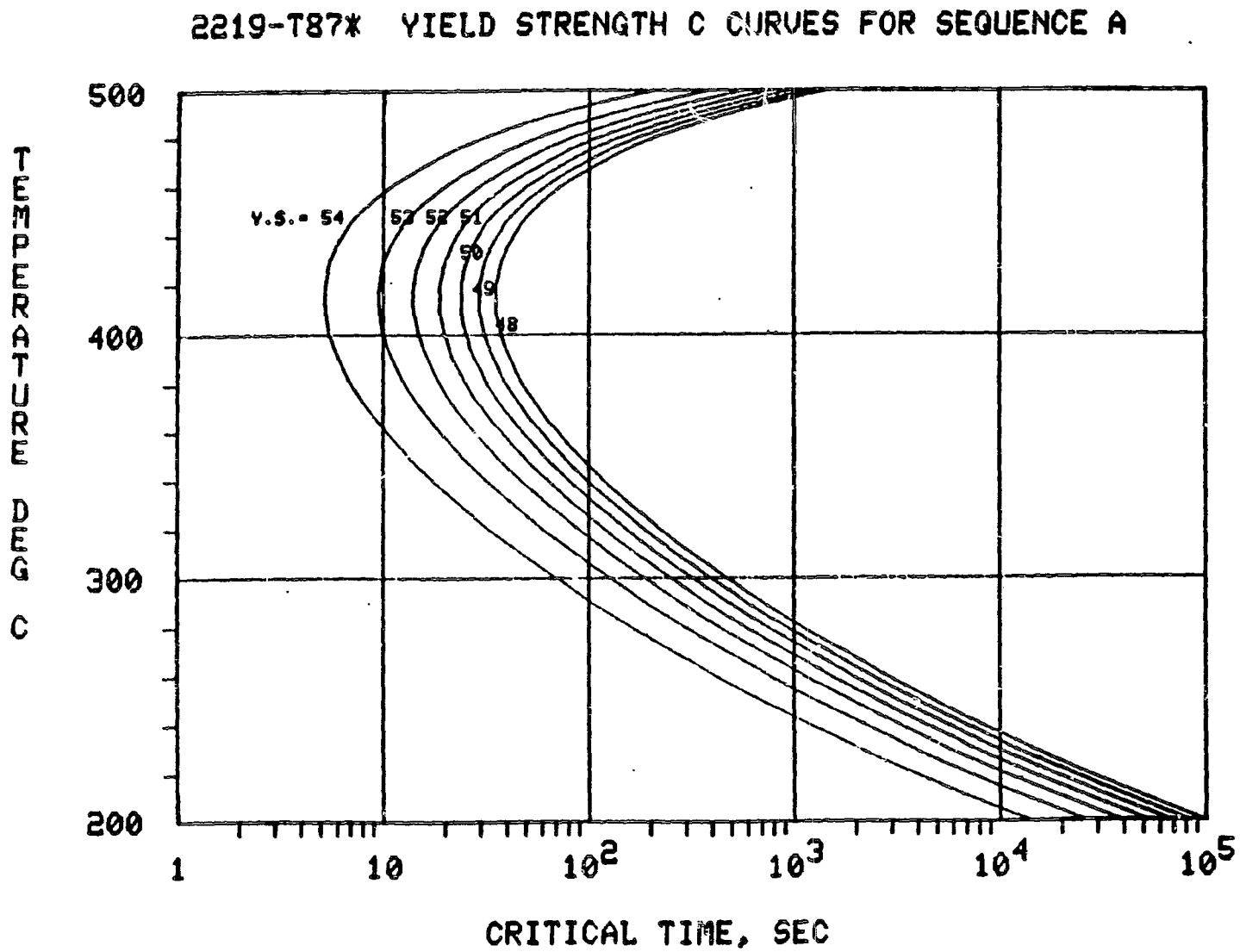

Figure 35. Yield strength C curve representation for sequence A alloys. The curves give the critical times for obtaining the indicated yield strength (0.2% offset) for an isothermal sequence A type heat treatment.

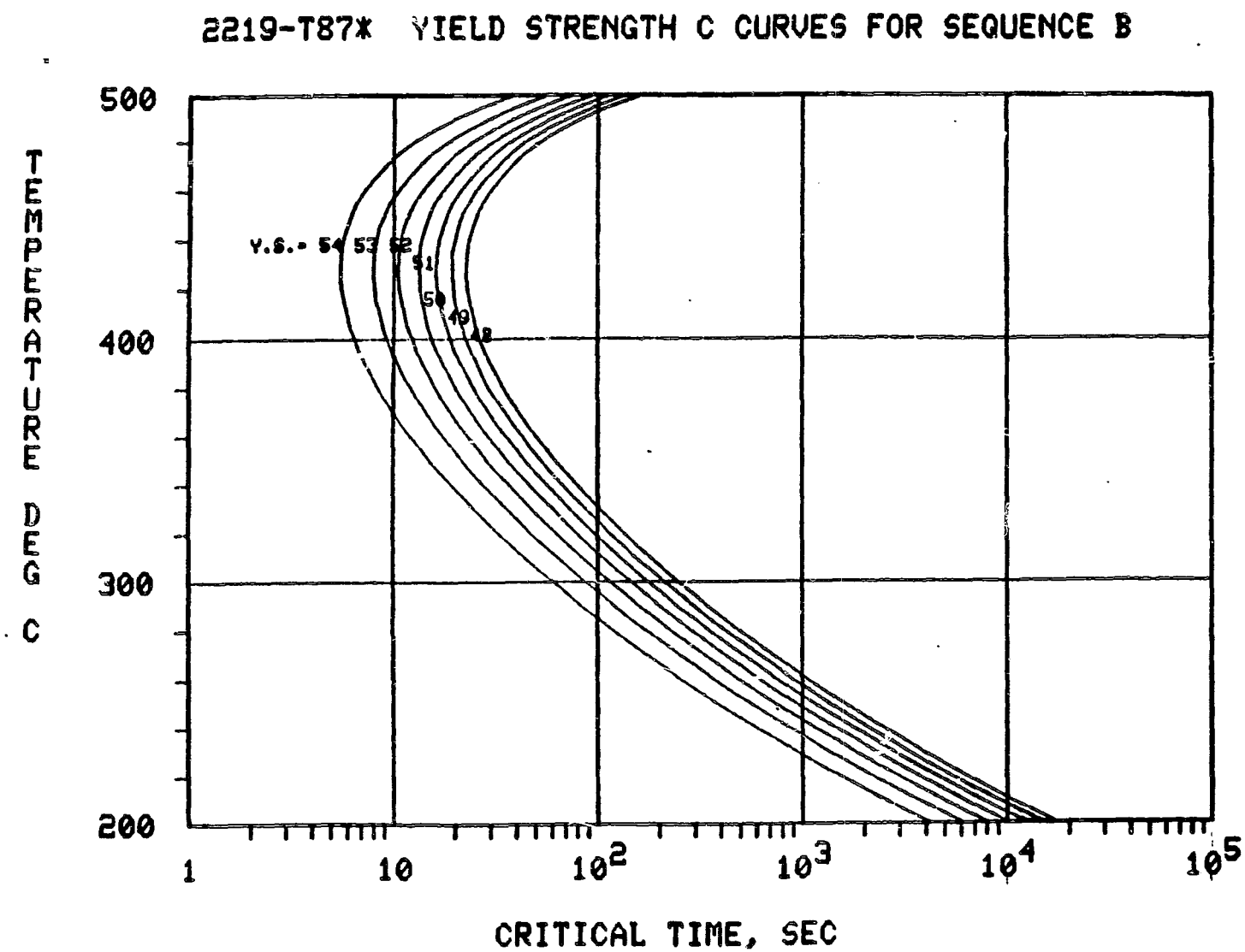

Figure 36. Yield strength C curve representation for sequence B alloys. The curves give the critical times for obtaining the indicated yield strength (0.2% offset) for an isothermal sequence B type heat treatment.

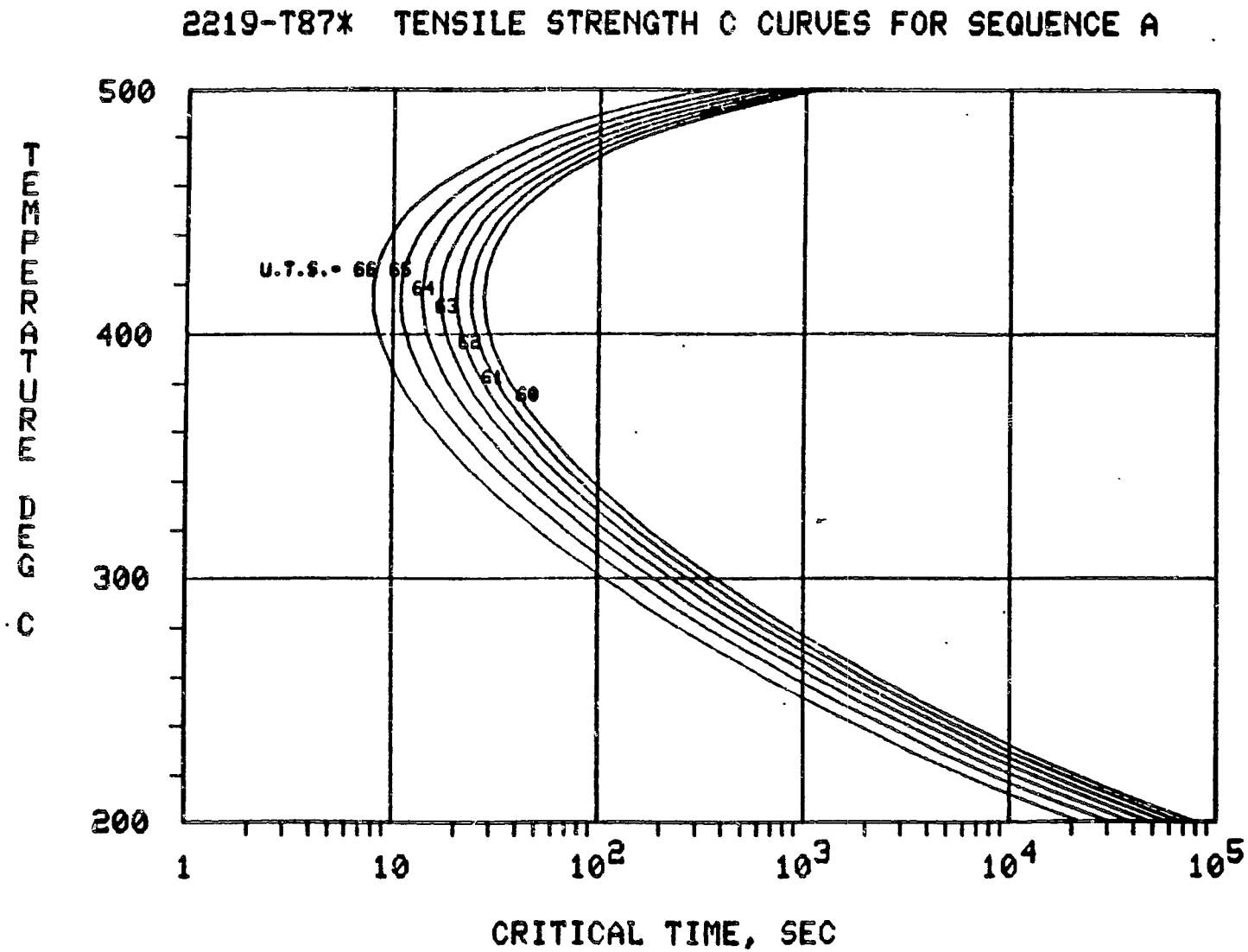

Figure 37. Tensile strength C curve representation for sequence A alloys. The curves give the critical times for obtaining the indicated ultimate tensile strength for an isothermal sequence A type heat treatment.

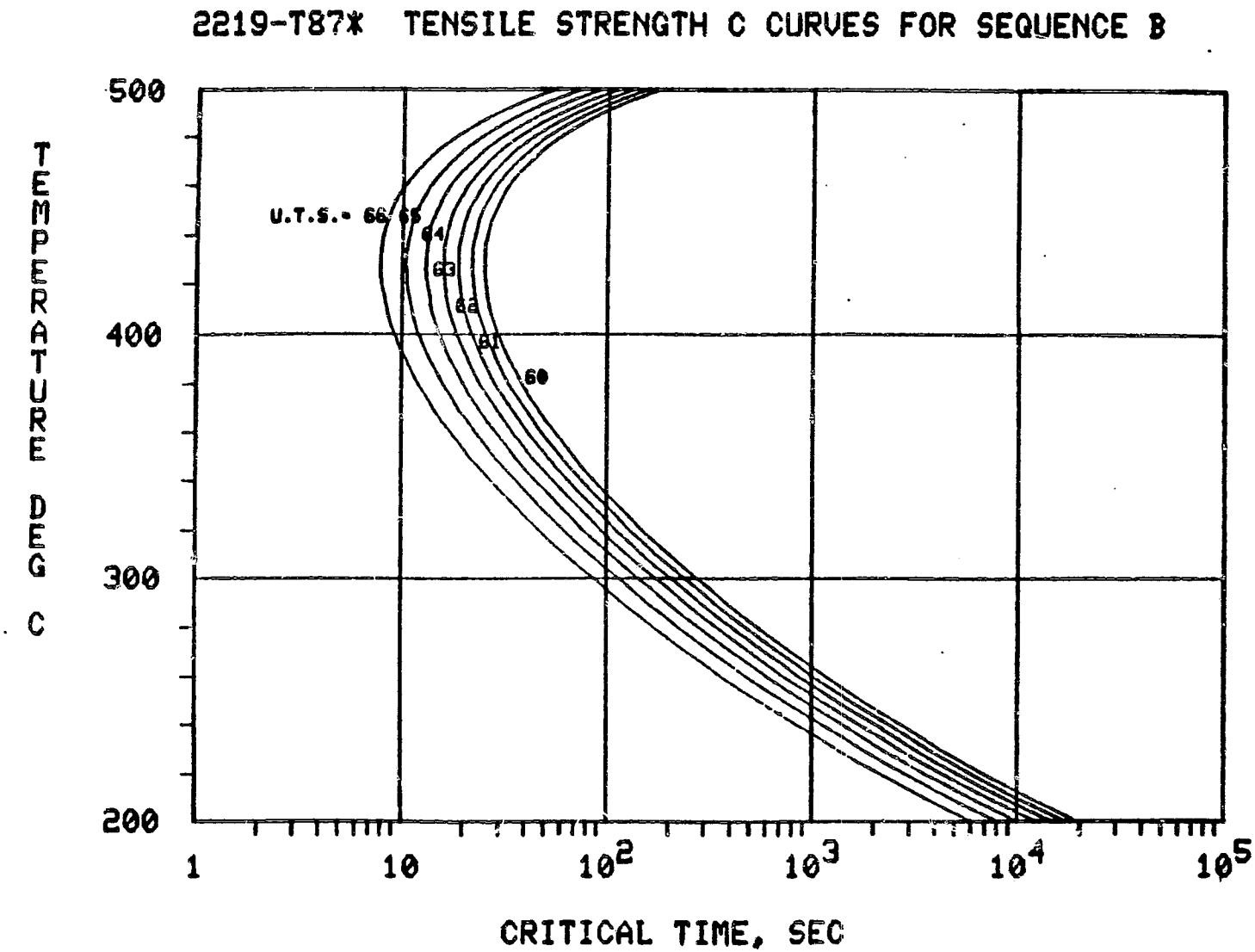

Figure 38. Tensile strength C curve representation for sequence B alloys. The curves give the critical times for obtaining the indicated ultimate tensile strengths for an isothermal sequence B type heat treatment.

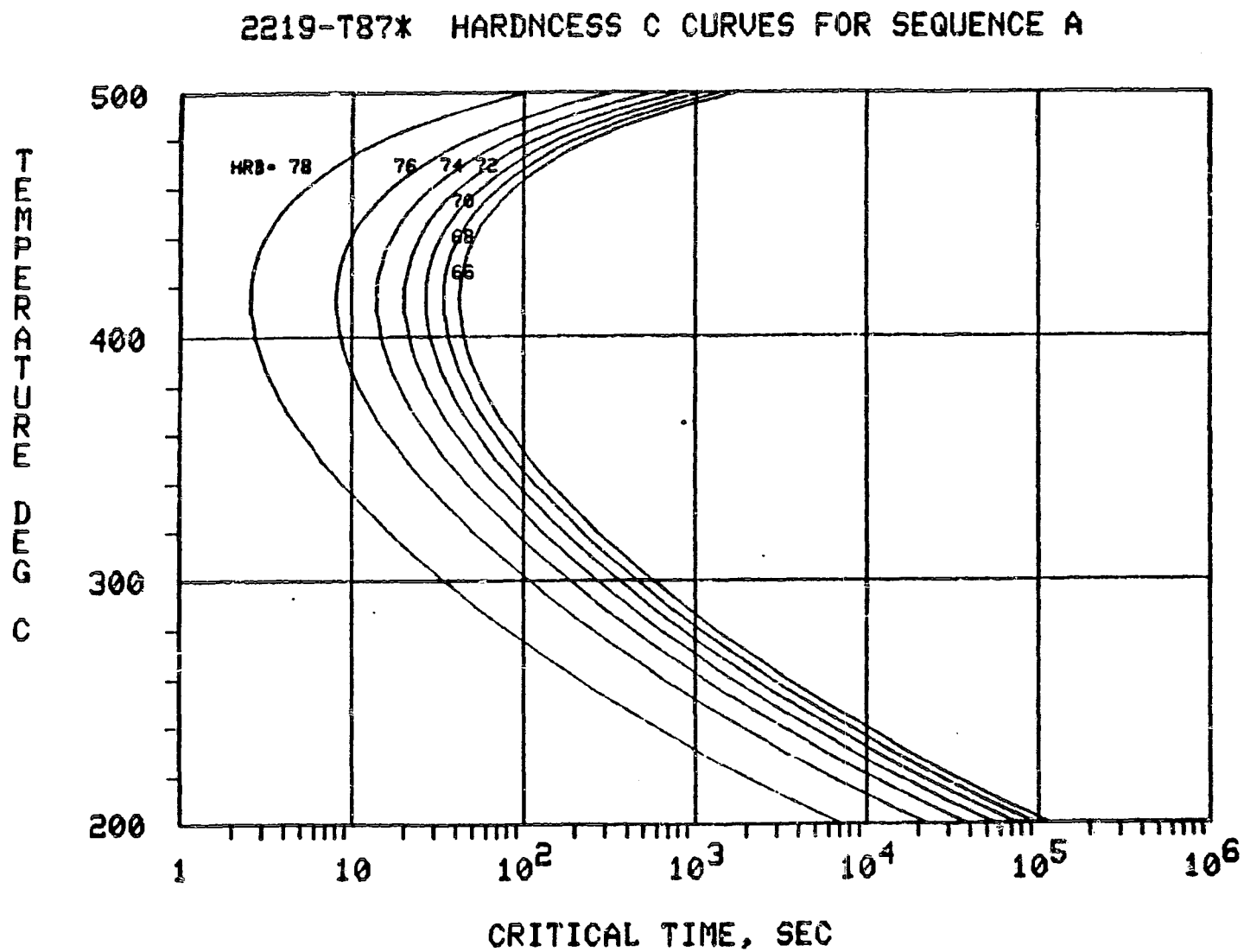

Figure 39. Hardness C curve representation for sequence A alloys. The curves give the critical times for obtaining the indicated hardness for an isothermal sequence A type heat treatment.

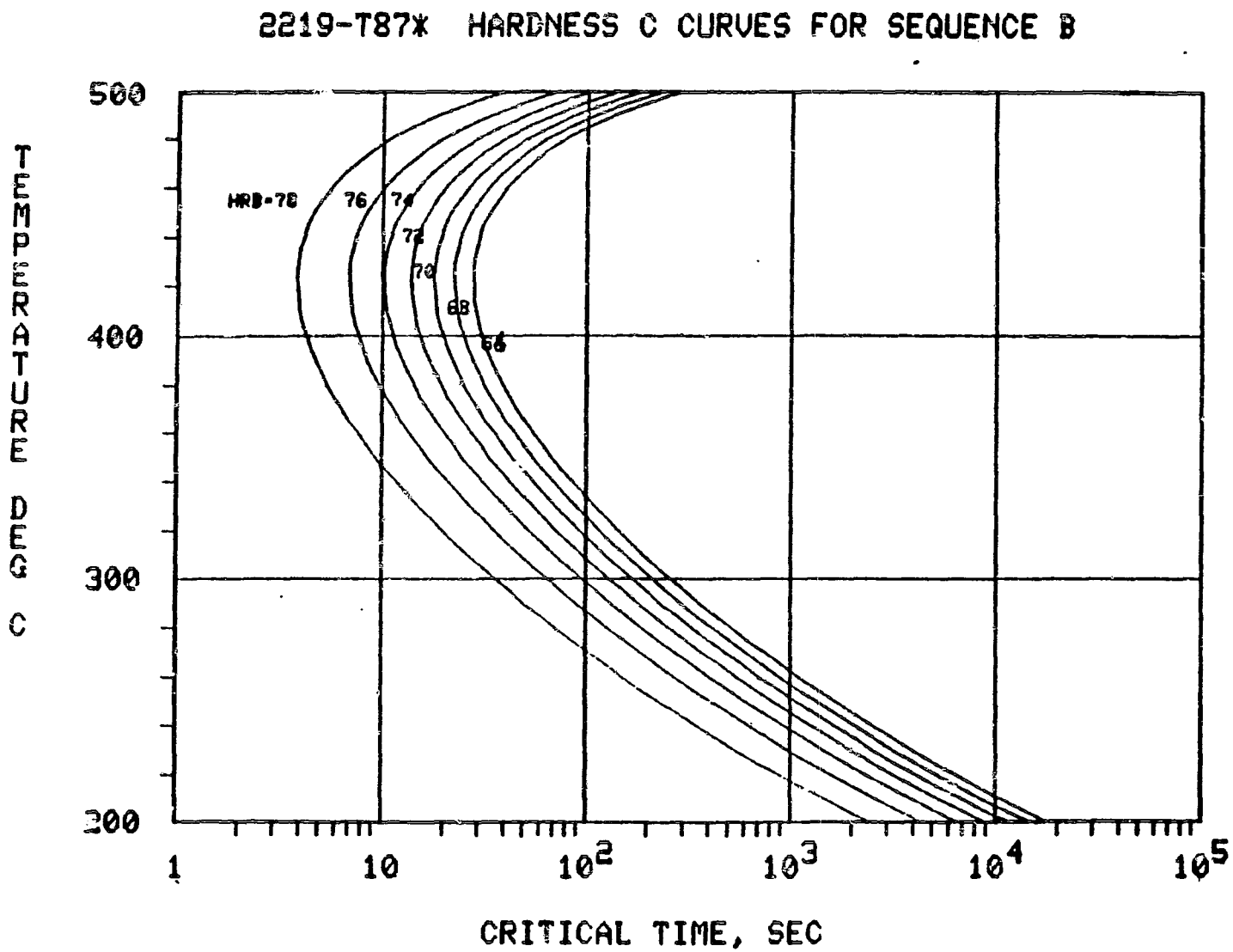

Figure 40. Hardness C curve representation for sequence B alloys. The curves give the critical times for obtaining the indicated hardness for an isothermal sequence B type heat treatment.

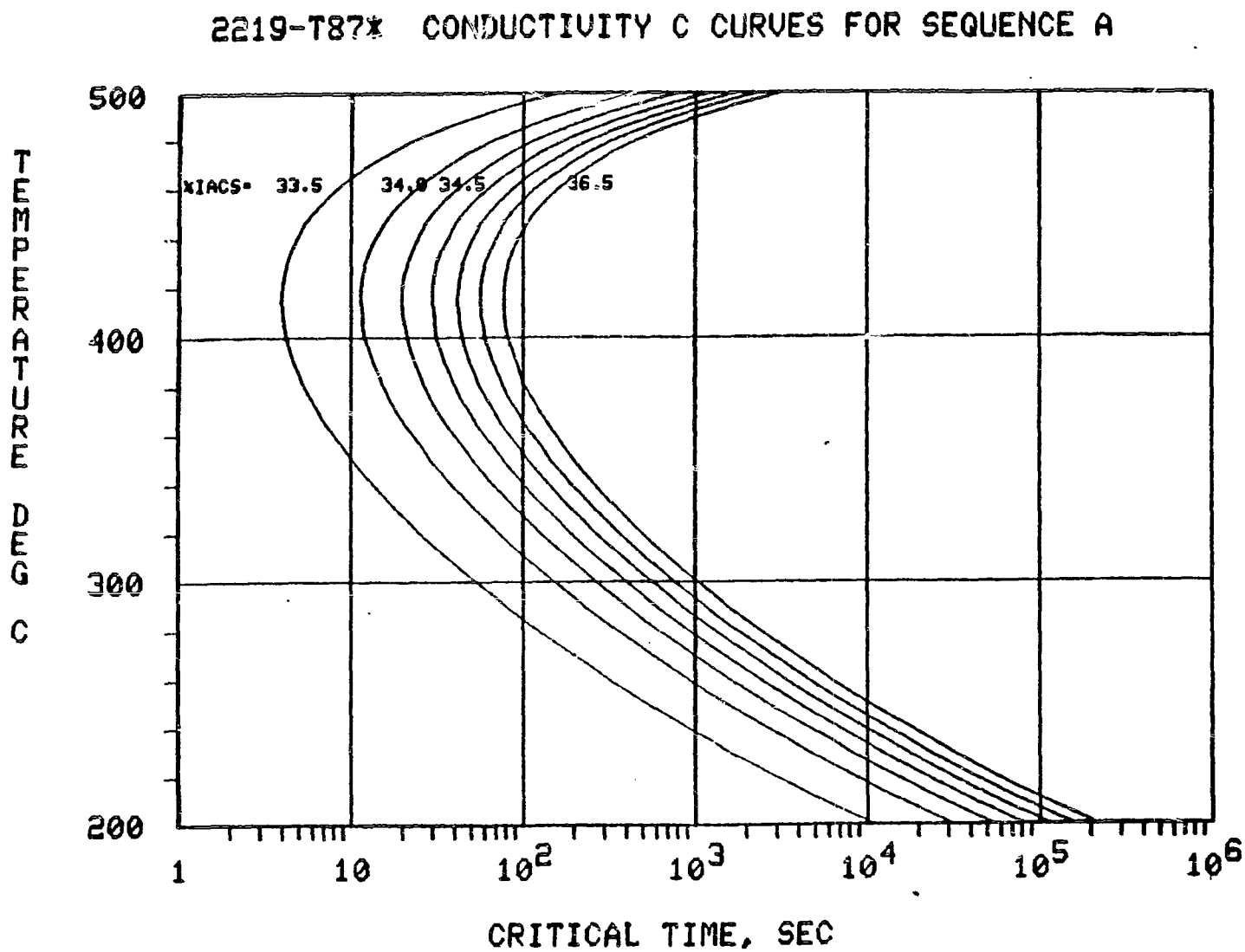

Figure 41. Conductivity C curve representation for sequence A alloys. The curves give the critical times for obtaining the indicated conductivity for an isothermal sequence A type heat treatment.

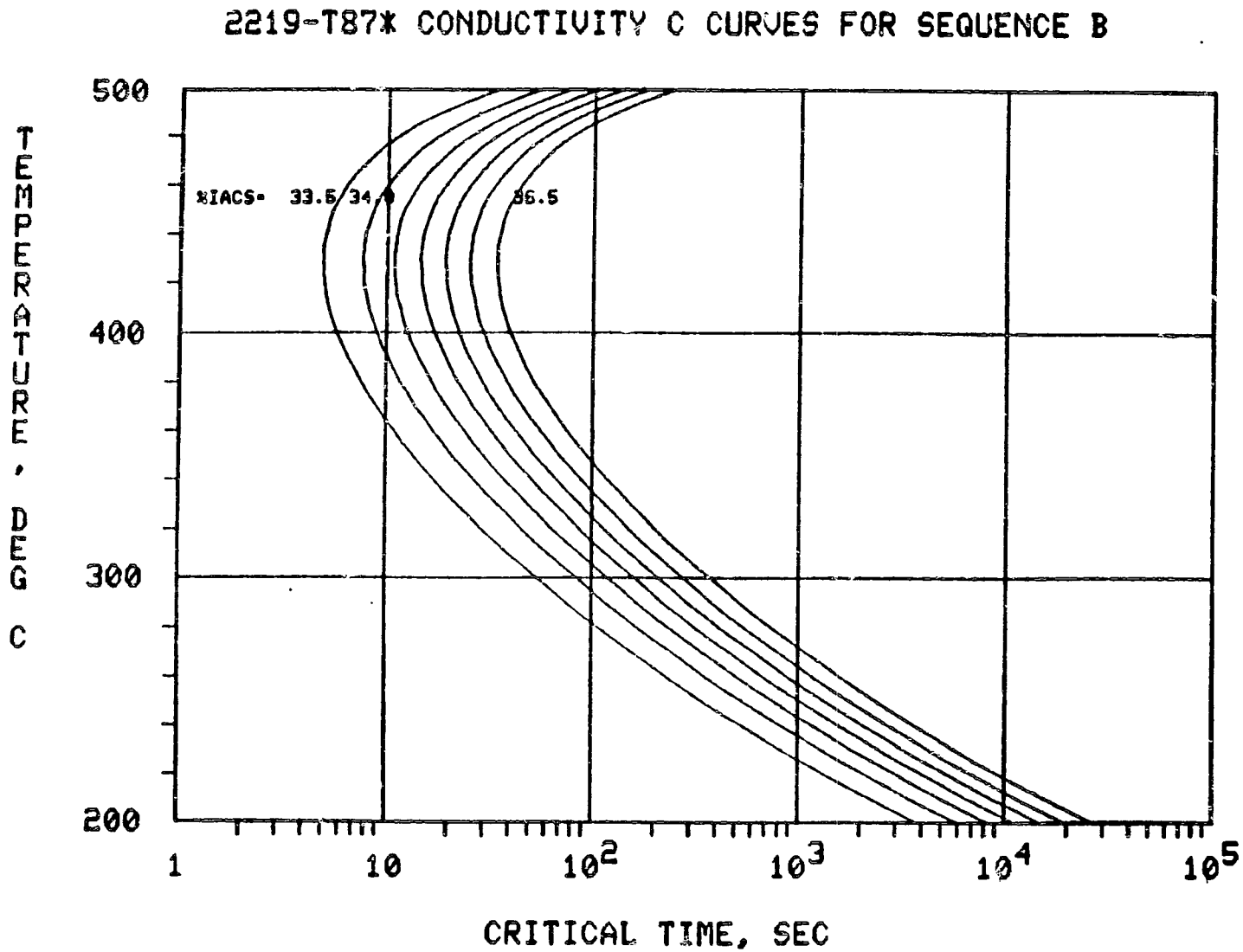

Figure 42. Conductivity C curve representation for sequence B alloys. The curves give the critical times for obtaining the indicated conductivity for an isothermal sequence B type heat treatment.

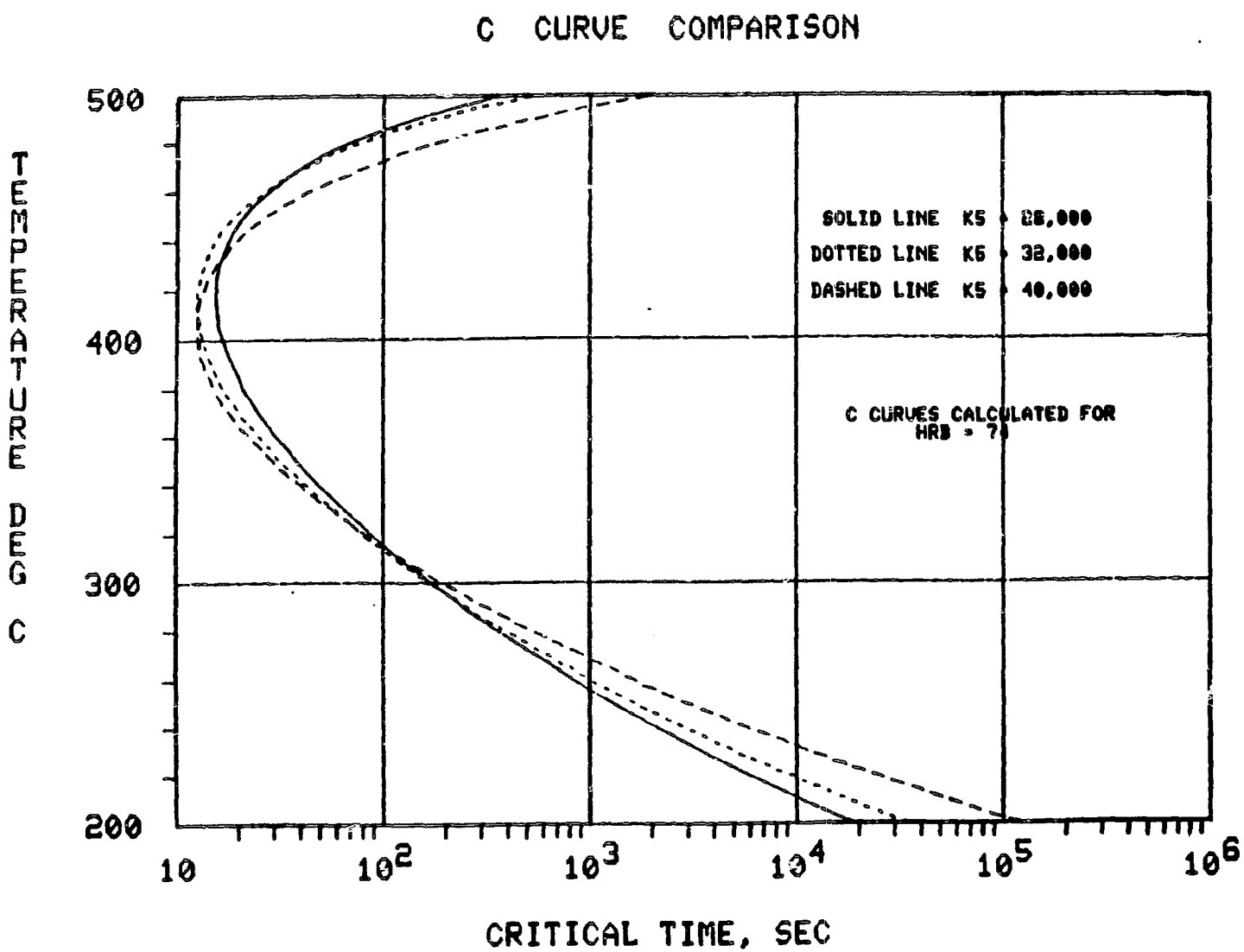

Figure 43. Comparison of hardness C curves obtained for three different values of the parameter K_5. The curves represent the critical times for obtaining a Rockwell B hardness of 74 for an isothermal sequence A type heat treatment.

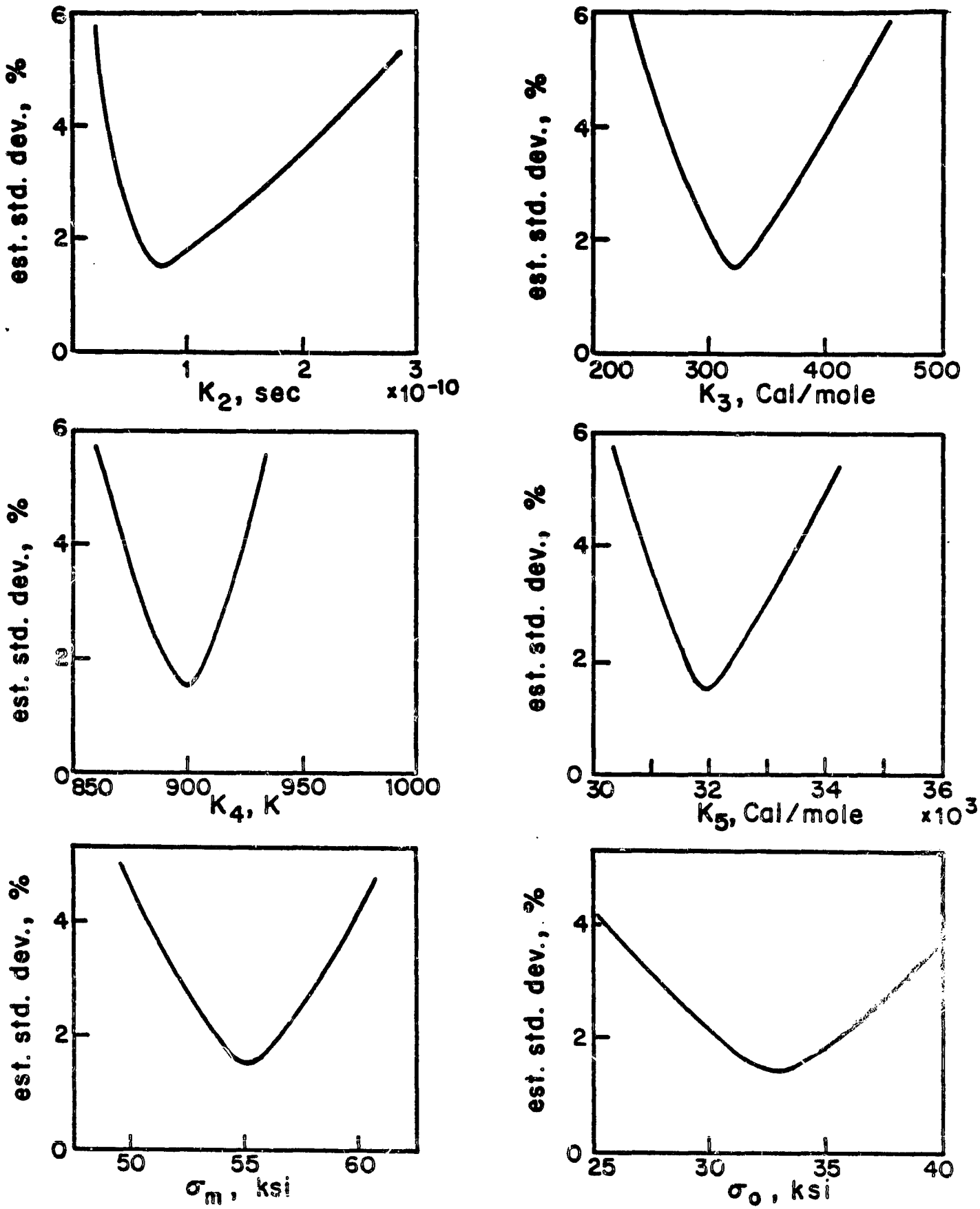

Figure 44. Estimated standard deviation for changes of only one C curve parameter at a time in the sequence A values for yield strength.

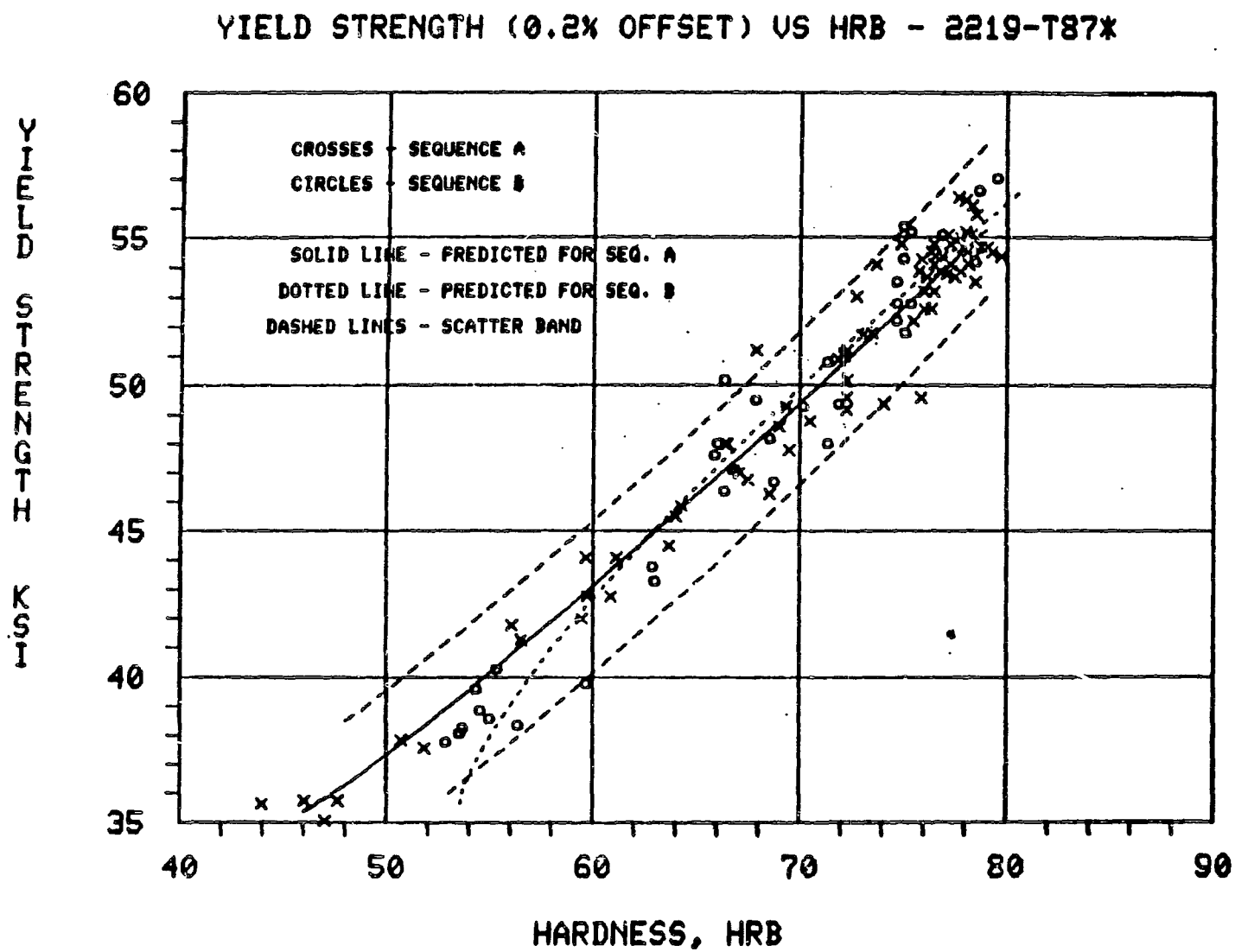

Figure 45. Comparison of yield strength vs. hardness data with the correlations predicted by the C curves. The dashed lines are the scatter band (~95% confidence level) obtained from a least squares quadratic fit to the data.

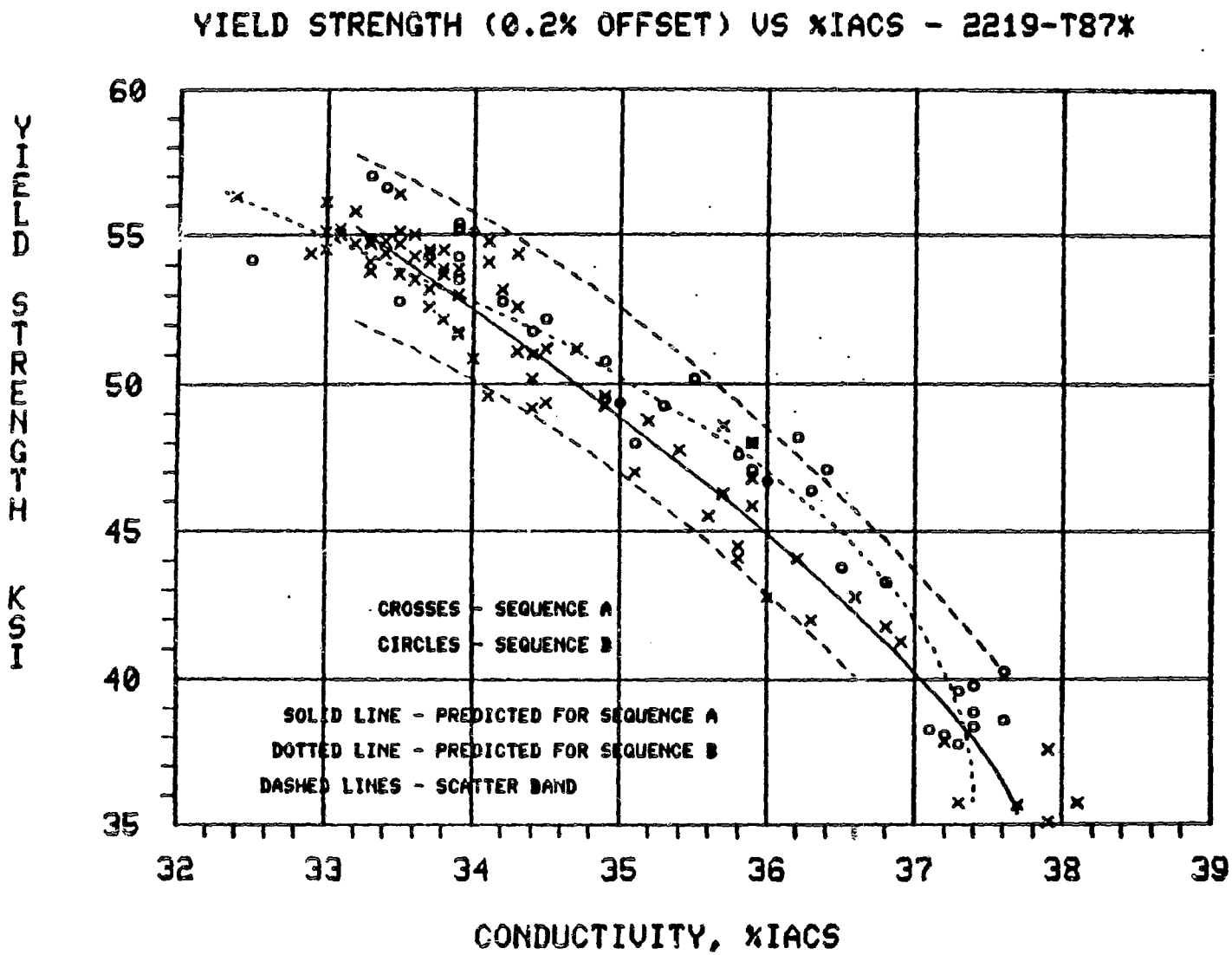

Figure 46. Comparison of yield strength vs. conductivity data with correlations predicted by the C curves. The dashed lines are the scatter band (~95% confidence level) obtained from a least squares quadratic fit to the data.

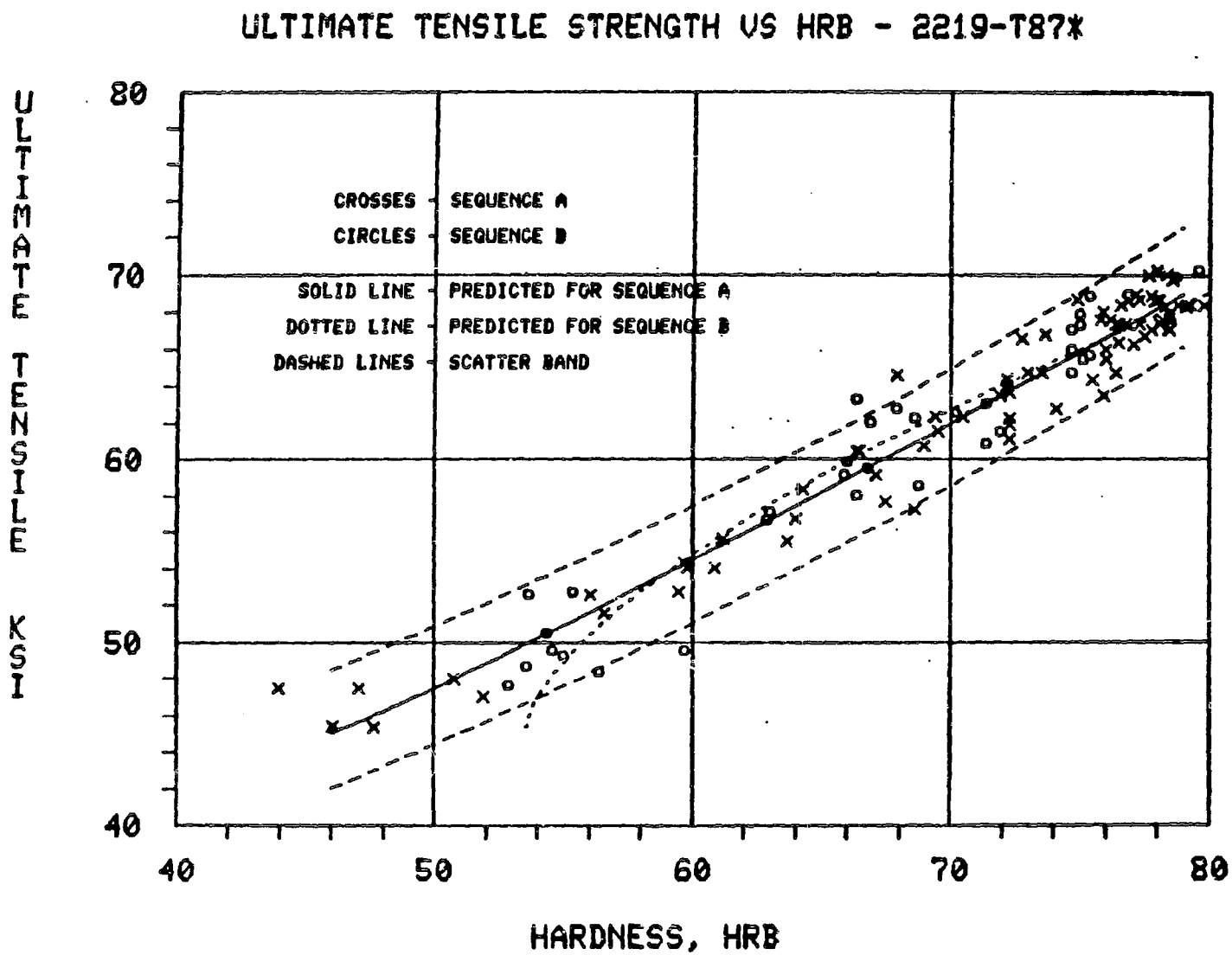

Figure 47. Comparison of tensile strength vs. hardness data with the correlations predicted by the C curves. The dashed lines are the scatter band (∿ 95% confidence level) obtained from a least squares quadratic fit to the data.

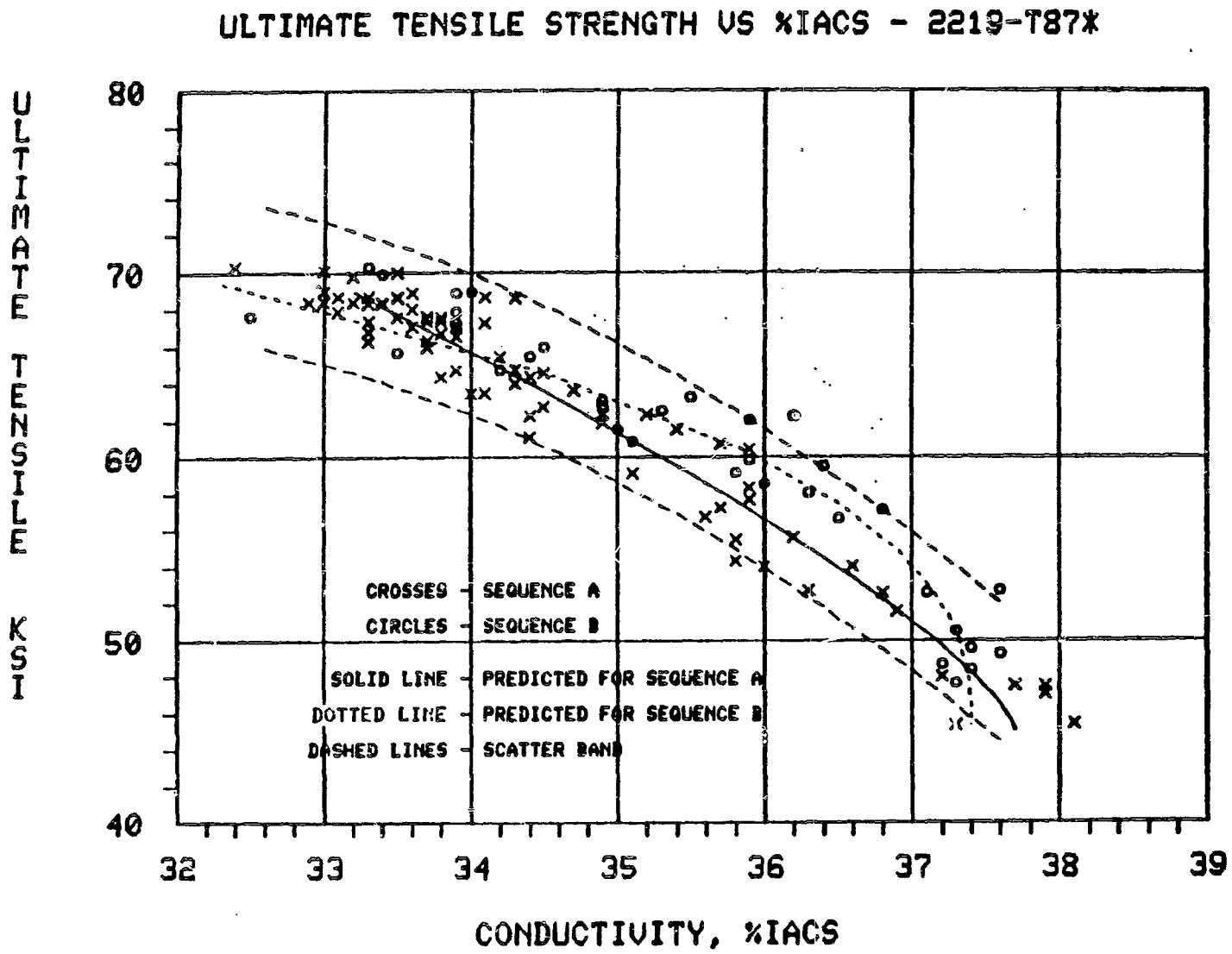

Figure 48. Comparison of tensile strength vs. conductivity data with the correlations predicted by the C curves. The dashed lines are the scatter band (∿ 95% confidence level) obtained from a least squares quadratic fit to the data.

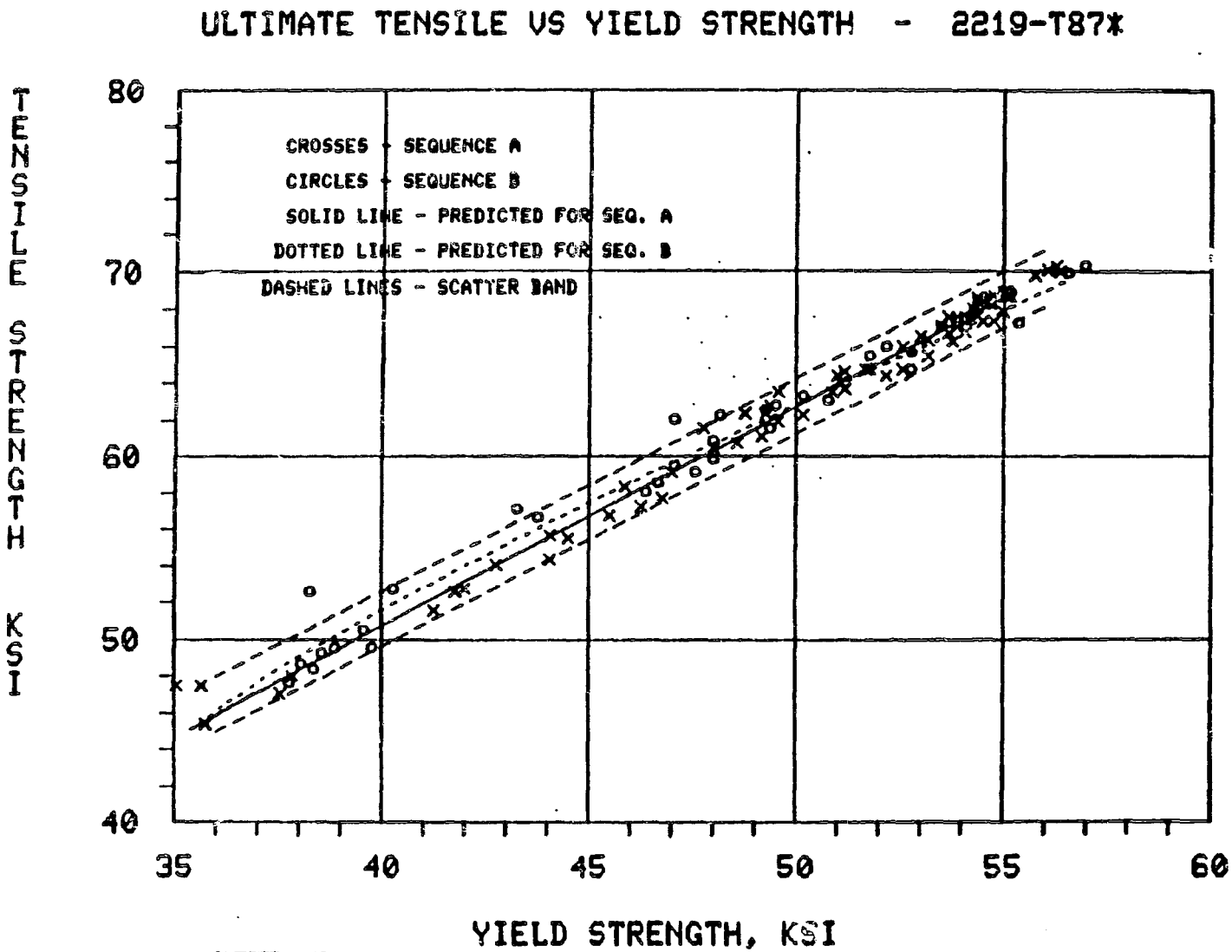

Figure 49. Comparison of tensile strength vs. yield strength with the correlations predicted by the C curves. The dashed lines are the scatter band (∿ 95% confidence level) obtained from a least squares quadratic fit to the data.

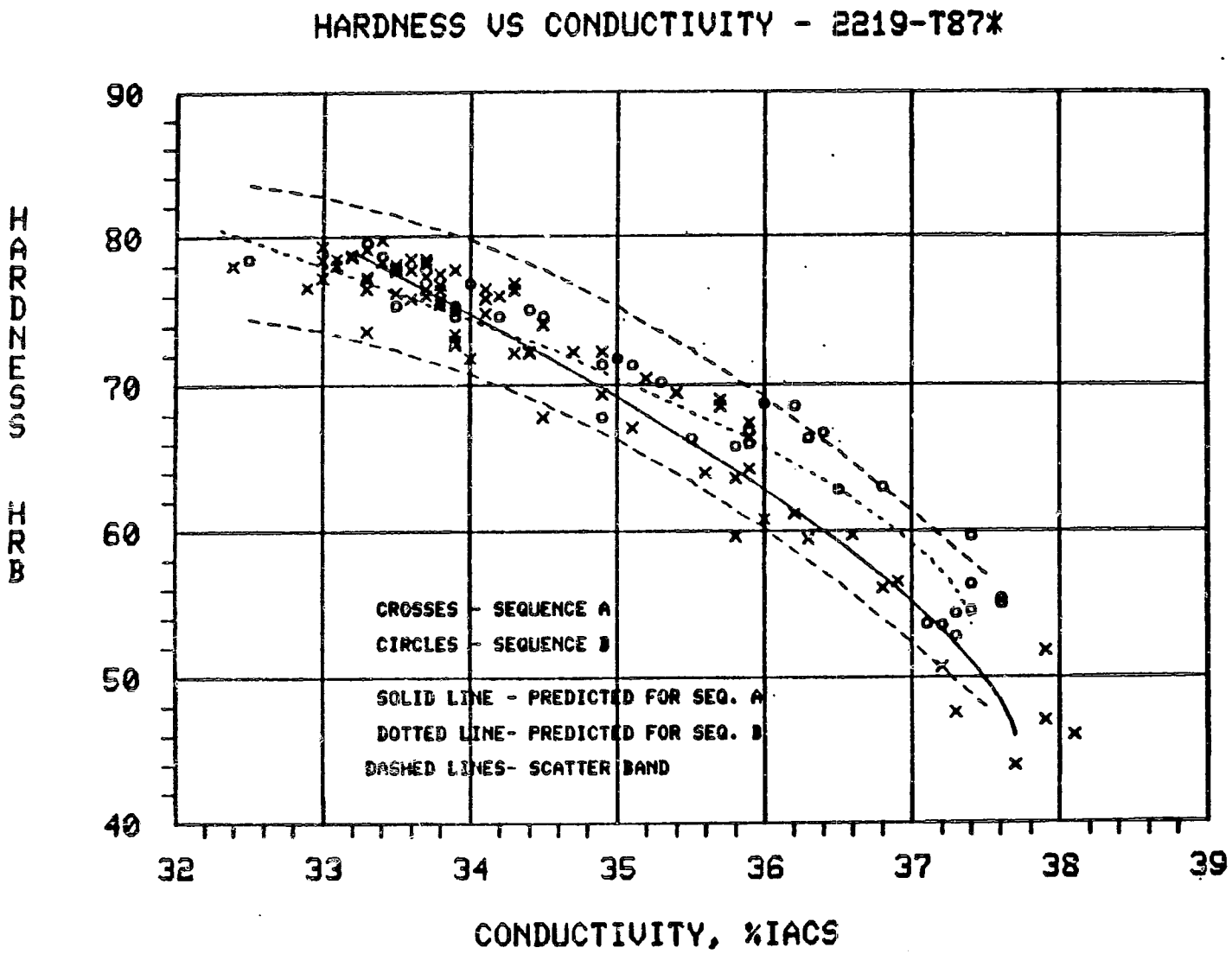

Figure 50. Comparison of hardness vs. conductivity data with the correlations predicted by the C curves. The dashed lines are the scatter band (∿ 95% confidence level) obtained from a least squares quadratic fit to the data.

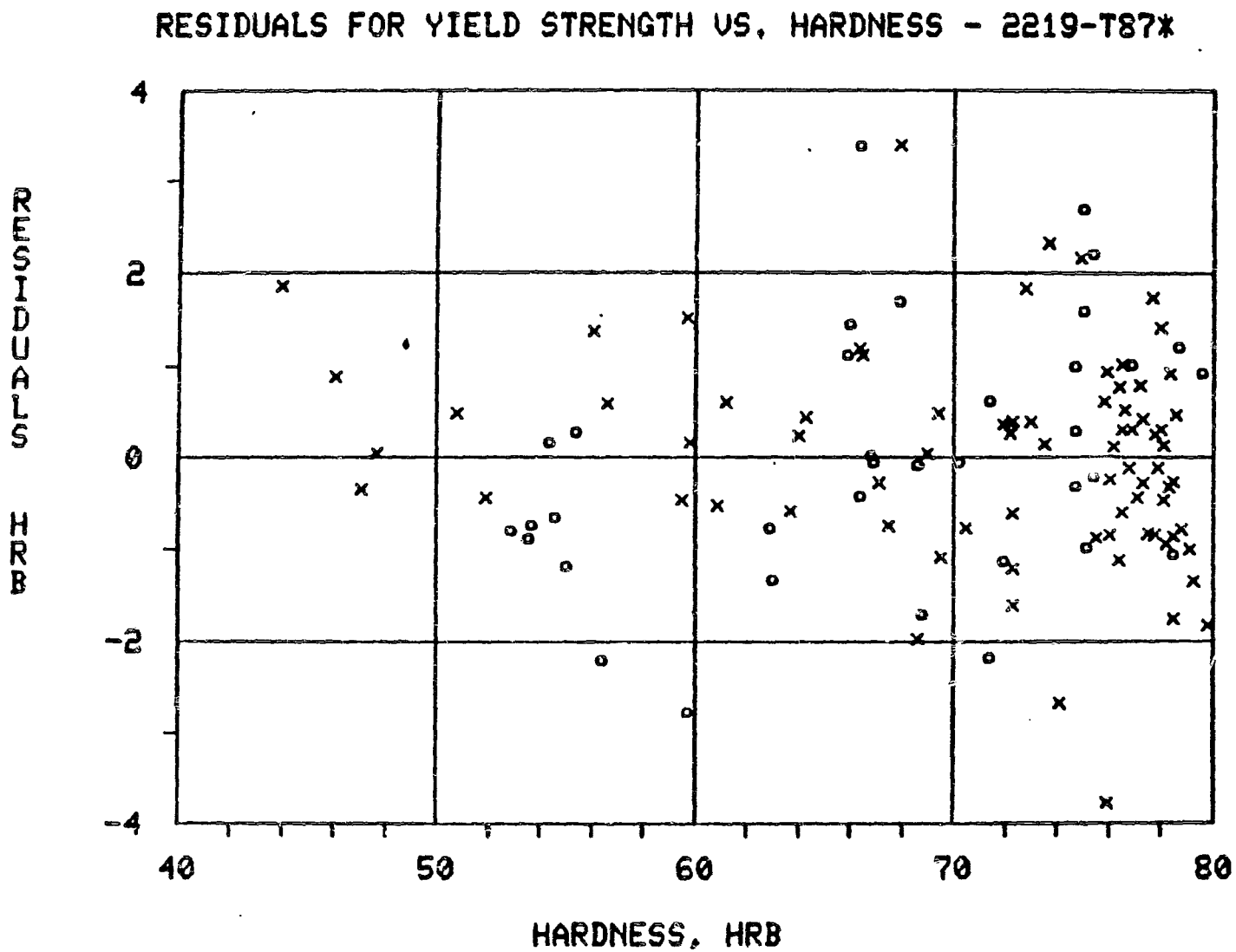

Figure 51. Residuals (measured minus least squares predicted values) for the fit of yield strength vs. hardness data. Shown in Figure 45.

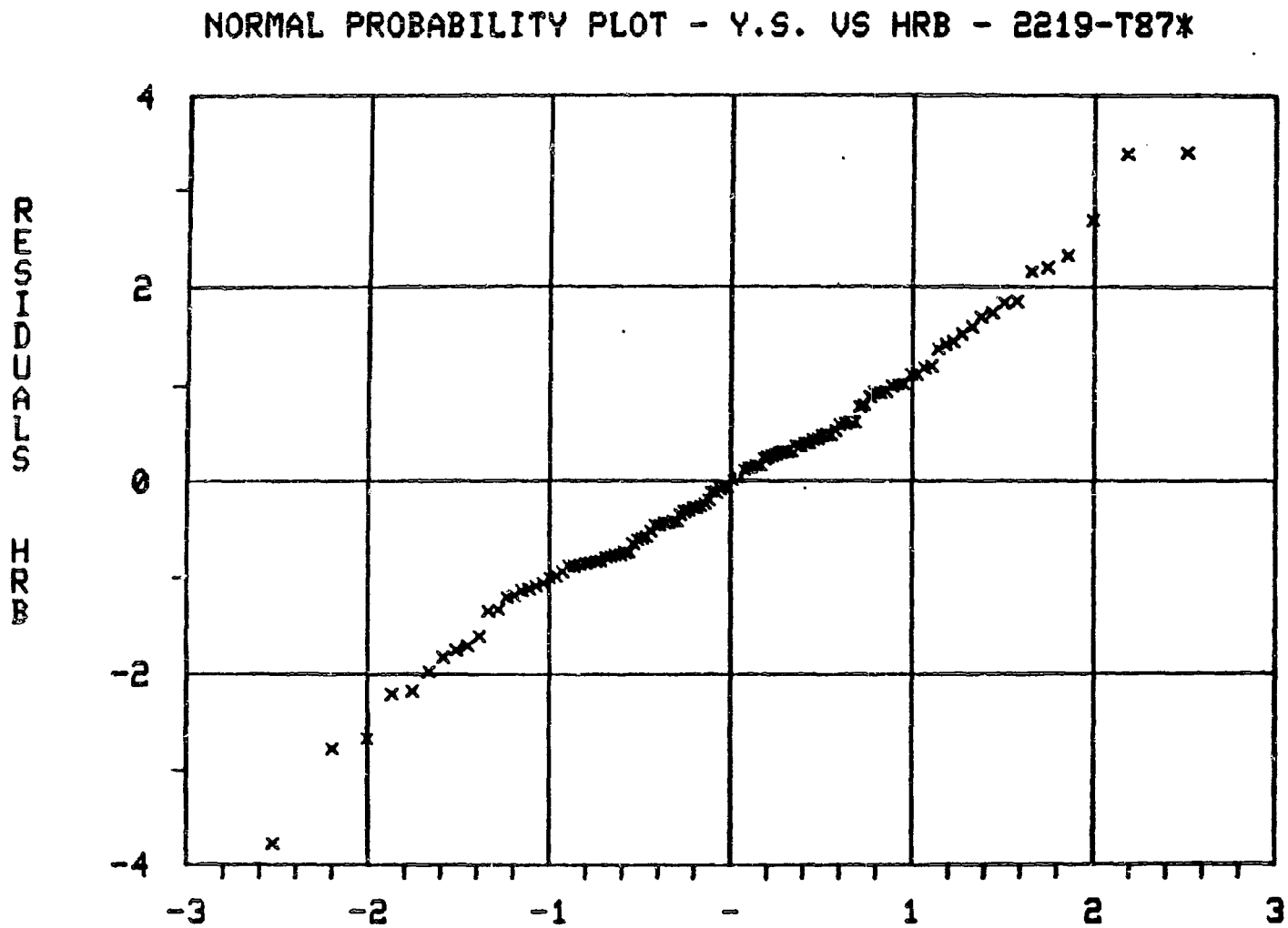

Figure 52. Normal probability plot of residuals from the least squares fit of yield strength vs. hardness data. Shown in Figure 45.

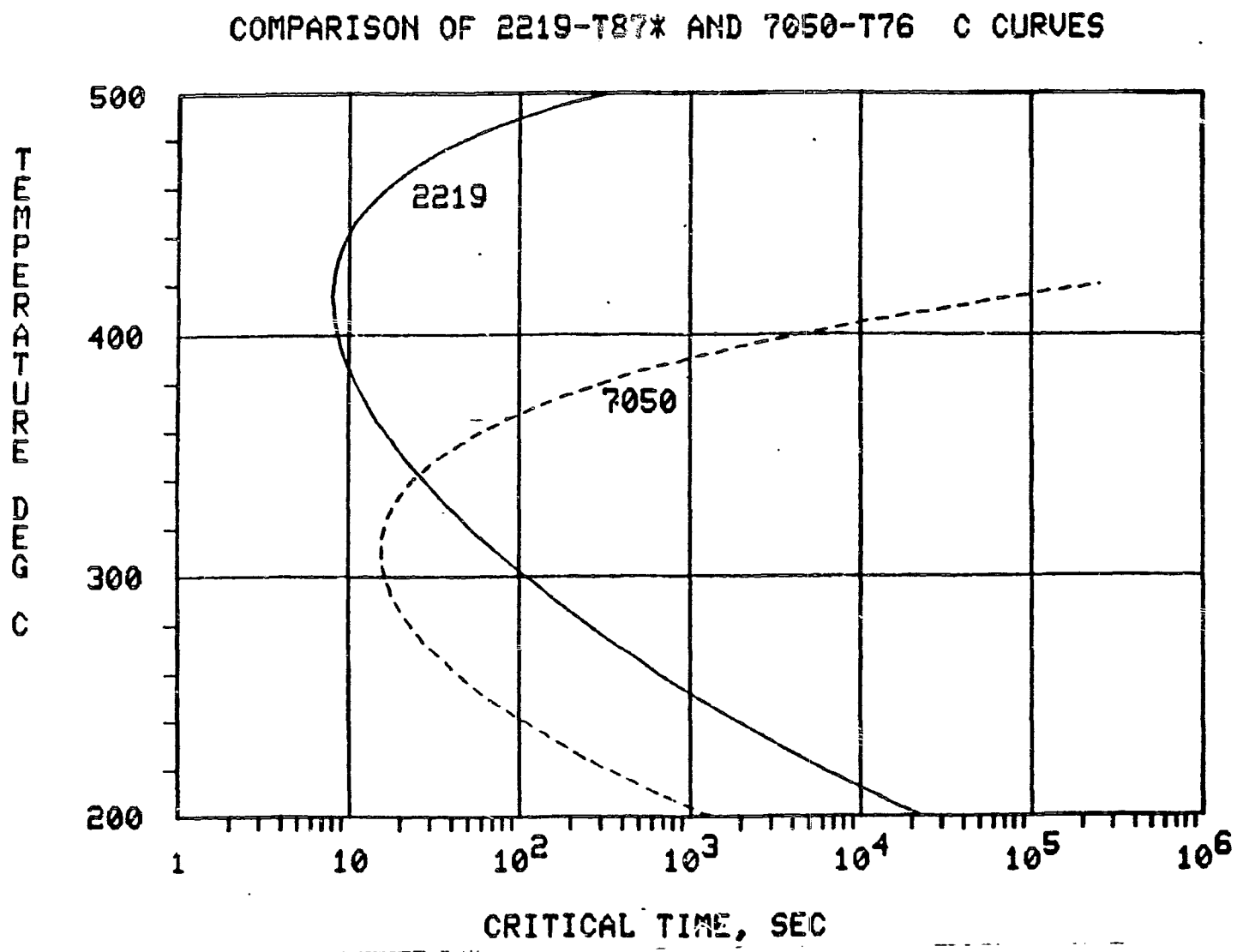

Figure 53. Comparison of the yield strength C curve of 2219-T87* with one determined by Evancho and Staley (Met. Trans. 5, 43, 1974) for 7050-T76. Plotted are the critical times for a sequence A isothermal anneal giving a 10% reduction in yield strength (assuming $\sigma_o << \sigma_m$).

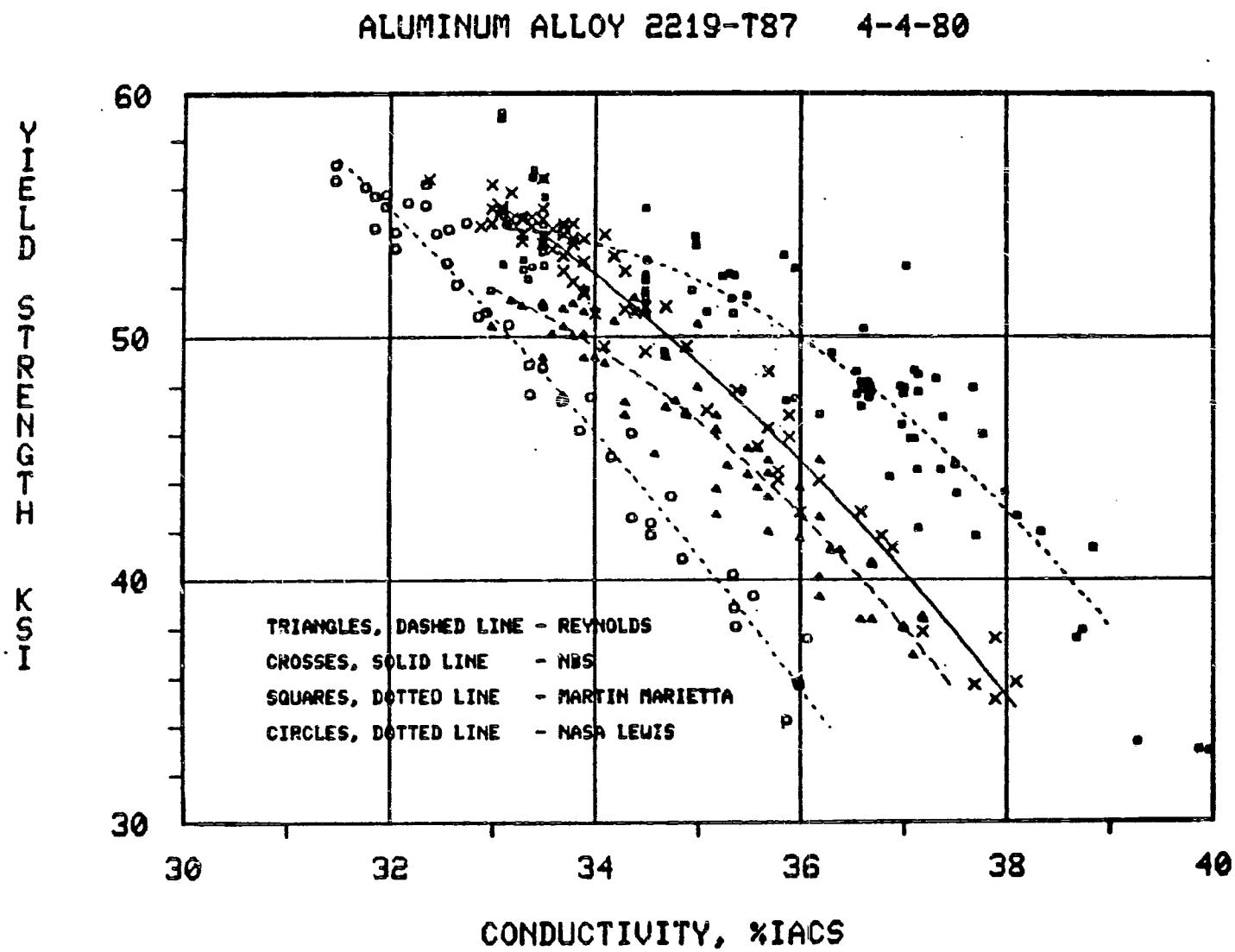

Figure 54. Comparison of yield strength vs. hardness for 2219-T87* as determined by four laboratories. The lines represent quadratic least squares fits to the data from the different laboratories, as indicated.

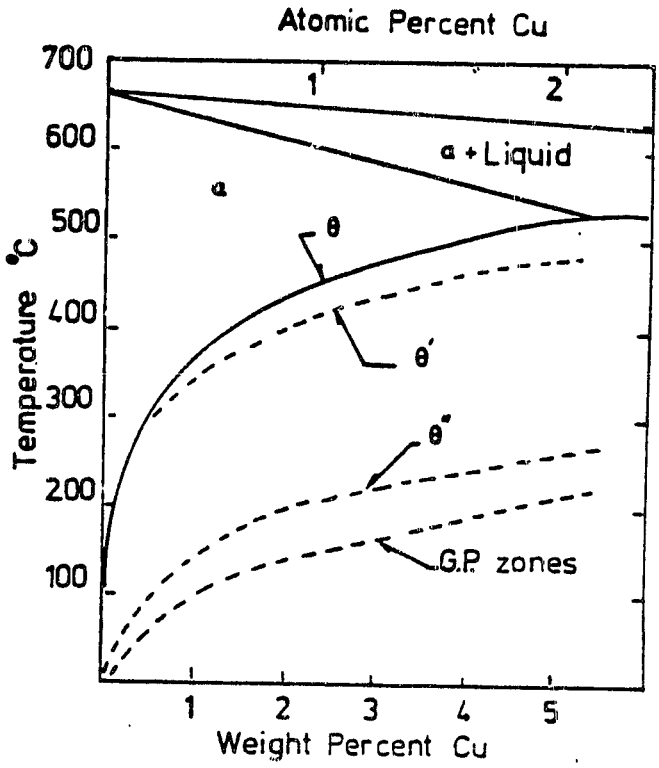

Figure 55. Al-rich portion of the Al-Cu binary equilibrium phase diagram, with G.P. zone, Θ" and Θ' metastable boundaries. From Lorimer (19) .

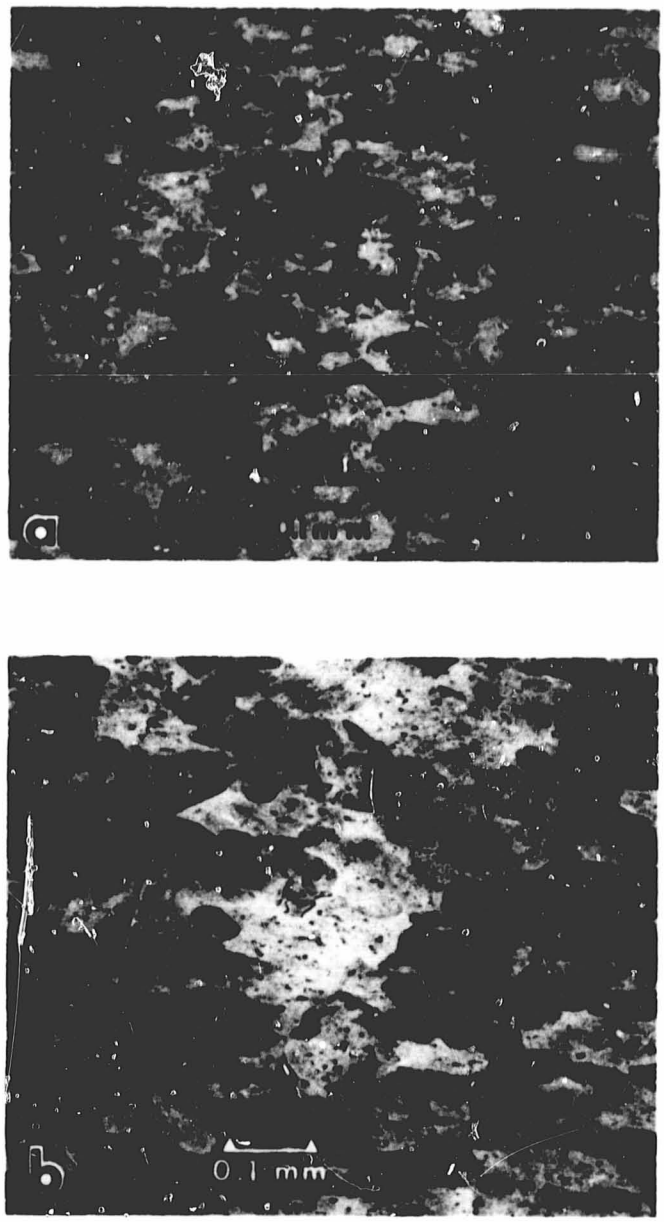

Figure 56. Optical micrographs showing grain structure of as-received plates of 2219 aluminum alloy (100X), (a) 0.625 cm thick plate in the T87* condition, (b) 3.81 cm thick plate in the T851 condition.

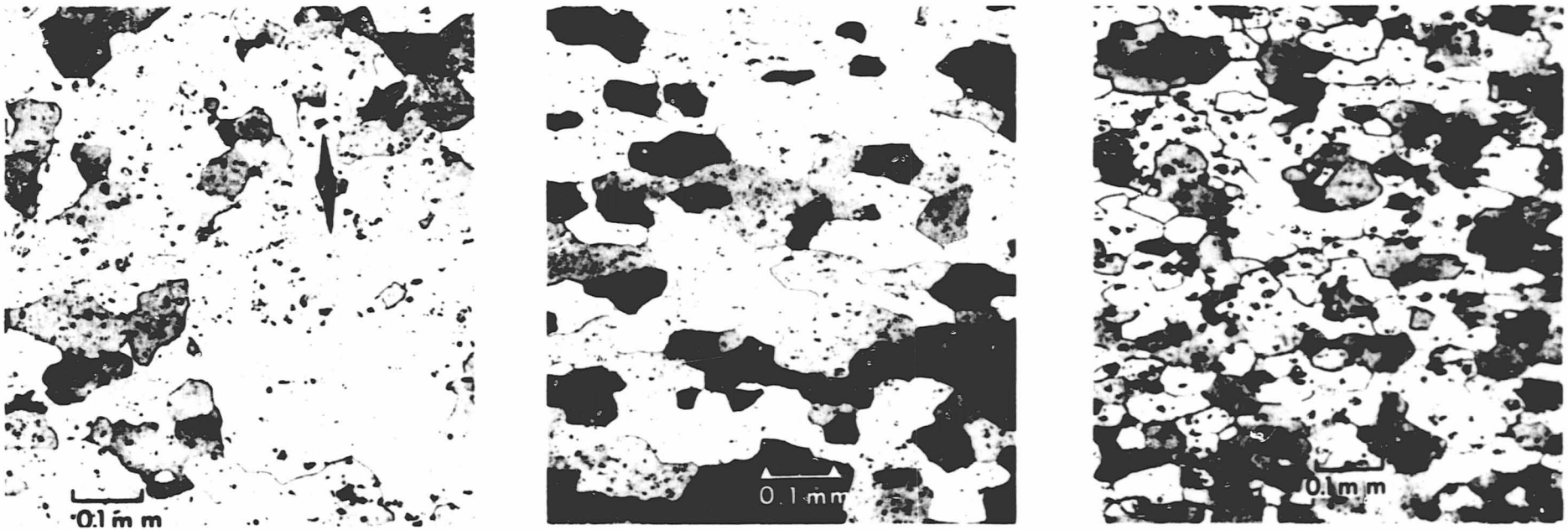

Figure 57. Optical micrographs showing grain structures of resolutionized and quenched plates of 2219 aluminum alloy (100X), (a) Initial material 0.625 cm thick T87* plate (b) Initial material 3.81 cm thick T851 plate, (c) Initial material 0.625 cm thick as-fabricated (F) plate.

Figure 58. TEM micrograph of solution heat treated and quenched (specimen #879-26). Sample preparation methods were used that minimized the introduction of dislocations. Most of the dislocations present are associated with networks and subboundaries.

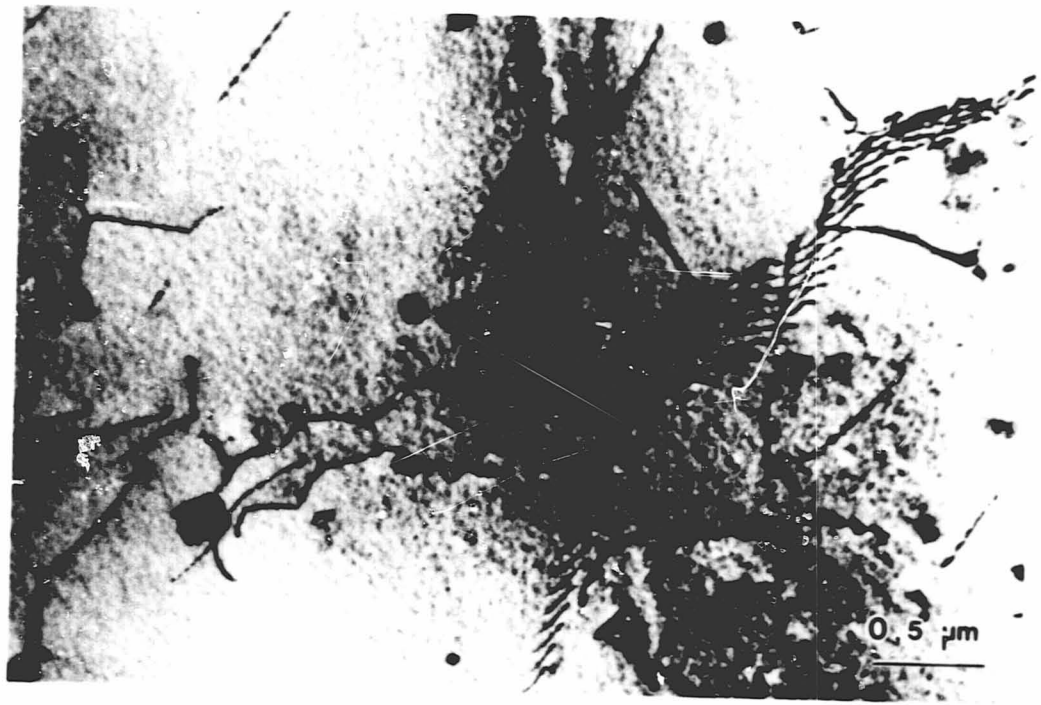

Figure 59. Dislocation network in as-quenched specimen (#879-26).

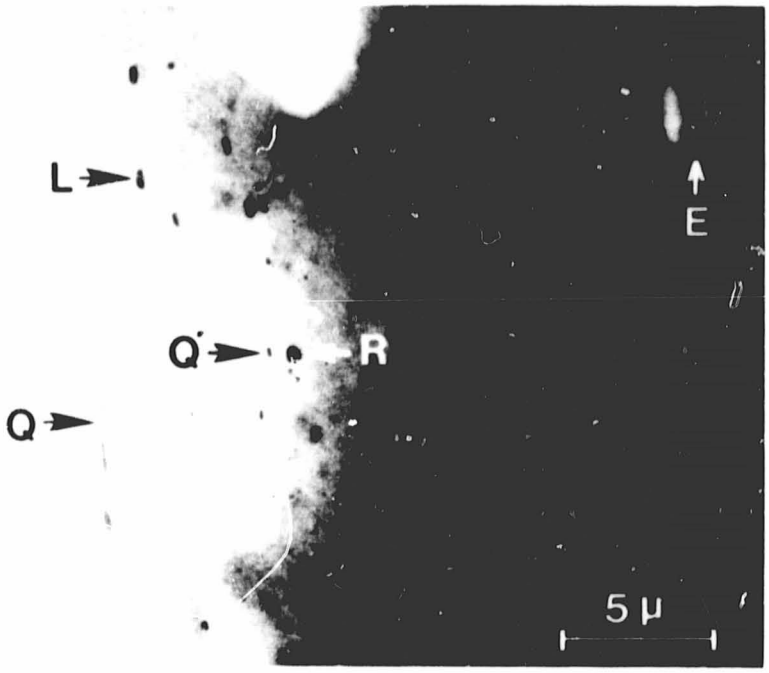

Figure 60. Low magnification STEM micrograph showing various phases that were subject to compositional and diffraction analysis. Q and Q' were found to be Cu_2FeAl_7, L and E were probably this phase also. R is as yet unidentified. Specimen #197 solution heat treated at 535°C for 75 minutes and quenched in ice water.

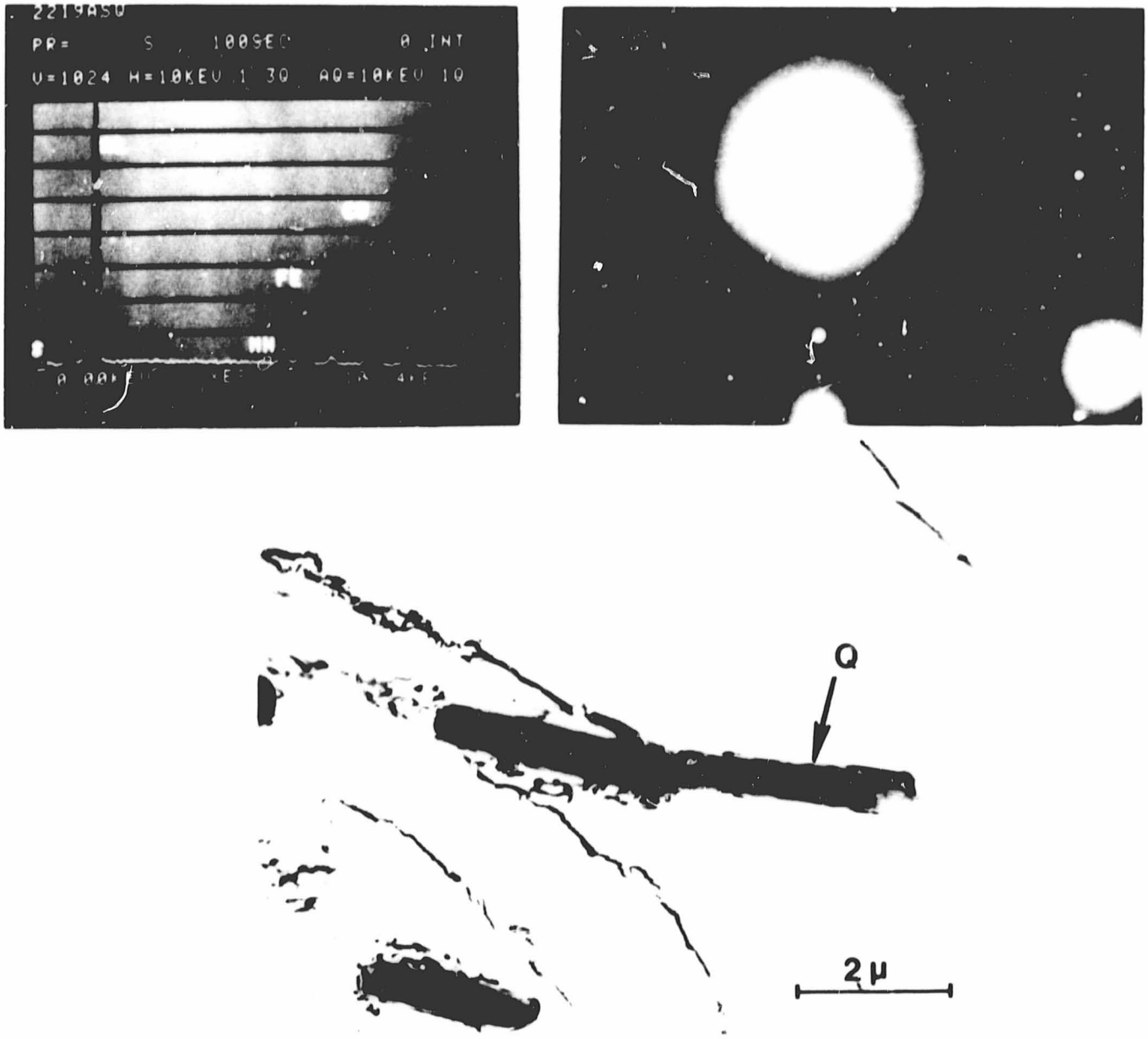

Figure 61. High magnification bright field image of Q shown in Figure59 with corresponding electron diffraction pattern and x-ray spectrum that identify it as Cu_2FeAl_7.

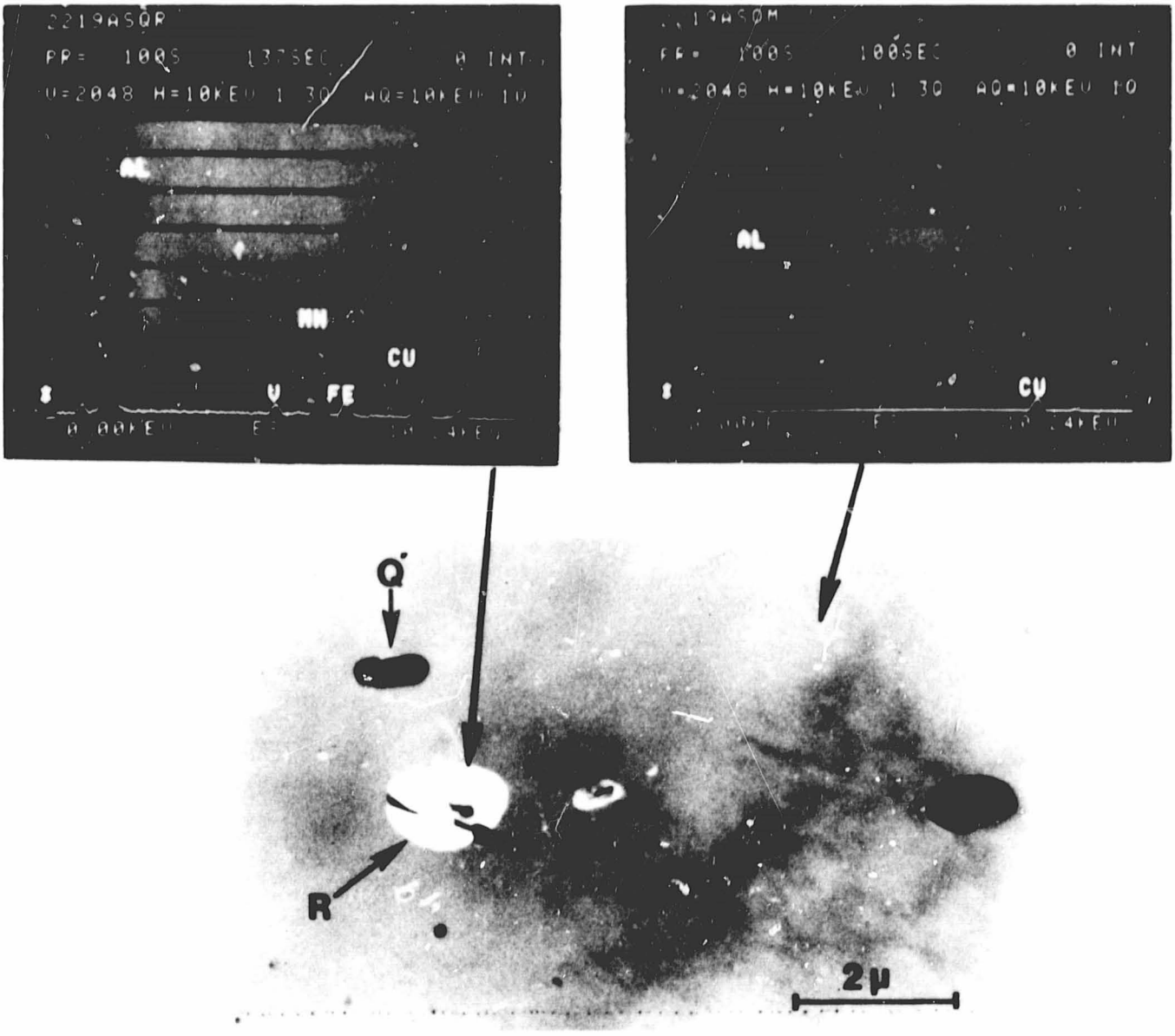

Figure 62. Precipitate R shown in dark field with corresponding x-ray spectrum. In addition to Al the precipitate contains a high concentration of Mn, Cu and some V. The precipitate may be the phase $Cu_2Mn_3Al_{20}$. The x-ray spectrum from the α-aluminum matrix is also shown. Only Al and Cu are present. The concentrations of other elements are too low to be detected.

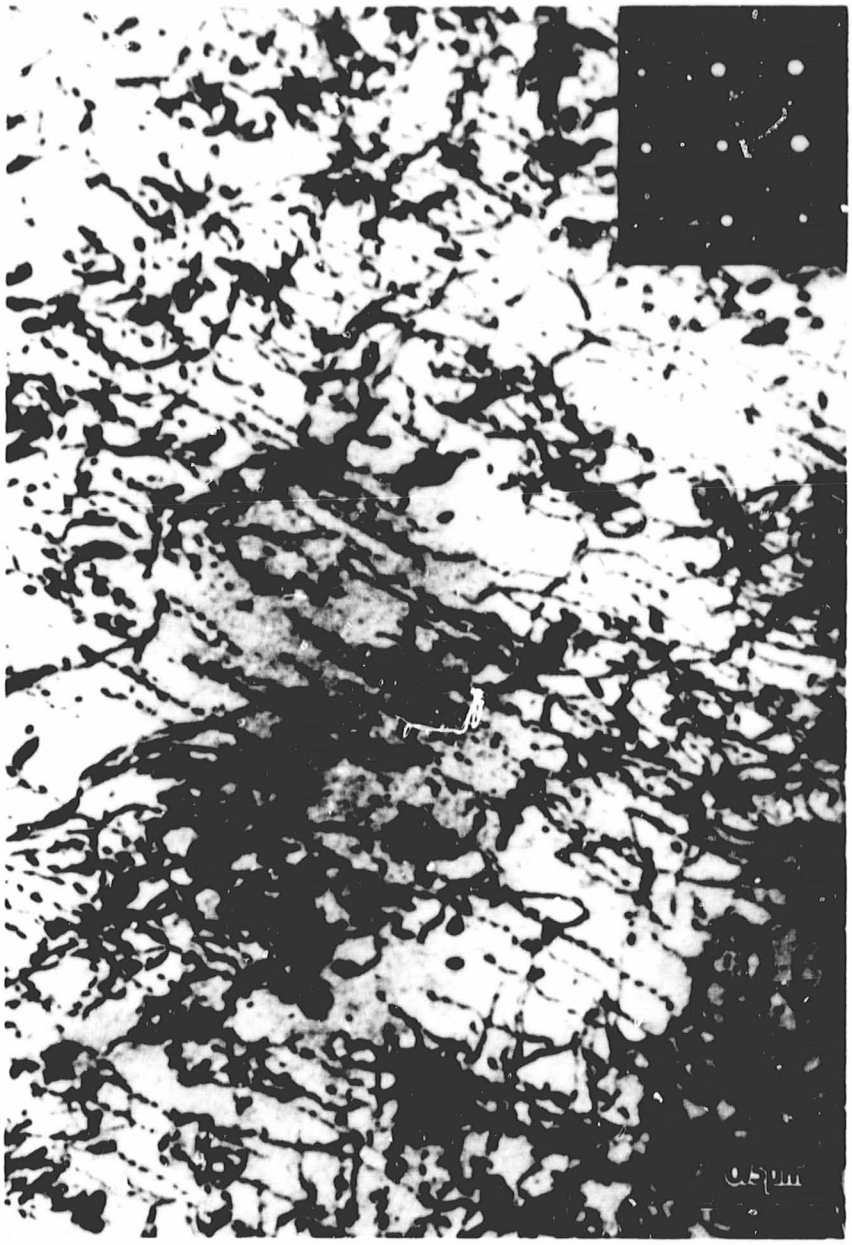

Figure 63. Micrographs showing dislocations and a few scattered inclusions in specimen which had been solutionized, quenched and stretched 2 1/4% (specimen #1). There is no evidence of a homogeneously distributed major precipitate phase.

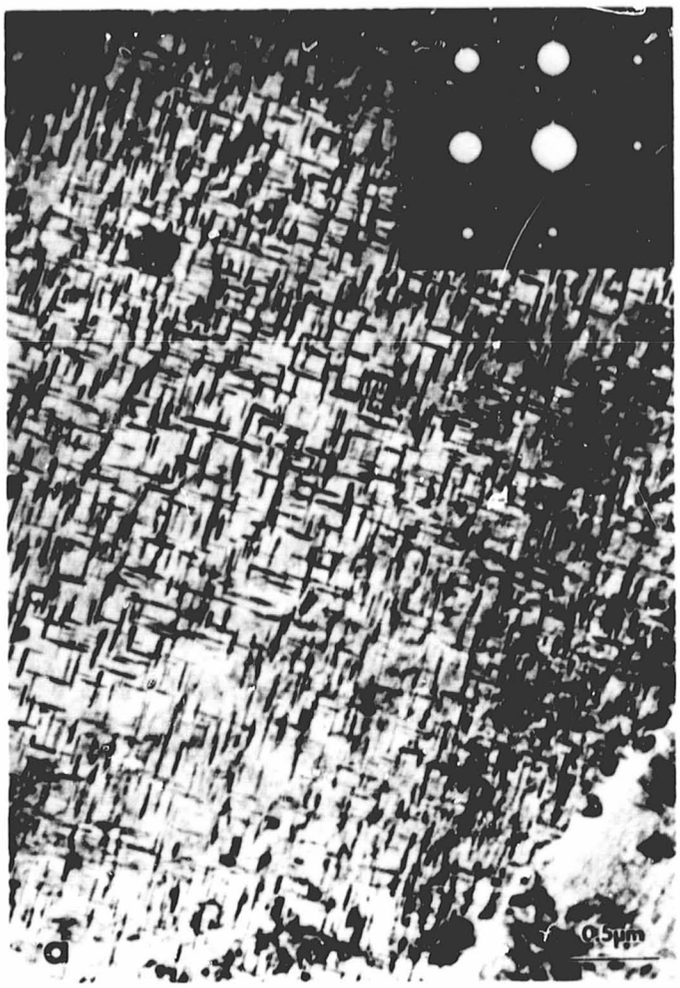

Figure 64a. Microstructure after resolutionizing and reprocessing to T851 conditions. Fine spots in the accompanying diffraction pattern serve to identify the precipitate phase as θ'. Specimen #1A.

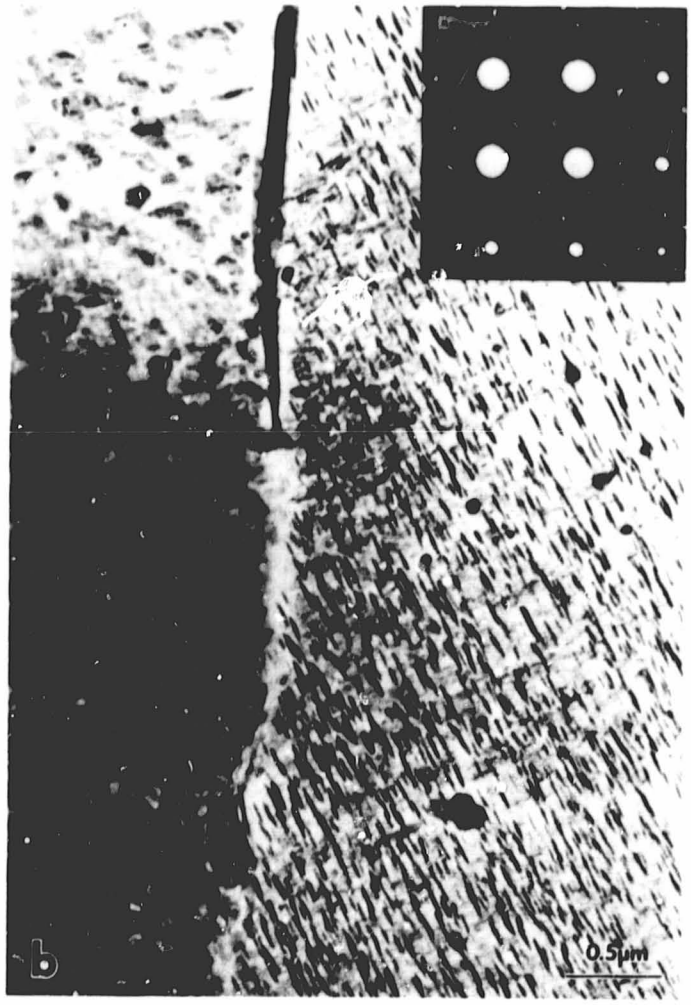

Figure 64b. TEM micrograph of specimen taken from T851 3.81 cm thick plate in as-received condition. The structures shown in Figure 64a and b are essentially identical. Specimen #879-55.

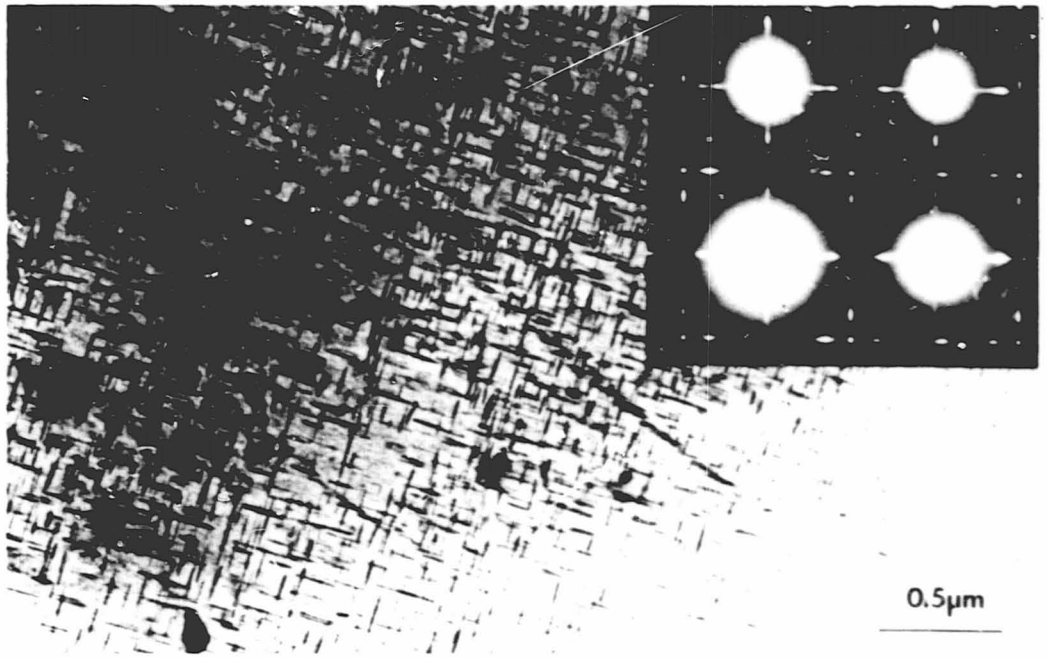

Figure 65. Microstructure after reprocessing according to T87* specifications (specimen #142). A high concentration of θ' precipitates is present.

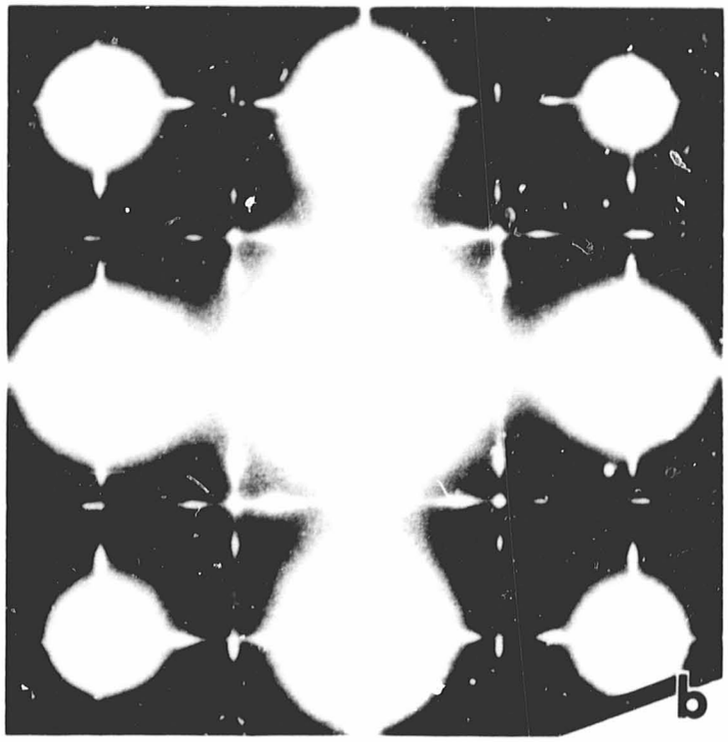

Figure 66. (a) Bright field micrograph showing relatively large θ' precipitates and smaller θ" precipitates. A cluster of θ" is present near the center of the photograph. (b) Electron diffraction pattern with intense α-aluminum matrix reflections and θ' reflections. θ" reflections cannot be distinguished. This specimen (#94) was given an interrupted quench at 400°C for 15s but otherwise was treated according to Reynold's T87* process.

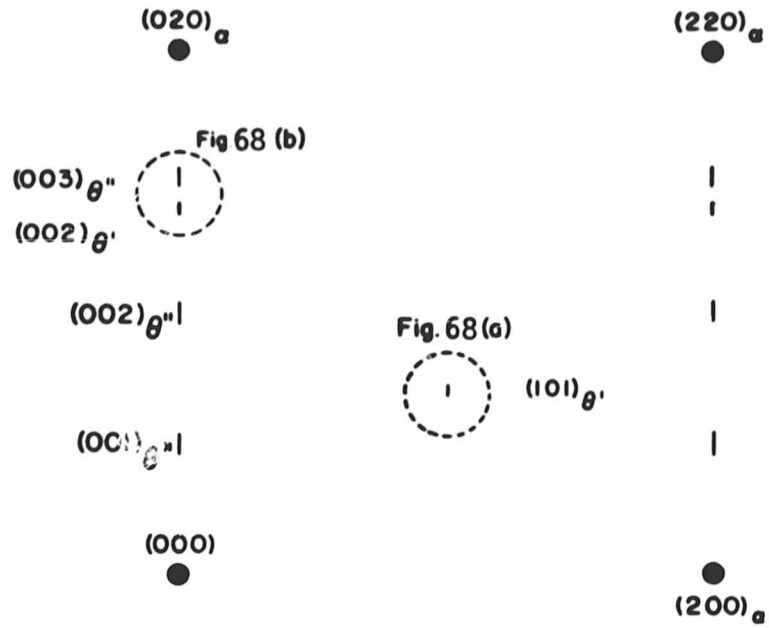

Figure 67. Schematic of diffraction pattern showing diffraction spots from which dark field images in Figure 68(a) and (b) were obtained.

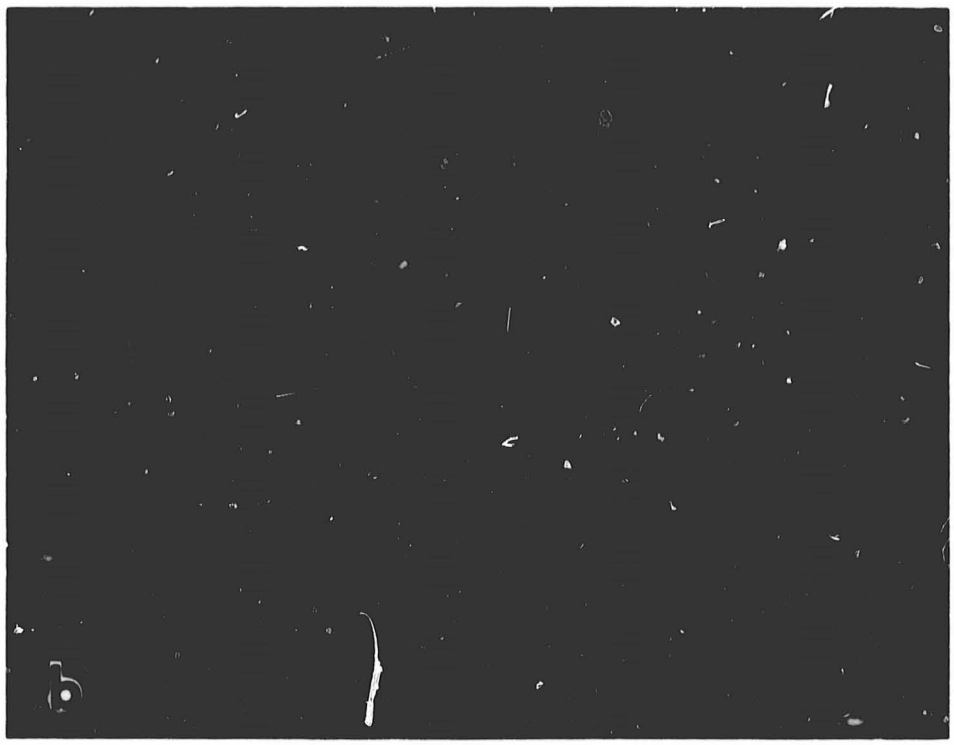

Figure 68. (a) & (b). Dark field micrographs demonstrating the presence of υ''. (a) Only υ' is imaged; operating reflection is $(101)_{\upsilon'}$. (b) Both υ' and υ'' are imaged; operating reflections are $(002)_{\upsilon'}$ and $(003)_{\upsilon''}$.

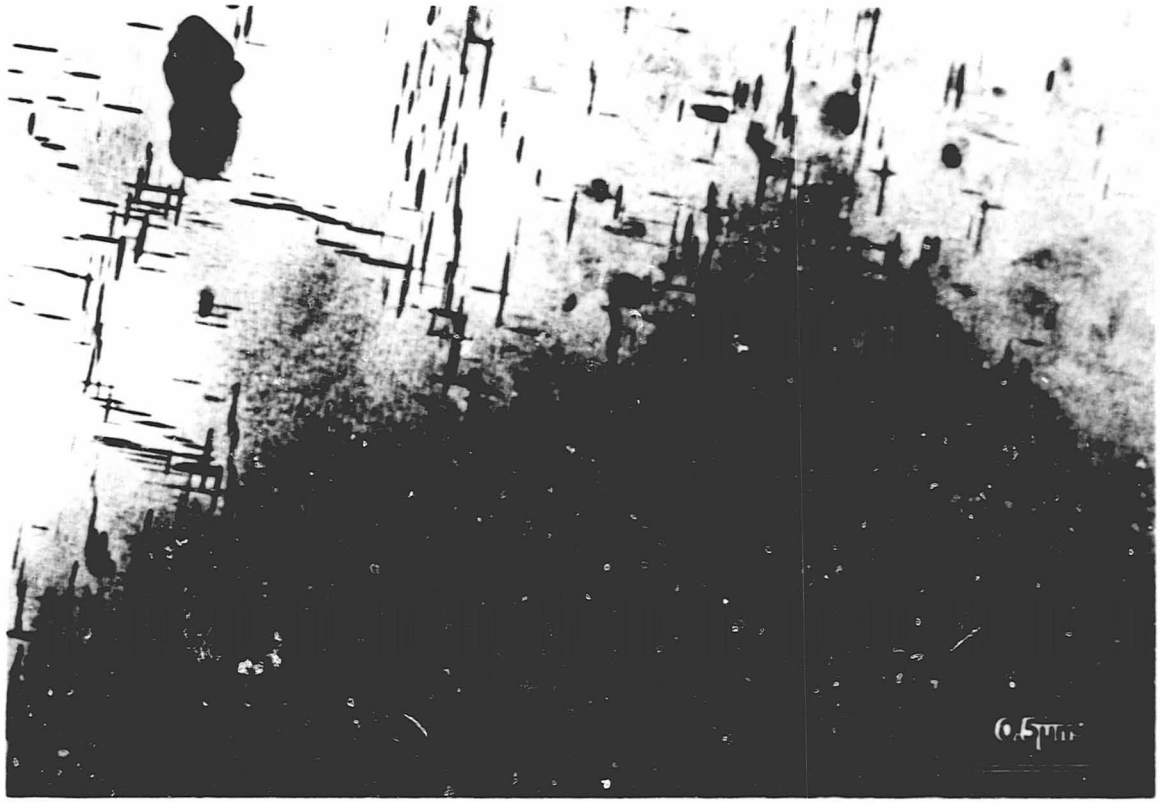

Figure 69. Typical microstructure after solution heat treatment, ice water quench and aging at 177°C for 18h, i.e., T851 without 2 1/4% stretch. Bands of large θ' precipitates are seen together with uniformly distributed fine θ" precipitates (specimen #879-35).

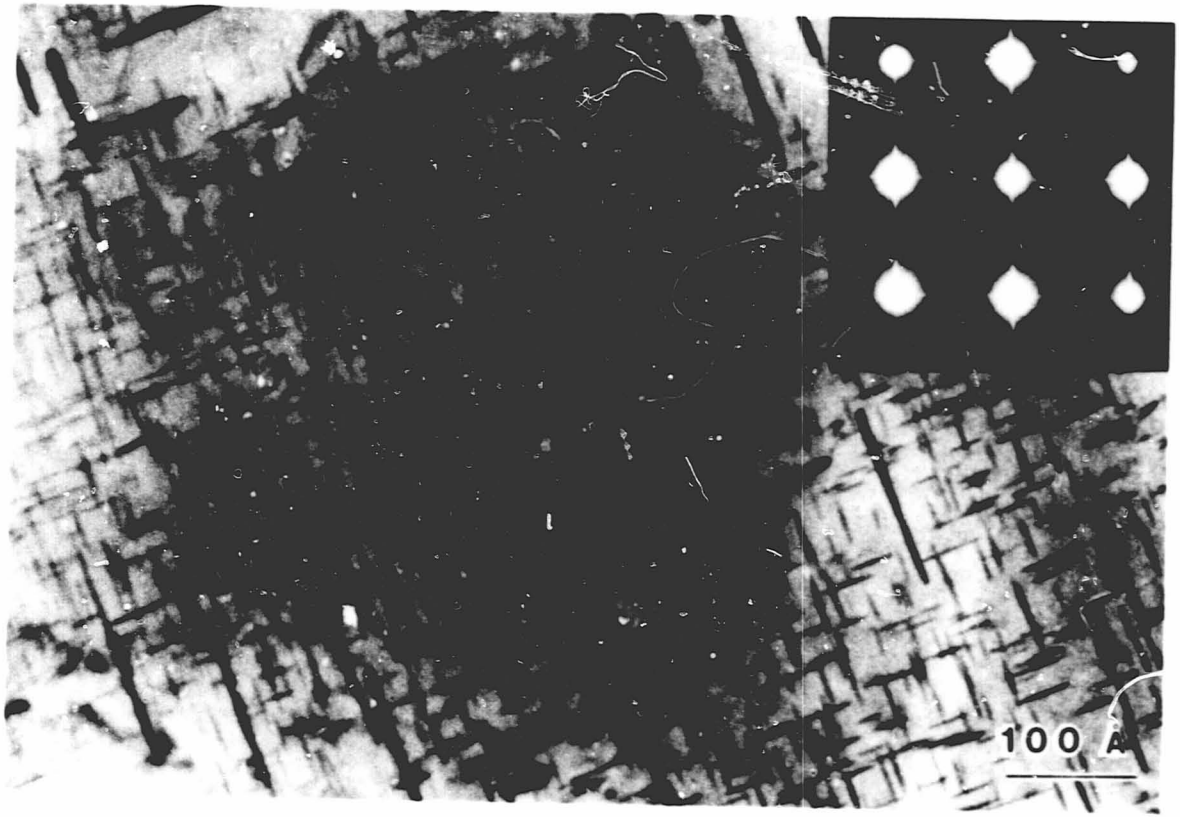

Figure 70. High magnification image of precipitates shown in Figure 68. Both the large θ' and small θ" precipitates have {100} habit planes. A denuded zone exists around the large θ' precipitates (specimen #879-35).

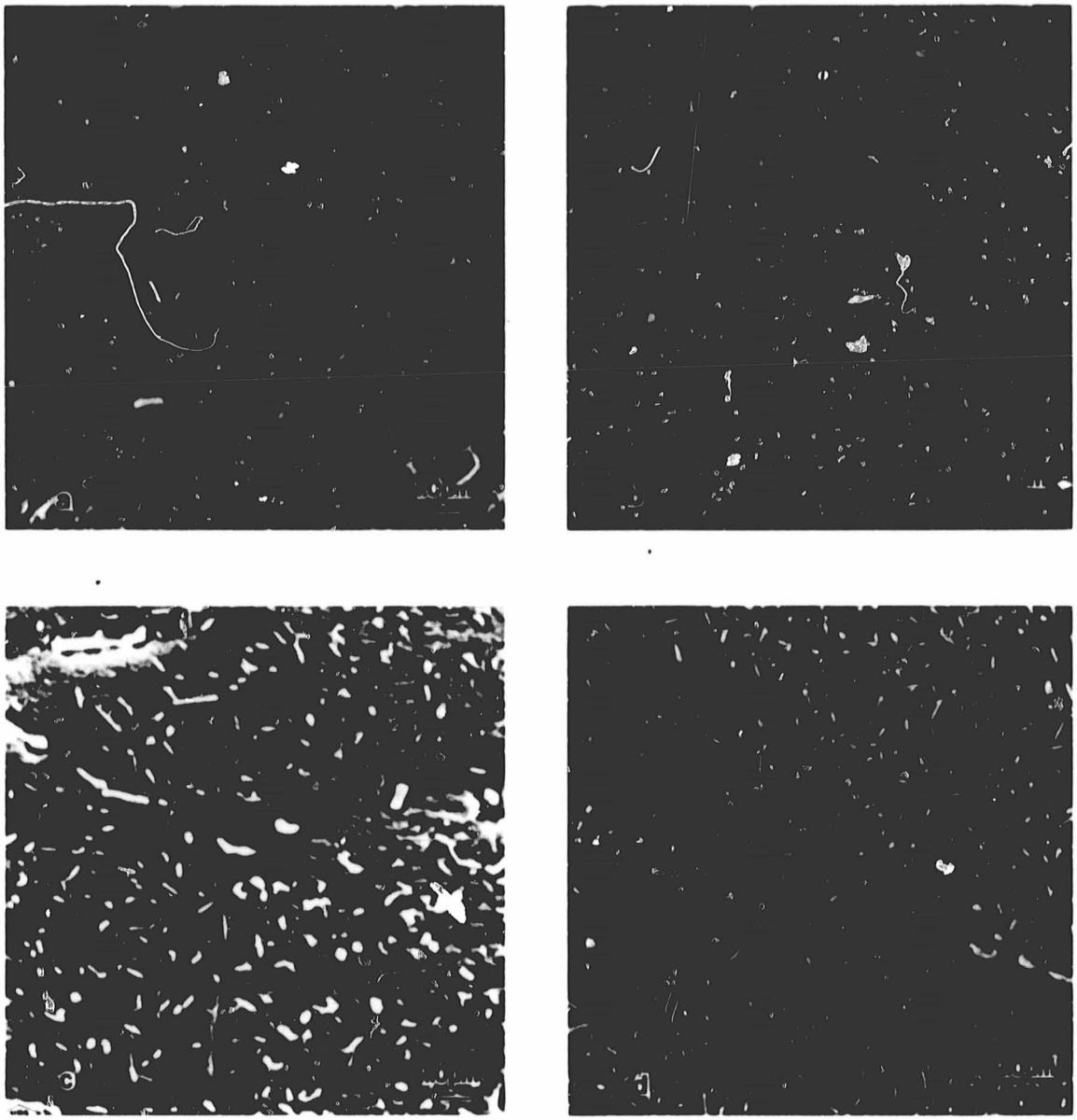

Figure 71. SEM micrographs of specimens after various sequence A quench treatments. The specimens were etched to reveal the presence of precipitates formed during the quench treatment, (a) Specimen #197, quenched without an interrupt, (b) Specimen #93, **pre-aged** at 400°C for 15s, (c) Specimen #81, **pre-aged at 400°C for** 30s, (d) Specimen #85, **pre-aged at 400°C for 60s.**

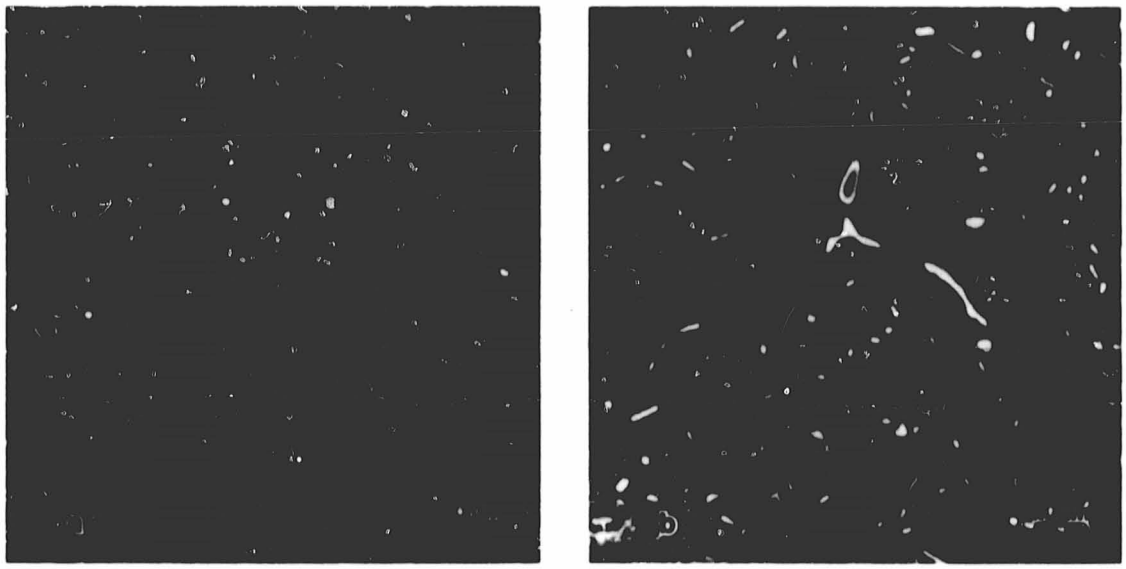

Figure 72. SEM micrographs of sequence A specimen #69, **pre-aged at 400°C** for 30s, a) Low magnification, b) High magnification.

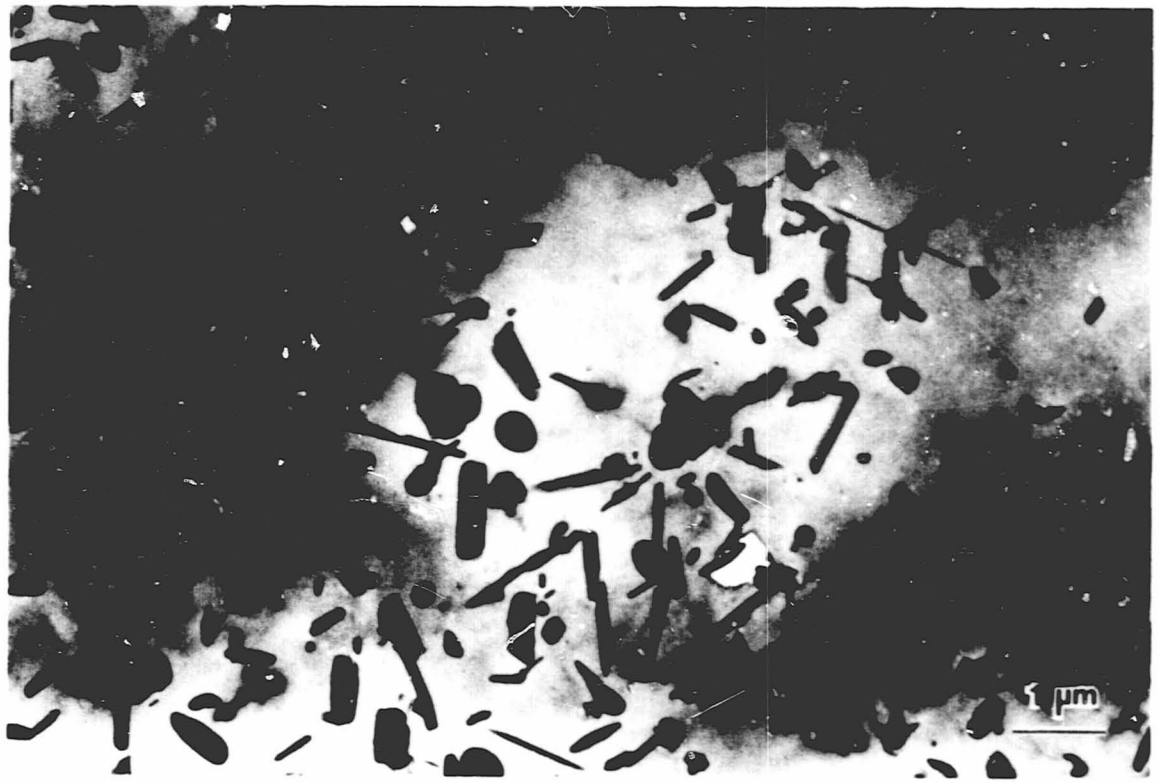

Figure 73. TEM micrograph of specimen #85, **pre-aged (sequence A) at 400°C for 60s.** Both θ' and θ precipitates are present.

Figure 74. Same specimen shown in Figure 73. Misfit dislocations can be seen at the interface of many precipitates. Numerous strain induced dislocations are present.

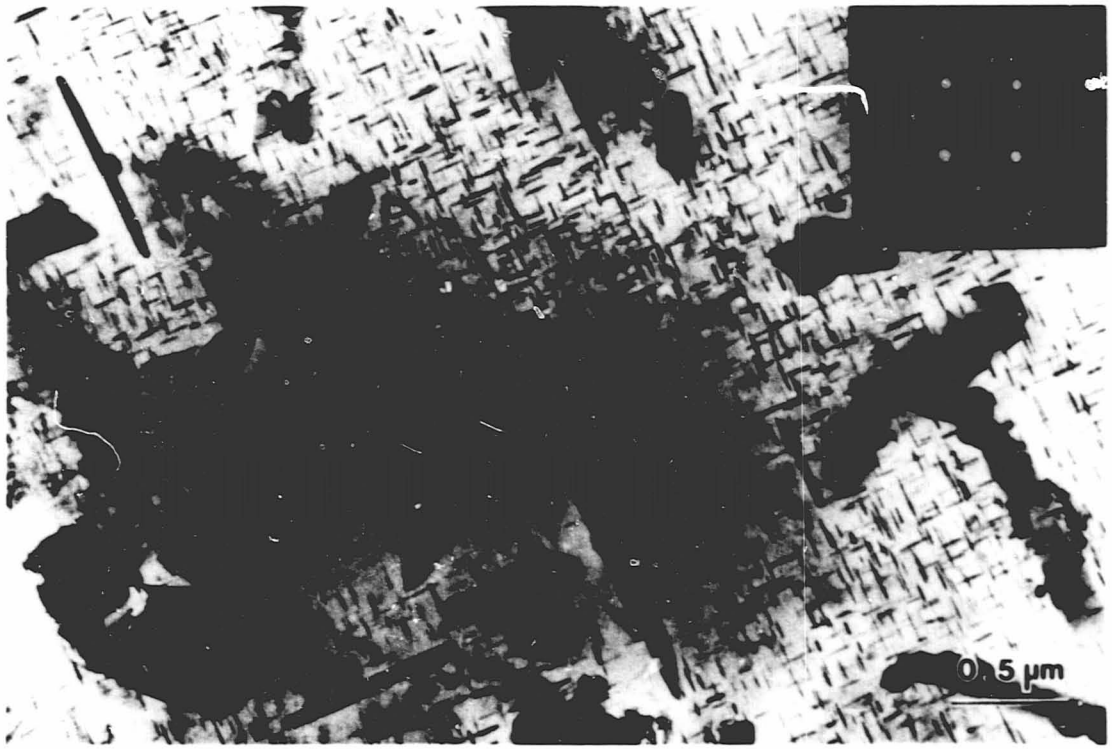

Figure 75. Specimen #86 given sequence A pre-aging at 400°C for 60s stretched 5% and aged at 172°C for 16h. Many of the large precipitates were produced during the interrupt period. Fine θ' precipitates (small spots in diffraction pattern) were produced on aging. Note precipitate free regions surrounding large particles.

Figure 76. Dark field image showing two Θ precipitates in bright contrast at a grain boundary and in contact with an inclusion. Specimen #105.

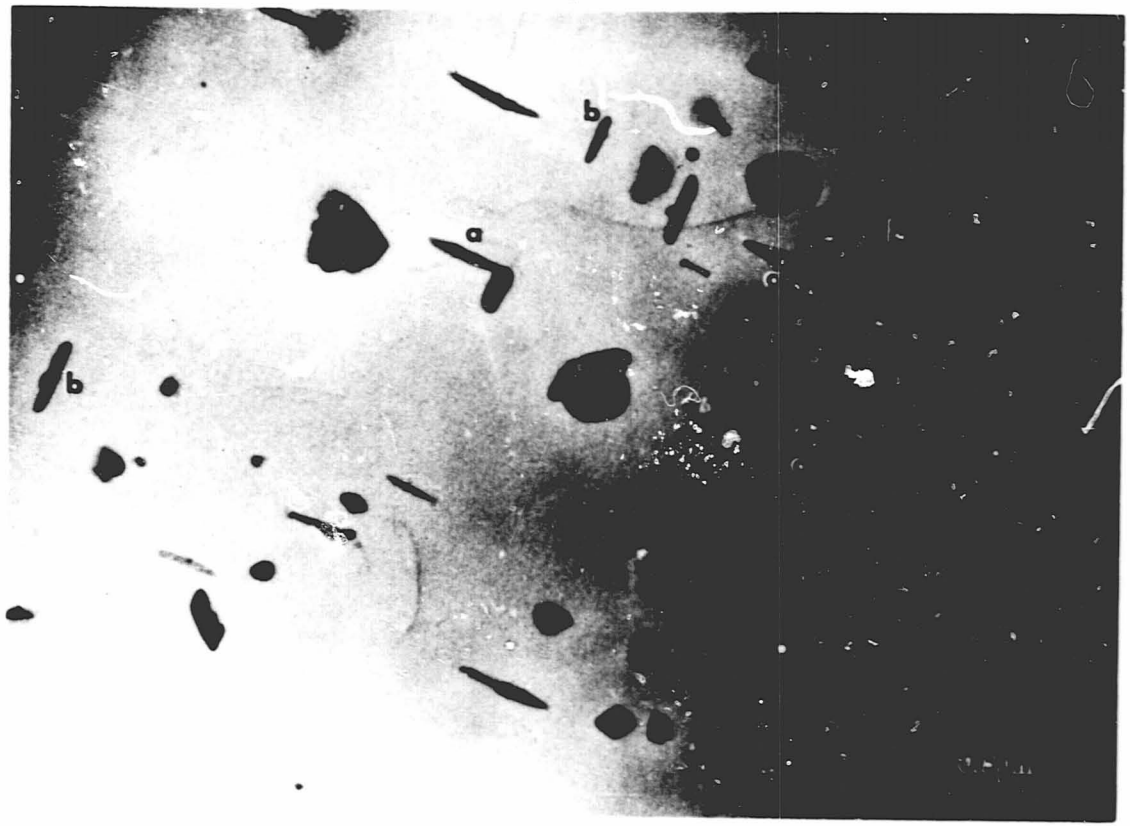

Figure 77. Specimen #6, quench pre-aged (sequence A) at 350°C for 15s. Many θ' precipitates are identified at a and b on two different {100} habit plane variants. Note black appearing particles associated with θ' precipitates.

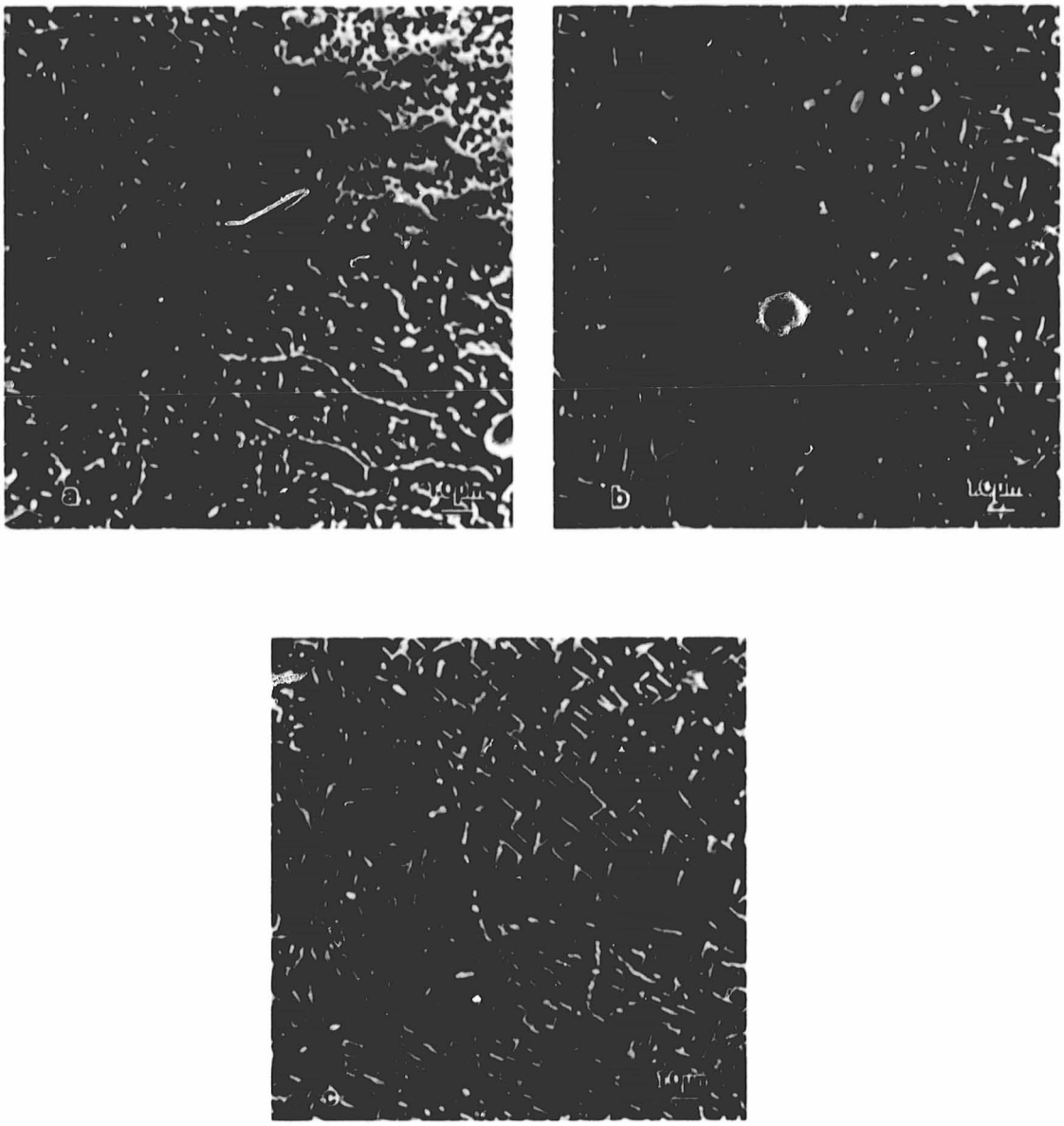

Figure 78. SEM micrographs of specimens after various sequence B **pre-aging** treatments. The specimens were etched to reveal the presence of precipitates formed during the quench treatment. a) Specimen #249, reheat to 450°C for 15s. b) Specimen #253, reheat to 450°C for 30s. c) Specimen #232, reheat to 400°C for 30s.

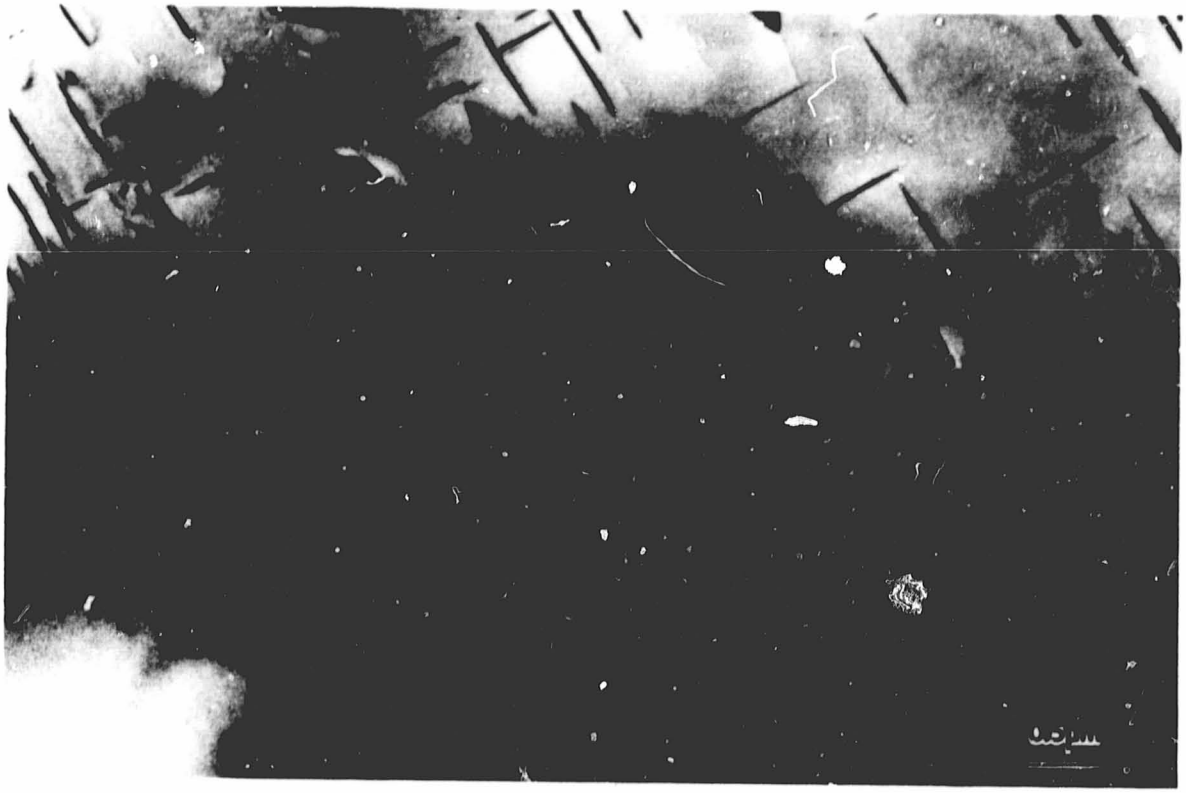

Figure 79. TEM micrograph showing Θ' precipitates formed during reheat 400°C for 30s. Specimen #232.(**Sequence B pre-aging.**)

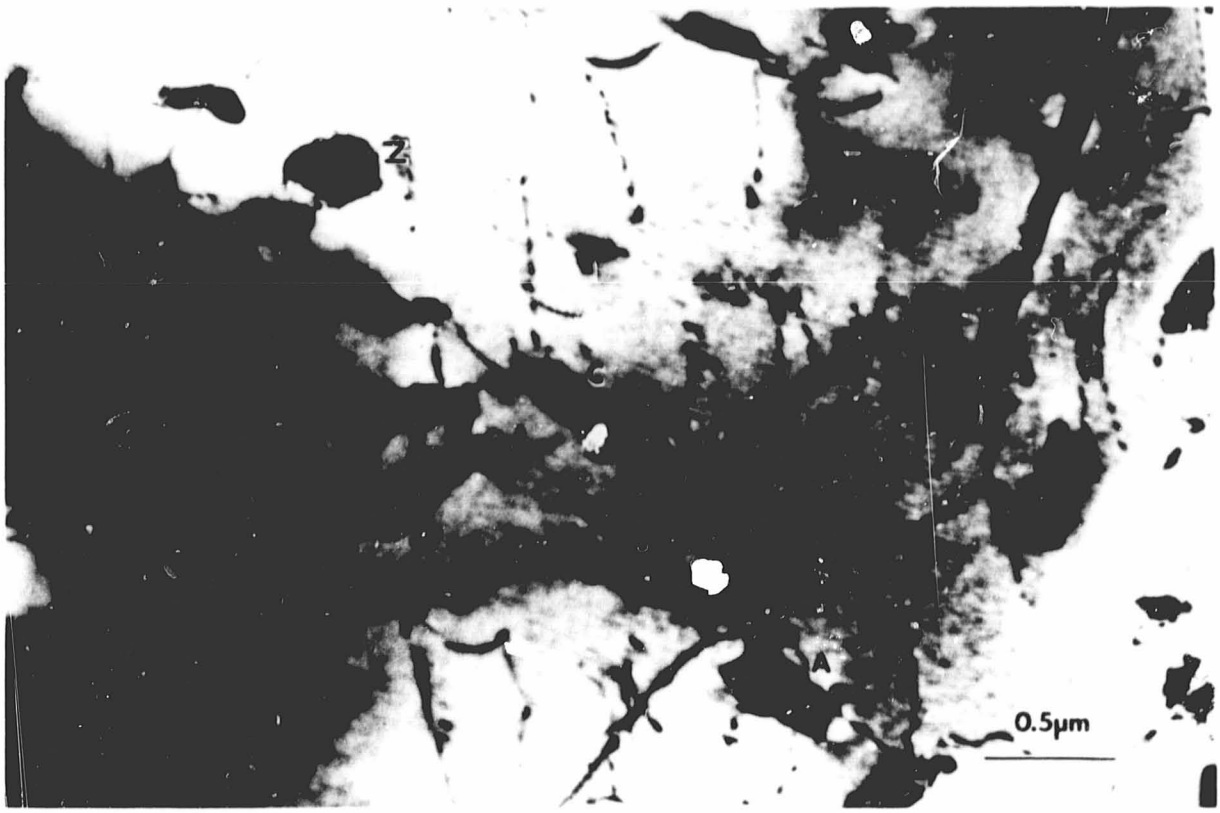

Figure 80. TEM micrograph showing precipitates from which x-ray spectra were obtained in Figure 81. Specimen #249, reheated to 450° for 15s. **(Sequence B pre-aging.)**

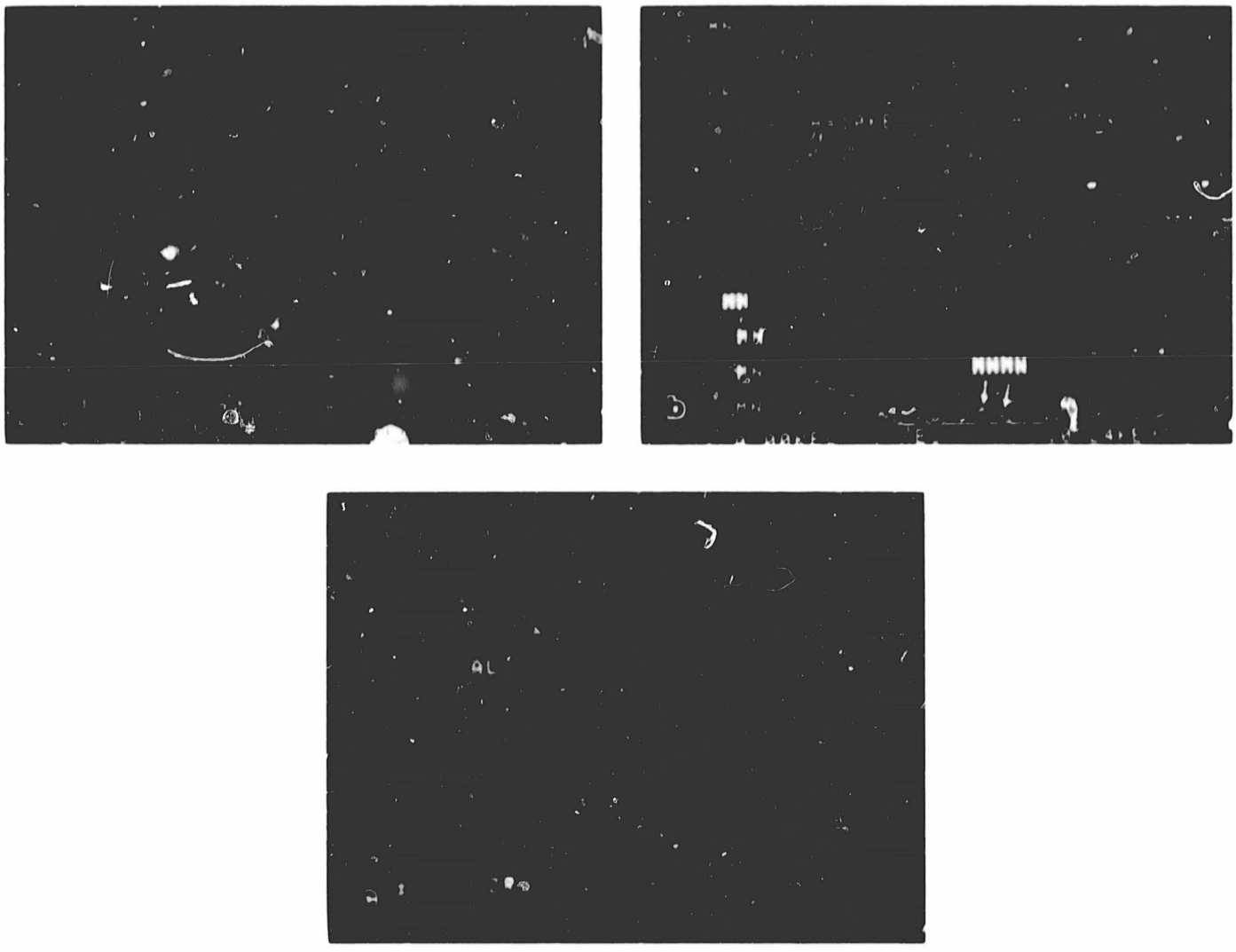

Figure 81. X-ray spectra of precipitates shown in Figure 80. a) Precipitate A. b) Precipitate B. Note, low energy Mn peaks which are labeled can not be detected above background. c) Precipitates at Z.

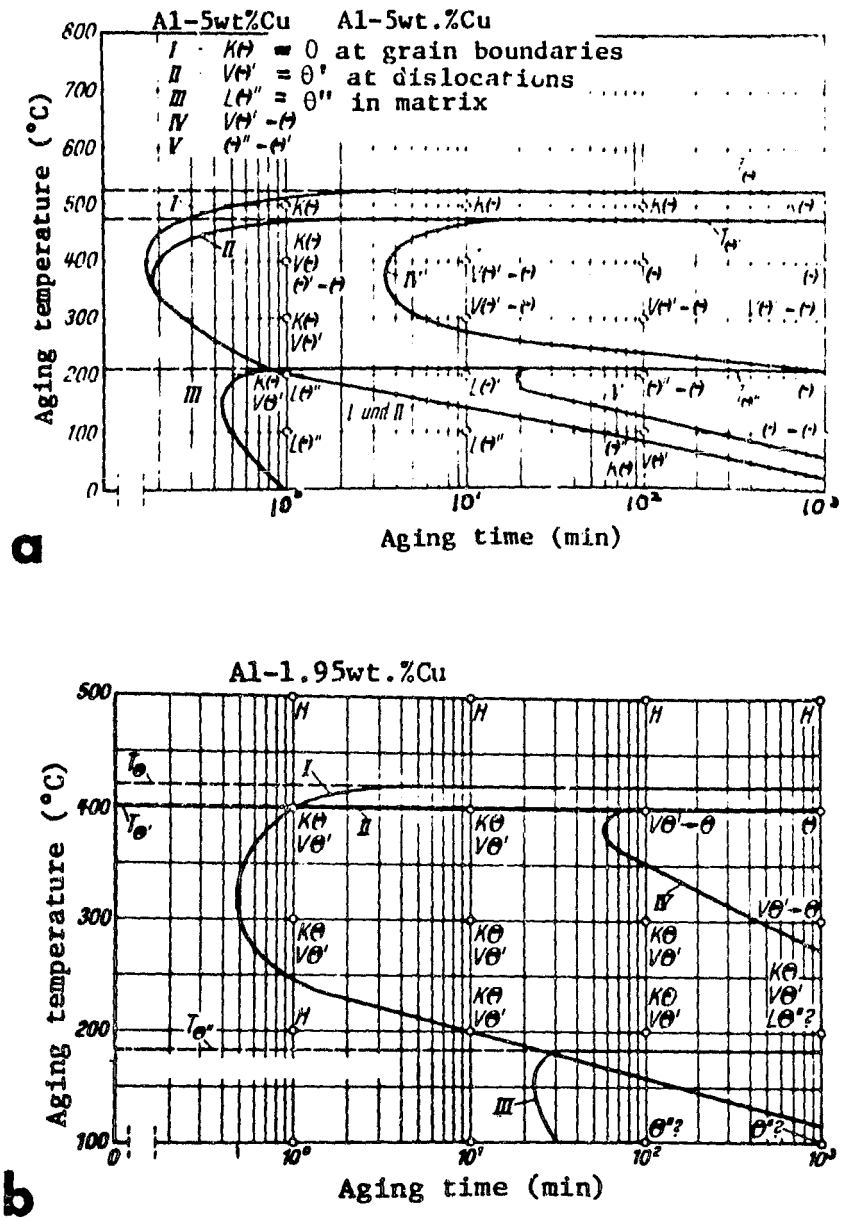

Figure 82. Nucleation diagrams for Al-Cu alloy from Reference (26). (a) Al-5wt% Cu alloy, (b) Al-1.95wt% Cu alloy.

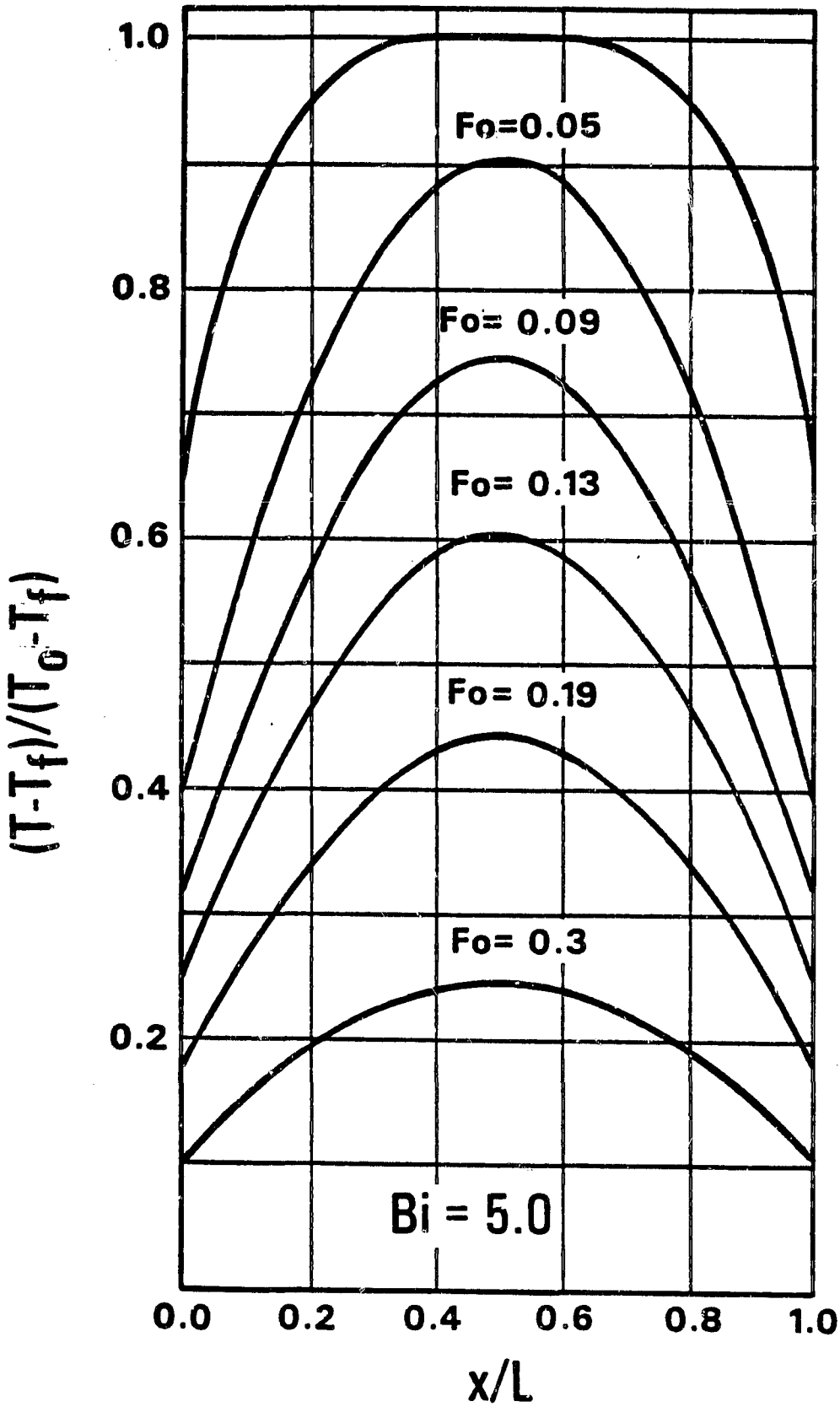

Figure 83. Dimensionless temperature profiles as a function of time in a plate subjected to symmetric cooling from both sides with a Biot number of 5.0.

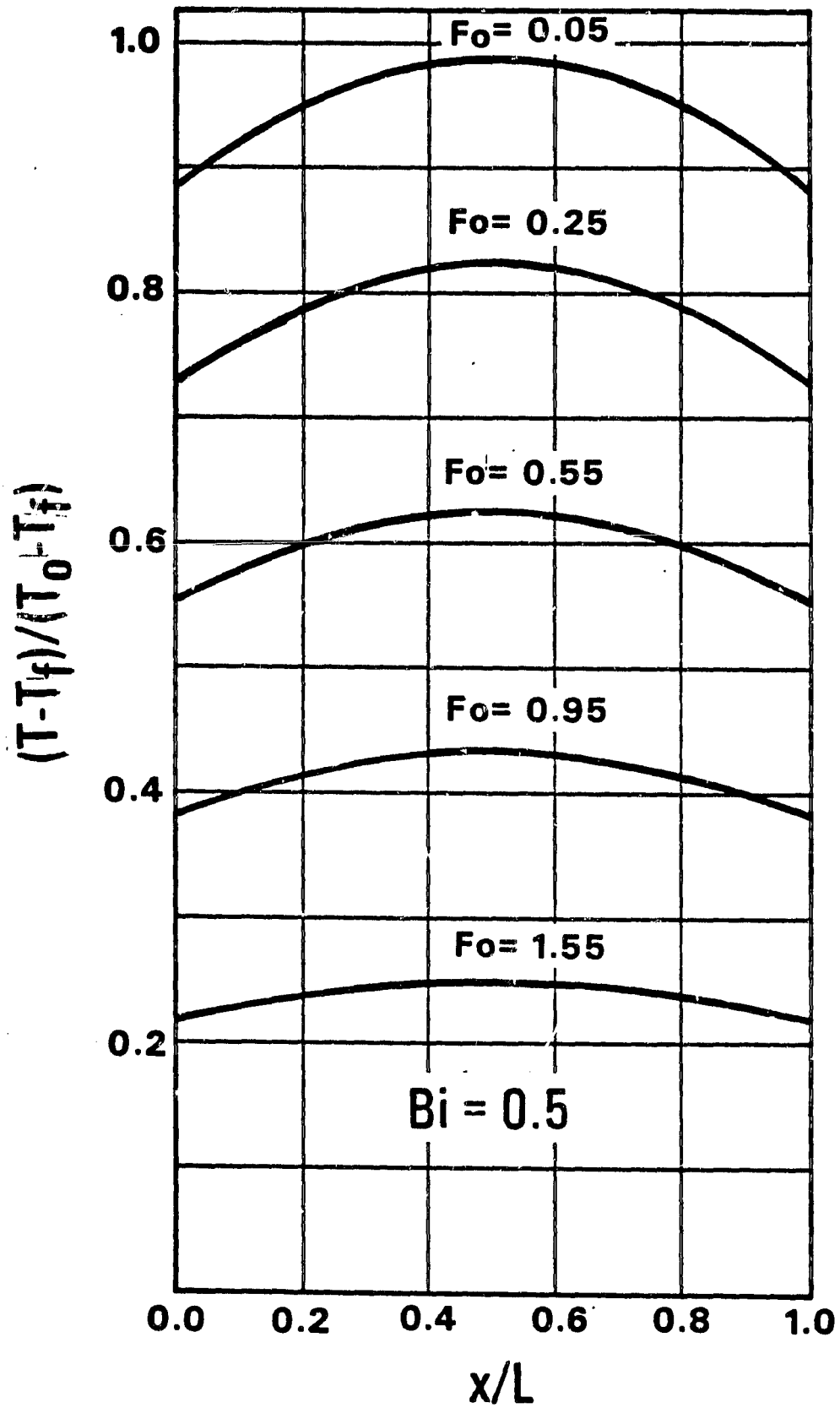

Figure 84. Dimensionless temperature profiles as a function of time in a plate subjected to symmetric cooling from both sides with a Biot number of 0.5.

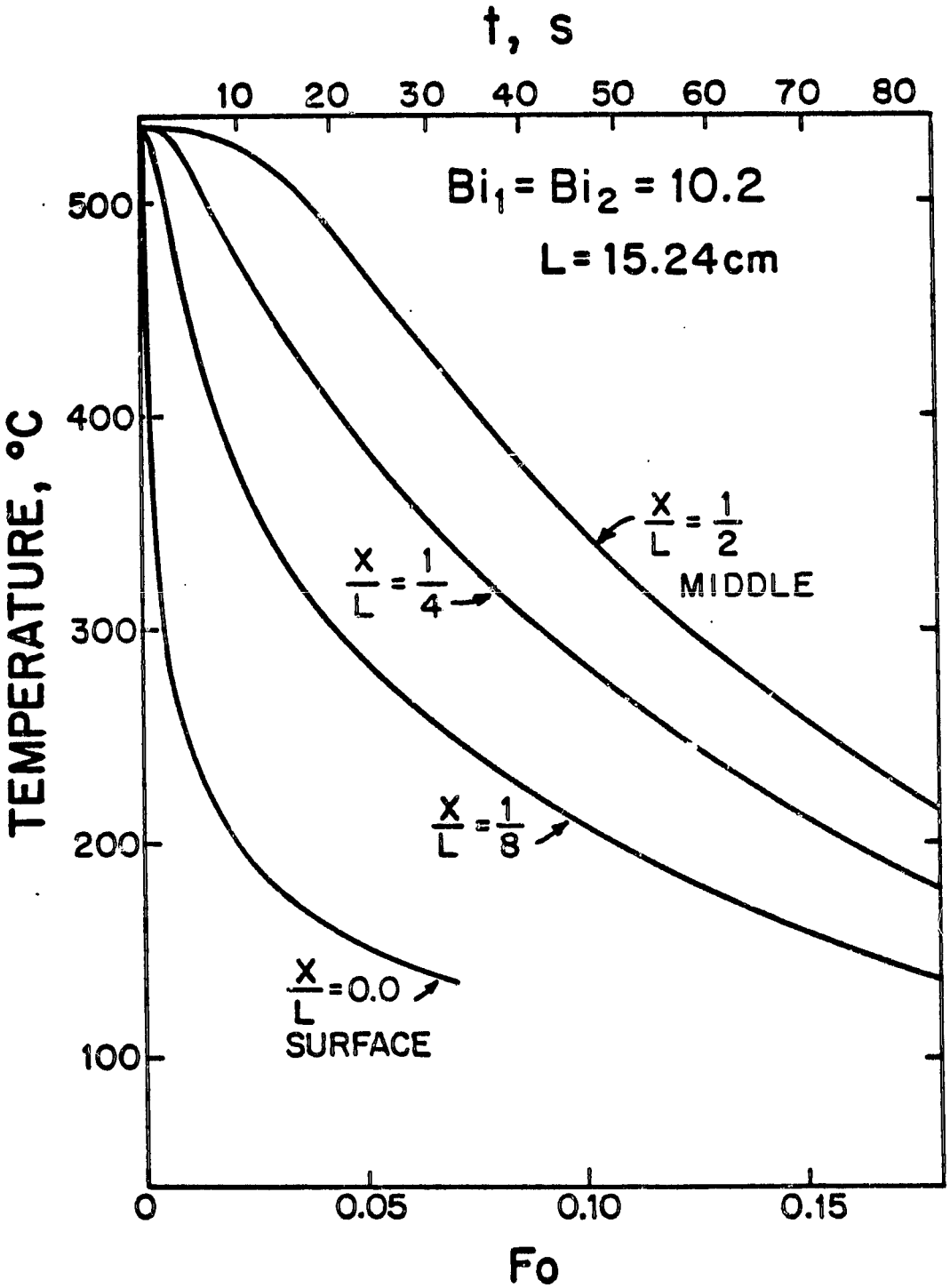

Figure 85. Calculated time-temperature profiles at four locations in a 15.24 cm thick plate of 2219 aluminum alloy cooled symmetrically from both surfaces from an initial temperature of 535 °C.

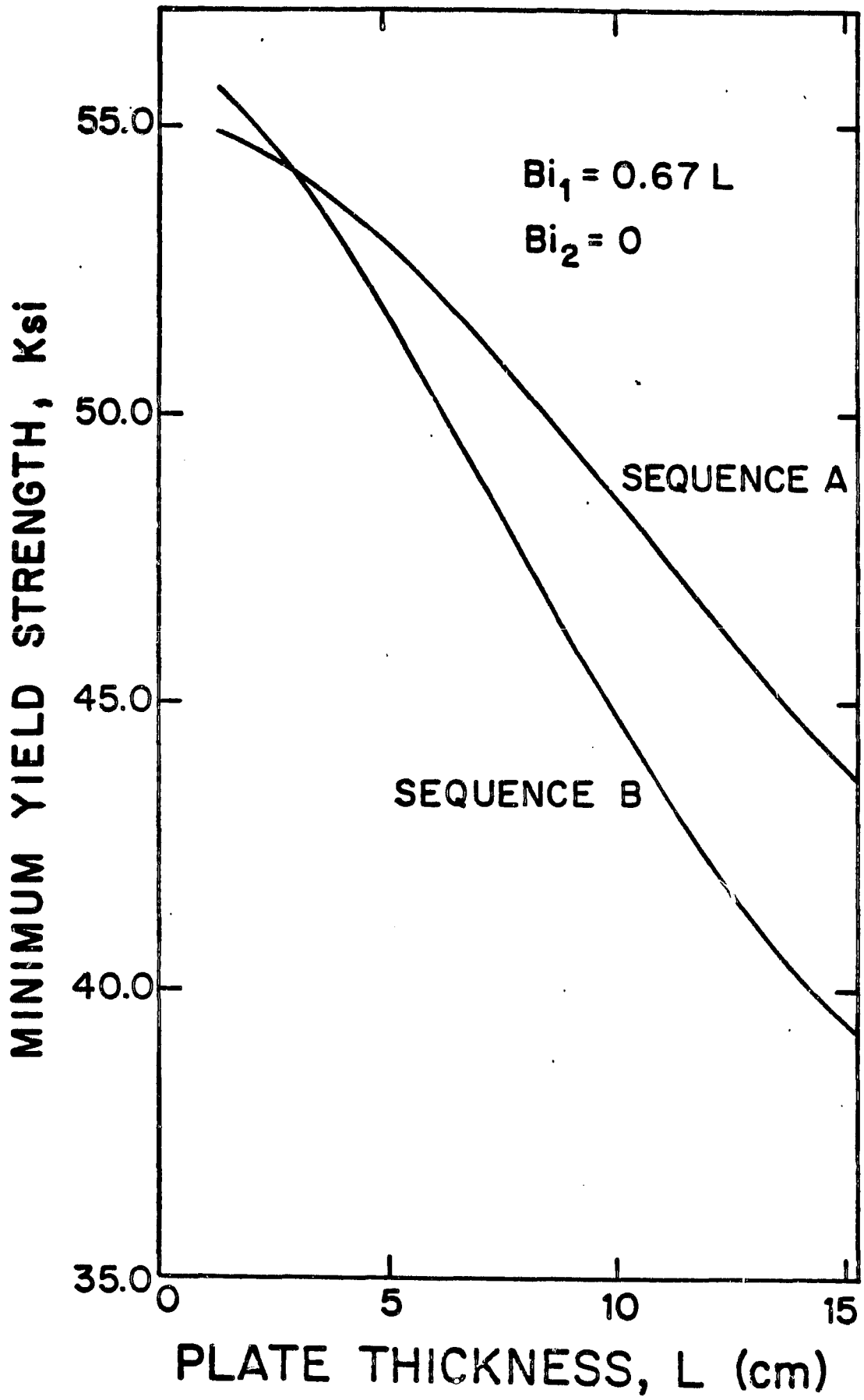

Figure 86. Predicted minimum yield strength versus plate thickness for plates cooled from the top surface. The minimum value corresponds to the bottom surface of the plate or the center of plates with twice the thickness, but cooled from both surfaces.

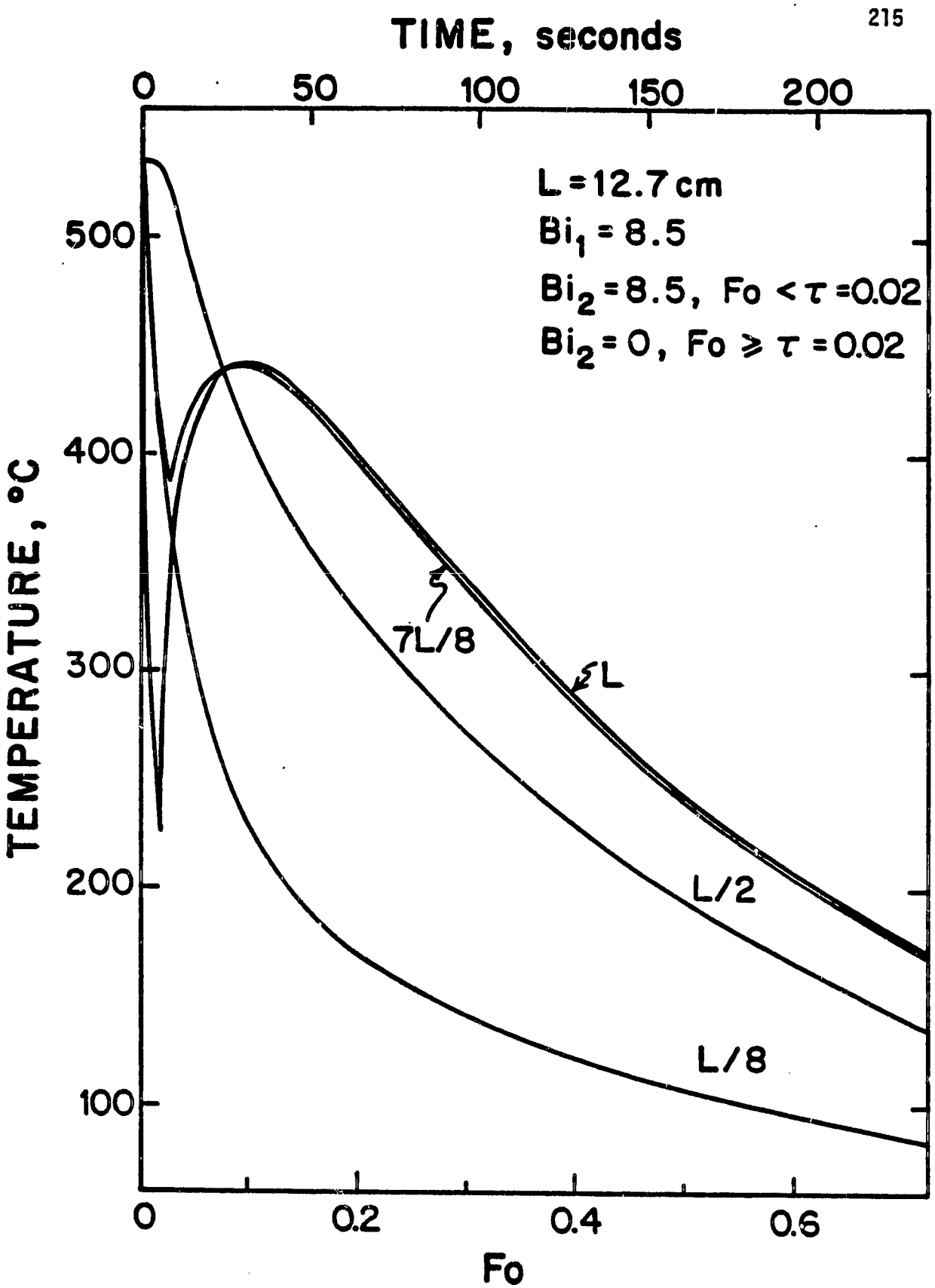

Figure 87. Calculated time-temperature profiles at four locations in a 12.7 cm thick plate of 2219 aluminum alloy subjected to an abrupt discontinuation of heat extraction from its bottom surface.

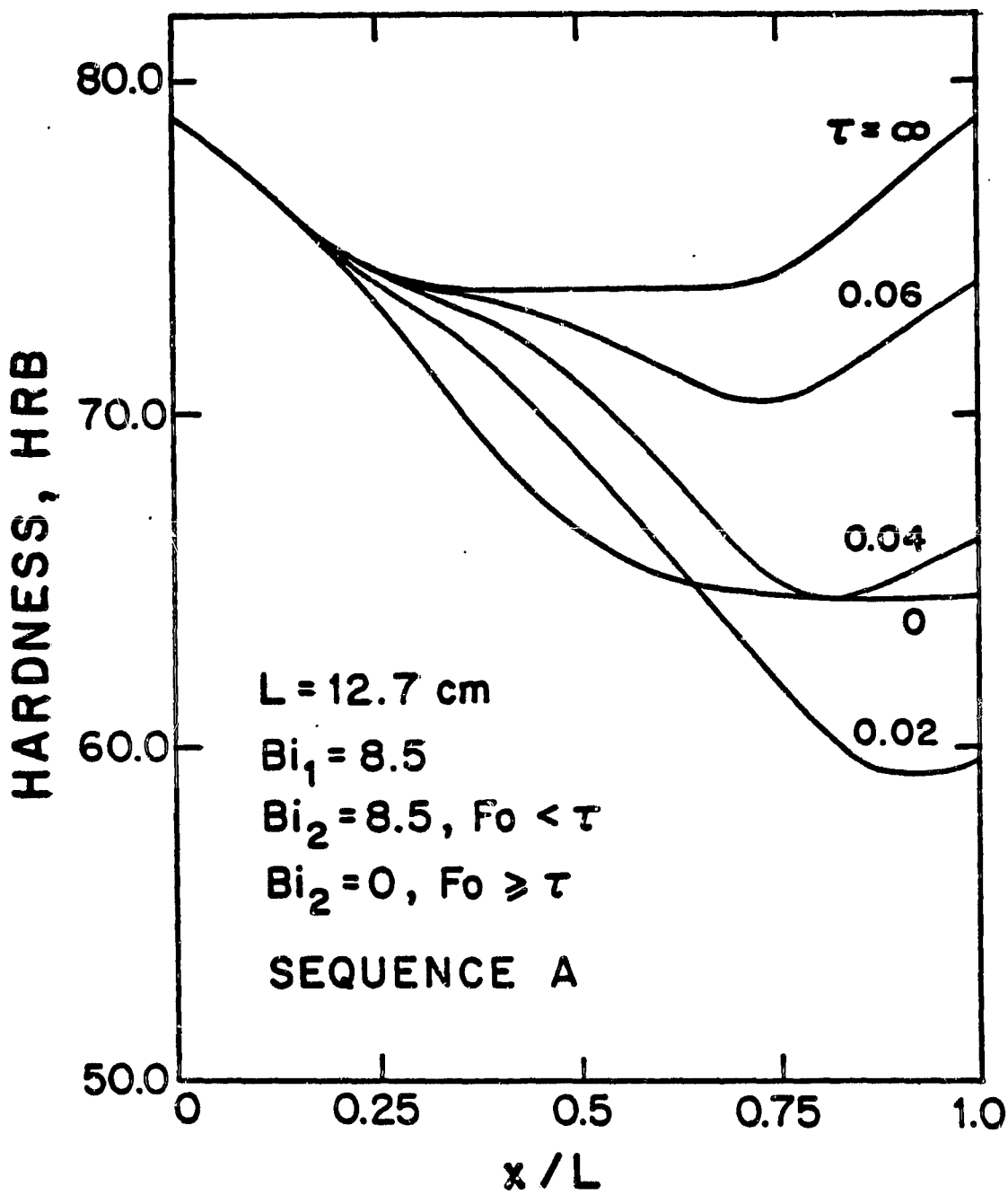

Figure 88. Predicted hardness versus distance from the top surface of 12.7 cm thick plates subjected to a variety of heat flow conditions at their bottom surfaces. Curve denoted by τ = 0.02 is for the time-temperature conditions shown in Figure 87.

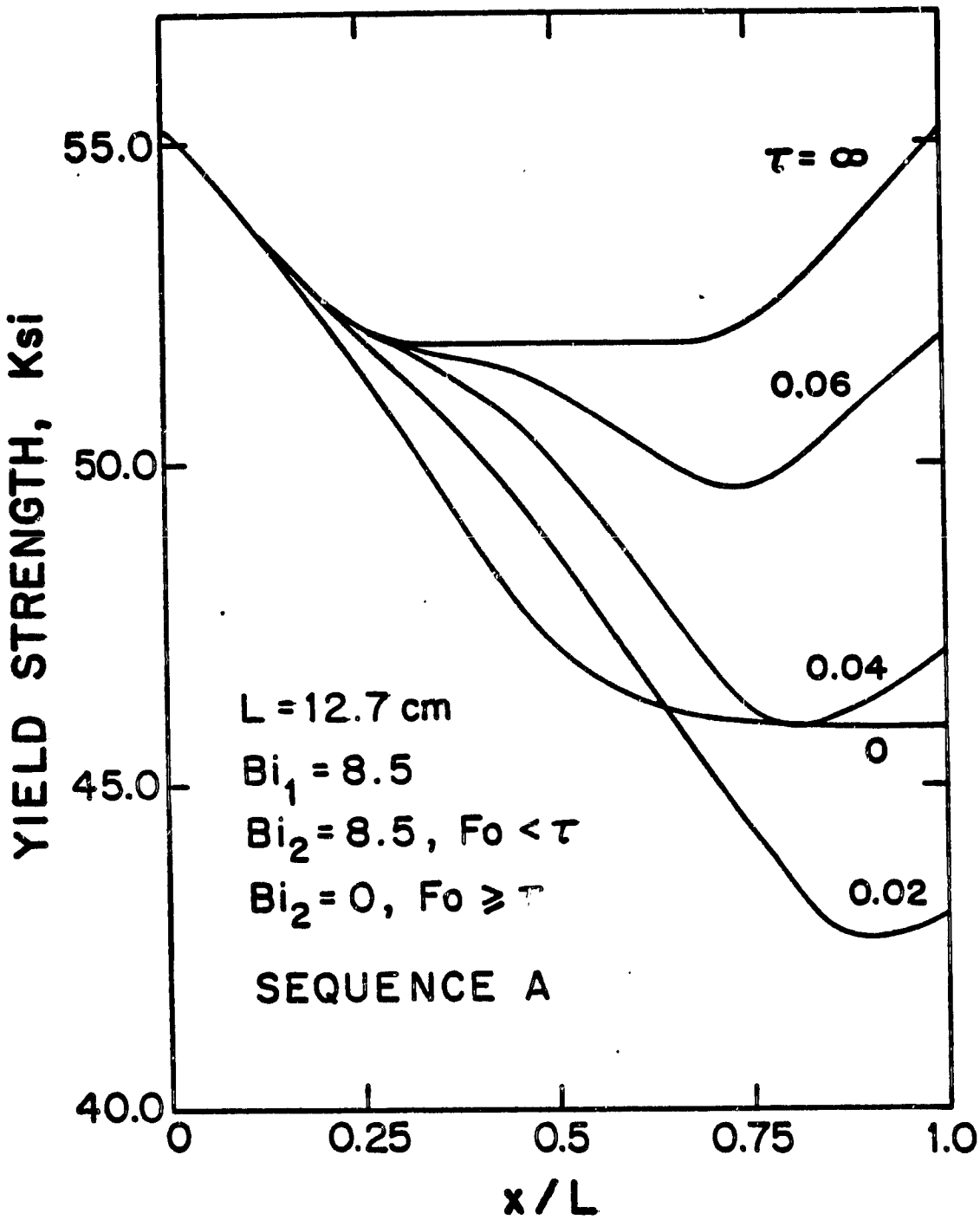

Figure 89. Predicted yield strength versus distance from the top surface of 12.7 cm thick plates subjected to a variety of heat flow conditions at the bottom surface. Curves are calculated using constants in Table VIII for sequence A.

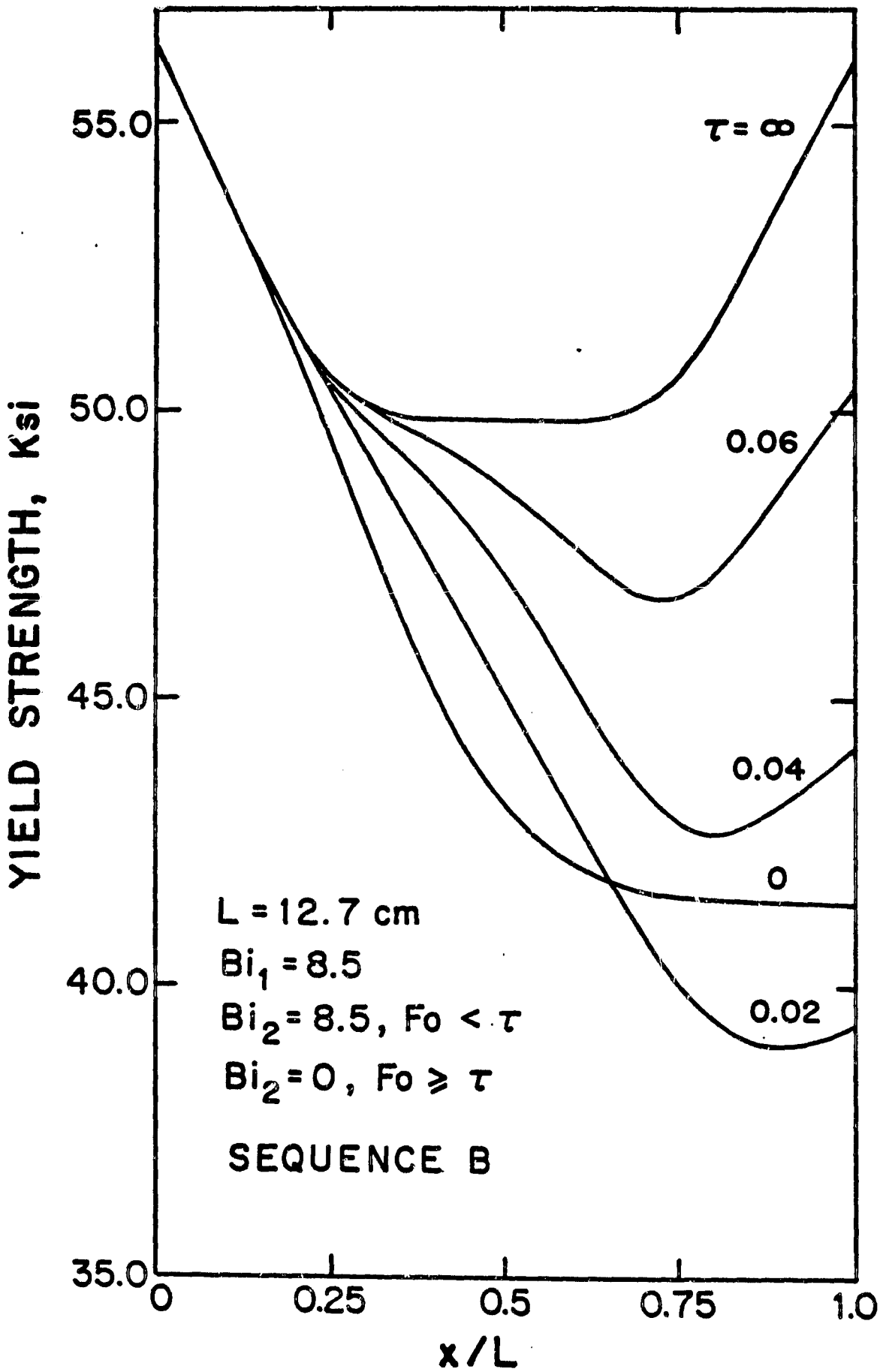

Figure 90. Predicted yield strength versus distance from the top surface of 12.7 cm thick plates subjected to a variety of heat flow conditions at the bottom surface. Curves are calculated using constants in Table VIII for sequence B.

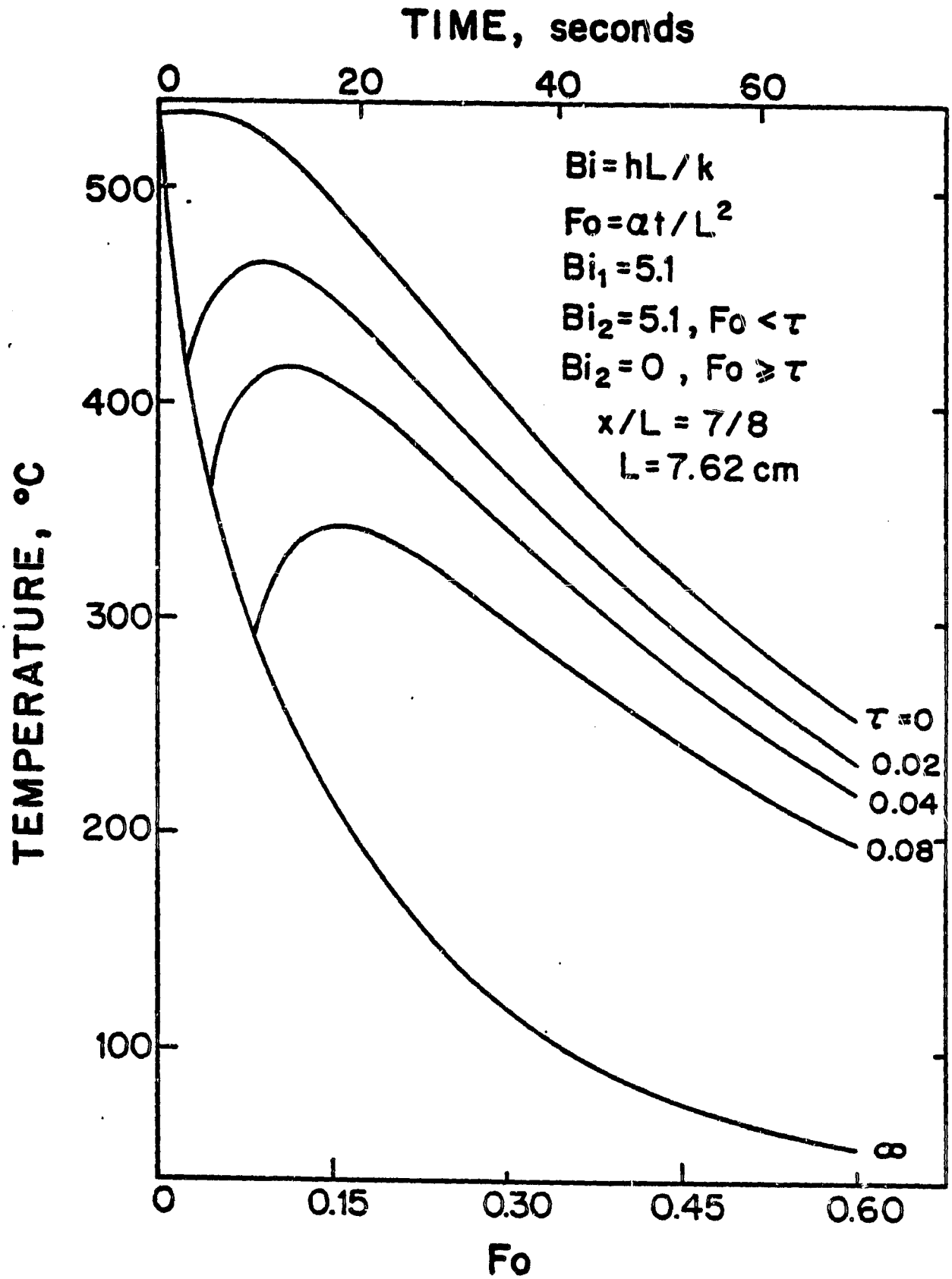

Figure 91. Calculated time-temperature profiles at a given location in a 7.62 cm thick plate of 2219 aluminum alloy subjected to a variety of heat flow conditions at the bottom surface.

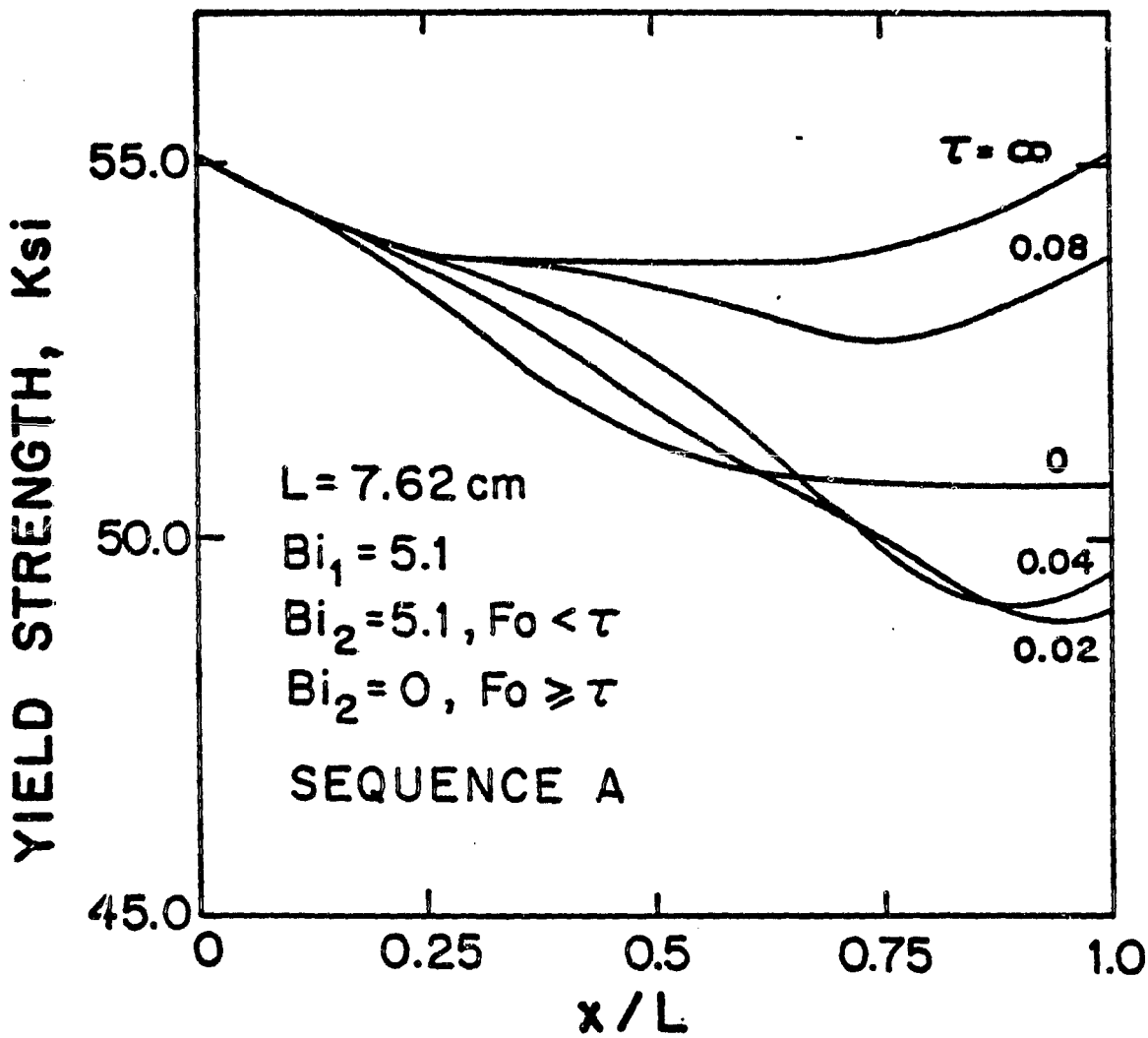

Figure 92. Predicted yield strength versus distance from the top surface of 7.62 cm thick plates subjected to a variety of heat flow conditions at the bottom surface. Curves are calculated using constants in Table VIII for sequence A.

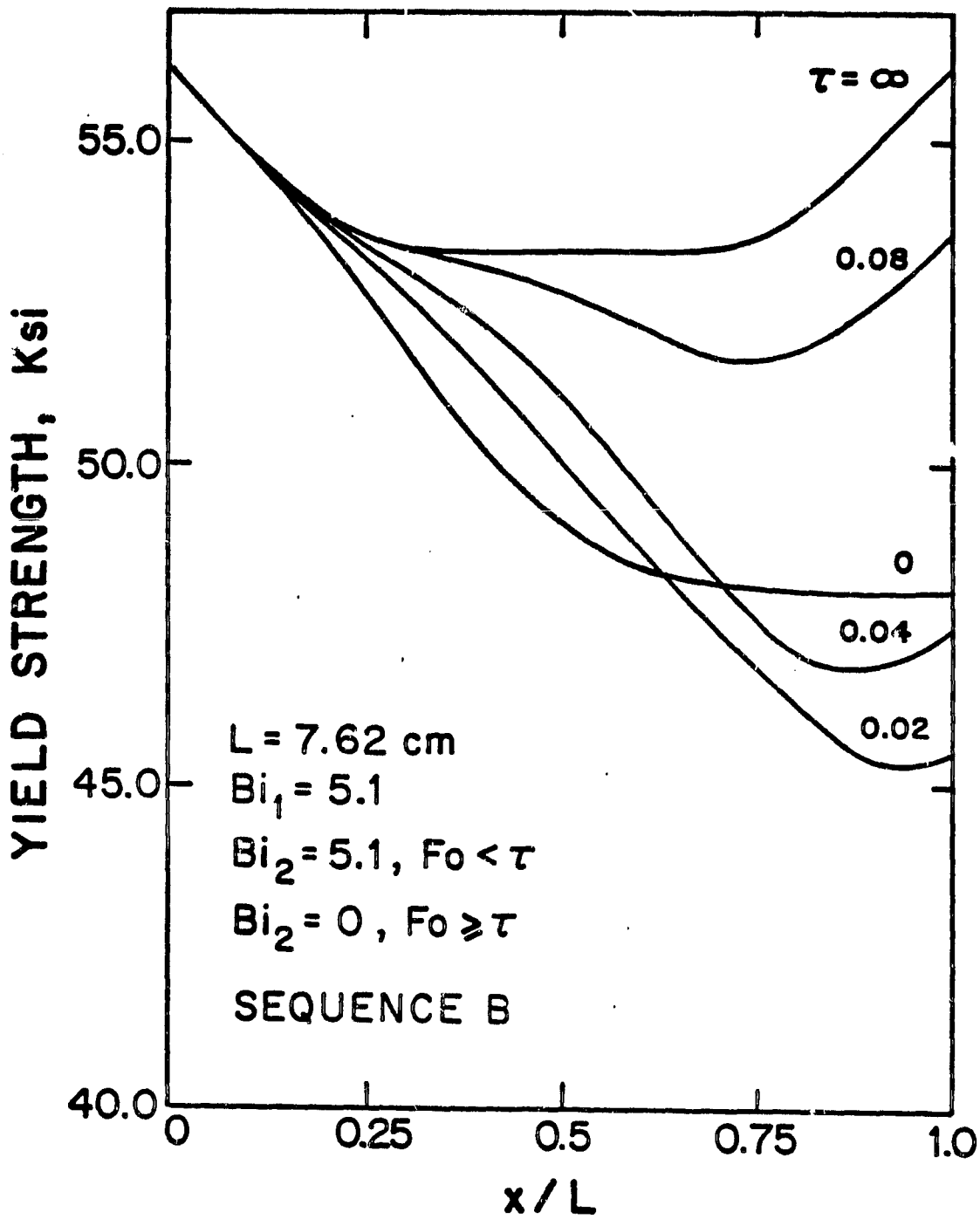

Figure 93. Predicted yield strength versus distance from the top of 7.62 cm thick plates subjected to a variety of heat flow conditions at the bottom surface. Curves are calculated using constants in Table VIII for sequence B.

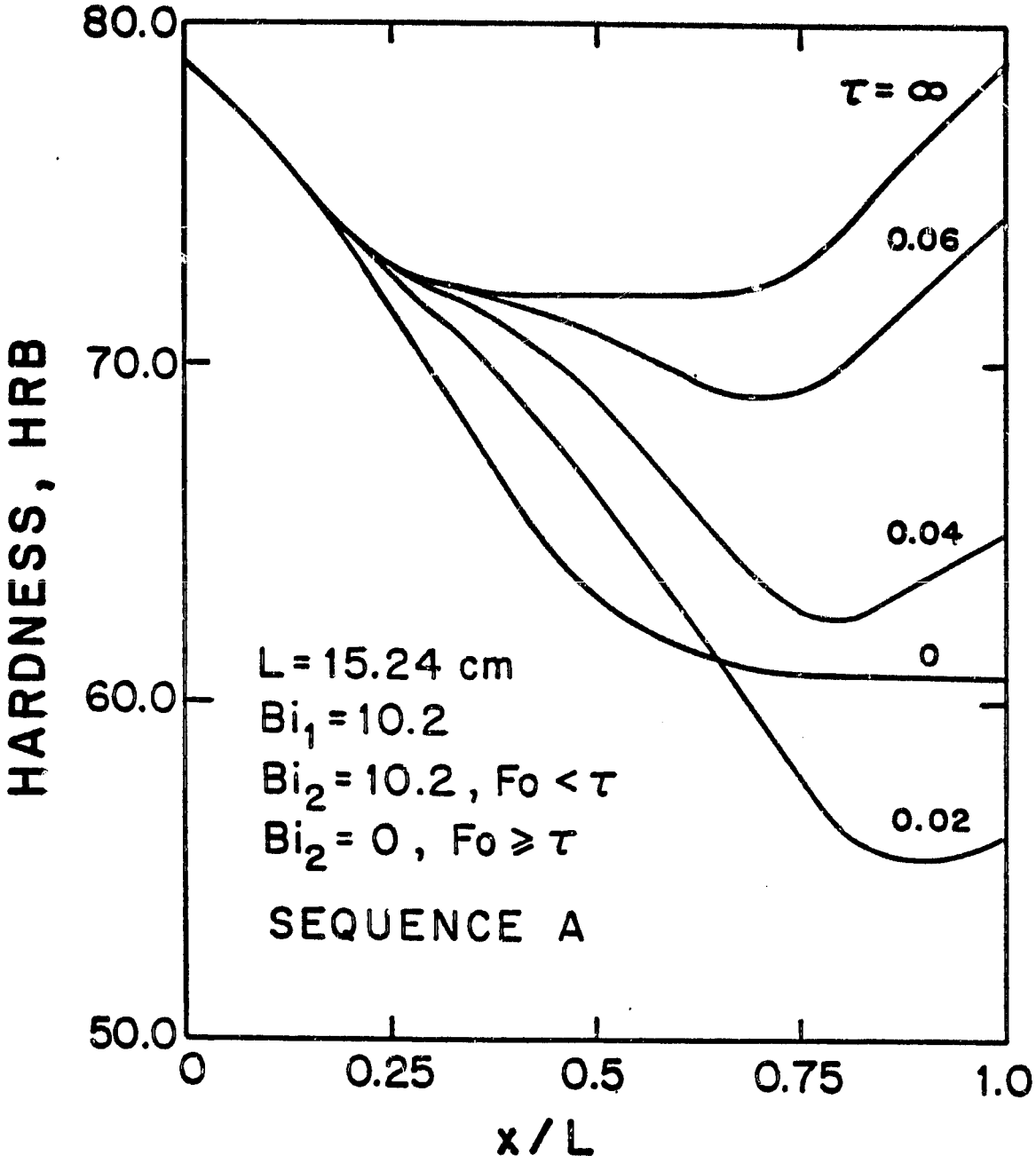

Figure 94. Predicted hardness versus distance from the top surface of 15.24 cm thick plates of 2219 aluminum alloy subjected to a variety of heat flow conditions at their bottom surfaces.

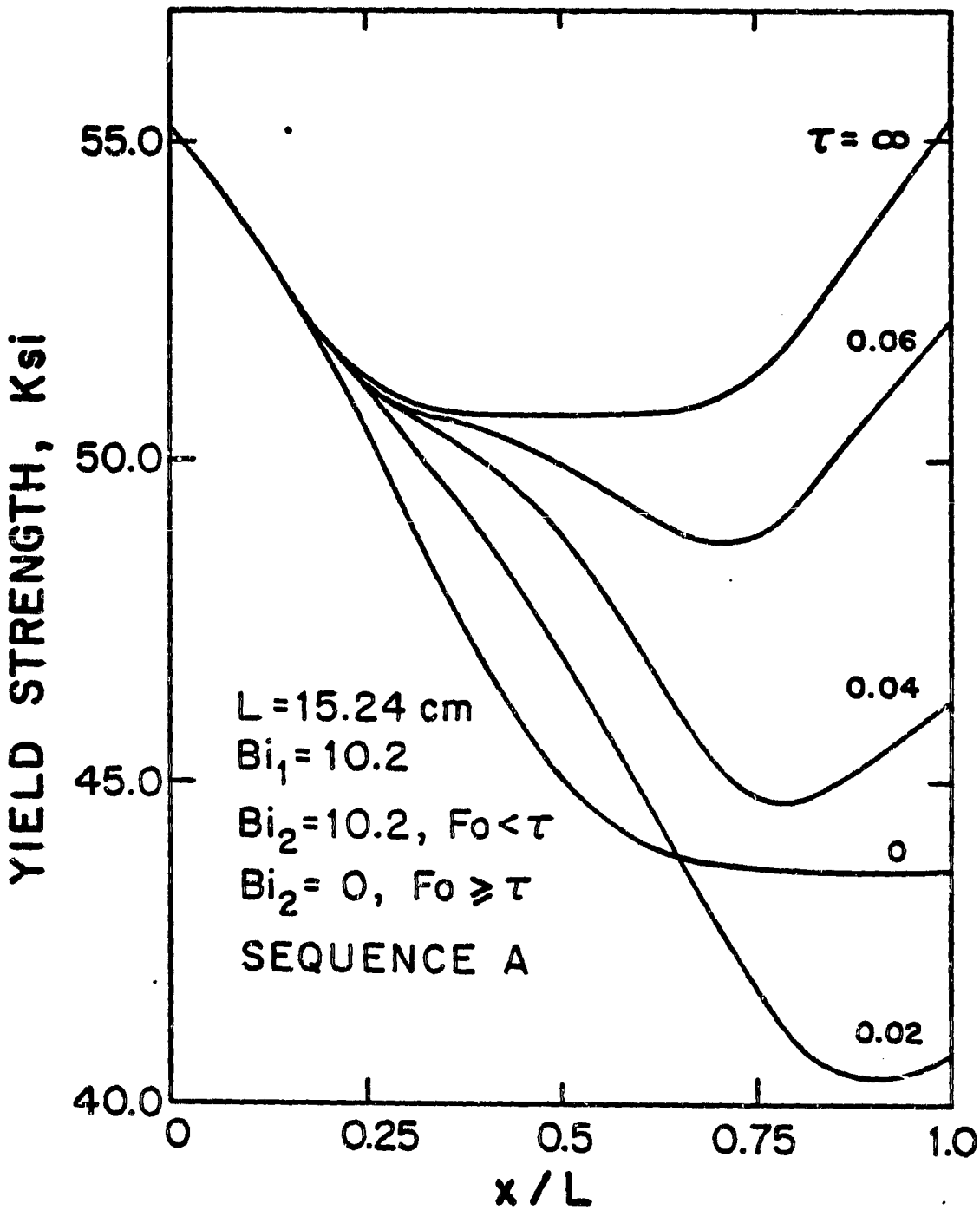

Figure 95. Predicted yield strength versus distance from the top surface of 15.24 cm thick plates subjected to a variety of heat flow conditions at the bottom surface. Curves are calculated using constants in Table VIII for sequence A.

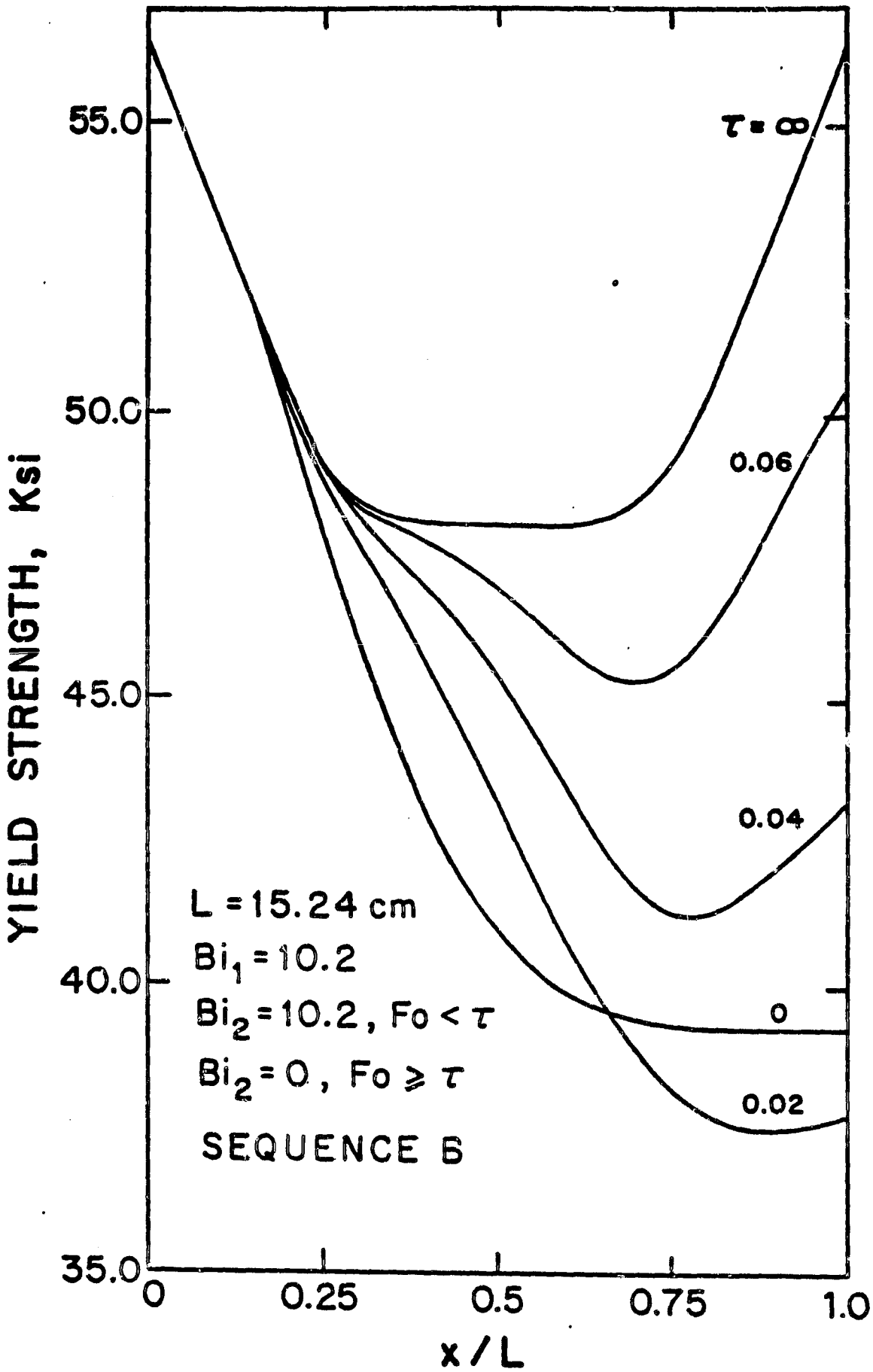

Figure 96. Predicted yield strength versus distance from the top of 15.24 cm thick plates subjected to a variety of heat flow conditions at the bottom surface. Curves are calculated using constants in Table VIII for sequence B.

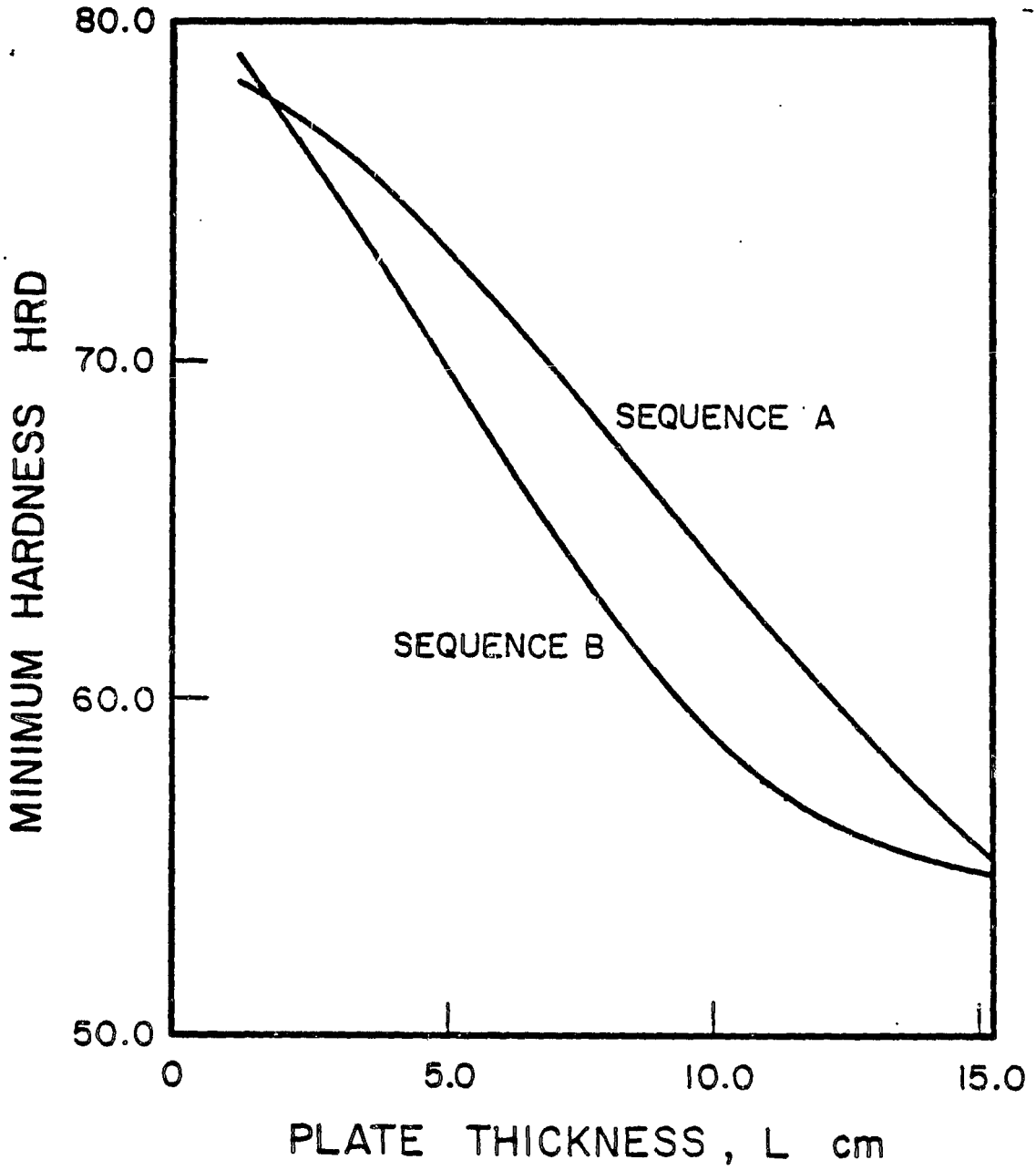

Figure 97. Predicted minimum hardness in different thickness plates under the "worst possible" heat flow conditions.

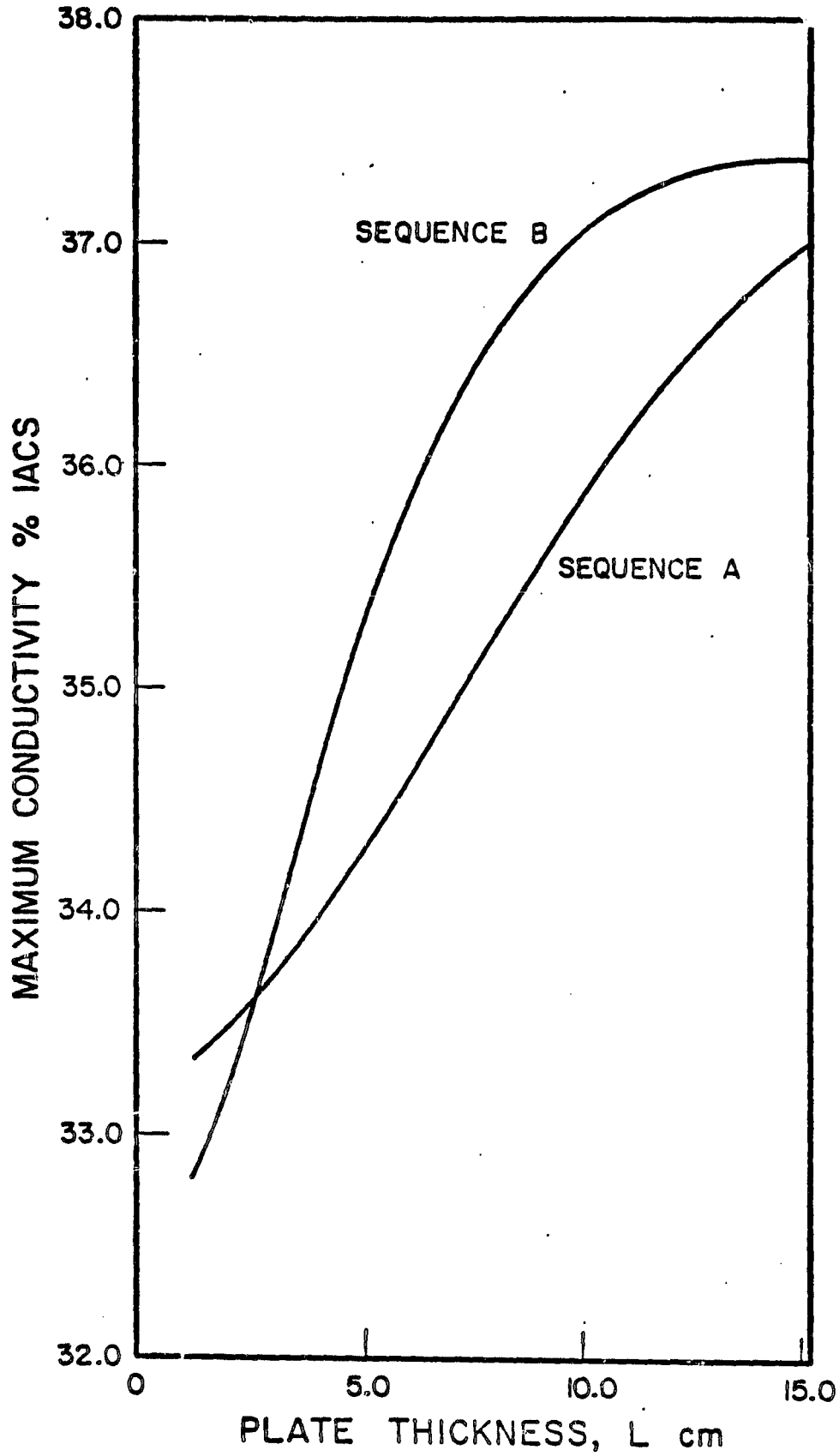

Figure 98. Predicted maximum conductivity in different thickness plates under the "worst possible" heat flow conditions.

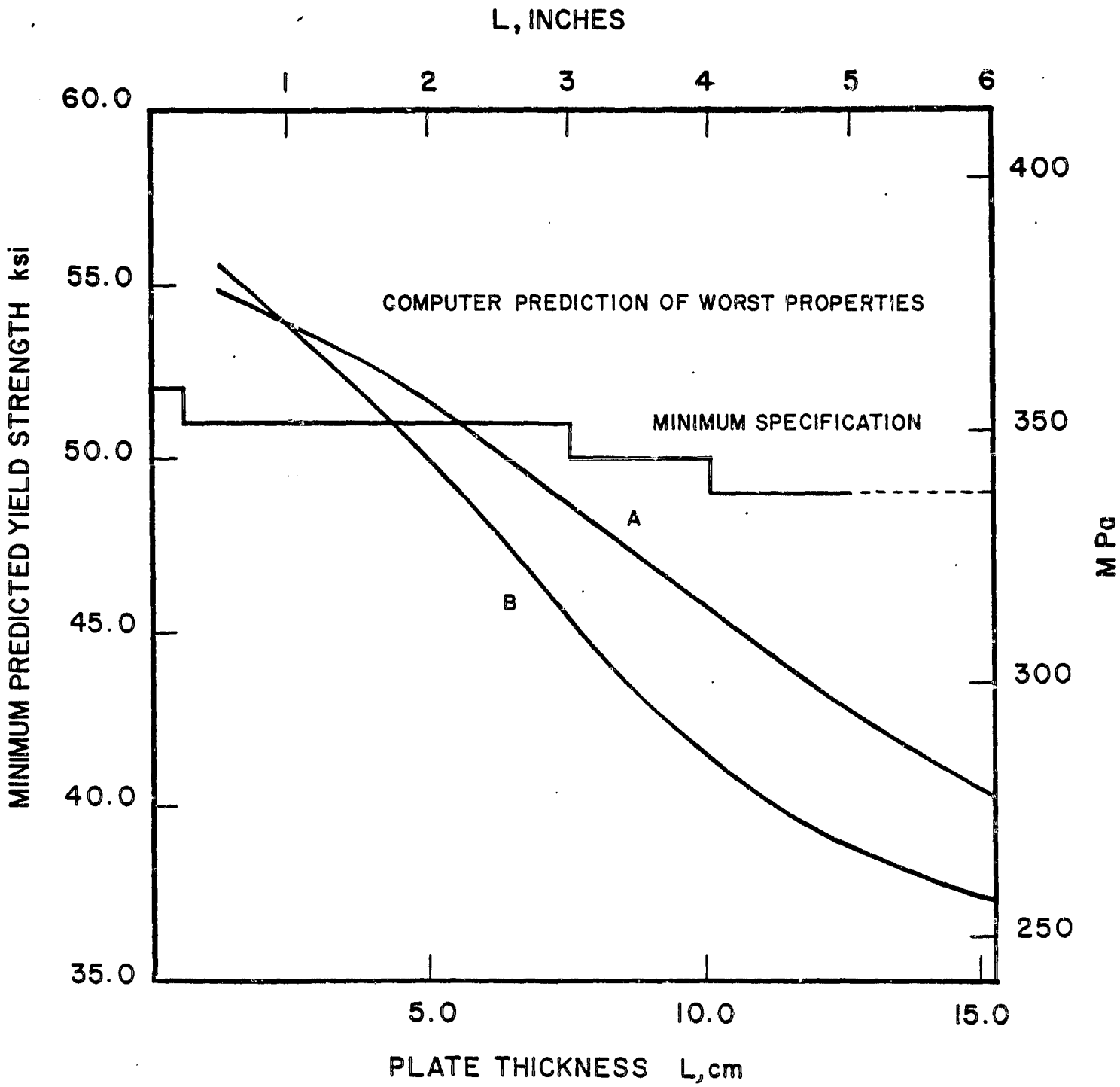

Figure 99. Predicted minimum yield strength in different thickness plates under the "worst possible" heat flow conditions using sequence A or B data.

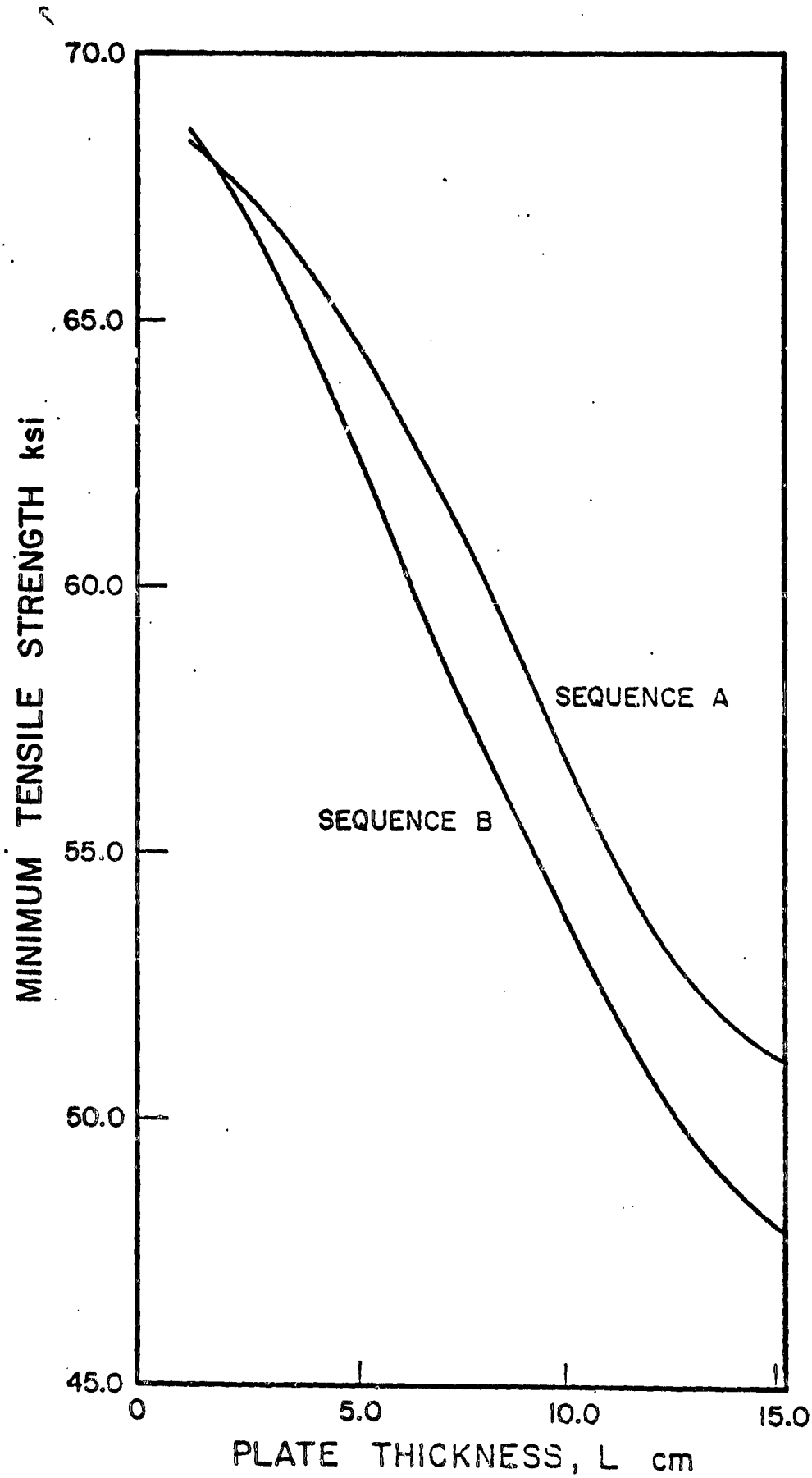

Figure 100. Predicted minimum ultimate tensile strength in different thickness plates under the "worst possible" heat flow conditions.

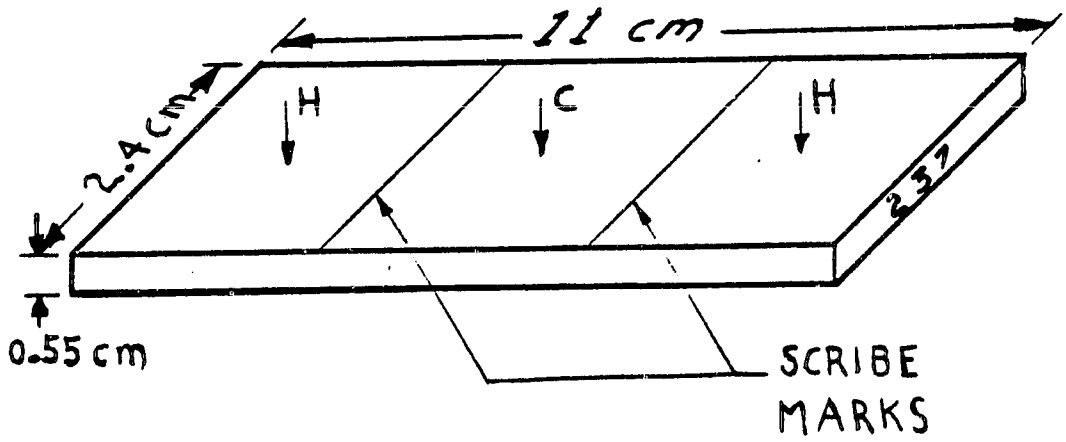

Figure 101. Geometry of aluminum samples used in the round robin. Each sample has an identifying number stamped on one end as shown. The sample surface was divided into three equal areas. Each laboratory made three hardness measurements in each of the areas H and three conductivity measurements in the area marked C.

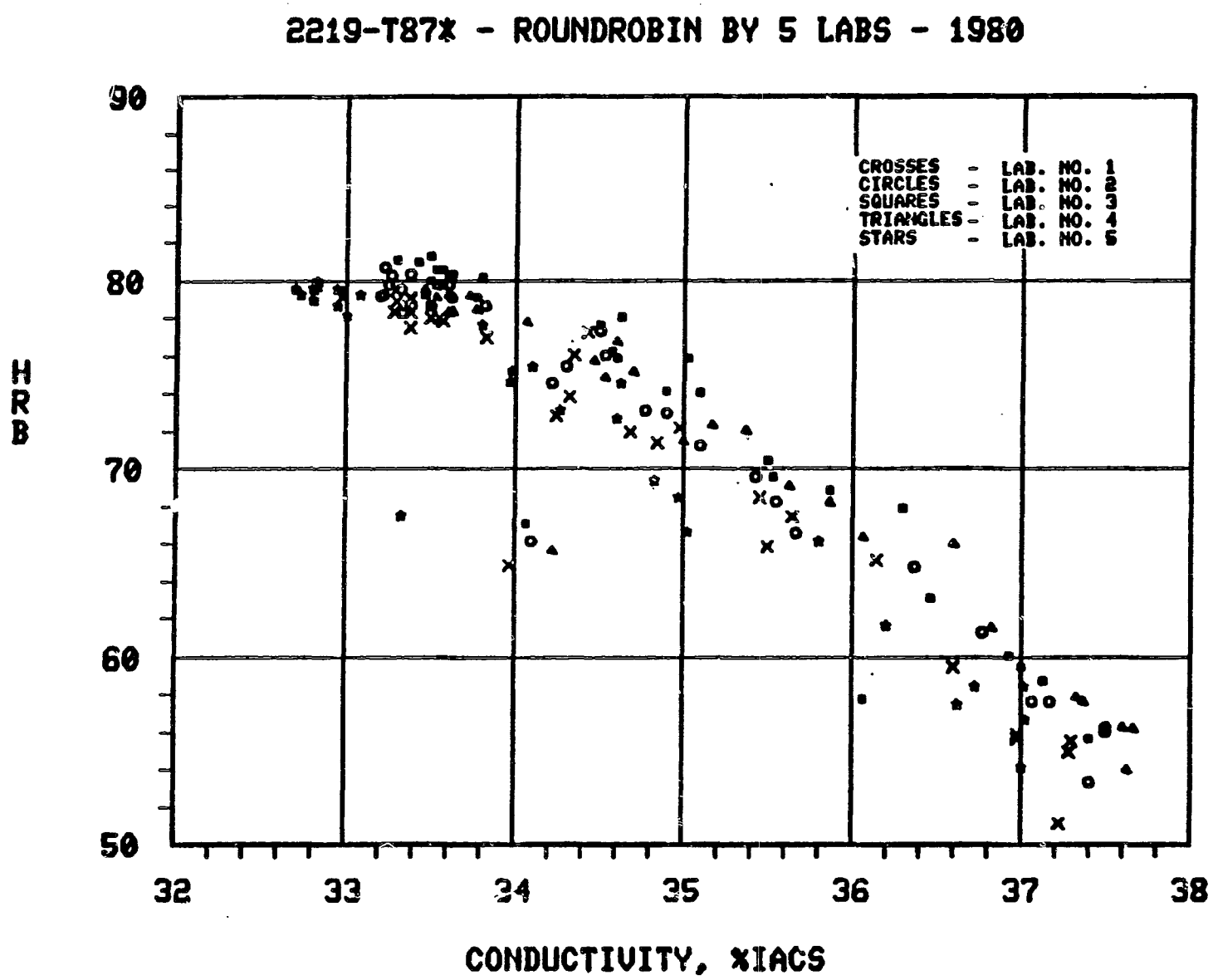

Figure 102. Rockwell B hardness vs. conductivity obtained on thirty round robin samples of 2219-T87* aluminum alloy. Each point represents the average of six hardness measurements and the average of three conductivity measurements as made by one laboratory on one sample.

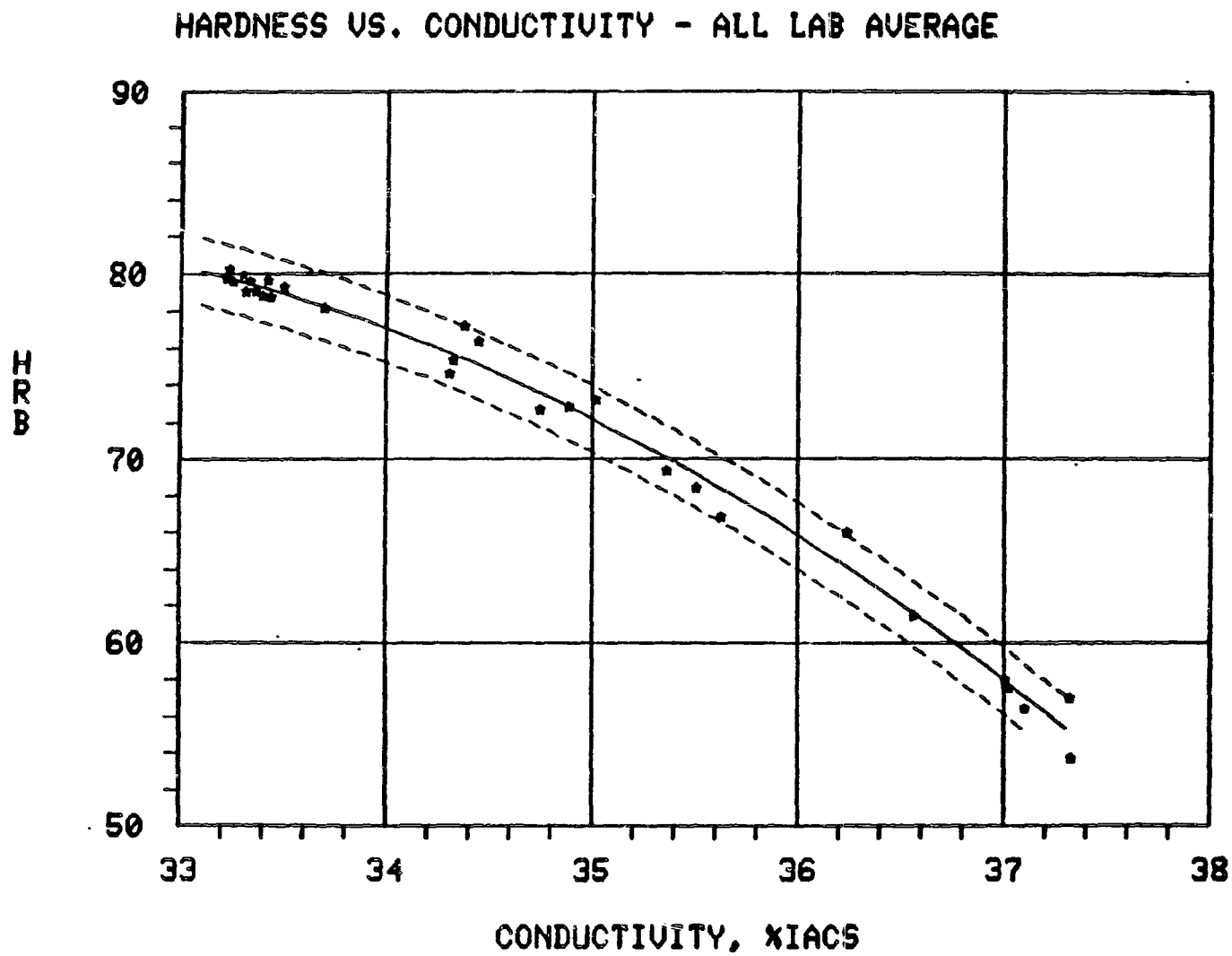

Figure 103. Rockwell B hardness vs. conductivity for the thirty round robin samples of 2219-T87* aluminum alloy when the hardness and conductivity measurements from five laboratories have been averaged for each sample. The solid line represents least squares fit to a quadratic equation and the dashed lines are the scatter band (approximately 95% confidence level).

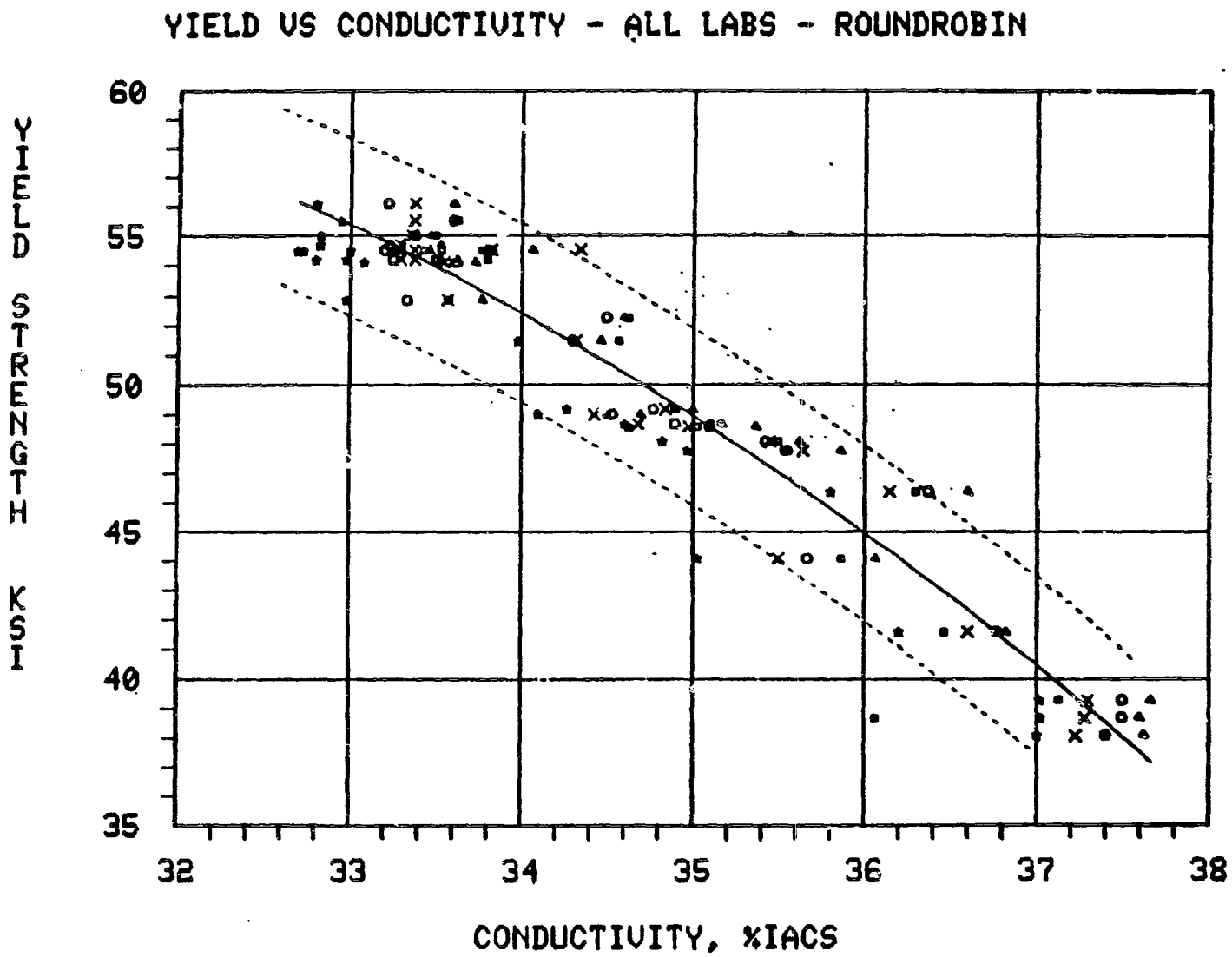

Figure 104. Yield strength (0.2% offset) vs. conductivity for the round robin samples of 2219-T87* aluminum alloy when the three conducitivty measurements from each of the five laboratories have been averaged. The solid line represents a least squares fit to a quadratic and the dashed lines are the scatter band (approximately 95% confidence level)

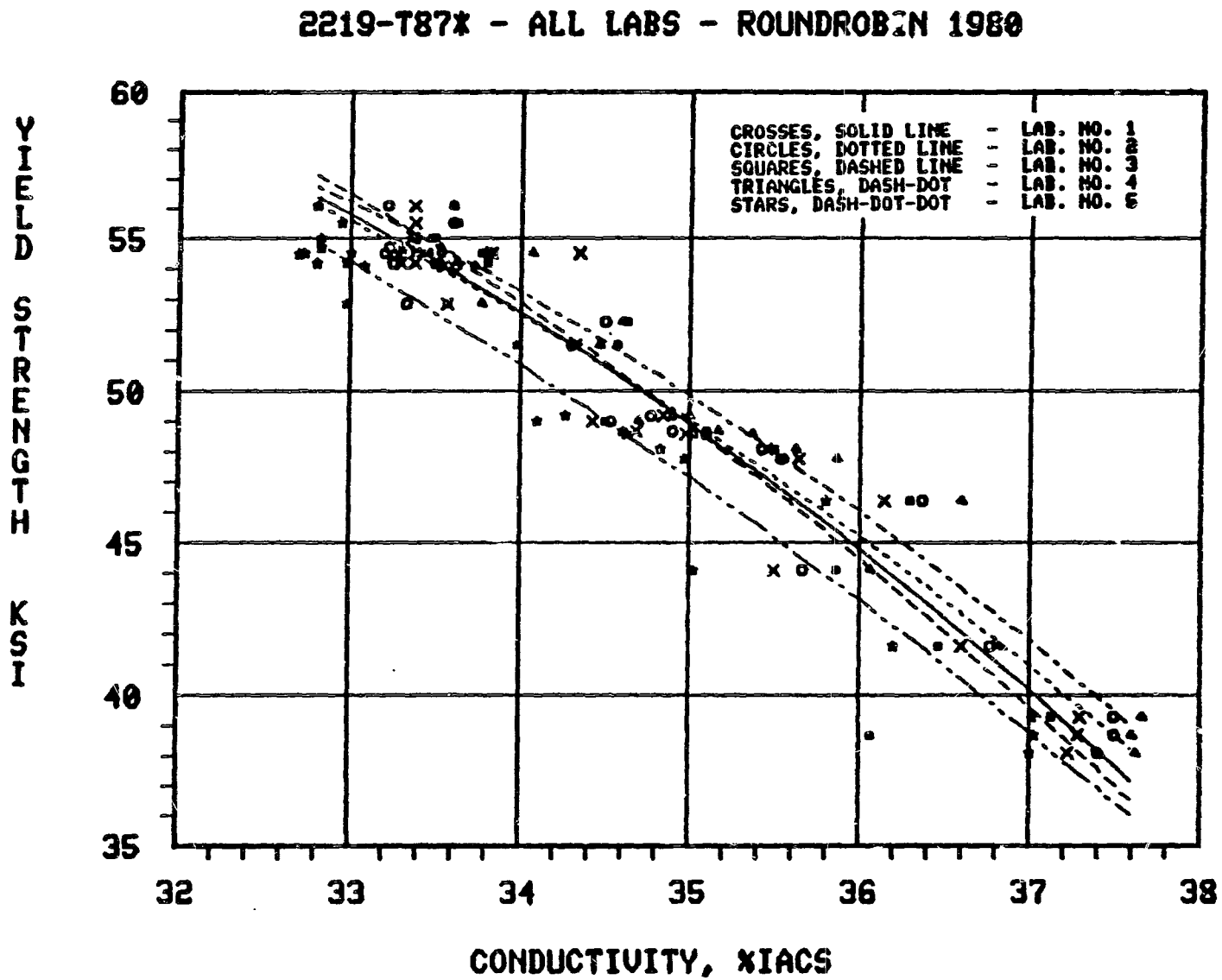

Figure 105. Curves obtained by least squares fitting the yield strength (0.2% offset) vs. the Rockwell B hardness of the 2219-T87* round robin samples as measured by each of the five participating laboratories.

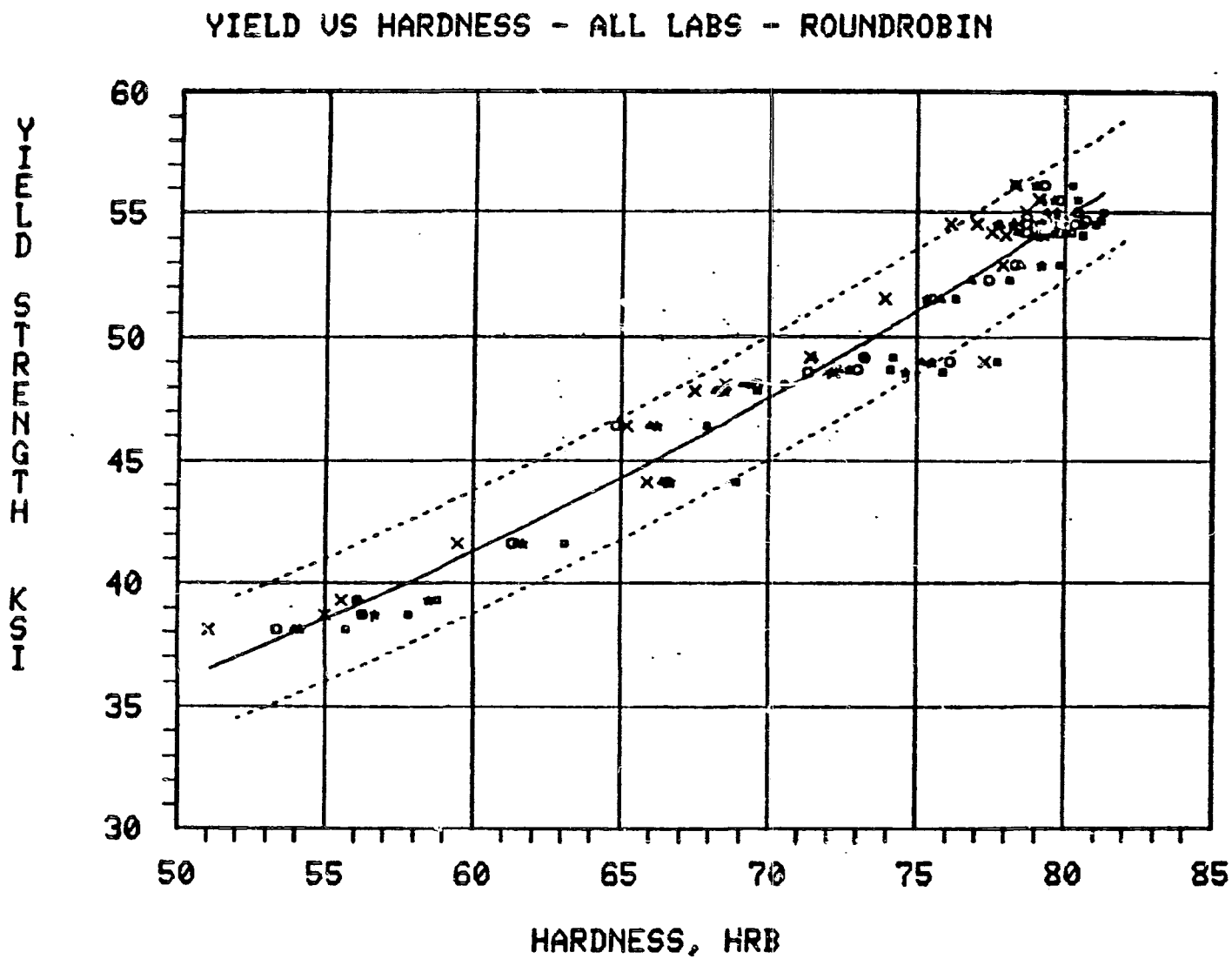

Figure 106. Yield strength (0.2% offset) vs. hardness for the round robin samples of 2219-T87* aluminum alloy when the six hardness measurements from each of the five laboratories have been averaged. The solid line represents a least squares fit to a quadratic equation and the dashed lines are the scatter band (approximately 95% confidence level).

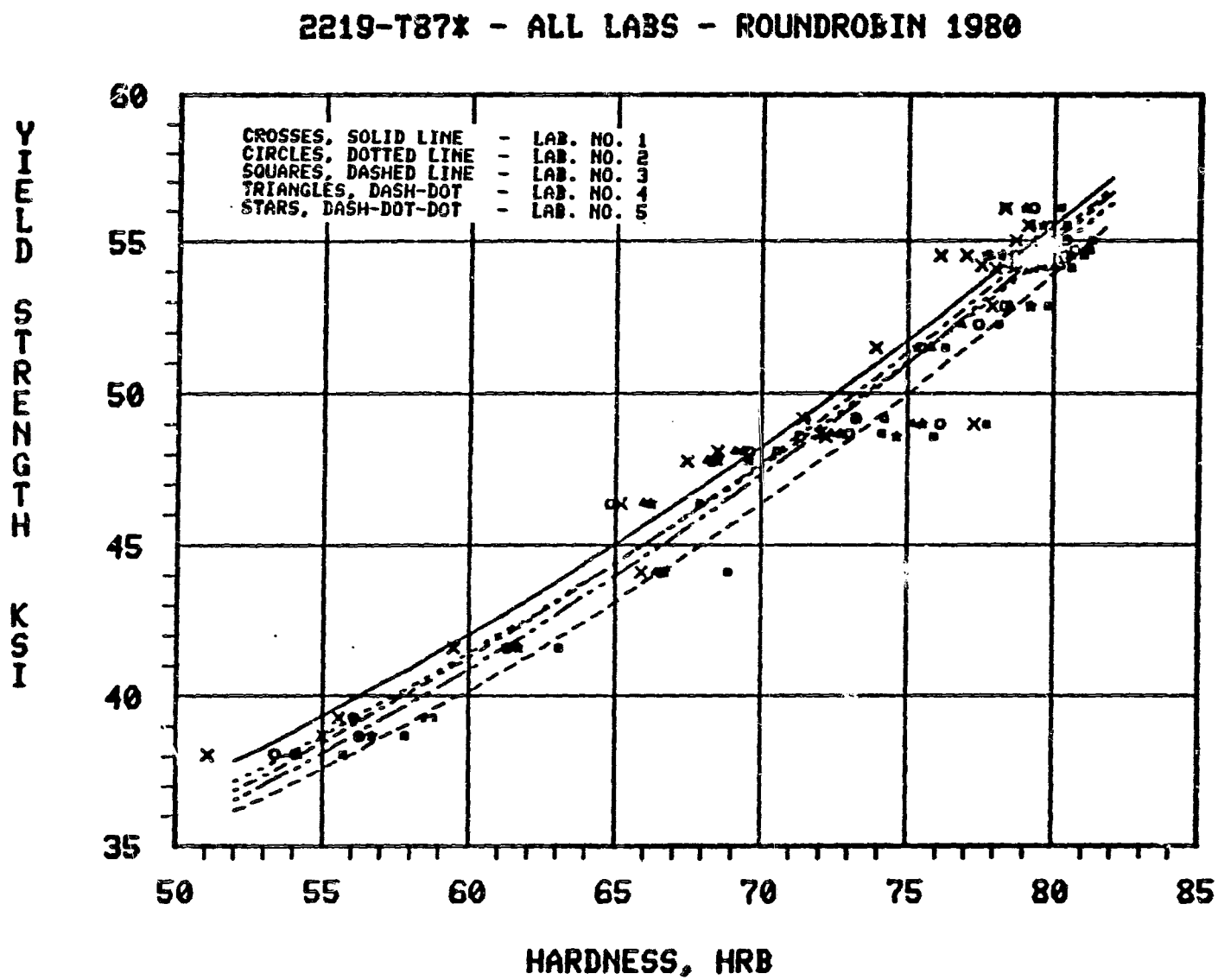

Figure 107. Curves obtained by least squares fitting the yield strength (0.2% offset) vs. the Rockwell B hardness of the 2291-T87* round robin samples as measured by each of the five participating laboratories.